Sr, Nd, Pb ISOTOPE AND TRACE ELEMENT GEOCHEMISTRY OF CALC-ALKALINE AND ALKALINE VOLCANICS, EASTERN TURKEY

by

LEVENT GULEN

B. Sc. (Hons), Hacettepe University, Ankara

(1976)

Submitted in partial fulfillment of the requirements for the

degree of

DOCTOR OF PHILOSOPHY

at the

MASSACHUSETTS INSTITUTE OF TECHNOLOGY

June.1984

Massachusetts Institute of Technology

Signature of Author _____
Center for Geoalchemy, Department of Earth, Atmospheric, and Planetary Sciences June 18, 1984

Certified by _____
Stanley R. Hart
Thesis Supervisor

Accepted by _____
Theodore R. Madden
Chairman, Department Committee on Graduate Students

Sr, Nd, Pb ISOTOPE AND TRACE ELEMENT GEOCHEMISTRY OF CALC-ALKALINE AND ALKALINE VOLCANICS, EASTERN TURKEY

by

LEVENT GULEN

Submitted to the Department of Earth, Atmospheric, and Planetary Sciences on June 18, 1984 in partial fulfillment of the requirements for the degree of Doctor of Philosophy

ABSTRACT

A Tertiary to Quaternary volcanic province, which includes both calc-alkaline and alkaline volcanics, covers wide areas just to the north of the Bitlis Suture Zone in Eastern Turkey. Investigations have been undertaken to provide constraints on the nature of the spatially and temporally coexisting calc-alkaline and alkaline volcanics and the magmato-tectonic evolution of this region. Two types of approaches have been utilized: 1-To study isotopic systematics (Sr, Nd and Pb), major and trace element abundances of carefully collected, representative volcanic rock samples. 2-To analyse tectonic deformations caused by the Miocene continental collision and still continuing convergence between the Arabian and "Turkish" plates, based on LANDSAT, SIR-A image analyses, field studies and existing geological data. Four major volcanoes of this volcanic province have been chosen to carry out geochemical investigations. Ararat and Suphan are calc-alkaline, Tendurek and Nemrut are alkaline volcanoes.

The calc-alkaline rocks of Ararat and Suphan include high-alumina basalts, andesites dacites and rhyolites. The results of this study show that the four volcanostratigraphic Ararat suites, distinguished by field studies, also form four coherent geochemical groups. Isotopic compositions of the Ararat suites are within the observed range for island-arc basalts. However a careful examination of their isotope systematics reveals a very limited involvement of a lower crustal component in their petrogenesis. In contrast to Ararat, Suphan lavas exhibit significant crustal contamination signatures. The obtained geochemical data indicate that various two-component magma mixing processes involving six end-members, that are derived from two distinct mantle-derived magmas by the interplay of fractional crystallization, limited crustal contamination and cumulate assimilation can account for the major, trace element and Sr, Nd, Pb isotopic composition of the Ararat lavas.

Alkaline products of Tendurek, Nemrut volcanoes and fissure lavas of the Lake Van region consist of rocks ranging in composition from alkali basalts, through hawaiites, benmoreites, mugearites and sodic trachytes to peralkaline commendites and pantellerites.

Alkali volcanism is basically sodic and Al-rich in character and the most primitive lavas are transitional to tholeiites. All of the alkaline suites studied have been variously affected by lower and/or upper crustal contamination. Derivation of the alkaline lavas by partial melting of a recently metasomatized, heterogeneous, hydrous phase-bearing (amphibole), depleted peridotite mantle source followed by variable degrees of crustal contamination and fractional crystallization is consistent with their overall geochemical characteristics.

Based on the geochemical compositions of the most primitive basalts as best exemplified by the Ararat high-alumina basalt suite, two distinct mantle sources can be inferred for the Eastern Turkish volcanics. The first one represents a mantle that has had a time-integrated depletion in Rb/Sr and Nd/Sm and similar to that of transitional-MORB and continental arc basalts. The second mantle source is characterized by relatively less depletion but quite radiogenic Pb 207/204 isotope composition. Models involving both an ancient subducted oceanic crust source or a segment of depleted subcontinental mantle that has been contaminated and metasomatized by a component carrying sediment signatures, during a previous subduction event, are isotopically plausible. However, considering all the geological and geochemical facts, the latter appears to be the most satisfactory petrogenetic model.

It is not possible to establish a direct link between the subduction of the Bitlis-Zagros ocean crust and the volcanism in Eastern Turkey. However, the assumption of a detached, sinking slab following Miocene continental collision along the Bitlis-Zagros Suture Zone, can be viewed as a plausible trigger for the generation of the calc-alkaline magmas and their emplacement within the continental crust. The calc-alkaline volcanism may be maintained to present by the continued sinking and dehydration of this detached slab, as well as by the continued tectonic deformations caused by continental collision. This creates mantle upwelling which not only initiates the alkali volcanism, but also keeps the calc-alkaline volcanism alive.

The consideration of the detailed geology, tectonic structures and their trends along with regional seismicity permits the identification of a number of deformational domains in eastern Turkey bounded by major shear zones, in which coherent deformational styles are displayed. The Van and the surrounding deformational domains formed and evolved under the influence of a continental collision, following the Late Miocene elimination of the Bitlis-Zagros ocean along the Bitlis-Zagros suture zone between the Anatolian-Iranian and Arabian blocks. Mainly three different, but nevertheless related deformational styles take up the still continuing continental convergence that is the result of the northward motion of the Arabian plate. These are: 1- Folding and thrusting within the Arabian platform and along the Caucasuses, 2- Displacements along NW-SE and NE-SW trending sets of oblique-slip faults, causing lateral escape, and 3- Tilting and bending of crustal blocks and thrusting of those blocks over a decollement surface within the continental crust. The contemporaneous development of extensional and compressional tectonic regimes along with calc-alkaline and alkaline volcanism can best be explained by limited thinning as opposed to thickening of the continental crust, as a result of wide scale compression in eastern Turkey. This is accomplished by the tilting and bending of slab like crustal blocks and thrusting of these blocks over a decollement surface within the continental crust, providing that there is an available "escape space" in the direction of the tilting and thrusting. It is suggested that the combined Black and Caspian Sea back-arc basins(marginal sea?) through the Caucasuses provided the required "escape space" in this region. However, the consumption of oceanic crust along the Caucasuses by the overthrusting continental margins, from both north and south, prevented the further development of an extensional regime in this region. The slab-like crustal blocks of the Van deformational domain, trapped between the converging Arabian and Scythian blocks

escape eastwards away from the maximum compression region along the NW-SE trending set of oblique-slip faults instead of thickening the crust by overthrusting onto each other. This model may offer plausible alternative explanations for the origin of an extensional regime, either immediately following or contemporaneously developing with a compressional regime in an adjacent region.

Thesis supervisor: Stanley R. Hart,
Professor of Geology and Geochemistry

ACKNOWLEDGEMENTS

I feel very lucky and honored by being a student of Stan Hart who is not only a very fine scientist, but also a very fine person. His constant encouragement and enthusiasm has been a prime source of inspiration. I would like to thank him also for taking his time patiently correcting the spelling and English of this thesis.

Special thanks to Fred Frey for help, advice and providing free access to his INAA facilities.

I would like to thank Nobu Shimuzu for advice, discussions, and for constructive critisism of Chapter 1.

Special thanks to Nafi Toksoz for help, advice, providing LANDSAT images, and for initiating my interest in SIR-B project, as well as in Cabernet Sauvignon.

I would especially like to acknowledge Clark Burchfiel, Peter Molnar, Wiki Royden, and Dave Walker for advice, discussions and their constructive critisism of Chapter 3.

The engineering expertise of Ken Burrhus has been extremely helpful in maintaining equipment of a high level performance. He taught me a lot about mass spec as well as Wall Street.

Special thanks to Donna Hall for being a good friend who cares and shares. She willingly took responsibility for graphics.

I would like to thank M. K. Roden for teaching me various analytical techniques.

Gile Beye and John Zannos helped with graphics.

I would like to gratefully acknowledge Gurol Ataman who provided continuous support during my college years and initiated my interest in geochemistry.

I gratefully acknowledge receipt of a Graduate Fellowship from the Scientific and Technical Research Council of Turkey (TUBITAK).

I acknowledge the logistic support by MTA (Institute of Mineral Research and Exploration) during the field work. I would like to thank E. Arpat, Y. Guner, and F. Saroglu of M.T.A. for introducing me to the geology of Eastern Turkey and for discussions.

Special thanks to my parents, who not only influenced my personal growth by giving me a certain "vision of life", but also unknowingly made me determined to be a geologist by telling a real life story when I was eight years old.

I am particularly grateful to my wife, Suna, for her constant encouragement, support, and patience. She also skillfully handled word-processing. This thesis is dedicated to Suna, without whom the world would have been dark for me.

Table of Contents

CHAPTER-3 Deformational domain continental tectonics in the Lake Van region, Eastern Turkey: implications on the origin of an extensional regime associated with compression

CHAPTER 1

GEOCHEMISTRY OF THE CALC-ALKALINE VOLCANICS

1.1 Introduction

A Tertiary to Quaternary volcanic belt which covers wide areas between the Caucauses (U.S.S.R) and Lake Van (Eastern Turkey) extends about 900 km. towards the Bijar region of northwest Iran (Figure-1.1). This volcanic belt is situated to the north of the Bitlis-Zagros suture zone. As a result of the overall convergence between the Arabian and Eurasian plates, the existing southern branch of Neo-Tethys was consumed by northward subduction; continental collision took place in the Miocene forming the Bitlis-Zagros suture zone (Rigo de Righi & Cortesini, 1966; Dewey et al., 1973; Hall, 1976; Stocklin, 1974). However, continental convergence is still taking place as manifested by active deformation and diffuse seismic activity in this region (Nowroozi, 1971; McKenzie, 1972; Rotstein & Kafka, 1982; Jackson & McKenzie, 1984). This volcanic province has certain peculiarities by which it can be distinguished from typical continental volcanic arcs. First of all, calc-alkaline and alkaline volcanics spatially and temporally coexist. Some of the volcanic centers that produced alkali volcanics are located just to the north of the presumed trench zone, which is represented by the Bitlis-Zagros Suture. Moreover, this volcanic belt attains it's maximum width in Eastern Turkey, where volcanic rocks extend northward, for about 350 km., from Lake Van area (Turkey) to the Caucasuses (U.S.S.R.). The existing volcanoes do not line up to form an elongate volcanic zone, subparallel to the presumed continental margin in Eastern Turkey, as they do in most continental arcs. Finally, major volcanoes were formed in Pliocene to Quaternary times, long after the Miocene continental collision.

Although the volcanics of this province have not been systematically dated (except the ones in the immediate vicinity of Lake Van and northwestern Iran), calc-alkaline volcanism appears to be represented by two main phases of activity. K/Ar dating by Innocenti et al.,(1976) indicates that the first phase of calc-alkaline, high-potassic activity

Figure-1.1

Distribution of Tertiary to Quaternary volcanic rocks in eastern Turkey and surrounding regions. Letters denote: a- Calc-alkaline, Ka- High-K calc-alkaline, b- Alkaline series. Shading patterns represent approximate age intervals by K-Ar dating. Shading patterns: 1- Upper Oligocene-Lower Miocene, 2- Lower-Middle Miocene, 3- Middle-Upper Miocene, 4- Upper Miocene-Pliocene, 5- Pliocene-Quaternary, 6- Quaternary, 7- Dominant pyroclastic products and ignimbrites. Bitlis-Zagros Suture Zone is located to the south of the volcanic province. Note that the volcanic belt attains it's maximum width between Lake Van and Tbilisi. The Lake Van area, indicated by a frame, is shown in detail in Figure-1.2. Map modified after Innocenti et al., 1982.

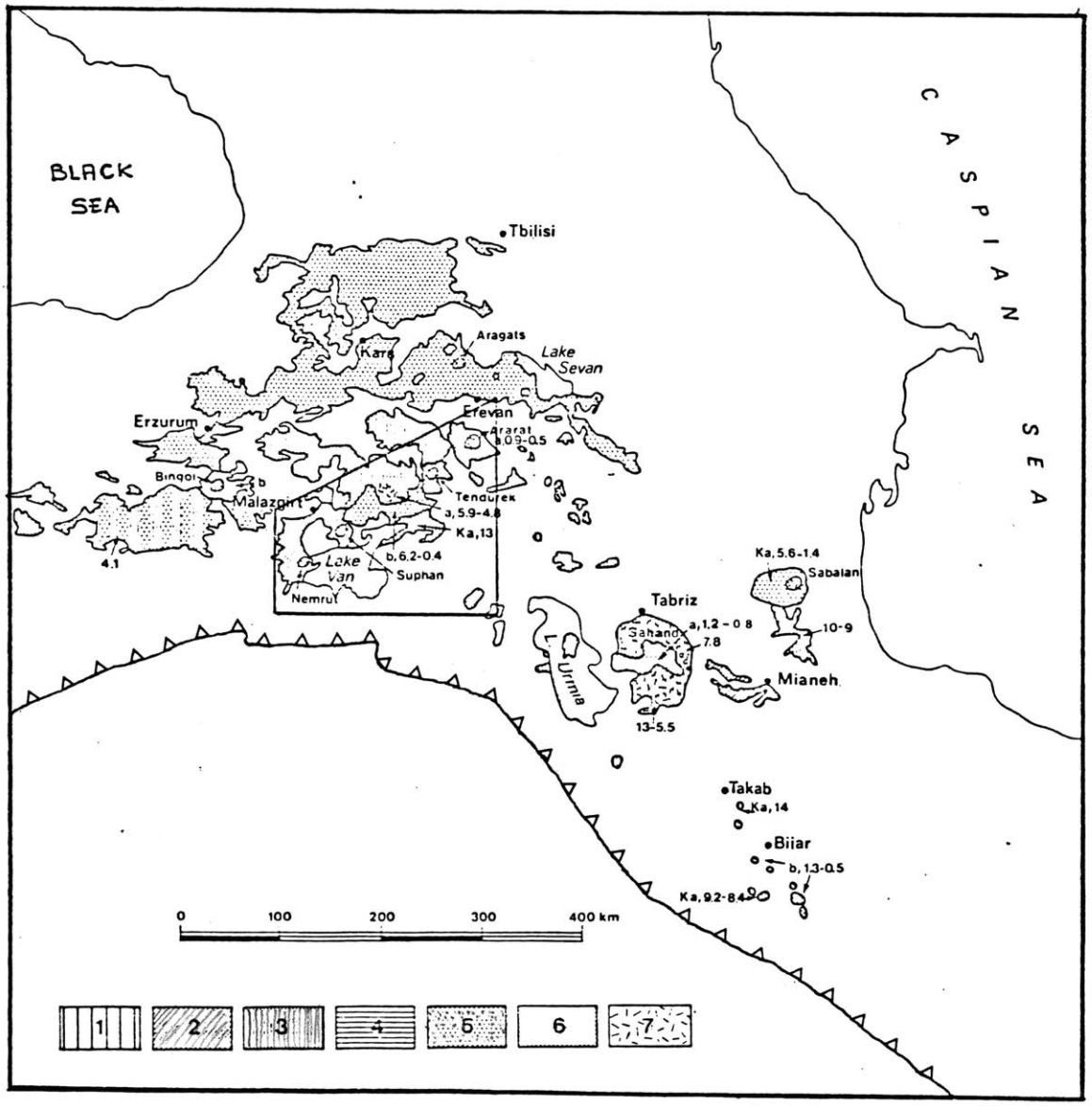
BLACK SEA
CASPIAN SEA
Tbilisi
Aragats
Kars
Lake Sevan
Erevan
Erzurum
Ararat
3.0-2.5
Bingol
Malazgirt
Tendurek
a, 5.9-4.8
Ka, 13
b, 6.2-0.4
Suphan
Lake Van
Nemrut
4.1
Tabriz
Sahand
a, 1.2 - 0.8
7.8
Lake Urmia
13-5.5
Ka, 5.6-1.4
Sabalan
10-9
Mianeh
Takab
Ka, 14
Biiar
b, 1.3-0.5
Ka, 9.2-8.4
0
100
200
300
400 km
1
2
3
4
5
6
7

produced large lava domes and flows and ceased, about 6my. ago, with repeated ignimbrite eruptions. Large stratovolcanoes of Pliocene to Quaternary age (such as Suphan, Sabalan, Ararat?) formed during the second phase of calc-alkaline activity.

The alkaline volcanism started about 6my. ago as fissure basalt eruptions and continued with the development of major cones such as Nemrut and Tendurek volcanoes.

1.2 Ararat Volcano

The Ararat volcano is situated in eastern Turkey, near the Turkey-Iran-U.S.S.R. triple border. It is one of the eight major volcanoes of the Tertiary to Quaternary volcanic province which covers extensive areas in this region (Figure-1.2). Apart from being famous for the biblical Noah's Ark story, it is a spectacular stratovolcano of 5165m. elevation. A permanent glacial cap is present above 4000m. elevation, at the summit of volcano. The lavas of Ararat occupy more than 1000 square km. A second major cone, Little Ararat (3903m. high) is located in the southeast, 12 km. from the Ararat peak.

The oldest exposed rocks in the vicinity of Ararat volcano are Devonian (Altinli, 1964-a), exposed as a small outcrop to the south of Little Ararat along the Iranian border. These rocks are composed of reddish schistose-sandstone and a limestone series underlying the base of the Permian limestone at this locality. The Brachiopod fossils that are found in the oldest limestone unit indicate Devonian age.

No rocks of Triassic to Lower Cretaceous age are found in this region. The Upper Cretaceous is represented by the widespread ophiolitic melange lithologies. (See the last chapter).

Figure-1.2

Simplified geological map of the Lake Van area, showing the distribution of calc-alkaline and alkaline volcanics and major volcanoes. Key to the patterns: 1- Alkaline volcanic rocks, 2- Calc-alkaline volcanic rocks, 3- Neogene and Quaternary sedimentary deposits, 4- Pre-Neogene basement. Map after Innocenti et. al., 1976.

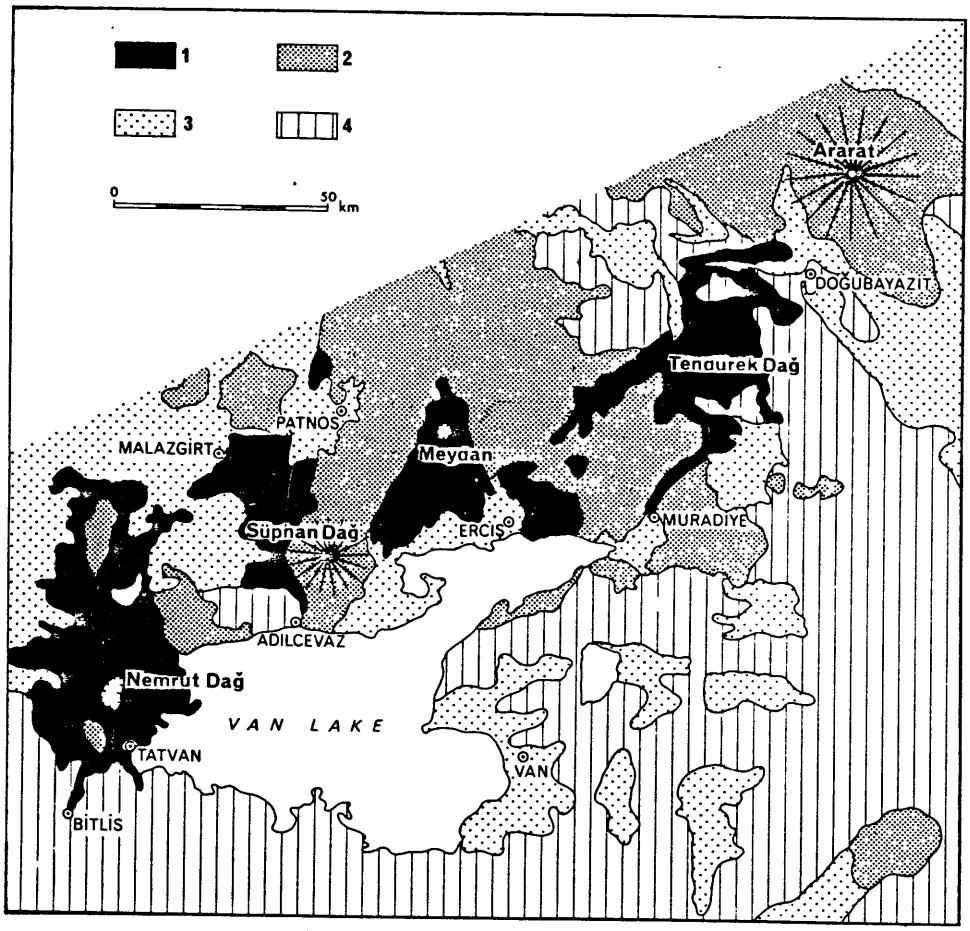
1
2
3
4
0
50 km
Ararat
DOĞUBAYAZIT
Tendurek Dağ
PATNOS
MALAZGİRT
Meydan
Süphan Dağ
ERCİŞ
MURADİYE
ADILCEVAZ
Nemrut Dağ
VAN LAKE
TATVAN
VAN
BİTLİS

The Ararat volcano is composed of high alumina basalts, basaltic andesites, andesites, dacites, rhyolites and minor amounts of pyroclastics. However, andesites and dacites are by far the most abundant lithology. Some scattered domes of gray colored andesites and dacites form the oldest exposed units. Due to the chemical similarities of these units to the Little Ararat products, they will be referred as the "Little Ararat Series" in the text. The oldest lava flows of the Ararat volcanic cone are reddish and pinkish colored andesites and dacites. These are well exposed to the north of Ararat along the Hell(Cehennem) valley. These lava flows will be referred to as the "Old Ararat Series". The high alumina basalts and basaltic andesites are found to the south of the volcano in the vicinity of the Ice Cave. They occupy an intermediate position in the Ararat volcanostratigraphy and are referred to as the "High Alumina Basalt Series". The youngest flows are black colored andesites and dacites and are referred to as the "Ararat Series". They erupted not only from the central vent, but also from post-glacial fissures, forming parasitic cones on the flanks of the volcano.

No geochronologic age data exists for the Ararat lavas. Sanver (1968) obtained a 0.4 my age for the youngest lavas of Ararat based on paleomagnetic studies.

1.3 Petrography

The samples of Ararat lava flows are highly porphyritic. There is an increase in phenocryst content, going from basalts to dacites. The most common phenocryst phases are plagioclase (An 50-60) and augite. Orthopyroxene is also common but it is not as abundant as clinopyroxene. The basalts and basaltic andesites contain minor amounts of olivine. Quartz is also common in the dacites and rhyolites. Apatite, ilmenite and magnetite are also present as accessory phases. Groundmass consists predominantly of

plagioclase, augite and oxide (titanomagnetite and ilmenite) microphenocrysts. Interstitial glass is generally present. Some samples (mostly silicic) have a holohyaline groundmass.

The plagioclase phenocrysts can reach up to 3-4 mm. length. Both normal and oscillatory zoning is present. As noted by Lambert et al (1974), some samples seem to have two generations of plagioclase. The first group is invariably more calcic and has relatively weak zoning compared to the other group. The presence of resorption of phenocrysts and the two types of plagioclases that are in disequilibrium indicate an important role for magma mixing processes in the generation of the Ararat lavas.

Isolated spherical aggregates of cpx+opx+plag+oxide exhibiting glomeroporphyritic textures are also present in some andesite samples.

1.4 Analytical Techniques

Utmost care was taken to obtain the freshest available samples in the field by sampling the crack/vein free cores of lava blocks. The sawn surfaces of sample slabs have been removed by abrasion with silicon carbide. The slabs were wrapped with plastic and aluminum foil and crushed down to 0.5 cm. chip size by hammer. Individually inspected rock chips that were free of alteration were cleaned ultrasonically in acetone and distilled water. After they were dried overnight in an oven at 110 C, they were ground in a WC shatter box and the rock powders were homogenized throughly. Major and trace elements were analyzed at Woods Hole Oceanographic Institution using the automated Phillips X-Ray Fluorescence spectrometer. Major elements were determined on fused glass discs and trace elements on pressed powder pellets using the techniques described in Schroeder et al. (1980). Based on numerous replicate analyses of U.S.G.S. rock standards,

the analytical uncertainties are in the 0.5-3% (with the exception of Na) and 1-5% range for major and trace elements respectively.

REE were determined by instrumental neutron activation analysis (INAA) (Frey et al., 1974). Nuclear irradiations were done at the Massachusetts Institute of Technology Research Reactor.

All isotope analyses were done on the 9-inch 60 mass spectrometer (NIMA-B) at the Massachusetts Institute of Technology. Chemical and mass spectrometric techniques for determination of Rb and Sr concentrations and Sr isotopic ratios are as described in Hart and Brooks (1977); for Sm and Nd concentrations and Nd isotopic ratios as adopted from Richard et al (1976) and summarized in Zindler et al (1979); for Pb isotopic compositions as adapted from Manhes et al (1978) and summarized in Pegram (1984). Procedural blanks are in the range of 20-35pg, 20-45pg and 0.8-1.2ng for Sr, Nd and Pb, respectively and, are all insignificant. Sr isotopic ratios are normalized to 0.70800 for E & A SrCO3 using 86Sr/88Sr = 0.1194. All Nd isotopic ratios are normalized to 0.51264 for BCR-1 using 144Nd/146Nd = 0.7219. Pb isotopic ratios are normalized for mass discrimination using the NBS SRM 981 common lead standard. Reproducibility is better than 0.05% per atomic mass unit. Quoted errors for Sr and Nd isotopic ratios are in-run statistics, and are representative of true precision as demonstrated by replicate analyses of various samples.

1.5 Results

1.5.1 Major and Trace Element Variation

The representative major and trace element analyses for the Ararat lavas are presented in Table 1.1. The major element compositions have been normalized to 100% volatile-free, with all Fe expressed as FeO (designated FeO T). The Ararat samples cover a wide composition range from basalt to rhyolite. Major element compositions range from 51-77% for SiO2, 14-19% for Al2O3, 1-9% for FeO, 0.2-6.5% for MgO, 0.8-8.5% for CaO, 3.8-5% for Na2O, 0.4-3.2% for K2O, 0.1-1.8% for TiO2, and 0.03-0.37% for P2O5. However, the variations of the major element compositions are not continuous within these ranges. In Figure-1.3, K2O is plotted versus SiO2. In the classification scheme of Peccerillo and Taylor (1976), the Ararat lava flows range from basalt to rhyolite, but andesites and dacites are by far the most abundant. As far as the K contents are concerned, all the analysed samples plot within the Medium-K field. The Ararat samples not only define linear trends but also form different groups in the major element variation diagrams (Figures-1.4,5) supporting the grouping based on the field observations. The Ararat lavas show an enrichment in incompatible elements (elements such as K, Ti, P, that are largely excluded from major fractionating phases such as cpx, opx, plag) from older to younger series. The Little Ararat lavas are depleted in incompatible elements in comparison with the other series, for a given SiO2 content. Being consistent with this, they have higher MgO and CaO contents. However they exhibit less Fe enrichment in comparison with the other series. Instead of having a moderate Fe enrichment trend which is typical for calcalkaline rocks, they define a linear trend on the AFM diagram (Figure-1.6) ending up with lower iron contents compared to the other series.

TABLE 1-1

	HIGH ALUMINA BASALTS						LITTLE ARARAT SERIES						
	A-30-1	A-30-5	A-30-10	A-30-12	A-13	A-36-A	A-43	A-48	A-51	A-47	A-46	A-12	A-54
SiO2	51.84	52.11	51.20	51.35	52.72	52.32	55.36	57.15	62.07	62.67	63.86	68.32	76.90
Al2O3	18.30	18.33	17.79	17.59	18.65	18.59	16.67	16.47	16.01	16.73	16.76	15.91	13.86
FeO(T)	8.89	9.06	9.07	9.08	8.81	8.70	7.20	6.48	4.92	4.36	4.45	2.69	1.11
MgO	5.06	5.20	6.22	6.54	4.87	4.85	6.04	4.95	3.41	2.77	2.55	1.47	0.16
CaO	7.99	7.97	8.32	8.47	7.84	7.84	7.95	7.30	6.06	5.64	5.82	4.59	0.81
Na2O	4.60	4.95	4.32	4.30	4.40	4.65	3.83	4.11	4.19	4.59	4.40	4.48	4.51
K2O	0.37	0.58	0.75	0.82	0.57	0.55	1.10	1.29	1.45	1.10	1.11	1.61	3.20
TiO2	1.78	1.79	1.74	1.73	1.78	1.77	1.18	1.04	0.75	0.76	0.75	0.37	0.11
MnO	0.14	0.14	0.15	0.15	0.15	0.15	0.12	0.11	0.09	0.07	0.08	0.05	0.06
P2O5	0.28	0.28	0.35	0.38	0.29	0.30	0.27	0.30	0.22	0.18	0.17	0.11	0.03
TOTAL	99.25	100.41	99.91	100.41	100.08	99.72	99.72	100.20	99.18	98.87	99.95	99.60	100.75
Mg#	50.4	50.6	55.0	56.2	49.6	49.8	59.9	57.7	55.3	53.1	50.5	49.3	20.4
Sr	424	459	536	566	434	431	382	415	384	360	372	347	100
Rb	9	10	11	13	8	10	26	36	39	31	34	50	87
Ba	93	105	147	160	154	161	335	488	525	437	508	620	934
Zr	184	193	190	188	182	181	150	157	152	133	134	125	109
Hf	4.09	-	-	4.00	4.16	?	-	3.61	3.54	-	-	2.50	-,
Nb	6	7	10	11	7	6	11	12	13	9	9	9	12
Y	29	29	30	28	30	29	24	24	17	16	17	12	28
Ni	46	46	78	94	42	43	76	77	56	26	26	21	4
Cr	23	28	91	123	19	18	158	132	87	20	24	25	-
Sc	22.8	-	-	23.5	21.7	23.6	-	19.9	14.7	-	-	5.7	-
V	171	164	160	165	153	156	155	136	92	77	82	51	7
Cu	32	36	42	49	28	11	49	51	36	30	32	10	-
Zn	69	69	64	70	64	35	59	60	52	36	35	29	35
K/Rb	341	481	566	619	591	457	351	297	309	295	271	267	305
K/Ba	33	46	42	43	31	28	27	22	23	21	18	22	28
K/Sr	7	10	12	12	11	11	24	26	31	25	25	39	266
Ba/Rb	10.33	10.50	13.36	12.31	19.25	16.10	12.89	13.56	13.46	14.10	14.94	12.40	10.74
Zr/TiO2	103	108	109	109	102	102	127	151	203	175	179	338	991
Zr/Hf	45.0	-	-	47.0	43.8	- -	-	43.5	42.9	-	-	49.4	-
Zr/Nb	30.67	27.57	19.00	17.09	26.00	30.17	13.64	13.08	11.69	14.78	14.89	13.89	9.08
Zr/Y	6.34	6.66	6.33	6.71	6.07	6.24	6.25	6.54	8.94	8.31	7.88	10.42	3.89
Zr/Ni	4.00	4.20	2.44	2.00	4.33	4.21	1.90	2.04	2.71	5.12	5.15	5.95	27.25
Zr/V	1.08	1.18	1.19	1.14	1.19	1.16	0.97	1.15	1.65	1.73	1.63	2.45	15.57

TABLE 1-1 (cont'd)

TABLE 1-1 (cont'd)

	ARARAT SERIES													
	A-1	A-4	A-5	A-6	A-8-B	A-9	A-10	A-17	A-19	A-32	A-42-H	A-42-I	A-42-J	A-42-K
SiO2	64.17	63.18	59.65	64.87	63.83	59.16	62.67	62.07	63.20	58.71	61.79	62.46	61.48	62.64
Al2O3	16.39	16.45	16.85	16.25	16.41	16.53	16.77	16.87	16.47	17.44	17.35	17.07	17.05	16.87
FeO(T)	4.90	5.24	6.30	4.64	4.89	6.04	5.19	4.98	5.06	7.02	5.16	5.25	5.30	5.19
MgO	1.64	1.87	2.72	1.43	1.60	4.13	2.14	2.20	2.18	2.71	2.39	2.18	2.28	2.20
CaO	4.54	4.86	6.03	4.47	4.53	6.57	5.21	5.29	4.99	6.08	5.31	5.17	5.34	5.23
Na2O	4.62	4.47	4.48	4.65	4.74	4.37	4.57	4.52	4.07	4.42	4.50	4.32	5.09	4.41
K2O	2.12	2.05	1.79	2.16	2.06	1.89	2.14	2.34	2.46	1.62	2.12	2.10	2.15	2.11
TiO2	0.94	1.00	1.17	0.88	0.95	1.01	0.96	0.96	0.93	1.30	0.92	0.96	0.96	0.94
MnO	0.09	0.09	0.11	0.08	0.09	0.11	0.10	0.09	0.10	0.12	0.09	0.09	0.09	0.09
P2O5	0.24	0.29	0.37	0.25	0.28	0.38	0.27	0.25	0.27	0.36	0.24	0.27	0.28	0.31
TOTAL	99.65	99.50	99.47	99.68	99.38	100.19	100.02	99.57	99.73	100.08	99.87	99.87	100.02	99.99
Mg#	37.4	38.9	43.5	35.5	36.8	34.9	42.4	44.1	43.4	40.8	45.2	42.5	43.4	43.0
Sr	344	377	460	330	352	525	399	393	366	409	420	418	420	417
Rb	62	59	44	65	62	47	58	56	58	35	54	57	56	55
Ba	583	568	457	606	590	550	569	585	590	447	569	636	594	594
Zr	245	240	217	250	244	191	218	223	219	188	219	213	214	213
Hf	-	5.50	4.94	-	-	4.73	-	-	-	4.54	-	-	5.42	-
Nb	10	10	12	10	11	14	13	15	13	14	13	13	14	13
Y	31	29	26	29	30	24	26	27	26	27	26	26	26	26
Ni	11	10	17	9	10	71	15	14	14	21	15	15	14	14
Cr	2	4	19	-	-	94	5	8	5	14	12	5	5	4
Sc	-	11.2	14.4	-	-	17.9	-	-	-	14.7	-	-	12.6	-
V	66	73	98	63	64	118	89	77	80	133	88	89	91	94
Cu	13	10	29	8	10	39	16	22	14	30	26	24	15	14
Zn	45	44	58	42	44	57	52	50	48	73	54	51	53	53
K/Rb	284	288	338	276	276	334	306	347	352	384	326	306	319	318
K/Ba	30	30	33	30	29	29	31	33	35	30	31	27	30	29
K/Sr	51	45	32	54	49	30	45	49	56	33	42	42	42	42
Ba/Rb	9.40	9.63	10.39	9.32	9.52	11.70	9.81	10.45	10.17	12.77	10.54	11.16	10.61	10.80
Zr/TiO2	261	240	186	284	257	189	227	232	236	145	238	222	223	227
Zr/Hf	-	43.6	43.9	-	-	40.4	-	-	-	41.4	-	-	39.5	-
Zr/Nb	24.50	24.00	18.08	25.00	22.18	13.64	16.77	14.87	16.85	13.43	16.85	16.39	15.29	16.39
Zr/Y	7.90	8.28	8.35	8.62	8.13	7.96	8.38	8.26	8.42	6.96	8.42	8.19	8.23	8.19
Zr/Ni	22.27	24.00	12.76	27.78	24.40	2.69	14.53	15.93	15.64	8.95	14.60	14.20	15.29	15.21
Zr/V	3.71	3.29	2.21	3.97	3.81	1.62	2.45	2.90	2.74	1.41	2.49	2.39	2.35	2.27

TABLE 1-1 (cont'd)

TABLE 1-1 (cont'd)

	OLD ARARAT SERIES																
	A-14	A-23A	A-23C	A-24	A-25	A-26	A-28B	A-33	A-34B	A-42A	A-42B	A-42C	A-42D	A-42E	A-42F	A-42G	A-45
SiO2	64.76	63.70	63.85	63.94	63.65	63.18	65.87	64.86	65.34	69.39	68.63	61.25	69.01	66.80	68.07	68.55	65.54
Al203	16.17	16.96	17.15	17.15	17.23	17.22	16.79	17.18	17.00	15.51	15.55	17.65	15.65	16.22	15.55	15.56	16.18
FeO(T)	4.38	5.04	5.68	5.00	5.20	5.22	4.27	4.48	4.45	3.37	3.42	5.31	3.38	3.40	3.42	3.33	4.25
MgO	1.98	1.49	1.49	1.43	1.53	1.59	1.12	1.24	1.22	1.08	1.13	2.21	1.08	1.64	1.37	1.31	1.91
CaO	4.64	4.73	4.69	4.64	4.77	4.88	4.11	4.19	4.26	3.41	3.49	5.74	3.33	4.38	3.76	3.72	4.69
Na20	4.64	4.55	4.46	4.80	4.44	4.57	4.48	4.75	4.46	4.32	4.64	4.78	4.70	4.19	4.26	4.37	4.57
K20	2.07	1.83	1.83	1.83	1.81	1.88	2.18	1.97	2.15	2.34	2.30	1.80	2.33	2.18	2.30	2.35	1.94
TiO2	0.78	0.82	0.83	0.82	0.86	0.87	0.63	0.71	0.66	0.64	0.63	0.95	0.62	0.58	0.58	0.56	0.71
MnO	0.08	0.10	0.10	0.10	0.11	0.10	0.10	0.10	0.10	0.07	0.08	0.09	0.07	0.07	0.07	0.07	0.08
P205	0.20	0.34	0.32	0.34	0.35	0.33	0.35	0.32	0.37	0.17	0.18	0.21	0.17	0.12	0.15	0.14	0.22
TOTAL	99.70	99.56	100.40	100.05	99.95	99.84	99.90	99.80	100.01	100.30	100.05	99.99	100.34	99.58	99.53	99.96	100.09
Mg#	44.6	34.5	31.9	33.8	34.4	35.2	31.9	33.0	33.2	36.4	37.1	42.6	36.3	46.2	41.7	41.2	44.5
Sr	319	383	383	385	382	381	420	363	418	262	262	378	268	260	275	273	338
Rb	56	43	42	44	42	42	52	46	50	61	60	46	61	57	65	67	52
Ba	573	535	533	546	526	546	668	573	667	659	644	515	679	603	634	692	583
Zr	194	188	189	188	186	186	210	199	206	194	195	182	191	185	186	187	187
Hf	-	4.39	-	-	-	-	-	-	-	-	4.45	-	-	-	-	4.58	
Nb	11	15	13	14	15	15	18	14	17	13	13	13	14	11	11	10	11.
Y	24	22	23	24	22	23	22	22	22	23	24	22	22	23	22	22	21
Ni	13	6	5	5	5	6	4	4	4	10	8	15	8	12	10	11	18
Cr	5	-	-	-	-	-	-	-	-	2	1	4	-	-	5	-	17
Sc	-	7.3	-	-	-	-	-	-	-	-	-	12.2	-	-	-	-	10.4
V	68	59	64	60	68	61	42	47	46	32	36	95	39	57	50	46	65
Cu	7	13	15	15	16	18	12	10	10	14	10	39	11	16	7	11	10
Zn	37	58	59	57	59	61	60	58	57	37	40	51	35	39	33	31	40
K/Rb	307	353	362	345	358	372	348	356	357	318	318	325	317	317	294	291	310
K/Ba	30	28	29	28	29	29	27	29	27	29	30	29	28	30	30	28	28
K/Sr	54	40	40	39	39	41	43	45	43	74	73	40	72	70	69	71	48
Ba/Rb	10.23	12.44	12.69	12.41	12.52	13.00	12.85	12.46	13.34	10.80	10.73	11.20	11.13	10.58	9.75	10.33	11.21
Zr/TiO2	249	229	228	229	216	214	333	280	312	303	310	192	308	319	321	334	264
Zr/Hf	-	42.8	-	-	-	-	-	-	-	-	-	40.9	-	-	-	-	40.8
Zr/Nb	17.64	12.53	14.54	13.43	12.40	12.40	11.67	14.21	12.12	14.92	15.00	14.00	13.64	16.82	16.91	18.70	17.00
Zr/Y	8.08	8.55	8.22	7.83	8.45	8.09	9.55	9.05	9.36	8.43	8.13	8.27	8.68	8.04	8.45	8.50	8.90
Zr/Ni	14.92	31.33	37.80	37.60	37.20	31.00	52.50	49.85	51.50	19.40	24.38	12.13	23.88	15.42	18.60	17.00	10.39
Zr/V	2.85	3.19	2.95	3.13	2.74	3.05	5.00	4.23	4.48	6.06	5.42	1.92	4.90	3.25	3.72	4.07	2.88

Figure-1.3

Plot of K_2O versus SiO_2 for the Ararat lavas. All the Ararat lavas have medium-K contents and andesitic-dacitic compositions dominate over basaltic and rhyolitic compositions. Note the systematic increase in K_2O, for a given SiO_2 content from the Little Ararat, through the Old Ararat to the Ararat series. Classification boundaries are from Peccerillo and Taylor (1976).

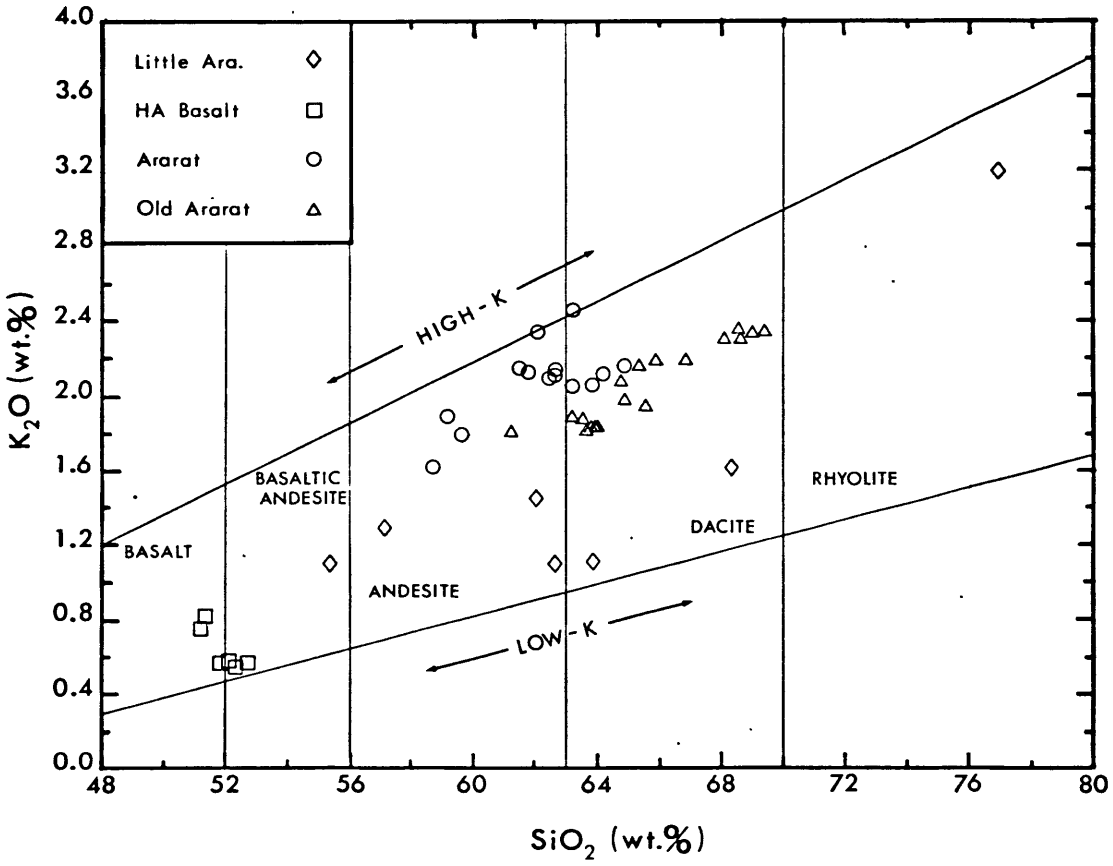
Little Ara.
HA Basalt
Ararat
Old Ararat
HIGH-K
LOW-K
BASALT
BASALTIC ANDESITE
ANDESITE
DACITE
RHYOLITE
K_2O (wt.%)
SiO_2 (wt.%)
4.0
3.6
3.2
2.8
2.4
2.0
1.6
1.2
0.8
0.4
0.0
48
52
56
60
64
68
72
76
80

Figure-1.4 and 1.5

Diagrams showing the variation of MgO, FeO(T), CaO, and TiO2 with SiO2 contents. All the series define distinct fields and linear trends on these major element variation diagrams. Note again the systematic differences in the major element contents for a given SiO2 content among the different suites.

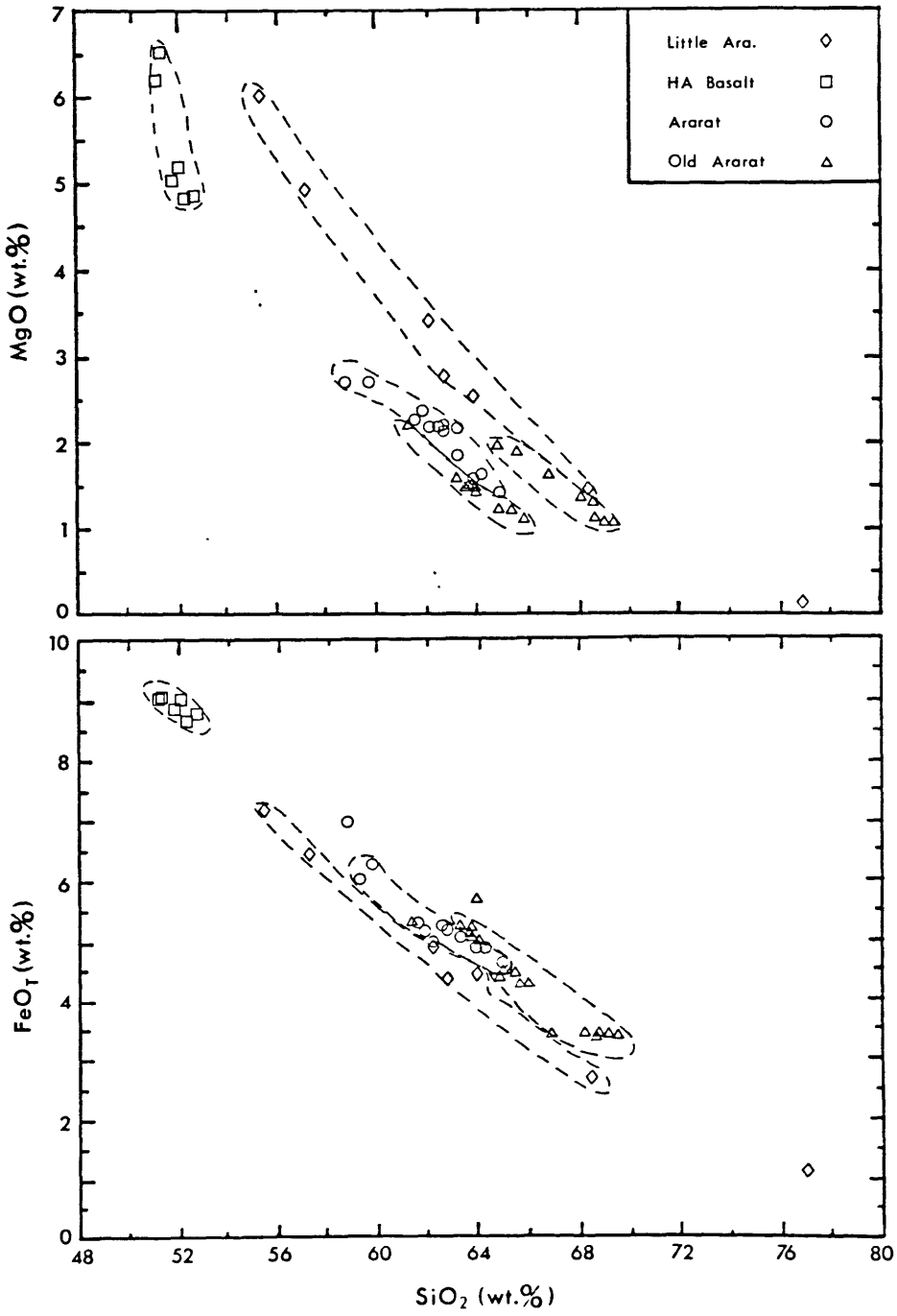
Little Ara.
HA Basalt
Ararat
Old Ararat
MgO (wt.%)
FeO$_T$ (wt.%)
SiO$_2$ (wt.%)
0
1
2
3
4
5
6
7
8
10
48
52
56
60
64
68
72
76
80

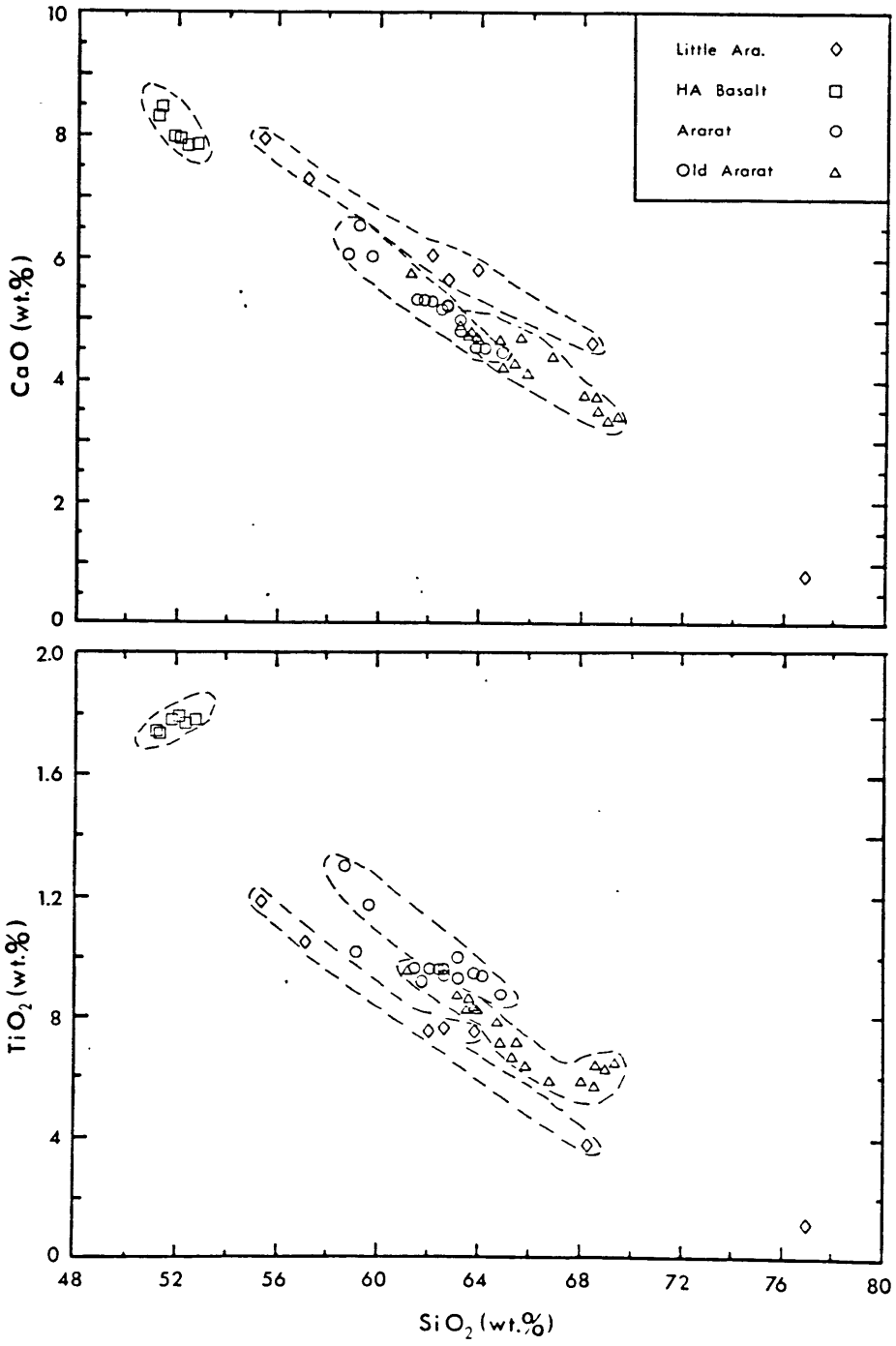
Little Ara.
HA Basalt
Ararat
Old Ararat
CaO (wt.%)
TiO2 (wt.%)
SiO2 (wt.%)
0
2
4
6
8
10
0
4
8
1.2
1.6
2.0
48
52
56
60
64
68
72
76
80

Figure-1.6

AFM diagram of the Ararat lavas. All the Ararat samples define a calc-alkaline trend. Different Ararat series not only form roughly linear trends but also form distinct fields as a result of systematic differences in their major element compositions.

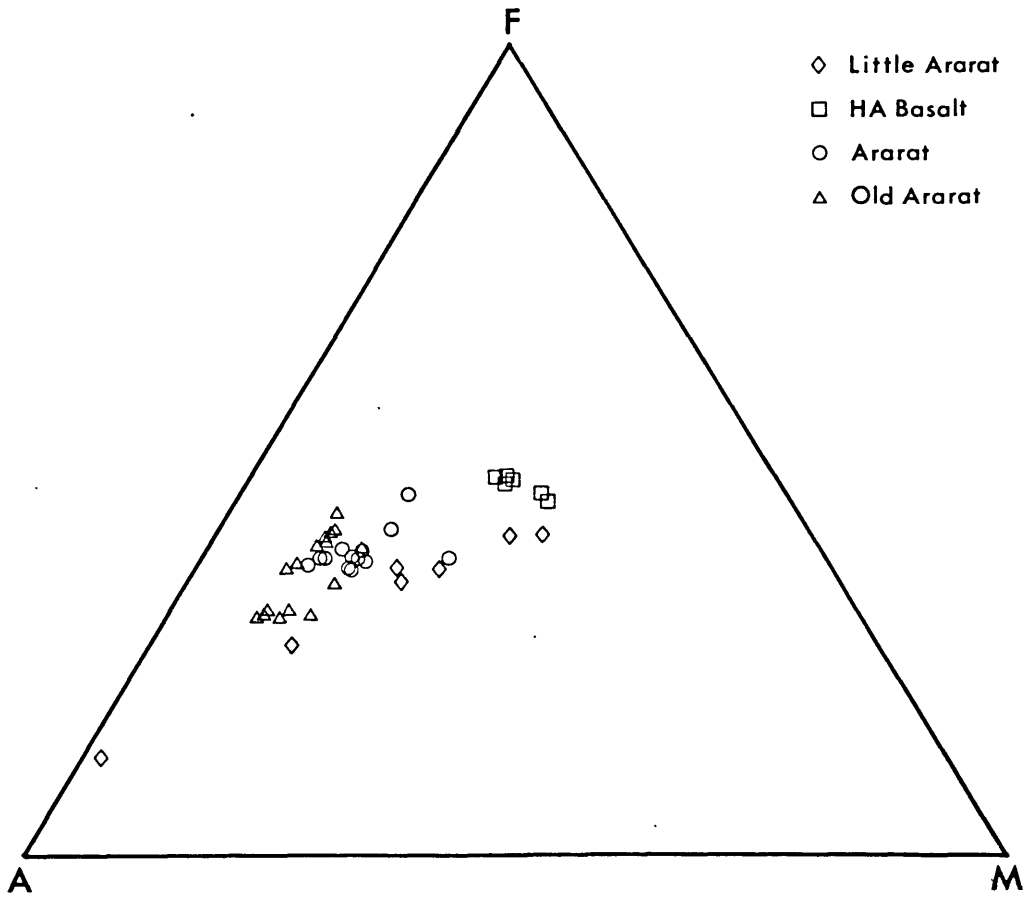
F
A
M
Little Ararat
HA Basalt
Ararat
Old Ararat

In the text, "High Alumina Basalt" term will be used to designate all rocks with $\leq$53% SiO2. High-Alumina basalts typically have high Al2O3 ($>$ 17%), moderate K2O (0.4-1.3%) and generally low TiO2 (~ 1.5%) contents (Escobar et al., 1977). The Ararat High alumina basalt major element compositions range from 51.2-52.3% for SiO2, 17.6 to 18.7% for Al2O3, 0.37-0.82% for K2O and 1.7 to 1.8% for TiO2. Their TiO2 contents are slightly high relative to the criteria defined in Escobar et al. (1977).

Molecular norms (Barth-Niggli Katanorm) have been calculated for all compositions after assigning %Fe2O3 = %TiO2 + 1.5, following Irvine and Baragar (1971). All the high alumina basalts are olivine and hyperstene normative. All the andesites, dacites and rhyolites are quartz and hyperstene normative.

The major element data indicate that the Ararat lavas represent a typical orogenic calcalkaline series according to the criteria established by Irvine and Baragar (1971), Jakes and White (1972), Miyashiro (1974) and Gill (1981).

Concentrations of trace elements and some trace element ratios are listed in Table 1-1. The Ararat lavas exhibit large variations in both absolute concentrations of incompatible trace elements and also in their ratios. Similar to the variation of K2O with SiO2, Rb and Ba contents positively correlate with SiO2 for all the series except the HA Basalts(Figure-1.7). High Alumina basalt K2O, Rb and to a lesser extend Ba contents correlate negatively with SiO2. They form separate linear trends for each series in these element versus element plots.

Figure-1.8 shows K/Rb plotted against K2O. The HA Basalts exhibit a very large range in K/Rb ratios (340 to 620) and form a well defined linear trend with a positive slope. The rest of the Ararat samples have a relatively limited range in K/Rb ratios (300-400)

Figure-1.7

Plots showing the variation of Rb and Ba abundances with SiO2 for the Ararat lavas. The distinct fields formed by each of the Ararat series and their linear trends are also apparent on these diagrams. Two samples from the Little Ararat series have higher Rb and Ba contents with respect to the trend defined by the other Little Ararat samples, possibly indicating crustal contamination.

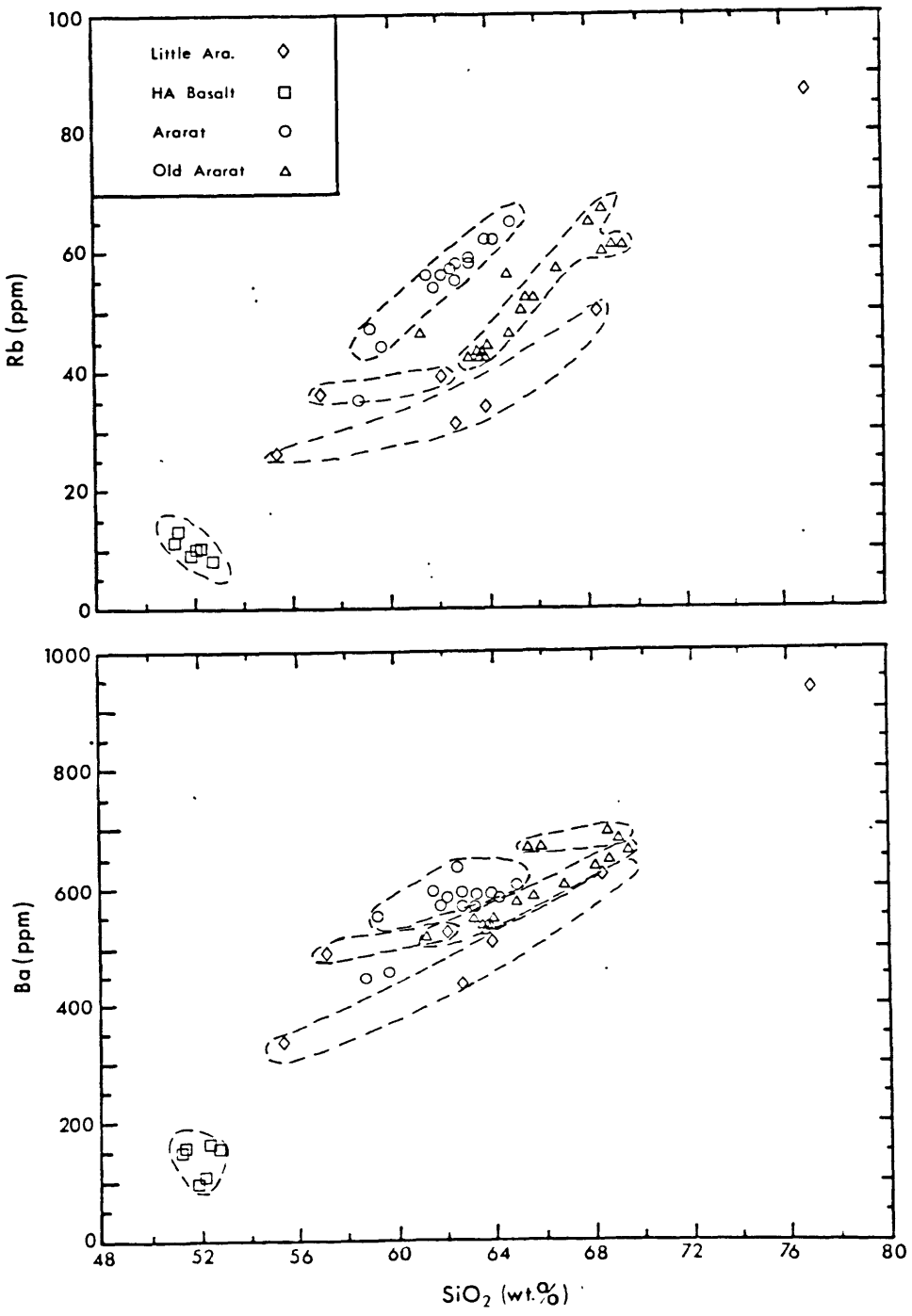
Little Ara.
HA Basalt
Ararat
Old Ararat
Rb (ppm)
Ba (ppm)
SiO2 (wt.%)
0
20
40
60
80
100
200
400
600
800
1000
48
52
56
60
64
68
72
76
80

Figure-1.8

Plot of K/Rb versus K2O for the Ararat lavas. Shaw's Main Trend (Shaw, 1968) is also shown. Although different Ararat series form different fields on this plot, there is an overlap between the fields of the Ararat and the Old Ararat series. HA basalts form an impressive linear trend with a positive slope. The K/Rb ratios of the HA basalts increase systematically from older to younger flows. The age progression is indicated by an arrow. The other series also exhibit a similar though more scattered variation, in comparison with the HA basalts, possibly due to fractionation effects.

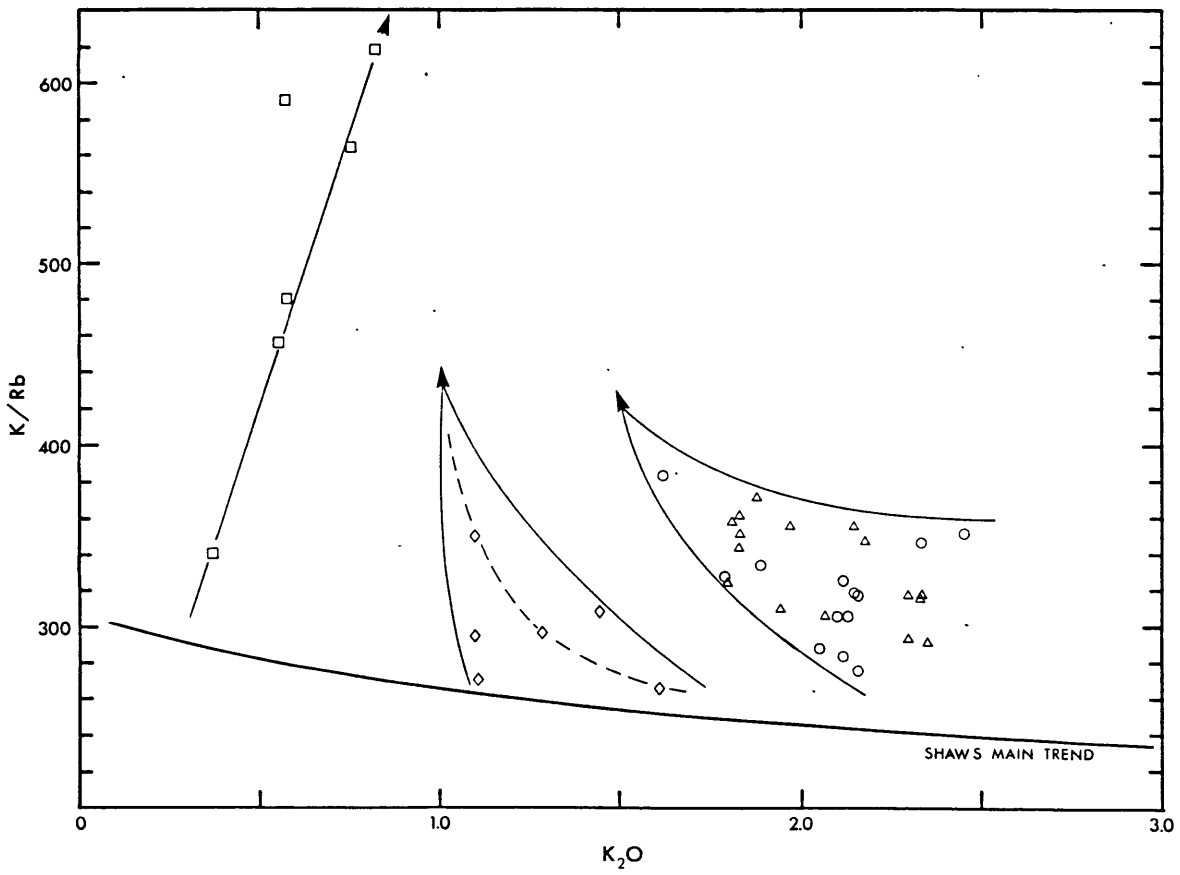
600
500
400
300
K/Rb
0
1.0
2.0
3.0
K_2O
SHAW'S MAIN TREND

and define two distinct fields due to the differences in K2O contents. As indicated by the arrows in Figure-1.8, the younger samples appear to have higher K/Rb ratios. In general, K/Rb ratios are correlated negatively with K2O contents for calc-alkaline rocks and this has been attributed to differentiation (Shaw, 1968). Although the K/Rb range observed for the Ararat lavas are within the range reported for orogenic calc-alkaline rocks (Jakes & White, 1970; Gill, 1981), they differ in two aspects. First, the K/Rb ratios become progressively higher for the younger lava flows, which is opposite in sense to a fractionation progession. Secondly, the HA basalts define a convincing positive trend with a very high slope. Similar atypical positive correlation between K/Rb ratios and K content has also been reported for submarine basalts from the Puerto Rico trench (Hart & Nalwalk, 1969). They suggested that sea water alteration might produce the observed positive trend. However this is not directly applicable to the Ararat case, because the subaerial lava flows of Ararat have never seen sea water (perhaps with the exception during Noah's journey!). In addition, the HA basalt sample with the lowest K/Rb ratio (A-30-1) is also the least radiogenic in Sr87/86 ratio. Contamination by a crustal material of low K/Rb can potentially decrease the K/Rb ratio of the original magma but with an increase in K2O content which in turn produces a negative correlation between K/Rb and K2O, and higher Sr87/86 ratios; this is not consistent with the Ararat HA basalt. In summary, the atypical positive correlation between K/Rb and K2O contents and increase in K/Rb ratio with age progression suggests two component magma mixing (one end member with low K/Rb and low K2O, the other with high K/Rb and high K2O) for the Ararat HA basalts. As far as the K/Ba and K/Sr ratios are concerned, the ranges observed for the Ararat lavas (21-46 and 6-70 respectively) are within the range of the calc-alkaline rocks (Gill, 1981; Morris & Hart, 1983).

Zr is plotted versus SiO2 in Figure-1.9a. The four series form different groupings, again showing linear trends. The interesting aspect of this plot is the presence of a very

Figure-1.9.a,b

Diagrams illustrating the variation of Zr with SiO2 and V abundances for the Ararat lavas. Plots involving Zr abundances are found to be very useful in distinguishing the various Ararat series. Note the large range observed for the Zr abundances (130-250 ppm.) for a given SiO2 content (64%). (see the text for further explanation).

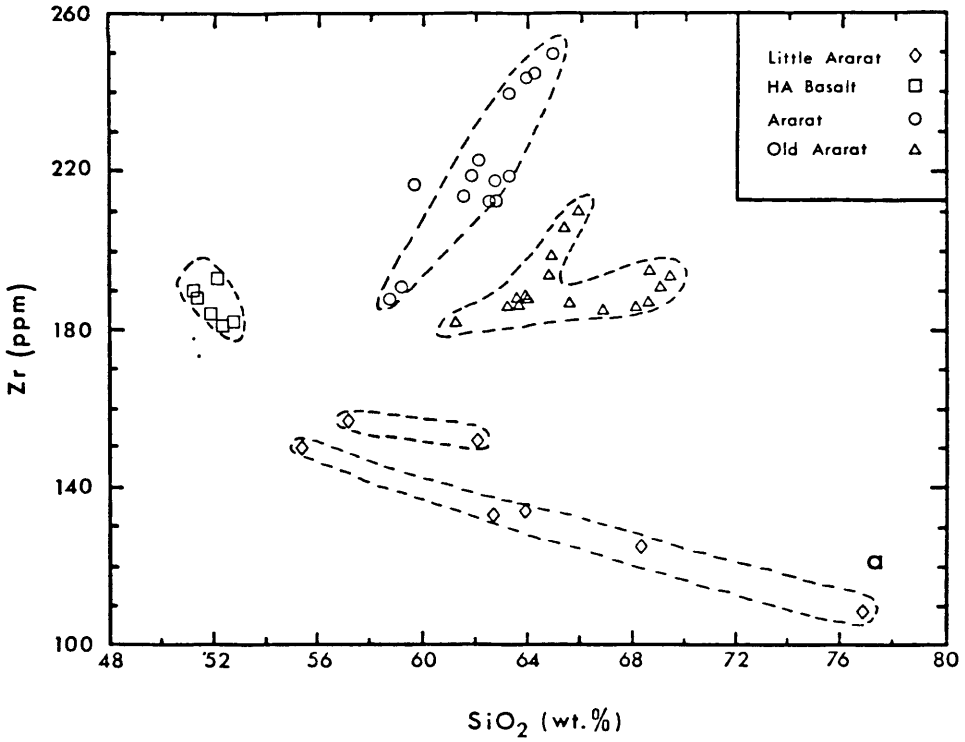
Little Ararat
HA Basalt
Ararat
Old Ararat
Zr (ppm)
260
220
180
140
100
48
52
56
60
64
68
72
76
80
SiO2 (wt.%)
a

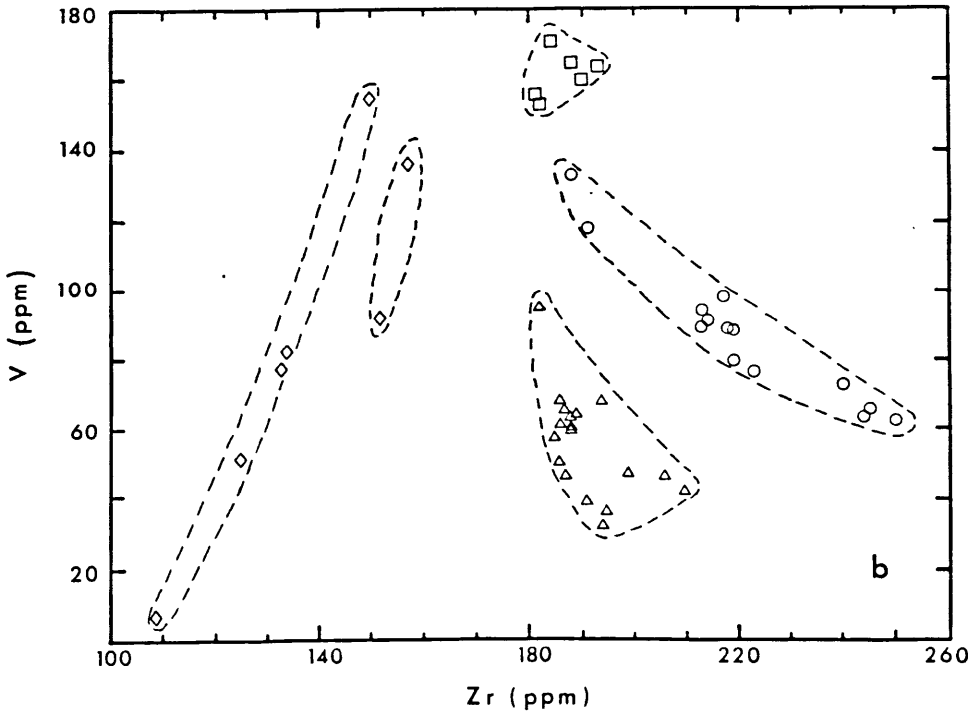
V (ppm)
180
140
100
60
20
100
140
180
220
260
Zr (ppm)
b

wide range in Zr content among the different series, for given SiO2. For example, Zr ranges from about 130 ppm. to 250 ppm. for samples containing about 64% SiO2. In light of this variation, the possibility that the different series are related to each other by fractional crystallization is inconceivable. Since Zr is an incompatible element for a reasonable fractionating phase assemblage (e.g. olivine-cpx-opx-plag-magnetite), the negative covariation of Zr with SiO2 for the HA Basalt and Little Ararat series would require either magma mixing or zircon fractionation, or a combination of the two. Despite the apparent zircon fractionation for A-54(rhyolite which contains zircon), mixing seems to be more likely as the dominant process because, in general, the onset of a new crystallizing phase causes a significant slope change in element versus element plots which involves one of the compatible elements for the newly fractionating phase. Also, simple fractionation does not produce any change in the isotope ratios. As will be discussed later, the Zr abundances are correlated with isotope ratios. Moreover, the volcanostratigraphy of the Ararat lavas also argues against simple fractional crystallization. The HA Basalt samples whose numbers start with A-30 were collected from successive lava flows, A-30-1 from the bottom of the volcanostratigraphic section (oldest) and A-30-12 from the top of the lava pile (youngest). The fact that the concentrations of Zr, Nb, Ni, Cr, Ba, Rb, Sr, K show a gradual increase from bottom to top (from oldest to youngest lava flows) rules out fractional crystallization as a viable process and suggests magma mixing as the cause of the observed variations.

Starting with the pioneering work of Gast (1968) and following the studies involving systematic treatment of trace element data (Allegre et al., 1977; Allegre and Minster, 1978; Langmuir et al., 1978; DePaolo, 1981), it has been well established that trace element data, especially the ratios of incompatible elements and incompatible versus compatible element variations can be effectively utilized to infer the source characteristics and

Figure-1.10.a,b

Plots of TiO2 versus Zr and Zr/TiO2 versus Zr for the Ararat lavas. As expected from two-component magma mixing, the Ararat lavas form linear trends on the element versus element diagrams and either linear or hyperbolic mixing trends (depending on the value of r, Langmuir et al., 1979) on the diagrams involving element ratios versus elements. All these mixing trends converge towards a common point.

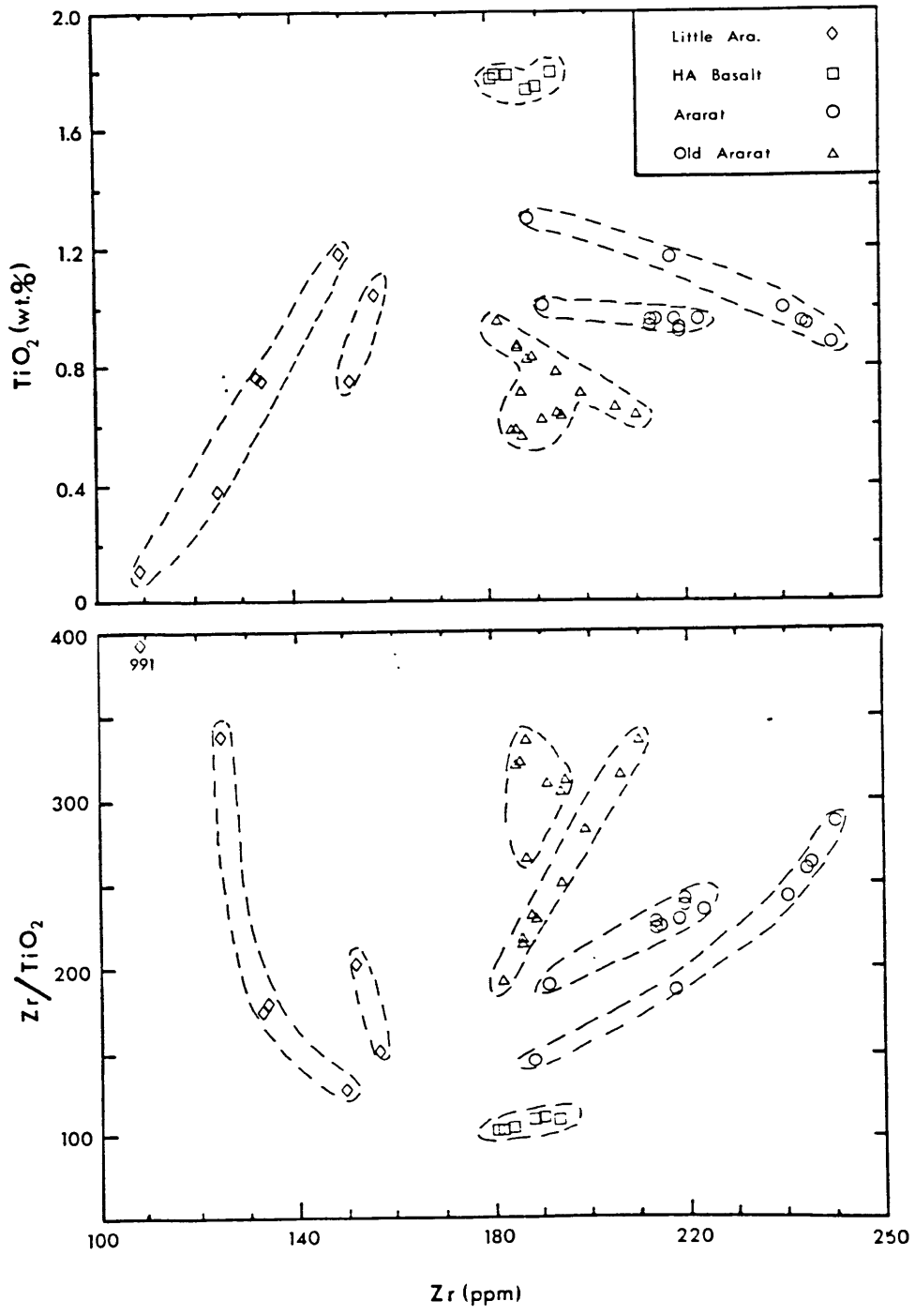
Little Ara.
HA Basalt
Ararat
Old Ararat
TiO_2 (wt.%)
2.0
1.6
1.2
0.8
0.4
0
991
400
300
200
100
Zr/TiO_2
100
140
180
220
250
Zr (ppm)

to identify magmatic processes such as partial melting, fractional crystallization, fractional crystallization accompanied by assimilation, magma mixing, source mixing etc.

Incompatible versus compatible element variations have proved to be very useful in defining the different Ararat series (e.g. V vs Zr, Ti vs Zr, Ni vs Zr). The V vs Zr and Ti vs Zr variations are illustrated in Figures-1.9b and 1.10a. In these figures, the different Ararat series not only form well-separated fields with different trends, but also appear to converge towards higher V, Ti and intermediate Zr values. Based on the volcanostratigraphic relationship of the lavas, the samples become progressively younger, along the trends defined for each suite, toward the higher V and Ti values. This variation is also just the opposite of that expected from simple differentiation. The viability of magma mixing can be further tested utilizing element ratio versus element and their companion plots (element ratio vs reciprocal of the denominator; Langmuir et al, 1978). If two-component mixing is the case, element ratio vs element plots, in general (if r not equal to 1), will produce hyperbolic trajectories and their companion plots will produce linear trends connecting the two end-members. Fractionation will produce curved trends on the companion plots. In Figure-1.11 two companion plots are shown; Zr/Ni vs 100/Ni and Zr/V vs 100/V. All of the Ararat series are clearly separated from each other and converge towards a common point. The well-defined linear trends for each of the Ararat series indicate that mixing is the dominant process.

In general, high field strength (charge/ionic radius) elements (Ti, Zr, Hf, Nb, Ta) are depleted in orogenic calc-alkaline rocks in comparison with MORB or OIB. This depleted character has been used to distinquish arc-derived rocks from others (Pearce and Cann, 1973; Wood et al, 1979). In order to compare the geochemical characteristics of MORB and Ararat lavas, the MORB normalized elemental abundances of the two Ararat HA basalt samples are plotted in Figure-1.12. The order of the elements are arranged, fol-

Figure-1.11.a,b

Plots of Zr/Ni versus 100/Ni and Zr/V versus 100/V for the Ararat lavas. Distinct linear trends are formed by each series on these companion plots, converging towards the lower left corner of the diagrams (high Ni, V and low Zr/Ni, Zr/V values), confirming different two-component magma mixing processes for each of the series.

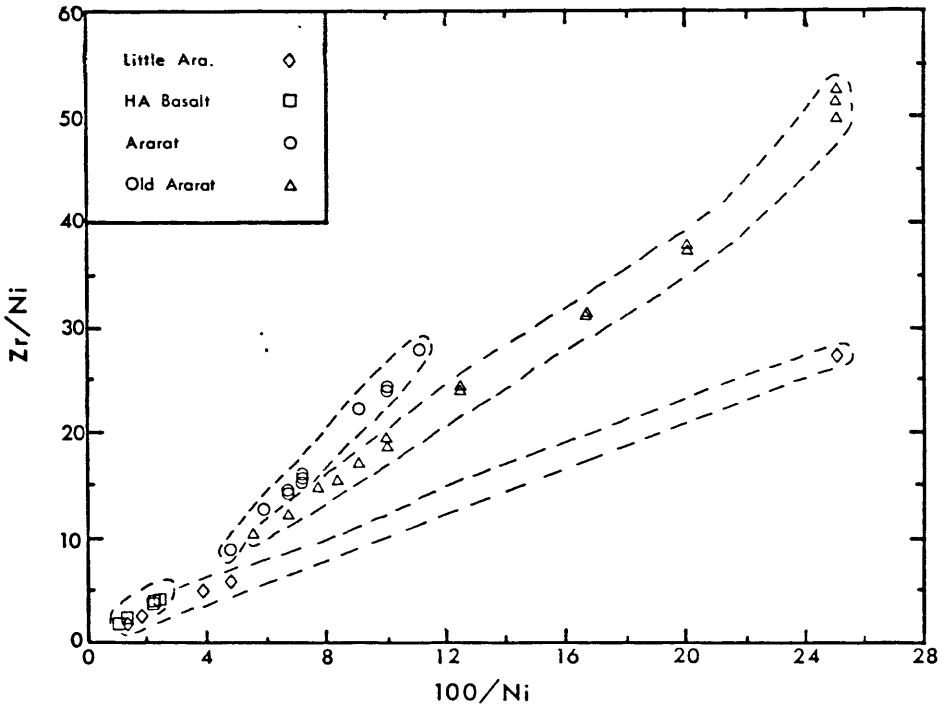
Little Ara.
HA Basalt
Ararat
Old Ararat
Zr/Ni
100/Ni
0
10
20
30
40
50
60
0
4
8
12
16
20
24
28

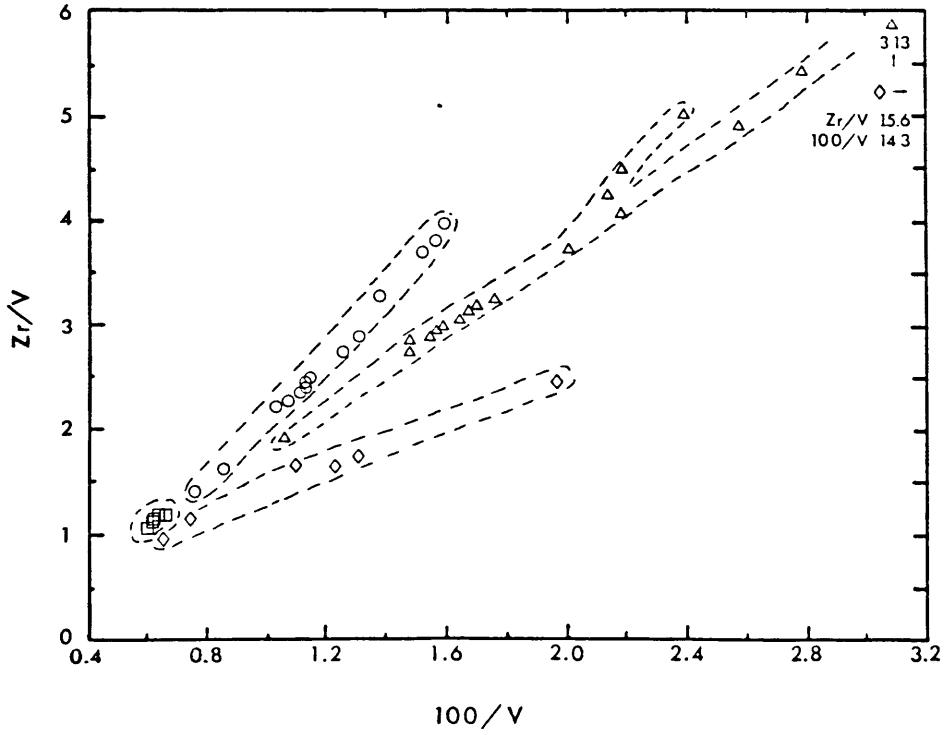
Zr/V 15.6
100/V 14 3
Zr/V
100/V
0
1
2
3
4
5
6
0.4
0.8
1.2
1.6
2.0
2.4
2.8
3.2

lowing Pearce(1983), on the basis of their ionic potential and of their bulk distribution coefficients between garnet lherzolite and melt. Also included in this figure are the normalized patterns of: one Hawaiian tholeiite, one New Hebrides calc-alkaline basalt (IAB), one Australian anorogenic basalt and average calc-alkaline basalt from Western U.S. Inspection of Figure-1.12 clearly shows the depleted nature of the IAB in high field strength elements with respect to MORB and OIB. The comparison of the patterns reveals that the one HA basalt from Ararat (A-30-1) closely mimics the pattern of the Hawaiian tholeiite, but with two exceptions. Nb is depleted and Th is enriched in A-30-1 with respect to the Hawaiian tholeiite pattern. Interestingly, the depletion in Nb in sample A-30-1 is not accompanied (even when allowance made for analytical uncertainty) by depletions in Hf, Zr and especially in Ti abundances. It is possible to attribute part of the depletion in Nb to oxide fractionation (e.g. titanomagnetite, rutile), since D-Nb Titanomagnetite/Melt ~ 13 (Ewart,1982) and D-Nb Rutile/Melt~16 (McCallum & Charette, 1978). However, fractionation of these phases will also create depletion of Ti. Unless there is a phase which is capable of fractionating Nb and Ti (without affecting Ti), then the observed Nb depletion of A-30-1 may reflect the depleted nature of the source in Nb or the presence of a residual phase which can retain Nb (but not Ti) during partial melting. Alternatively, an already depleted source region enriched with either a partial melt or a metasomatic fluid which carries along with it the depleted Nb signature (e.g. Nb retaining phase in the ultimate source of the enriching fluid; in the lower mantle or in a subducted slab), can produce the MORB normalized pattern of A-30-1 upon partial melting. Unfortunately, existing knowledge of the partitioning behavior of Nb is too meagre to further elaborate and explain this apparent decoupling of Ti and Nb. The comparison of the normalized patterns for basalts representing different tectonic settings also suggests that the degree of HFSE depletions decrease, with the exception of Nb depletion, from oceanic arc basalts to continental arc basalts. No depletion in Nb is observed for anorogenic basalts outside of the analytical precision limits. The patterns

Figure-1.12

MORB normalized trace element patterns for the two Ararat HA basalts. Also included for comparison are basalt patterns representing different tectonic environments. The MORB normalization values, and the order of the elements are adopted from Pearce, (1983). Data sources for the basalts include Pearce (1983) and Ewart (1982).

Figure-1.13

MORB-normalized patterns of three andesites. Two of them (A-5, A-9) are from the Ararat series and the third (A-48) is from the Little Ararat series.

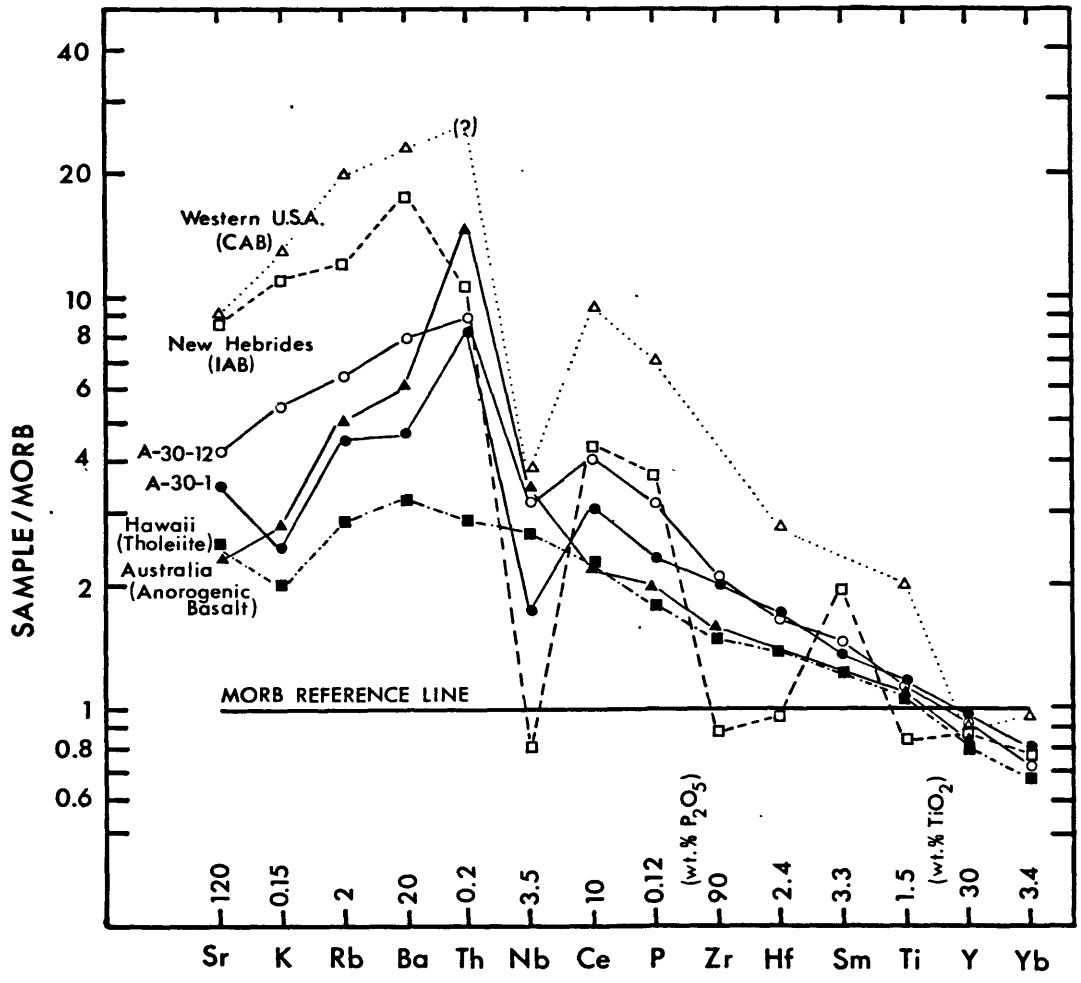
SAMPLE/MORB
40
20
10
8
6
4
2
1
0.8
0.6
(?)
Western U.S.A.
(CAB)
New Hebrides
(IAB)
A-30-12
A-30-1
Hawaii
(Tholeiite)
Australia
(Anorogenic
Basalt)
MORB REFERENCE LINE
120
0.15
2
20
0.2
3.5
10
0.12
(wt.% P_2O_5)
90
2.4
3.3
1.5
(wt.% TiO_2)
30
3.4
Sr
K
Rb
Ba
Th
Nb
Ce
P
Zr
Hf
Sm
Ti
Y
Yb

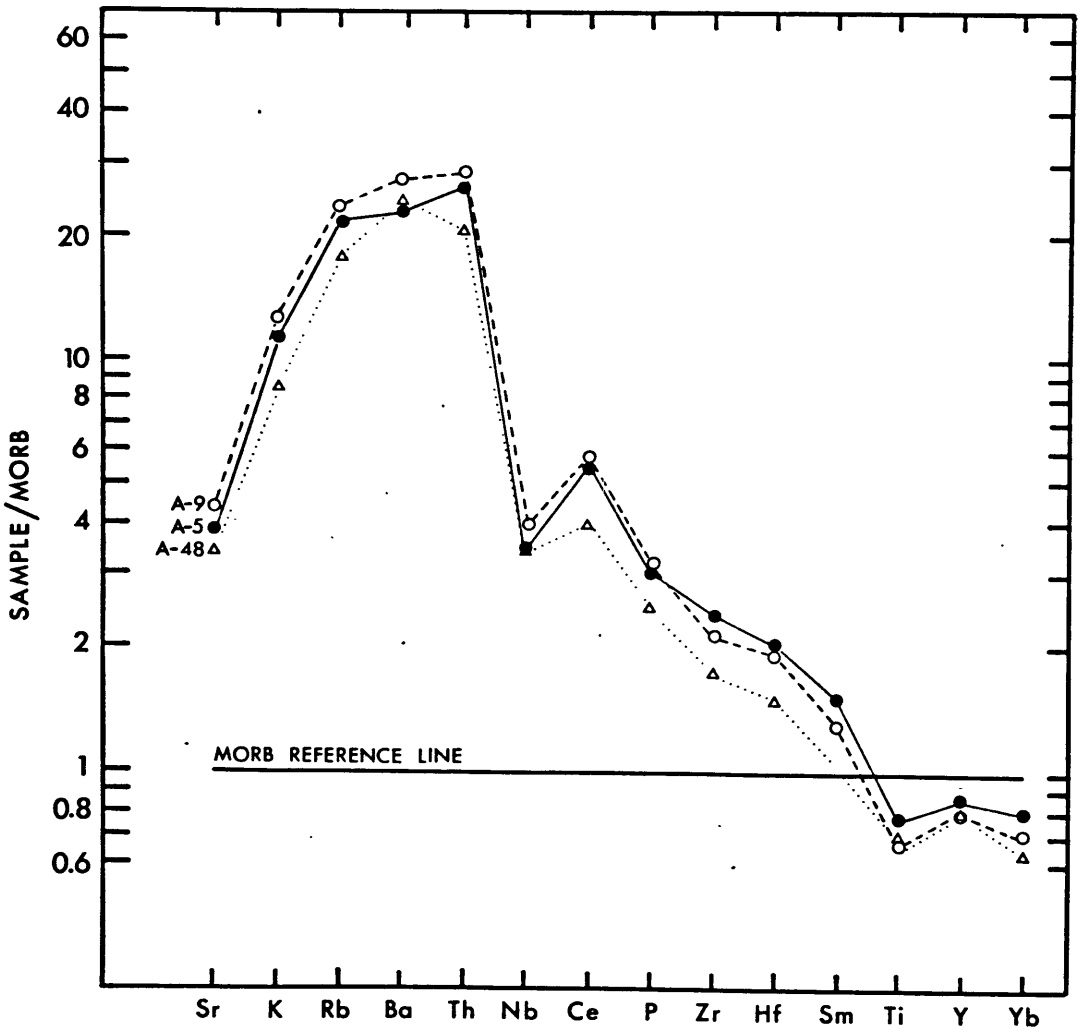
60
40
20
10
8
6
4
2
1
0.8
0.6
SAMPLE/MORB
A-9
A-5
A-48
MORB REFERENCE LINE
Sr
K
Rb
Ba
Th
Nb
Ce
P
Zr
Hf
Sm
Ti
Y
Yb

of the Ararat HA basalts are broadly similar to the Western U.S.A. (continental arc basalt) pattern.

Two andesites from the Ararat series (A-9 and A-5) and one andesite from the Little Ararat series (A-48) are normalized with respect to MORB and plotted in Figure-1.13. The overall patterns of these samples closely resemble each other. However, their patterns differ significantly from the patterns of the HA Basalts, in that they are more enriched in K, Rb, Ba, Th and Ce. They also exhibit Ti depletion, as expected for Ti-bearing oxide phase fractionation, as well as Nb depletion. Their MORB normalized Sr values are comparable with those of the HA basalts. A-9 and A-48 seem to have small negative Zr anomalies, but no Hf anomaly.

1.5.2 Rare Earth Elements

Chondrite normalized REE abundances for the Ararat samples are plotted in Figure-1.14 and the REE data are listed along with chondrite abundances in Table 1-2. All of the Ararat samples are LREE enriched ((La/Yb)e.f. (enrichment factor relative to chondrites) = 2.6-8.6 (La/Sm)e.f. = 1.4-4.3). The LREE abundances of Ararat lavas vary by a factor of 3 (34-103xchondrites) while the HREE abundances are relatively constant (10+3xchondrites), excluding sample A-12, which is a dacite from the Little Ararat series. A-12 has significantly lower REE abundances and the most fractionated REE pattern ((La/Yb)e.f.=11), with a negative Eu anomaly. The HA basalts and Little Ararat series (except A-12) have small positive Eu anomalies, while the Old Ararat and Ararat series lavas have small negative Eu anomalies. These positive and negative Eu anomalies can be generated by accumulation and fractionation of plagioclase respectively. Alternatively, they can be inherited from the source, but this is not likely for calc-alkaline rocks in general, based on the data obtained from experimental petrological studies. All of the Ararat

TABLE 1-2

	LITTLE ARARAT SERIES			HIGH ALUMINA BASALTS				
	A-12	A-48	A-51	A-13	A-30-1	A-30-12	A-36-A	CHONDRITIC ABUND. (1)
La	14.6	20.4	21.1	11.3	11.9	17.6	13.1	0.33
Ce	24	40	38	29	31	41	32	0.88
Nd	9.2	17.2	15.5	17.5	18.5	21.5	18.3	0.60
			(14.49)(2)		(17.65)	(21.56)	-	
Sm	1.98	3.48	3.02	4.34	4.66	4.87	4.36	0.181
			(3.02)(2)		(4.51)	(4.92)	-	
Eu	0.52	1.28	1.02	1.70	1.75	1.77	1.76	0.069
Tb	0.36	0.45	0.48	0.84	0.86	0.90	0.86	0.047
Yb	0.8	2.2	1.6	2.6	2.7	2.5	2.9	0.20
Lu	0.11	0.36	0.26	0.41	0.40	0.36	0.45	0.034
La/Ce	0.61	0.51	0.56	0.39	0.38	0.43	0.41	
La/Sm	7.37	5.86	6.99	2.60	2.64	3.58	3.00	
La/Yb	18.25	9.27	13.19	4.35	4.41	7.04	4.52	

	OLD ARARAT SERIES			ARARAT SERIES				
	A-23-A	A-42-C	A-45	A-4	A-5	A-9	A-32	A-42-J
La	25.6	24.1	25.6	24.2	27.7	34.1	25.8	31.3
Ce	50	46	47	48	55	58	50	59
Nd	20.7	18.3	18.7	21.8	24.1	23.8	22.4	23.7
Sm	4.15	4.16	3.55	4.57	4.97	4.30	4.53	4.35
Eu	1.27	1.29	1.10	1.37	1.52	1.35	1.60	1.41
Tb	0.69	0.71	0.60	0.82	0.81	0.87	0.86	0.76
Yb	2.0	2.1	2.0	2.6	2.4	2.4	2.6	2.4
Lu	0.30	0.33	0.33	0.38	0.38	0.37	0.41	0.39
La/Ce	0.51	0.52	0.54	0.50	0.50	0.59	0.52	0.53
La/Sm	6.17	5.79	7.21	5.30	5.57	7.93	5.70	7.20
La/Yb	12.80	11.48	12.80	9.31	11.54	14.21	9.92	13.04

(1) Chondritic abundances are from Frey et al., (1968).
(2) Concentrations in parentheses are determined by isotope dilution.

Figure-1.14

Diagrams showing the ranges for the chondrite normalized REE patterns of the Ararat series. Chondrite normalization values are listed in Table-1.2.

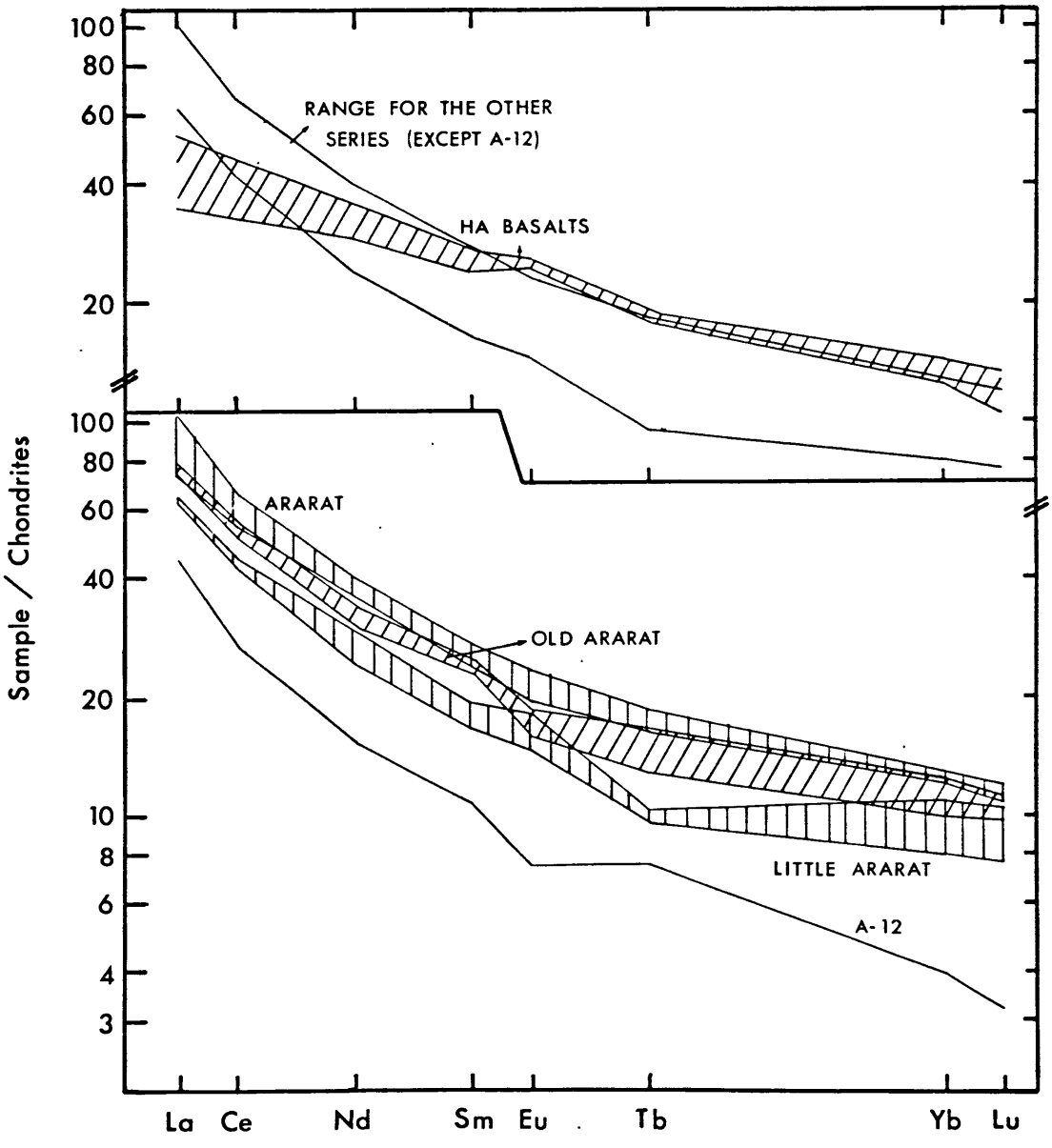
Sample / Chondrites
100
80
60
40
20
RANGE FOR THE OTHER
SERIES (EXCEPT A-12)
HA BASALTS
100
80
60
40
20
10
8
6
4
3
ARARAT
OLD ARARAT
LITTLE ARARAT
A-12
La
Ce
Nd
Sm
Eu
Tb
Yb
Lu

andesites, and dacites seem to also have small negative Ce anomalies (Ce/Ce*=0.92-0.99). However the Ce anamolies are within the analytical uncertainty limits. The chondrite-normalized REE patterns of the Ararat samples (Figure-1.14) distinguish the same four groupings, as the grouping based on major and trace element data. The HA basalts exhibit the least LREE enrichment ((La/Yb)e.f.=2.6-3.0) among the Ararat series. Chondrite normalized REE patterns of two HA Basalt samples (A-30-1 and A-30-12), which represent the oldest and youngest lava flows of this series, respectively, are plotted in Figure-1.15. A-30-12 is more enriched in LREE, while more depleted in HREE, relative to A-30-1. It is possible to explain the REE abundances of A-30-1 and A-30-12 by different degrees of partial melting of a single mantle source. A-30-12 could be generated by a smaller degree partial melt, being LREE enriched and HREE depleted relative to A-30-1. However, the isotope data preclude such an explanation. Based on major, trace element and Sr-Nd-Pb isotope data, the HA basalts represent two component magma mixing. One end-member (similar to A-30-1) is a MORB-like magma, and the second end-member is an alkali basalt magma. The chondrite-normalized pattern of A-30-12 can be explained by addition of an alkali basalt component to A-30-1. Because this second end-member is more enriched in LREE and depleted in HREE relative to A-30-1, the REE pattern of A-30-1 is rotated around the chondrite normalized Tb abundance to generate the REE pattern of A-30-12 as a result of magma mixing (Figure-1.15). The lavas of the Little Ararat Series have lower total REE contents in comparison to the Old Ararat and Ararat series. Their La/Yb ratios are negatively correlated with Mg#, La and Zr abundances (Figure-1.16). The REE patterns of the Old Ararat series occupy an intermediate position between the Little Ararat and Ararat series. The lavas of the Ararat series have the highest total REE contents. La/Yb ratios are positively correlated with Mg# and La abundances for the Old Ararat and Ararat series. Zr abundances of the Ararat series lavas are correlated negatively with both La and La/Yb ratios (Figure-1.17).

Figure-1.15

Diagram illustrating the effect of magma mixing on the chondrite normalized REE patterns of the Ararat HA basalts. Apparently, the pattern of A-30-1 is rotated around a point in the middle to heavy REE region, resulting in enrichments in LREE and depletions in HREE, due to magma mixing.

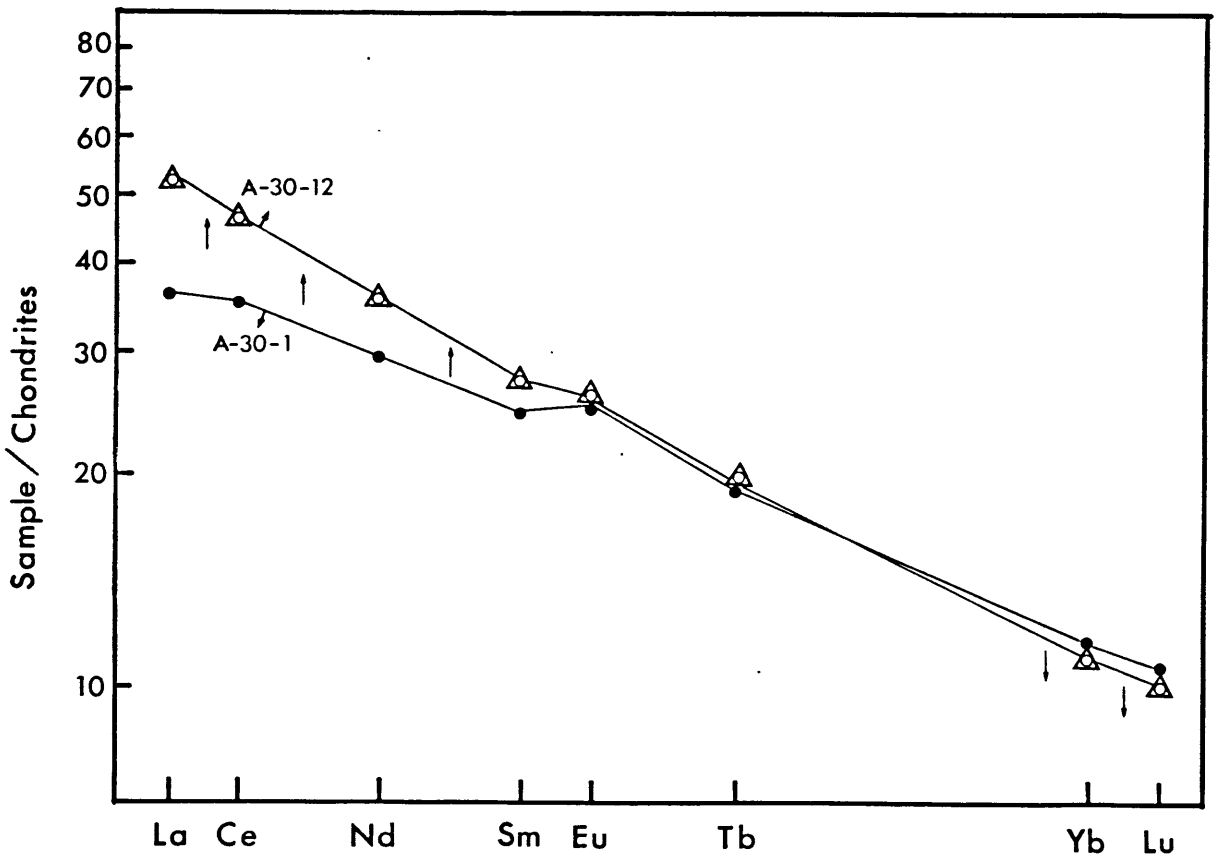
80
70
60
50
40
30
20
10
Sample / Chondrites
A-30-12
A-30-1
La
Ce
Nd
Sm
Eu
Tb
Yb
Lu

Figure-1.16.a,b

Diagrams illustrating the relationship between the degree of LREE enrichment (La/Yb ratio) and Mg# and La abundances. The distinct fields and trends not only distinguish the Ararat suites, but also exhibit the magma mixing relations.

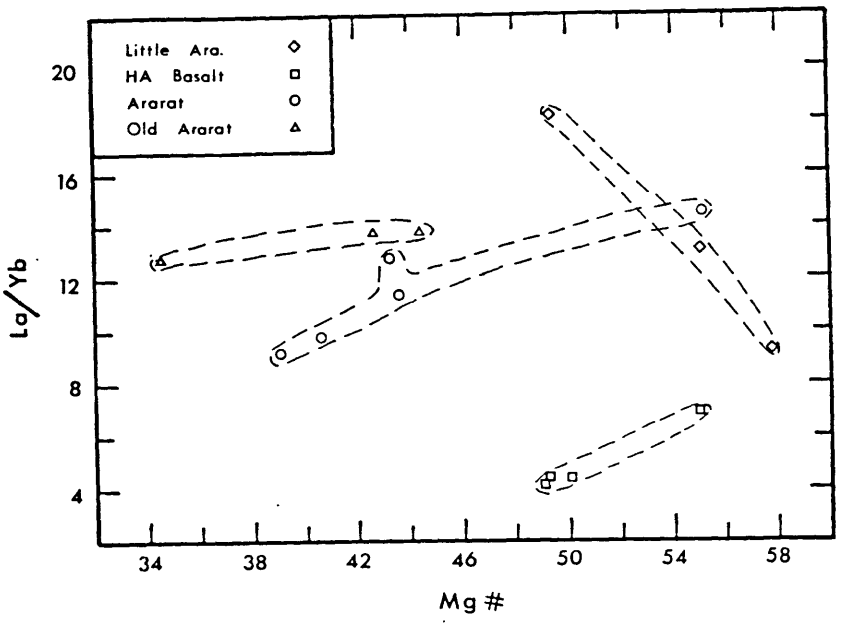
Little Ara.
HA Basalt
Ararat
Old Ararat
La/Yb
Mg #
20
16
12
8
4
34
38
42
46
50
54
58

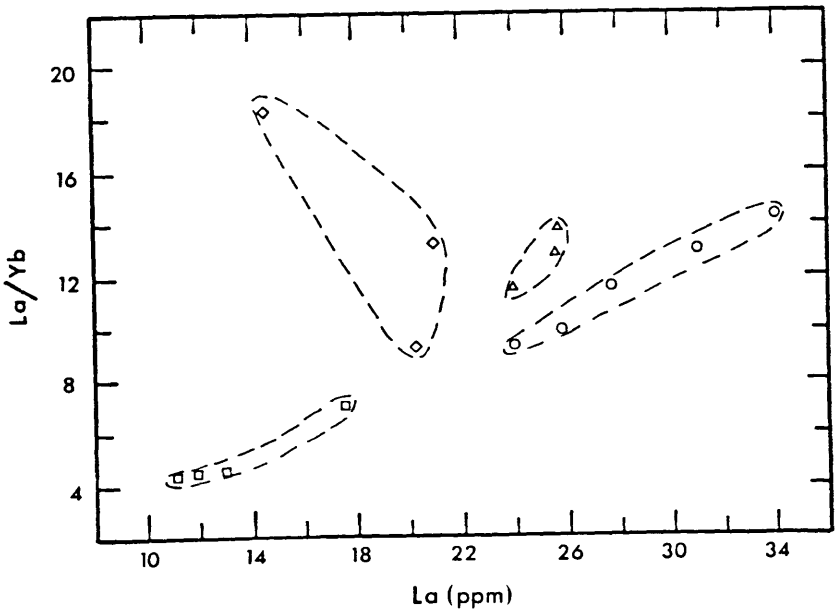
La/Yb
La (ppm)
20
16
12
8
4
10
14
18
22
26
30
34

Figure-1.17.a,b

Plots of La versus Zr and La/Yb versus Zr for the Ararat lavas. Note the negative correlation between the La and Zr abundances for the Ararat series lavas. Also negative correlations exist between La/Yb and Zr abundances for the Little Ararat and the Ararat series.

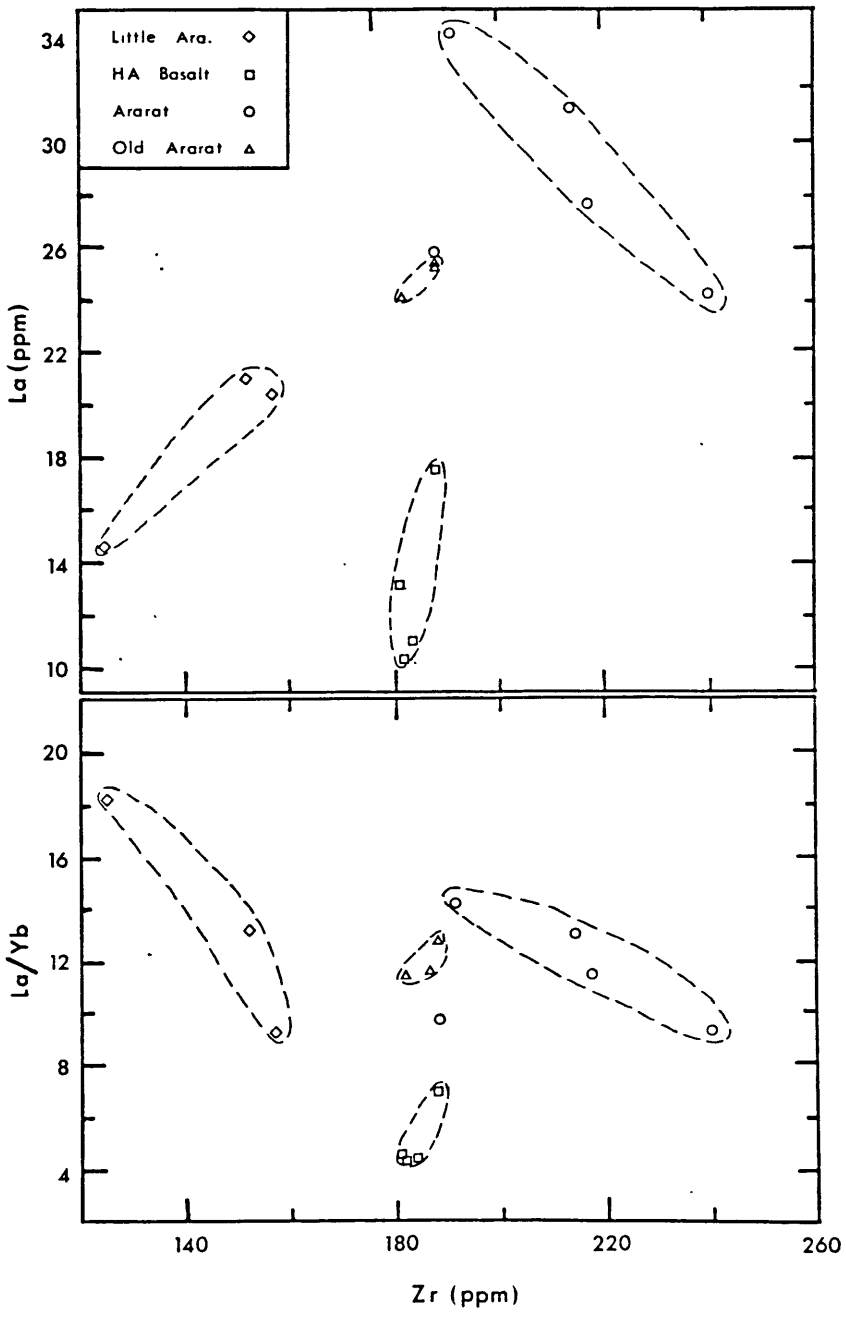
Little Ara.
HA Basalt
Ararat
Old Ararat
La (ppm)
La/Yb
Zr (ppm)
34
30
26
22
18
14
10
20
16
12
8
4
140
180
220
260

1.5.3 Isotope Geochemistry

Sr, Nd and Pb isotopic compositions, along with Rb, Sr, Sm and Nd abundances for the Ararat lavas are listed in Table-1.3. Sr 87/86 ratios range from 0.70339 to 0.70442, and Nd 143/144 ratios range from 0.51297 to 0.51280. The observed Pb isotopic composition ranges are 18.80-19.02 for Pb 206/204, 15.56-15.67 for Pb 207/204, and 38.76 to 39.14 for Pb 208/204.

1.5.3.1 Sr and Nd Isotope Variation

Isotopic compositions of the Ararat lavas are broadly correlated with major and trace element abundances. However, consideration of possible disturbances due to fractionation on the covariation of isotopic compositions with major and trace element abundances, makes such correlations even more convincing. In Figure-1.18 Sr 87/86 ratios are plotted against SiO2 and MgO contents. The Sr 87/86 compositions of Ararat samples are correlated negatively with SiO2 and positively with MgO contents. The four different series of Ararat lavas form distinct trends and fields on these plots. Sr isotope ratios are also correlated negatively with Rb/Sr ratios for Little Ararat, Ararat and Old Ararat series (Figure-1.19a). The HA Basalts exhibit a wide range in Sr 87/86 ratio (0.70339-0.70376) at almost constant Rb/Sr ratios. The data presented so far suggest the predominance of magma mixing in the petrogenesis of the Ararat lavas. One test for mixing processes is to plot isotopic ratios versus the reciprocal of the relevant element's abundance. If the concentrations of individual samples are not significantly affected by crystal fractionation or contamination, such plots will produce linear trends for simple two-component mixing processes. In Figure-1.19b Sr 87/86 ratios are plotted against 100/Sr for the Ararat samples. All the Ararat series form distinct linear trends with negative slopes, indicating

TABLE 1-3

SAMPLE #	Sr 87/86 (1) (6)	Nd 143/144 (2) (6)	Pb 206/204 (3)	Pb 207/204 (3)	Pb 208/204 (3)	Rb (4)	Sr (4)	Sm (5)	Nd (5)	Rb/Sr	Sm/Nd	Sr/Nd
					HIGH ALUMINA BASALTS							
A-13	0.70339 ∓2	0.51297 ∓2	18.933	15.616	38.941	8	434	4.34	17.49	0.018	0.248	24.81
A-30-1	0.70339 ∓3	0.51296 ∓2	18.924	15.614	38.910	9	424	4.51	17.65	0.021	0.256	24.02
A-30-5	0.70351 ∓3	0.51294 ∓2	18.940	15.625	38.957	10	459	4.49	17.71	0.022	0.254	25.92
A-30-10	0.70366 ∓4	0.51291 ∓2	18.965	15.635	39.001	11	536	4.77	20.29	0.021	0.235	26.42
A-30-12	0.70376 ∓2	0.51288 ∓2	18.982	15.648	39.042	13	566	4.92	21.56	0.023	0.228	26.25
A-36-A	0.70339 ∓3	0.51295 ∓2	18.916	15.601	38.890	10	431	4.36	18.29	0.023	0.238	23.56
					LITTLE ARARAT SERIES							
A-12	0.70423 ∓4	0.51292 ∓2	18.832	15.563	38.756	50	347	1.98	9.18	0.144	0.216	37.80
A-43	0.70433 ∓3	0.51284 ∓2	18.941	15.639	38.997	26	382	-	-	0.068	-	-
A-46	0.70403 ∓4	0.51289 ∓2	18.802	15.601	38.837	34	372	2.50	11.19	0.091	0.223	33.24
A-47	0.70401 ∓3	0.51290 ∓2	18.810	15.611	38.870	31	360	-	-	0.086	-	-
A-48	0.70439 ∓3	0.51280 ∓2	18.962	15.660	39.069	36	415	3.48	17.15	0.087	0.203	24.20
A-51	0.70423 ∓4	0.51286 ∓3	18.958	15.673	39.139	39	384	3.02	14.49	0.102	0.208	26.50
A-54	0.70385 ∓3	0.51291 ∓2	18.921	15.603	38.912	87	100	3.22	14.38	0.870	0.224	6.95
					ARARAT							
A-1	0.70382 ∓4	-	-	-	-	62	344	-	-	0.180	-	-
A-4	0.70386 ∓4	0.51291 ∓2	-	-	-	59	377	4.57	21.82	0.157	0.209	17.28
A-5	0.70418 ∓4	0.51288 ∓2	-	-	-	44	460	4.97	24.06	0.096	0.207	19.12
A-6	0.70387 ∓4	0.51292 ∓2	18.890	15.605	38.884	65	330	4.58	20.65	0.197	0.222	15.98
A-8-B	0.70391 ∓4	-	-	-	-	62	352	-	-	0.176	-	-
A-9	0.70418 ∓4	0.51286 ∓2	18.960	15.617	38.979	47	525	4.30	23.80	0.090	0.181	22.06
A-10	0.70405 ∓4	-	-	-	-	58	399	-	-	0.145	-	-
A-17	0.70398 ∓5	0.51291 ∓2	18.956	15.620	38.988	56	393	-	-	0.143	-	-
A-32	0.70433 ∓3	0.51284 ∓2	18.981	15.633	39.022	35	409	4.53	22.35	0.086	0.203	18.30
A-42-H	0.70404 ∓4	-	-	-	-	54	420	-	-	0.129	-	-
A-42-I	0.70401 ∓4	-	-	-	-	57	418	-	-	0.136	-	-
A-42-J	0.70412 ∓4	0.51288 ∓2	18.963	15.625	39.001	56	420	4.35	23.74	0.133	0.183	17.69
A-42-K	0.70409 ∓4	-	-	-	-	55	417	-	-	0.132	-	-

(cont'd.)

(1) Sr 87/86 ratios normalized to 0.70800 for E & A SrC03 using Sr 86/88 = 0.1194
(2) Nd 143/144 ratios normalized to 0.51264 for BCR-1 using Nd 146/144 = 0.7219
(3) Pb isotope ratios are normalized for mass discrimination using that obtained for NBS SRM 981. Reproducibility is better than 0.05% AMU-1.
(4) Concentrations in ppm by XRF.
(5) Concentrations in ppm by isotope dilution, with precision for Nd, and Sm ~0.3%.
(6) Quoted errors for Sr and Nd isotopic ratios are in-run statistics, and are representative of true precision as demonstrated by replicate analysis of various samples.

TABLE 1-3 (Cont'd)

SAMPLE #	Sr 87/86 (1) (6)	Nd 143/144 (2) (6)	Pb 206/204 (3)	Pb 207/204 (3)	Pb 208/204 (3)	Rb (4)	Sr (4)	Sm (5)	Nd (5)	Rb/Sr	Sm/Nd	Sr/Nd
					OLD ARARAT SERIES							
A-14	0.70416 ∓4	-	-	-	-	56	319	-	-	0.176	-	-
A-23-A	0.70441 ∓4	0.51283 ∓2	-	-	-	43	383	4.15	20.71	0.112	0.200	18.49
A-23-C	0.70441 ∓3	-	-	-	-	42	383	-	-	0.110	-	-
A-24	0.70442 ∓4	-	-	-	-	44	385	-	-	0.114	-	-
A-25	0.70431 ∓4	-	-	-	-	42	382	-	-	0.110	-	-
A-26	0.70430 ∓4	-	-	-	-	42	381	-	-	0.110	-	-
A-28-B	0.70428 ∓4	0.51284 ∓3	19.018	15.618	39.032	52	420	-	-	0.124	-	-
A-33	0.70439 ∓4	-	-	-	-	46	363	-	-	0.127	-	-
A-34-B	0.70432 ∓4	-	-	-	-	50	418	-	-	0.120	-	-
A-42-A	0.70412 ∓4	0.51286 ∓3	-	-	-	61	262	-	-	0.233	-	-
A-42-B	0.70434 ∓4	-	-	-	-	60	262	-	-	0.229	-	-
A-42-C	0.70440 ∓4	0.51283 ∓2	18.916	15.620	38.961	46	378	4.16	18.29	0.122	0.227	20.67
A-42-D	0.70409 ∓4	-	-	-	-	61	268	-	-	0.228	-	-
A-42-E	0.70408 ∓4	0.51288 ∓2	18.912	15.610	38.920	57	260	-	-	0.219	-	-
A-42-F	0.70411 ∓4	-	-	-	-	65	275	-	-	0.236	-	-
A-42-G	0.70423 ∓4	-	-	-	-	67	273	-	-	0.245	-	-
A-45	0.70409 ∓4	0.51285 ∓2	-	-	-	52	338	3.55	18.74	0.154	0.189	18.04

(1) Sr 87/86 ratios normalized to 0.70800 for E & A SrC03 using Sr 86/88 = 0.1194
(2) Nd 143/144 ratios normalized to 0.51264 for BCR-1 using Nd 146/144 = 0.7219
(3) Pb isotope ratios are normalized for mass discrimination using that obtained for NBS SRM 981. Reproducibility is better than 0.05% AMU-1.
(4) Concentrations in ppm by XRF.
(5) Concentrations in ppm by isotope dilution, with precision for Nd, and Sm ~0.3%.
(6) Quoted errors for Sr and Nd isotopic ratios are in-run statistics, and are representative of true precision as demonstrated by replicate analysis of various samples.

Figure-1.18.a,b

Plots showing the variation of Sr 87/86 ratios with SiO2 and MgO contents. Despite the fractional crystallization effects (shown by the arrows), all of the series have distinct trends and fields. Note that the negative correlations between Sr 87/86 and SiO2, and positive correlations between Sr 87/86 and MgO are just the opposite in sense to that expected for crustal contamination.

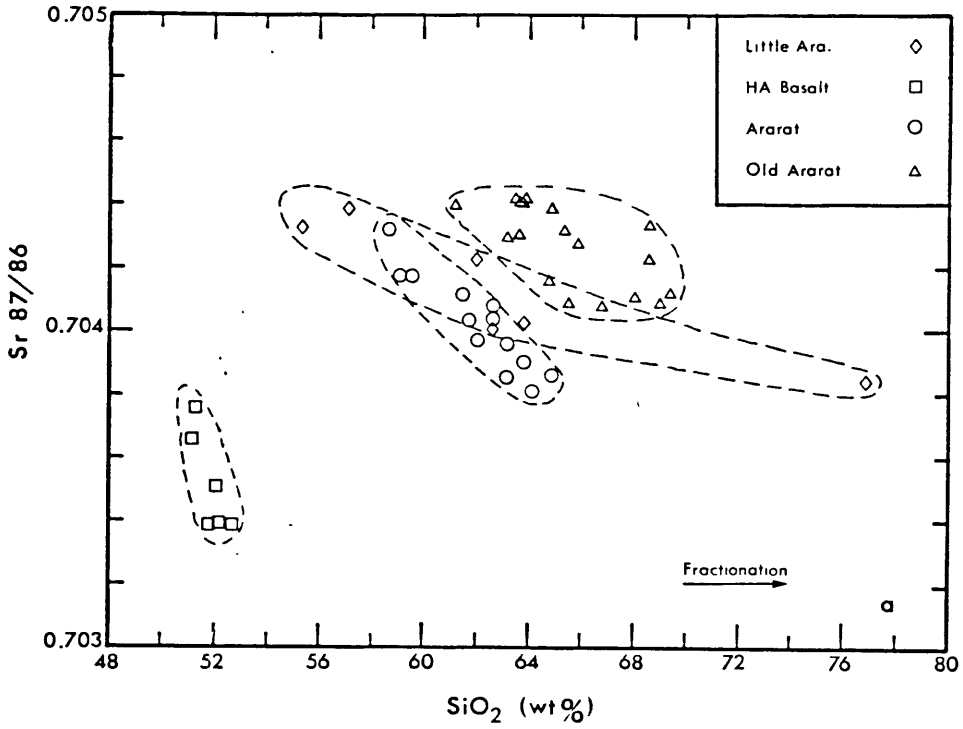
0.705
0.704
0.703
Sr 87/86
48
52
56
60
64
68
72
76
80
SiO2 (wt%)
Little Ara.
HA Basalt
Ararat
Old Ararat
Fractionation
a

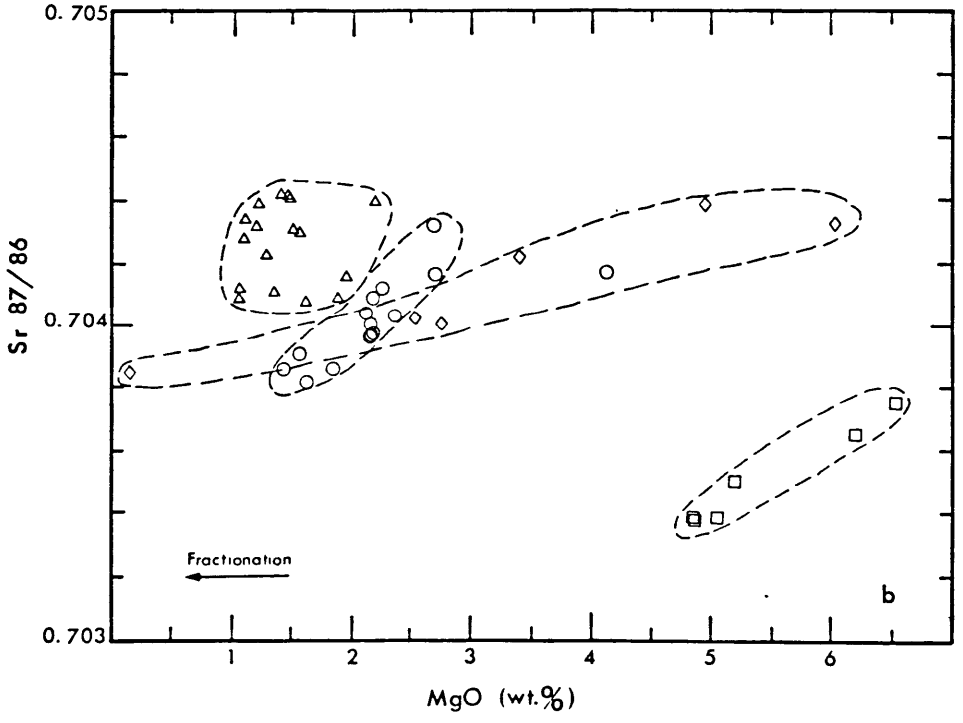
0. 705
0. 704
0. 703
Sr 87/86
1
2
3
4
5
6
MgO (wt.%)
Fractionation
b

Figure-1.19.a,b

Diagrams illustrating the variation of Sr 87/86 ratios with Rb/Sr and the reciprocal Sr concentration for the Ararat lavas. The linear correlations observed for each of the Ararat series on these plots demonstrate the viability of magma mixing for the Ararat lavas.

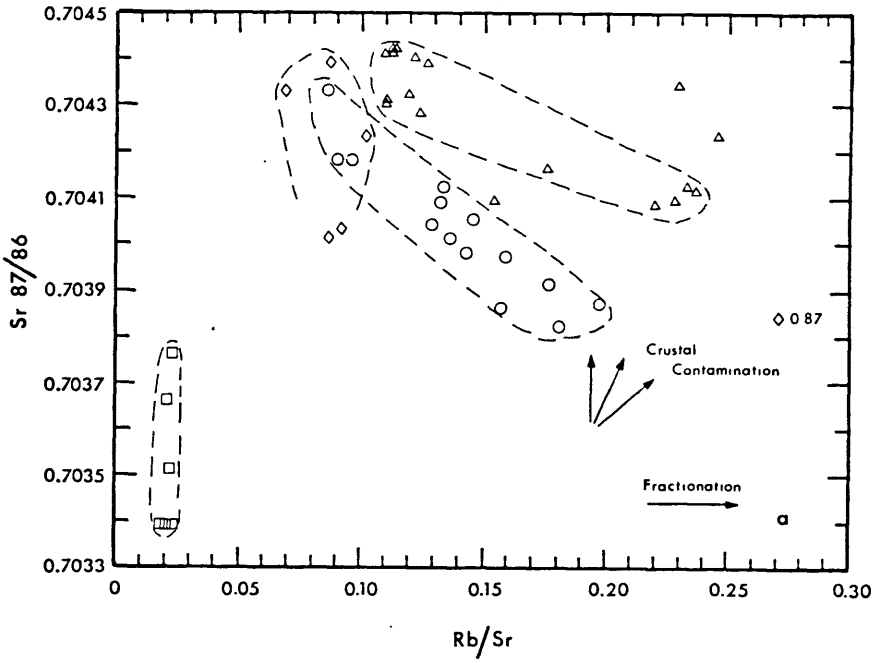
0.7045
0.7043
0.7041
0.7039
0.7037
0.7035
0.7033
Sr 87/86
0
0.05
0.10
0.15
0.20
0.25
0.30
Rb/Sr
◇ 0.87
Crustal
Contamination
Fractionation
a

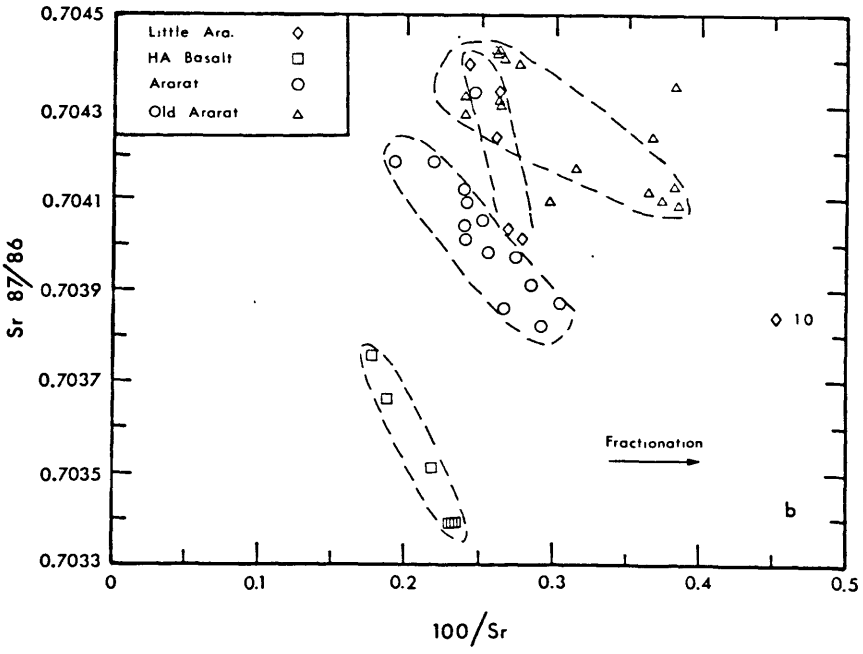
Little Ara. ◇
HA Basalt □
Ararat ○
Old Ararat △
0.7045
0.7043
0.7041
0.7039
0.7037
0.7035
0.7033
Sr 87/86
0
0.1
0.2
0.3
0.4
0.5
100/Sr
◇ 1.0
Fractionation
b

different two component magma mixing processes for each of the Ararat series. Details of magma mixing will be discussed in the next section.

The Sr and Nd isotope compositions of the Ararat lavas are presented in a Sr 87/86-Nd 143/144 correlation diagram in Figure 1.20. Also shown are the fields for MORB and some island-arc suites. In order to avoid overcrowding, only the Azores field of OIB is shown. The general OIB field, overlapping with the lower end of the MORB field, extends as a broad field more or less along the oceanic regression line. The Ararat data form two narrow elongate fields along the oceanic regression line. The HA Basalts plot virtually on the oceanic regression line, starting from the lower end of the MORB field and extending towards lower Nd 143/144 and higher Sr 87/86 values. The rest of the Ararat series lavas, composed mainly of andesites and dacites, define a elongate field subparallel to the oceanic regression line but shifted towards the more radiogenic Sr 87/86 side. All of the Ararat samples plot within the OIB field and also overlap with the field of the Central Japan, Azores and Dominica volcanics. The data point for one alkali basalt sample (S-60) from NE of the Suphan volcano is also plotted in Figure-1.20. Assuming that the Nd 143/144 - Sr 87/86 correlation represents two-component mixing for each of the Ararat series, then the isotopic composition of S-60 is a plausible common lower end-member. Nd isotopic compositions of the Ararat lavas are also correlated with major and trace element abundances (e.g. positive correlation with SiO2, negative correlation with MgO contents; figures are not given here). Nd 143/144 ratios are also correlated negatively with Nd abundances and positively with Sm/Nd ratios (Figure-1.21). In these diagrams, differentiation could potentially cause significant scatter. The best correlation is displayed by the HA Basalts, since they are the least differentiated lavas among the Ararat suites. The linear mixing trends defined by the Ararat suites converge to a common point which is characterized by Nd143/144 0.51273, Nd 30ppm and Sm/Nd 0.2. In fact, the most primitive alkali basalt (S-60, plotted in

Figure-1.20

Sr-Nd isotope correlation diagram for the Ararat lavas. Fields for MORB, Island arc and one oceanic island (Azores) are shown for comparison. Bulk Earth values and the "Oceanic Regression Line" are from Allegre et al., (1984). All Nd data normalized to Nd146/144=0.51264 for BCR-1. Data sources: Hawkesworth et al., (1977, 1979); Hawkesworth and Powell (1980); Cohen and O'Nions (1982); DePaolo and Johnson (1979); McCulloch and Perfit (1981); Morris and Hart (1983); White and Hofmann (1982); Cohen et al., (1980); O'Nions et al., (1977); Ito et al., (1981); White (1979); Nohda and Wasserburg (1981); Stern (1981); Allegre et al., (1979).

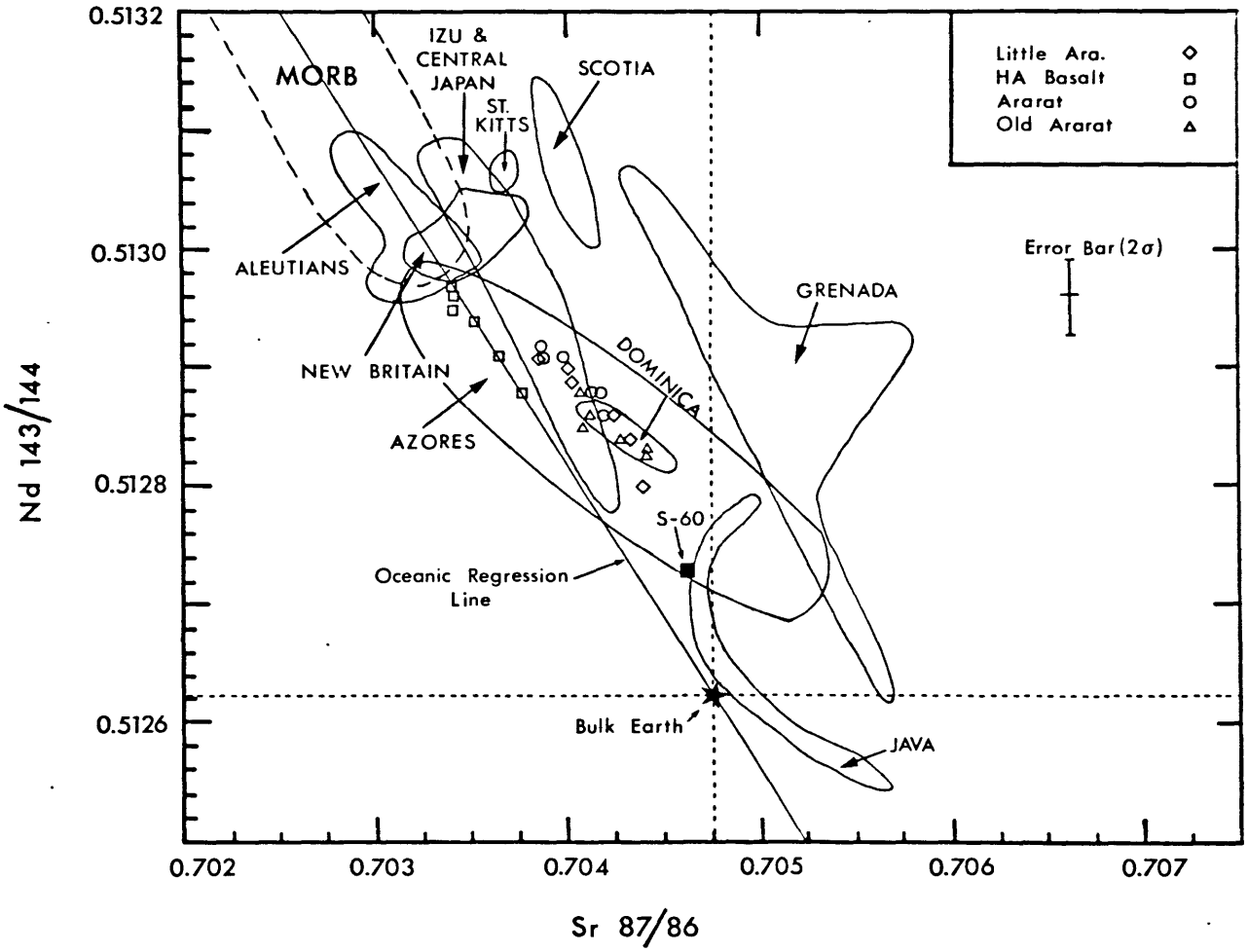
0.5132
0.5130
0.5128
0.5126
Nd 143/144
0.702
0.703
0.704
0.705
0.706
0.707
Sr 87/86
MORB
IZU &
CENTRAL
JAPAN
ST.
KITTS
SCOTIA
ALEUTIANS
NEW BRITAIN
AZORES
GRENADA
DOMINICA
S-60
Oceanic Regression
Line
Bulk Earth
JAVA
Little Ara.
HA Basalt
Ararat
Old Ararat
Error Bar (2σ)

Figure-1.21a

Variation between Nd 143/144 ratio and reciprocal Nd abundance for the Ararat lavas. The lines are drawn to approximate the linear trends exhibited by the Ararat suites, despite of the disturbances due to fractional crystallization. These trends are interpreted as two-component mixing trends. Note that they all converge towards a common point which has a Nd 143/144 ratio of 0.51273 and Nd abundance of 30-35ppm. The isotopic composition of this "end-member" is almost identical to sample S-60 (also shown in the figure) which is the most "primitive" alkali basalt fissure lava flow, sampled from an area to the northwest of the Suphan volcano.

Figure-1.21b

Variation between Nd 143/144 ratio and Sm/Nd ratio for the Ararat lavas. Note the trends with positive correlations, disturbed by fractional crystallization, for the Ararat suites. The trends all converge towards a common field.

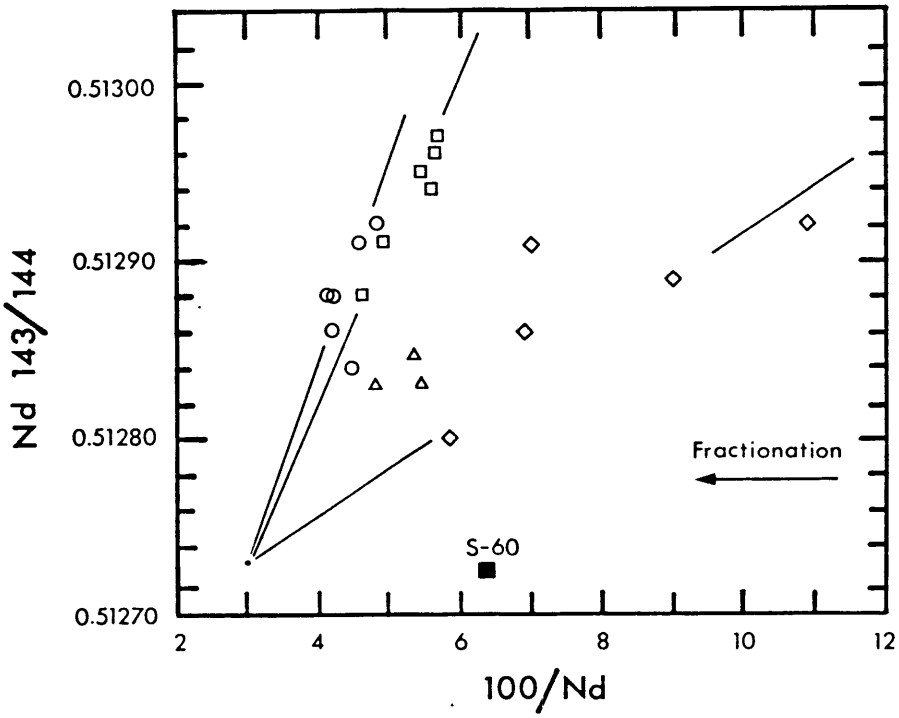
0.51300
0.51290
0.51280
0.51270
Nd 143/144
2
4
6
8
10
12
100/Nd
Fractionation
S-60

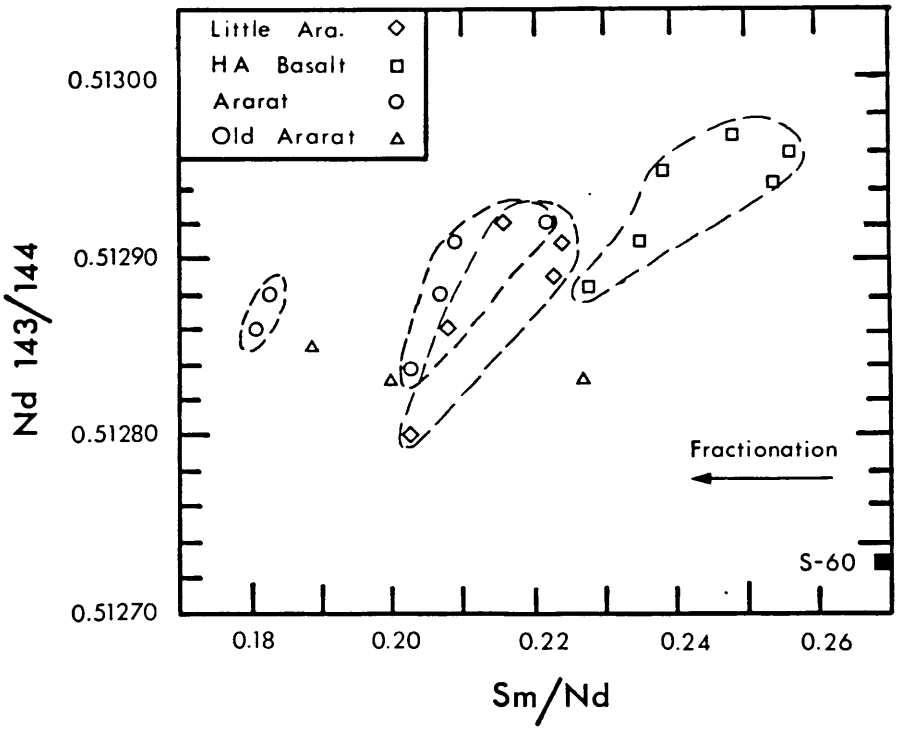
Little Ara.
HA Basalt
Ararat
Old Ararat
0.51300
0.51290
0.51280
0.51270
Nd 143/144
0.18
0.20
0.22
0.24
0.26
Sm/Nd
Fractionation
S-60

Figure-1.21) is identical to this end-member in terms of Nd and Sr isotopic composition but differs from it in Sm/Nd ratio and Nd abundance. This suggets that the common end-member for mixing trends of the Ararat suites may represent a smaller degree partial melt derived from the same mantle source as the alkali basalt. Similarly, the trends formed by the Ararat suites converge towards a common field on the Sr 87/86 versus Rb/Sr and 100/Sr diagrams (Figures-1.19a,b). Sr isotopic composition of this convergence point is almost identical to the Sr 87/86 ratio of S-60 (0.70470 vs 0.70462).

1.5.3.2 Pb Isotope Variation

The Pb isotope compositions of the Ararat lavas are plotted on Pb isotope correlation diagrams in Figure-1.22. Also included are various island arc, ocean island basalt and Tethian ophiolite fields. The Ararat lavas form a steep, narrow array on the 207/204 Pb versus 206/204 Pb diagram. Most of the Ararat samples do not plot within the mantle array as defined by MORB and some OIB (e.g. Hawaii, Iceland and NE Pacific seamounts). However the lower 207/204 Pb end of the Ararat array is within the mantle array and also overlaps with the fields of Tethian ophiolites (Troodos, Baer-Bassit and Semail). The radiogenic 207/204 end of the ophiolite fields are mostly characterized by the rocks of upper ophiolite sequence (e.g. basalts, diabeses and upper level gabbros). Most of the Ararat samples plot within the field defined by Reunion (an Indian ocean island) volcanics, though some extend to more radiogenic values which are typical of rocks from the Indian Ocean Islands (e.g. Crozet, Amsterdam) and also of oceanic sediments.

Although the trends that are defined by the HA Basalt and Ararat series lavas are quite narrow and well-defined on the 207-206-204 Pb diagram, the Little Ararat series form a wide field. In other words, for a given 207/204 Pb ratio, the Little Ararat Series

Figure-1.22

Pb-Pb isotope correlation diagrams for the Ararat lavas. Included for comparison are the fields for a variety of island arcs, OIB and Tethian ophiolites. The mantle array is drawn using the data from the North Atlantic, and Pacific Ocean MORB and some OIB (e.g. Hawaii, Iceland, and NE Pacific Seamounts). Data sources: Dupre and Allegre (1980,1983); Dupre et al., (1982); Oversby (1972); Sun (1980); Tatsumoto (1969, 1978); Meijer (1976); Cohen & O'Nions (1982); Oversby and Ewart (1972); Hamelin et al., (1984); Chen & Pallister (1981); Barreiro (1983); Davidson (1983); Cohen et al., (1980).

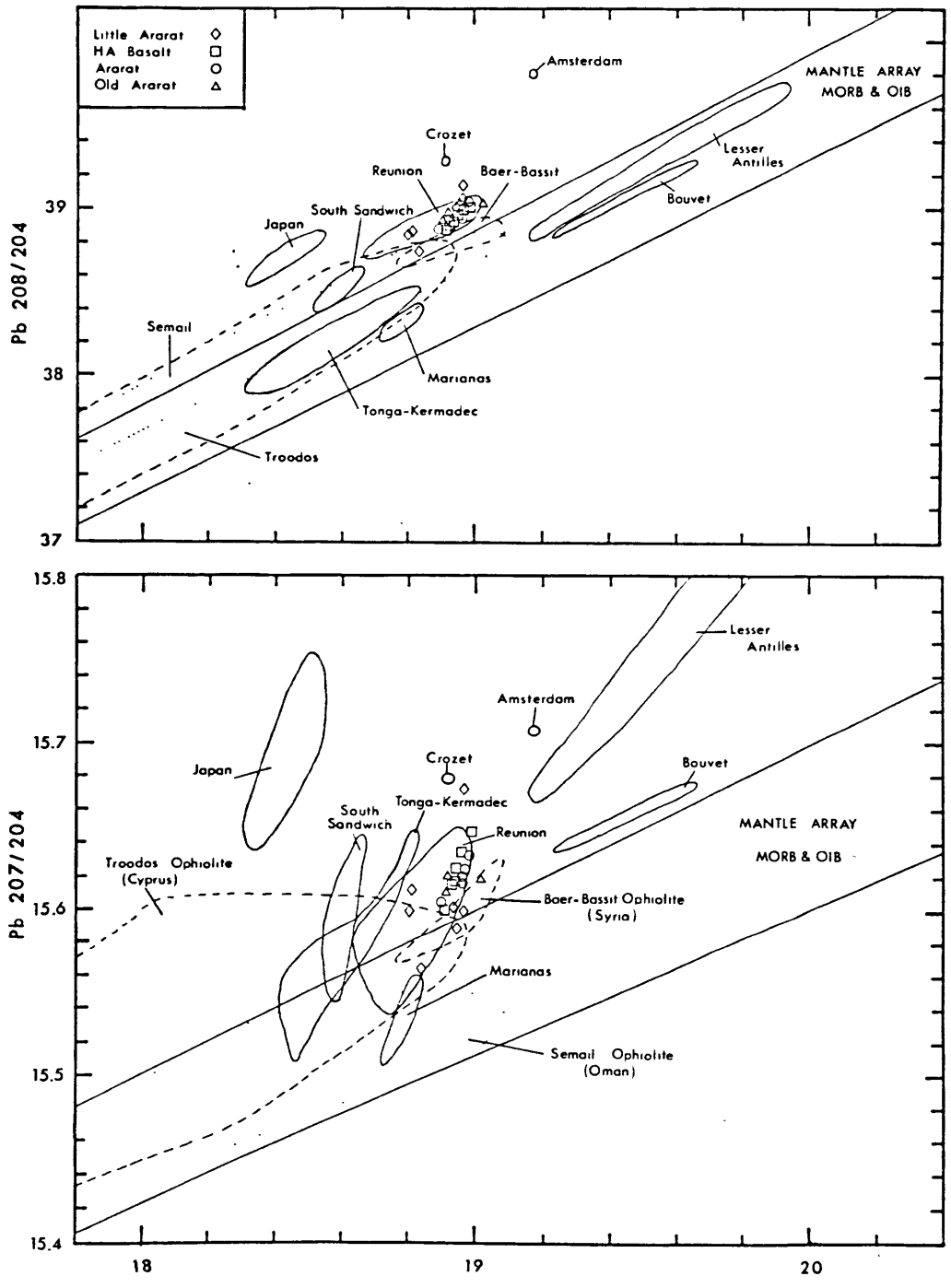
Little Ararat
HA Basalt
Ararat
Old Ararat
Amsterdam
MANTLE ARRAY
MORB & OIB
Crozet
Reunion
Baer-Bassit
Lesser
Antilles
Bouvet
South Sandwich
Japan
Semail
Marianas
Tonga-Kermadec
Troodos
Pb 208/204
39
38
37
15.8
15.7
15.6
15.5
15.4
Lesser
Antilles
Amsterdam
Japan
Crozet
Bouvet
Tonga-Kermadec
South
Sandwich
Reunion
MANTLE ARRAY
MORB & OIB
Troodos Ophiolite
(Cyprus)
Baer-Bassit Ophiolite
(Syria)
Marianas
Semail Ophiolite
(Oman)
Pb 207/204
18
19
20
Pb 206/204

Figure-1.23

Nd-Pb and Sr-Pb correlation diagrams showing the coherent correlations involving all three isotope systems. Nd 143/144 ratios are correlated negatively with Pb 206/204 ratios, whereas a positive correlation exists between Sr 87/86 and Pb 206/204 ratios for the Ararat lavas.

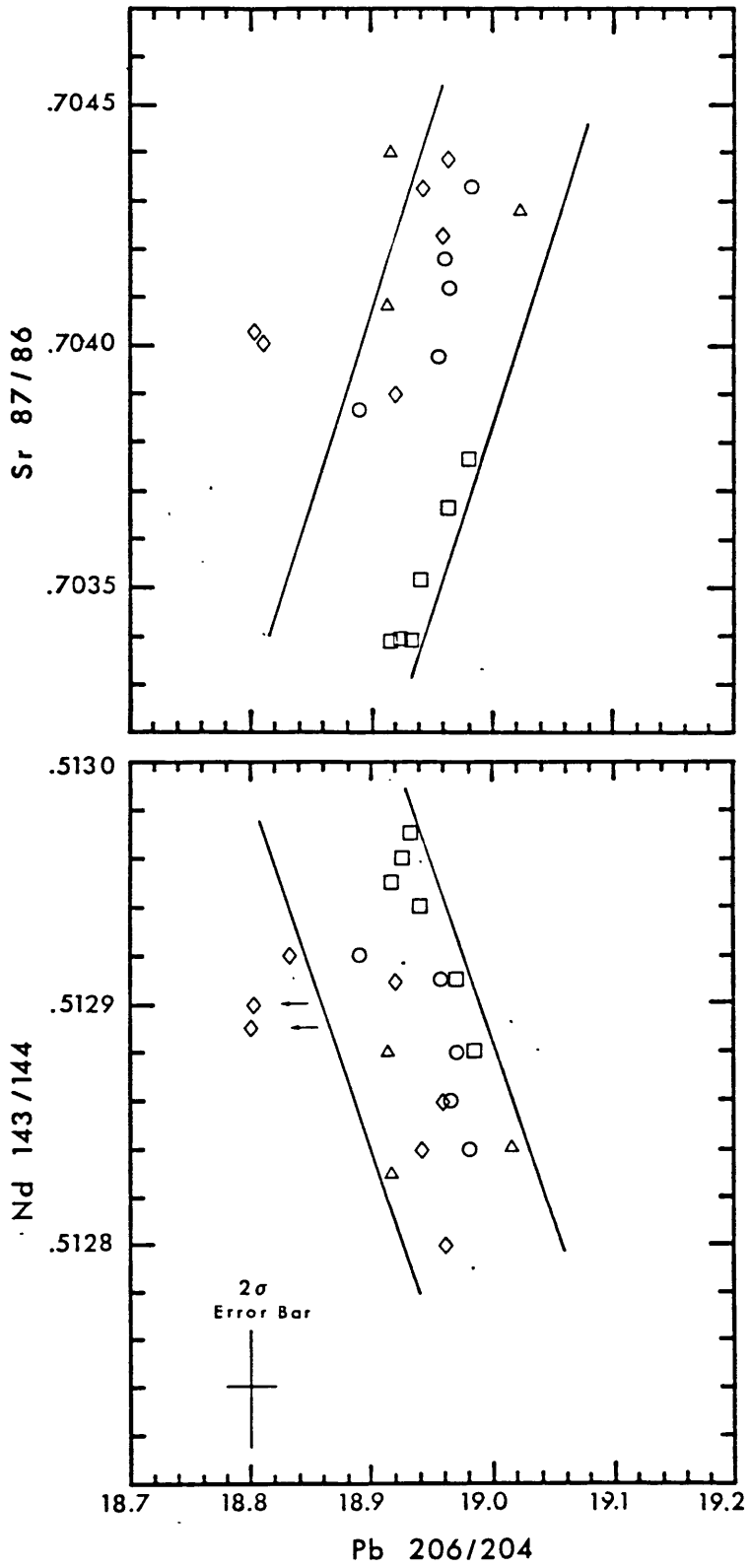
.7045
.7040
.7035
Sr 87/86
.5130
.5129
.5128
Nd 143/144
2σ
Error Bar
18.7
18.8
18.9
19.0
19.1
19.2
Pb 206/204

lavas have a wider range in 206/204 ratios in comparison with the other series. This suggests involvement of a Pb-bearing component with low U/Pb and possibly low Th/U (see 208-206-204 Pb diagram) values in the petrogenesis of the Little Ararat series (see the discussion on crustal contamination).

Nd, Sr and Pb isotope ratios of Ararat lavas are coherently correlated. These correlations are illustrated for 143/144 Nd-206/204 Pb and 87/86 Sr-206/204 Pb in Figure-1.23. 206/204 Pb ratios are correlated negatively and positively with 143/144 Nd and 87/86 Sr, respectively. These correlations are similar in slope, but not in absolute position to those reported for Atlantic and Pacific MORB (Allegre et al. 1980; Cohen et al. 1980; Dupre & Allegre, 1980).

1.6 Discussion

1.6.1 Crustal Contamination

Since the Ararat lavas were erupted in a continental setting and exhibit isotopic variations even among the successive lava flows, the possibility of crustal contamination has to be evaluated before starting any discussion of possible mantle source characteristics.

The continental crust has been recognized as a potential contaminant for modifying the chemistry of magmas since the early days of igneous petrology (Bowen, 1928). Because of the large differences in isotopic characteristics of mantle derived magmas and continental crust, the increasing application of isotope studies in igneous petrology has provided abundant evidence for crustal contamination of mantle derived magmas from a variety of regions, rock types and ages (e.g. Pankhurst, 1969; Carter et al, 1978; Moorbath & Thompson, 1979; Taylor, 1980; Tilton & Barreiro, 1980; Zindler et al, 1981;

James, 1982; Myers et al, 1984). Moreover, contours obtained from the Pb and Sr isotope systematics of Mesozoic and younger igneous rocks, reflecting crustal contamination, have been successfully used to delineate the age and/or geochemical nature of the underlying basement of the Western United States and Canada (Kistler & Peterman, 1973; Zartman, 1974; Armstrong et al, 1977). More recently, experimental work done on basalt/continental crust interactions has shed same light on the details of processes operating during crustal contamination (Watson, 1982; Watson & Jurewicz, 1984). Crustal contamination of magmas may be divided into six categories:

1. Mixing of mantle derived magmas with crustal melts.
2. Selective contamination of magmas en route to the surface.
3. Wall rock assimilation accompanied by crystal fractionation.
4. Isotope exchange between the magmas and their host rocks, without assimilation.
5. Solid state mixing prior to partial melting.
6. Any combination or permutation of the above.

Even though the effects of crustal contamination may be somewhat different depending on the type of crustal material, the actual contamination site and the mechanism of contamination and also on the physical and chemical characteristics of the magma, some broad generalizations can be made about the typical geochemical indicators of crustal contamination assuming an "average" crustal material.

Crustal contamination, in general, modifies magmas in the direction of radiogenic Sr, unradiogenic Nd, and Hf isotope ratios, and high δ18-O values. The Pb isotopes may be unradiogenic or radiogenic depending on the U/Pb, Th/Pb ratios and the age of the crust. The abundances of alkali elements increase (possibly with the exception of Na; Watson & Jurewicz, 1984) as do ratios such as Rb/Sr, Rb/K and Cs/K ratios. The Sr isotope ratios

may also correlate positively with Rb/Sr, and to a lesser extend with SiO2 and Sr content.

Interestingly, the within-suite variations of the different Ararat series, when considered in light of the above generalizations, exhibit just the opposite trends and correlations to those expected from crustal contamination. These can be summarized as follows:

1. Positive K/Rb-K2O correlation for the HA Basalts. (Figure-1.8)
2. Negative Sr 87/86 vs SiO2 and positive Sr 87/86 vs MgO correlation for all the Ararat suites (Figure-1.18)
3. Negative correlation between Sr 87/86 and Rb/Sr ratios for all the Ararat suites except the HA basalts. Practically constant Rb/Sr ratios of the HA basalt lavas, despite progressive increase in Sr 87/86 ratios from 0.70339 to 0.70376 (Figure-1.19a).
4. Negative correlation between Sr 87/86 and 100/Sr ratios for all Ararat suites (Figure-1.19b)

However, the observed wide range in 206/204 Pb ratios for the Little Ararat series (Figure-1.22,23) could have been caused by crustal contamination. Samples A-46, A-47 and A-51 (see Table-1.3) deserve special attention, because they do not plot within the well-defined, narrow Ararat array in Figures-1.22,23 and they are shifted towards the unradiogenic 206/204 Pb side of the array. A typical example of this kind of a shift has been convincingly demonstrated as a diagnostic signature of crustal contamination for the Arequipa and Barroso volcanics of southern Peru (Tilton & Barreiro, 1980). The unradiogenic 206/204 Pb signature in 206-207-204 Pb diagram indicates an old crustal component with a low U/Pb ratio and high Pb content. If this unradiogenic signature is accompanied by an unradiogenic 208/204 Pb signature in the 206-208-204 Pb diagram,

then an additional constraint, that of low Th/Pb ratio, can be imposed on the chemistry of the contaminant. Among the geologically viable contaminants, lower crustal rocks will generally have low U/Pb and high Th/U whereas K-feldspars from the upper crust will generally have low U/Pb and Th/Pb. The identification of the type of crustal contaminant is not very easy due to the difficulties involved in a choice for a reference point for 208/204 Pb ratios. However the relative positions of A-46 and A-47, with respect to the Ararat array in the 208-206-204 Pb diagram, appear to indicate that the contaminant does not have an unusually high Th/U ratio.

Although crustal contamination of the Ararat lavas cannot be ruled out, and indeed occurs to a certain extend (as will be clarified in the magma mixing section), it is highly unlikely to be the principal cause of the observed isotopic variations, which are considered to reflect mixing of magmas.

1.6.2 Fractional Crystallization

Because of the phenochryst rich nature of calc-alkaline rocks, in general, fractional crystallization certainly plays a role in their petrogenesis. After an extensive review Gill (1981) concluded that the POAM fractionation (plag.+opx/olivine+augite+magnetite) is the most common process in the petrogenesis of orogenic andesites.

Lambert et al., (1974), based on their major and trace element study of the Ararat lavas, have concluded that garnet and extensive amphibole fractionation (up to 40%) could generate the Ararat lavas. They also distinguished two different series with respect to the major and trace element characteristics of the Ararat lavas (High-Y and Low-Y series). However, their classification does not correspond one to one with the different series described in this paper (e.g. In the Low-Y series, HA-basalts, Little Ararat rocks

and some Old Ararat lavas have been grouped altogether). Lambert et al.,(1974) account for the differences in trace element characteristics between the Low-Y and High-Y series by suggesting that, following an early stage of garnet fractionation, amphibole fractionation under hydrous conditions in a magma chamber generates the Low-Y series and, after the loss of volatiles, the remaining magma follows a liquid line of descent outside of the hornblende stability field, forming the High-Y series.

However, this model has several serious problems. First of all, no horblende and/or garnet is found in the Ararat lavas. In fact, Lambert et al. (1974) postulated the garnet and amphibole fractionation based on the presence of glomeroporphyritic aggregates (crystal clots) composed of plag+opx+oxide, and "an isolated crystal of resorbed brown hornblende" that they found in only one dacite sample. Although the overall major element compositions of some crystal clots may be analogous to the composition of garnet or amphibole, they are generally interpreted as cognate-primary igneous phase assemblages and not the products of mineral reactions with melt (Garcia & Jacobson, 1979; Luhr & Carmichael, 1980). Some amphiboles in andesitic and dacitic rocks do display a breakdown reaction of amphibole = plag+cpx+opx+mag, but these aggregates, unlike those of the clots, typically have a relict amphibole crystal outline and a fine-grained texture (Kuno, 1950; Luhr & Carmichael, 1980).

At first glance, amphibole fractionation has certain appealing aspects in the petrogenesis of calc-alkaline rocks, in terms of suppressing Fe-enrichment (tholeiite trend) and lowering presumed higher K/Rb ratios of parental basaltic magmas in the direction of more siliceous compositions (Yoder & Tilley, 1962; Shaw, 1968; Cawthorn & O'Hara, 1976; Boettcher, 1977). These effects derive from the high Fe/Mg ratios of amphibole and a distribution coefficient for K in amphibole which is about six times higher than that for Rb (0.33 and 0.05 respectively, Philpotts & Schnetzler, 1970).

Assuming about a four to sixfold difference in the distribution coefficients of K and Rb, 40% amphibole crystallization would cause a 15-20% decrease in K/Rb ratio and 50% increase in K content. Consideration of possible changes in the partitioning behaviour of these elements in the course of fractional crystallization, and the assumption of some crustal contamination, may lead to a more efficient decrease in K/Rb ratio. The observed twofold difference in K/Rb ratios of the HA basalts, and the positive linear trend of K/Rb versus K at practically constant SiO2 content simply cannot be generated by amphibole fractionation alone. A smooth decline in K/Rb ratio accompanied by an increase in K2O would be expected of amphibole fractionation, whereas the Ararat lavas define completely distinct fields and trends with no indication of amphibole fractionation. They also exhibit an overall increase in K/Rb ratios with time, as indicated by consecutive lava flows (e.g. A-30-1 to A-20-12). Moreover, extensive amphibole and/or garnet fractionation would have profound effects on the REE patterns of the Ararat lavas, because partition coefficient patterns of amphiboles for andesitic and more silicic compositions exhibit convex upward patterns, having negative Eu anomalies and values greater than unity for the middle to HREE (Nagasawa & Schnetzler, 1971; Arth, 1976; Nicholls & Harris, 1980). Garnets are capable of strongly fractionating the light and heavy REE (by exclusively incorporating HREE and excluding LREE from their structure) (Irving & Frey, 1978; Shimizu & Kushiro, 1975; Nicholls & Harris, 1980; Apted & Boettcher, 1981). Thus, liquids derived by large amounts of amphibole fractionation will have concave upward REE patterns with positive Eu anomalies relative to the parental magma. The REE distributions of the Ararat lavas show no hint of such a pattern (Figure-1.14). In fact, on this basis Escobar et al.(1977) noted that "no andesitic rocks have trace element features that could be explained by extensive amphibole loss from geographically associated island arc tholeiites or high alumina basalts". On the other hand, garnet fractionation would significantly deplete HREE and enrich LREE of the parental magma and produce liquids with fractionated REE patterns and high La/Yb ratios. With the exception of A-12

(Figure-1.14), the REE patterns of the Ararat lavas do not display such characteristics either. Although A-12 has a high La/Yb ratio (=18.25, Table 1-2), it shows an overall depletion in REE with a negative Eu anomaly. Assuming the HA basalts as a parental magma, a crossover of REE patterns would be expected between HA basalts and A-12 as a result of garnet and/or amphibole fractionation. It may be plausible to generate the REE pattern of A-12 by a number of combinations of POAM (plag+olivine/opx+augite+magnetite)+-garnet+zircon+apatite fractionation. However this solution is not unique, and more importantly, is not consistent with the isotope characteristics of the Little Ararat lavas.

1.6.3 Magma Mixing

The increasing application of integrated geochemical studies (petrographic analysis, major, trace element and isotope studies) on the same set of samples have shifted the long standing magma mixing controversy towards the acceptance of the viability of magma mixing in igneous petrology (see the reviews of Anderson, 1976; McBirney, 1980). Calc-alkaline rocks, in general, contain abundant petrographic evidence indicative of magma mixing, such as disequilibrium among phenocrysts (e.g. assemblages of calcic and sodic plagioclase, iron rich hyperstene and iron poor augite, magnesian olivine and quartz, resorption of phenocrysts, compositional zoning of minerals in opposite trends etc.), and the presence of glass inclusions with widely varying compositions (Kuno, 1950; Eichelberger, 1975; Anderson, 1976; Sparks et al., 1977; Sakuyama, 1979; Grove et al., 1982). Also, the failure to obtain consistent observed and calculated trace element abundances and ratios by simple fractional crystallization and partial melting models (especially when the observed abundances are higher for both incompatible and compatible element abundances) may be partly due to magma mixing processes. Based on this fact, O'Hara (1977) has proposed a model involving fractionation of a magma in a

repeatedly-filled magma chamber, in an attempt to account for large differences in trace element abundances. Magma mixing is not only suggested for calc-alkaline rocks, but also for MORB (Rhodes et al., 1979), Hawaiian basalts (Wright & Fiske, 1971; Chen & Frey, 1983) and large stratiform intrusions, such as the Muscox intrusion, where the formation of monomineralic chromitite bands has been succesfully explained by magma mixing (Irvine, 1977). Although the most likely place for magma mixing to occur is in a magma chamber; it can also take place during the ascent of mantle plumes or diapirs by mixing of incipient melts derived from wall rocks with the partial melt derived from the rising mantle diapir or plume, as suggested by Chen & Frey (1983).

Depending on the actual process magma mixing may or may not be diagnosed by using isotopic tracers. If magma mixing takes place in a magma chamber in which an uncontaminated, differentiated magma mixes with a more primitive magma derived from the same mantle source, no isotopic evidence indicative of magma mixing will be obtained. However, if differentiation is accompanied by crustal contamination and magma mixing takes place between contaminated, differentiated magma and more primitive magma, derived from the same mantle source, then isotopic data along with petrographic and trace element evidence for magma mixing can be used for modelling contamination and magma mixing processes. Note that in this case additional evidence, other than isotopic data, is required to indicate magma mixing. If eruption takes place after differentiation of the mixed magma, major element evidence for magma mixing (e.g. linear trends in the Harker variation diagrams) may be obscured by the fractional crystallization process. However, if it can be assumed that each new input of magma to the magma chamber causes eruption, then additional evidence for magma mixing may not be necessary and magma mixing can be viewed as a very common process. A third possibility, for which isotopes can provide evidence, is the mixing of magmas derived from isotopically distinct mantle sources. Of course, any combination or permutation of the above is also possible.

In the last two decades, geochemical literature has witnessed a significant development in the quantitative theoretical modelling of the above processes with increasing sophistication (Faure, 1977, Ch. 7 and it's references; Vollmer, 1976; O'Hara, 1977; Langmuir et al., 1978; Allegre & Minster, 1978; Briqueu and Lancelot, 1979; Taylor, 1980; DePaolo, 1981; O'Hara & Mathews, 1981). As emphasized by Langmuir et al. (1978), in the ideal case of two-component magma mixing all of the elemental and isotopic data for a suite of samples must be consistent with mixing, and the relative positions of samples on all plots must be the same. However, it should not be forgotten that in nature hardly anything is ideal and more than one process may operate simultaneously, such as some of the examples given above, for which even the end-member compositions may change. So the complications of nature may destroy some of the relationships expected for the ideal case. Keeping in mind all of the above points, we can go back to the Ararat data and evaluate magma mixing in detail.

The Ararat samples contain abundant petrographic evidence indicative of magma mixing, such as the presence of at least two types of plagioclase with different anorthite contents, signs of resorption among phenocryst phases, the presence of calcic plagioclase in rhyolites, and possible compositional differences in the glass inclusions. This latter possibility has not yet been proven by microprobe analysis, but the first three points have been confirmed by preliminary electron microprobe analysis (Lambert et al., 1974). Despite the detailed the description of these disequilibrium features among phenocrysts, Lambert et al., (1974) have not recognized magma mixing in the petrogenesis of the Ararat lavas.

The geochemical evidence that implies or, is consistent with magma mixing for the Ararat lavas can be summarized as following:

1. The linear trends defined by each Ararat series in the major element variation diagrams (Figure-1.4, 1.5) and in the AFM diagram (Figure-1.6).
2. The broad linear trends obtained in the Ba and Rb vs SiO2 diagrams, despite of disturbances due to fractional crystallization (Figure-1.7; note the elevated Ba and Rb contents of A-46 and A-48 with respect to the Little Ararat trend possibly due to crustal contamination).
3. The positive correlation between K/Rb ratio and K2O for the HA Basalts, with a progressive increase in K/Rb ratio with age progression (Figure-1.8).
4. The impressive linear trends obtained in the Zr/Ni vs 100/Ni and Zr/V vs 100/V companion plots and their convergence towards a common point (Figure-1.11).
5. The rotation of the chondrite normalized REE pattern of A-30-1, pivoting around the normalized Tb abundance with age progression (Figure-1.15).
6. The covariation of La/Yb ratio with Mg#, La, and Zr abundances indicating different magma mixing relations for each of the Ararat series (Figure-1.16, 1.17).
7. Correlated variation of all the isotopes (Sr, Nd, Pb) with each other, as well as with the major and trace elements (Figure-1.18 to 1.23).

After recognition of the above facts, which indicate that magma mixing processes are responsible for the generation of the different volcanic suites, it is possible to investigate the details of magma mixing processes and estimate the end-member compositions.

After numerous combinations and permutations among the isotopic ratios, trace element ratios and abundances different diagrams were constructed. It is found that six compositionally distinct end-members are responsible for the generation of four distinct trends that represent volcanologically and geochemically coherent four Ararat suites. The compositions of the five end-members have been estimated utilizing various diagrams by taking advantage of hyperbolic magma mixing trends, their asymptotic values and inter-

cepts between two curves. The estimated compositions are listed in Table-1.4. The composition of end-member #6 has not been estimated due to the scattered nature of the Old Ararat Series data. However, it represents a more fractionated and contaminated version of the end-member #3.

One of the best plots to use to test for mixing, are companion plots (i.e. both axes have the same denominator), because on companion plots mixing forms linear trends. Although end-member compositions are constrained to lie along the linear trends on companion plots, it may not be possible to obtain end-member compositions using only one linear trend. However, if more than one linear trend converge towards a common point indicating a common end-member, then it is possible to obtain the composition of that particular end-member. For example using Figure-1.21a, it is possible to obtain the Nd abundance and Nd 143/144 ratio of one end-member by taking advantage of the convergence of more than one linear trends. This, in turn provides an opportunity for the estimation of the Sr 87/86 and Pb isotope ratios of this end-member using isotope ratio versus isotope ratio plots, since they are correlated.

In addition to the linear trends and their intercepts on companion plots, hyperbolic mixing curves obtained from plots involving ratio versus ratio and ratio versus element variations may provide additional constraints on the end-member compositions. The curvature of the mixing hyperbola is determined by the r coefficient which, in turn, is determined by the composition of the end-members (Langmuir et al., 1978). The asymptotic nature of a mixing curve can be used to determine either a minimum or maximum value for one of the ratios in each end-member. End-member compositions are better constrained when the r value is either too small or too large relative to 1.

Table 1-4

ESTIMATED END MEMBER COMPOSITIONS

	(1)	(2)	(3)	(4)	(5)
Sr 87/86	0.70470	0.70385	0.70375	0.70455	0.70330
Nd 143/144	0.51272	0.51294	0.51294	0.51281	0.51300
Pb 206/204	19.00	18.81	18.87	18.99	18.90
Pb 207/204	15.68	15.55	15.59	15.63	15.59
Pb 208/204	39.10	38.65	38.80	39.05	38.80
Rb/Sr	0.025	0.12	0.20-0.23	0.05-0.07	0.02
Sm/Nd	0.19	0.23	0.22	0.19-0.20	0.26
Sr/Nd	26	39-40	15-16	25	23-24
La/Yb	8-9	20	8-9	15-16	4
Zr/Nb	13	14	27	11	32
K/Rb	770	250	260	500	320
K	15-16K	11-12K	17-18K	15K	2-3K
Rb	15-20	45-55	65-70	25-35	7-9
Sr	750-800	300-350	325	700	400
La	21	13-14	22	36	10-11
Nd	30	9	19-20	28	17
Sm	5.7	1.9-2.0	4.2	5.5	4.3-4.4
Yb	2.3	0.67	2.75	2.25	2.75
Zr	165	120	265	175	170
Nb	13	8-9	9-10	16	5-6

La/Yb ratios are plotted against Mg# in Figure-1.24. The trends of four Ararat series are clearly separated from each other. The approximate fields of the end-members are also shown. Hereafter the end-members will be referred according to the numbers assigned them in this figure. The Old Ararat and Ararat series trends converge towards a common end-member, similarly the Little Ararat and HA basalt series trends also converge towards another common end-member. The La/Yb ratios of these convergent points are approximately 8-9 for the end-member #1 and 15-16 for the end-member #4. The La/Yb ratios of the other end-members are not as well-constrained as the #1 and #4, but can be roughly inferred assuming that the compositions of the samples that plot in the extreme end of the different trends, closely approximate the compositions of the corresponding end-members. Thus, La/Yb ratios of 20 for #2, 8-9 for #3, 4 for #5 and 12 for #6 were obtained. The validity of the inferred La/Yb ratios of the end-members can be further tested by plotting La/Yb ratios against some other variables.

In Figure-1.25 La/Yb ratios are plotted against Zr/Nb ratios. The end-member fields are also shown on this plot. The independently obtained La/Yb ratios for the end-members from this diagram are identical to the ones that were obtained from the La/Yb versus Mg# plot. This consistency not only confirms the validity of the inferred La/Yb ratios for the end-members, but also makes it possible to estimate the corresponding Zr/Nb ratios of the end-members (see Table-1.4). It is also possible to estimate the abundances of La and Yb of the end-members by using the estimated La/Yb ratios and by plotting La/Yb ratios of Ararat samples against La abundances (Figure-1.16b).

The estimated La/Yb ratios of the end-members can be further tested by using Nd 143/144 versus La/Yb plot (Figure-1.26). This plot has two additional advantages over the two previous plots (La/Yb vs Mg# and vs Zr/Nb). Nd 143/144 ratios do not change with simple partial melting and fractional crystallization processes. In addition, Nd

Figure-1.24

La/Yb versus Mg# plot for the Ararat samples.

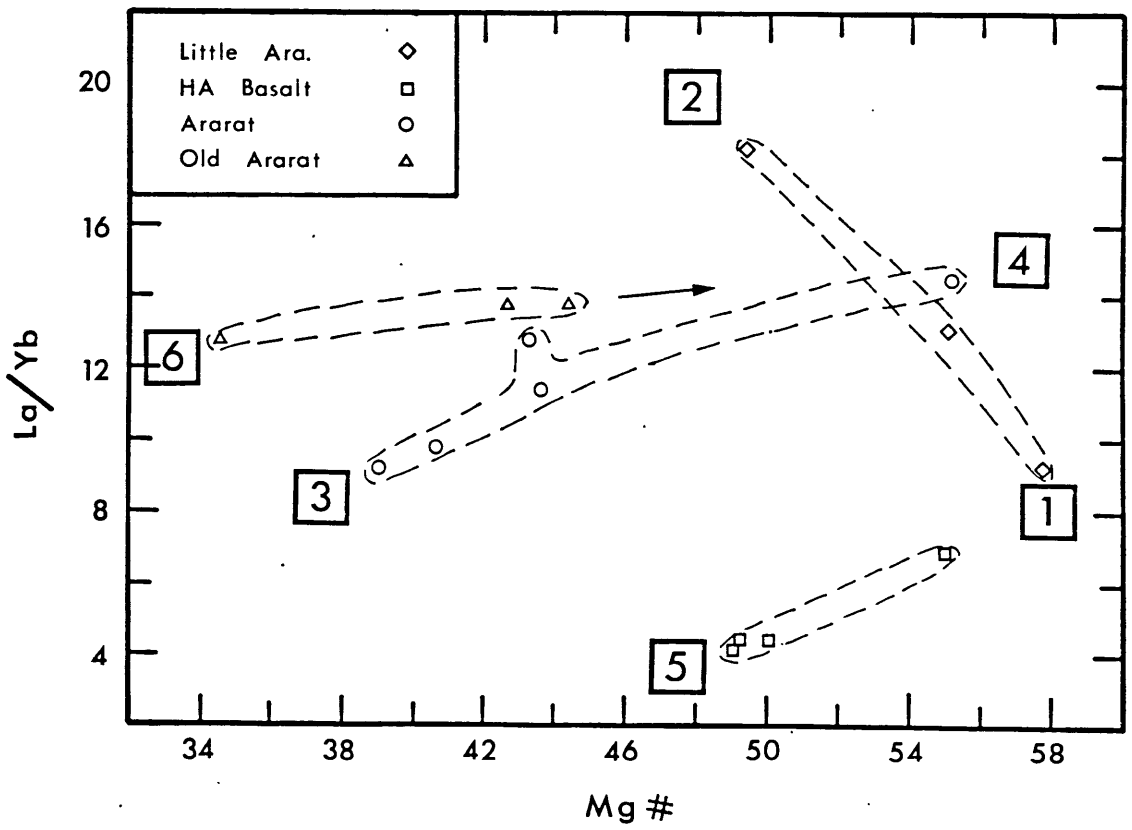
Little Ara.
HA Basalt
Ararat
Old Ararat
20
16
12
8
4
La/Yb
34
38
42
46
50
54
58
Mg #
1
2
3
4
5
6

Figure-1.25

Plot of La/Yb versus Zr/Nb for the Ararat lavas. This diagram illustrates the magma mixing relations among the different end-members (indicated by numbers) in the generation of Ararat suites.

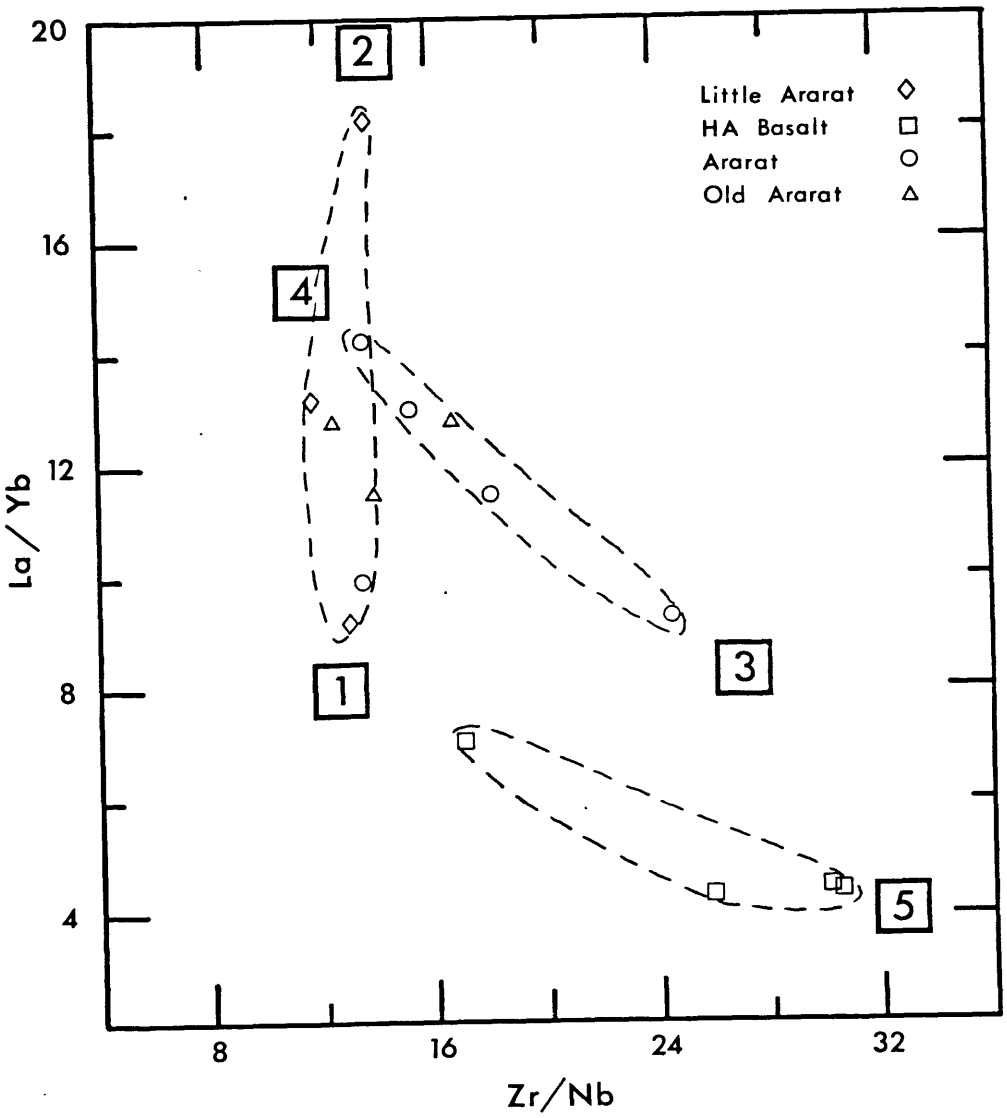
20
16
12
8
4
La/Yb
8
16
24
32
Zr/Nb
1
2
3
4
5
Little Ararat
HA Basalt
Ararat
Old Ararat

Figure-1.26

Plot of Nd 143/144 versus La/Yb for the Ararat lavas. The approximate end-member fields that generate the Ararat suites by two component magma-mixing are also shown. Numbers refer to the different end-members (see Table 1.4). (for further explanations see the text).

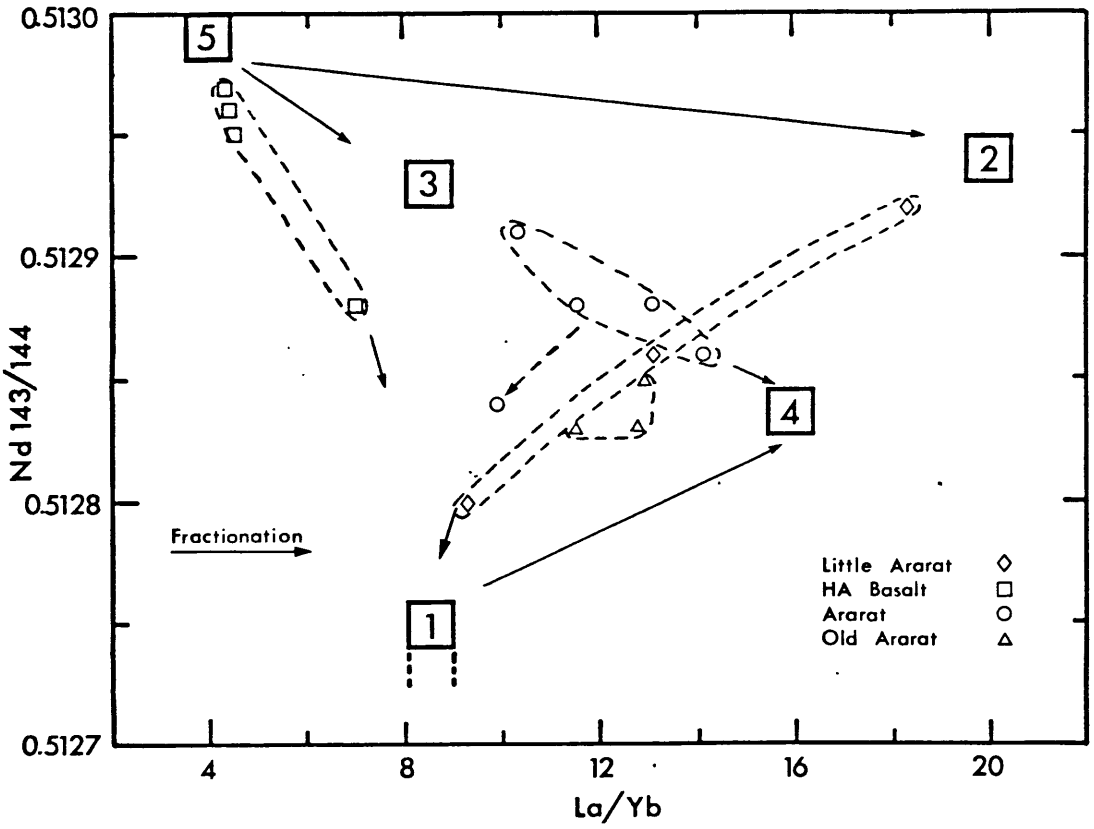
0.5130
0.5129
0.5128
0.5127
Nd 143/144
4
8
12
16
20
La/Yb
5
2
3
4
1
Fractionation
Little Ararat
HA Basalt
Ararat
Old Ararat

143/144 ratios of the end-members are also constrained by the Nd 143/144 versus 100/Nd plot (Figure-1.21a). If end-member compositions obtained from the different trends formed by the Ararat suites on this plot are consistent with the ones obtained from Nd 143/144 vs 100/Nd, La/Yb vs Mg# and La/Yb vs Zr/Nb, then the estimated end-member La/Yb, Zr/Nb, Nd 143/144 ratios and Nd, La, Yb abundances can be assumed to be constrained very well. The investigation of Figure-1.26 reveals that the obtained end-member compositions on this plot are all consistent with the other diagrams mentioned above. These consistent and coherent relations which involve a number of independent geochemical parameters convincingly indicate the reliability of the estimated end-member compositions and the existence of magma mixing processes which produce the observed distinct trends involving these end-members.

Similarly the end-member compositions listed in Table-1.4 were obtained by choosing one geochemical parameter at a time and studying its variation with other geochemical parameters (trace element abundances and ratios, isotope ratios) and by testing the consistency of the different trends formed by the Ararat suites as well as the inferred end-member compositions.

The interpretation of two plots require special explanation. The Sr 87/86 ratio vs 100/Sr variation of the Ararat lavas was presented previously in Figure-1.19. The extrapolation of the well-defined linear trend of the HA basalts towards the estimated Sr 87/86 ratio of end-member #1 (=0.70470) gives an unreasonably high Sr abundance of 3000 ppm. for this end-member. This unreasonably high Sr content may indicate simultaneous operation of a second process along with magma mixing, possibly fractional crystallization. However, Sr has to behave as an incompatible element during fractionation, which in turn implies that plagioclase cannot take part in this process. Experimental studies carried out by Yoder & Tilley (1962) demonstrated a major effect

of water pressure in depressing the crystallization field of plagioclase relative to the ferromagnesian minerals. Using the equations of De Paolo (1981) for magma mixing-fractionation and using the estimated Nd and Sr isotopic compositions of end-members 1 and 5 and the Sr and Nd abundances for end-member 5, a Sr abundance (800ppm.) has been estimated for end-member 1. In Figure-1.27, the results of the calculated and observed Sr isotopic ratios and abundances are illustrated for the Ararat HA basalts.

Although the fit between the observed and the calculated Sr isotopic ratios and abundances are quite good (Figure-1.27), this process does not seem to be reasonable. First, the assumed ratio of the rate of magma mixing to fractional crystallization is very low. Second, the observed difference in the Zr content from A-30-1 to A-30-12 is about 4-6 ppm. which is low with respect to the required amount of plagioclase-free fractional crystallization, unless Zr the abundance is buffered by an unknown fractionating phase. In fact, this inconsistency probably requires an additional process, along with magma mixing, and fractionation. Based on the estimated end-member Nd isotopic compositions and abundances, a mixture of 25% of end-member #1 and 75% of end-member #5, should duplicate the Sr isotopic composition and abundance of A-30-12 (0.70376 and 566ppm.) respectively. However, using the same magma mixing percentages that are obtained from Nd, and the estimated Sr isotopic compositions and abundances for end-members #1 and #5, values of 0.70386 and 500ppm are obtained. The calculated Sr isotopic ratio is more radiogenic and the Sr abundance is higher than the observed composition for A-30-12. This independent check of magma mixing relations and possible plagioclase effects using Nd can be considered reliable, because the plagioclase/liquid distribution coefficient for Nd is quite low. Probably the best way out of this Sr inconsistency is to assume that the new batch of magma which enters the magma chamber resorbs some plagioclase from the existing cumulates in the magma chamber. This proc-

Figure-1.27

Diagram comparing the observed and calculated Sr isotope compositions and Sr abundances of the HA basalts. The curve indicated by "Simple mixing" was obtained by modelling two-component magma mixing using the end-member compositions of #1 and #5. The tick marks indicate the percentage of end-member #1 in the mixture.

The other two curves, which best fit the data, were obtained by modelling the simultaneous operation of two-component magma mixing and fractional crystallization (without plagioclase). The tick marks indicate the mass fraction of the magma that remains in the magma chamber. In this model, the compositions of end-members #1 and #5 were used along with bulk distribution coefficients of 0.25 and 0.15 for Sr and a value of 0.8 for r (the ratio of magma mixing to fractional crystallization). Although this model accounts well for Sr isotopic composition and Sr abundance, it fails to explain the Zr abundances.

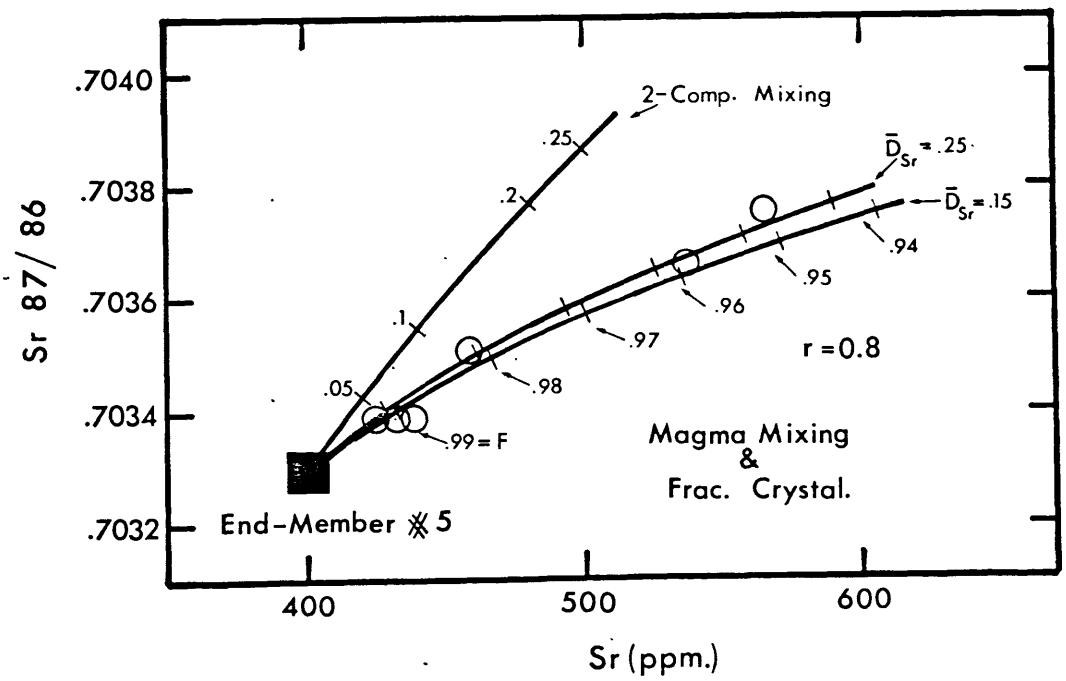
.7040
.7038
.7036
.7034
.7032
Sr 87/ 86
400
500
600
Sr (ppm.)
2-Comp. Mixing
.25
.2
.1
.05
.99 = F
.98
.97
.96
.95
.94
$\bar{D}_{Sr}$ = .25
$\bar{D}_{Sr}$ = .15
r = 0.8
Magma Mixing
&
Frac. Crystal.
End-Member ※ 5

ess is not only geologically reasonable, but also capable of explaining the less radiogenic Sr isotopic composition and higher Sr abundance observed for A-30-12, compared to that expected. Probably the best way to describe this process is to refer to it as "assimilation of cumulates". If this process is a ubiquitous one, then the potential dangers of extrapolating linear trends on isotopic ratio versus reciprocal concentration plots (especially for Sr) to obtain end-member compositions, should be emphasized. This process can also account for the lack of convergence on the Sr 87/86 versus 100/Sr diagram towards the common end-member #1, for the Little Ararat and HA basalt series trends (Figure-1.19b).

In Figure-1.28 the covariation of Pb 206/204 ratios with Nd 143/144 and Sr 87/86 ratios are shown. Since these diagrams only involve isotopic ratios, the positions of the end-members are not affected by simple fractional crystallization. Magma mixing trajectories are indicated by the dashed lines connecting the various end-members. One point of significance on these diagrams is the observed shifts of end-members #2 and #3 in the direction of unradiogenic Pb 206/204 and Nd 143/144 and radiogenic Sr 87/86 values; possible paths are shown with arrows. These shifts may be indicative of crustal contamination effects during the derivation of the distinct end-members #2 and #3, from a common mantle-derived end-member (#5). However, the magma mixing trends of the Ararat series (between #3 and #4) and the HA basalt series (between #1 and #5) are not affected by crustal contamination.

It has become clear from the data presented so far that there are two main mantle derived magmas, represented by the the two end-members (#1 and #5) and that the remaining four end-members (#2, #3, #4 and #6) are derivatives of them (or derivatives of their equivalents). These latter end-members (#2, #3, #4 and #6) are apparently the result of the interplay between differentiation, crustal contamination and possibly assim-

Figure-1.28

Diagram providing a close-up look at the correlated variations among Nd 143/144, Sr 87/86, and Pb 206/204 ratios for the Ararat lavas. Approximate locations of the end-members, along with possible mixing trends, are also indicated. Arrows indicate possible trajectories for obtaining end-members #3 and #2 from #5, unless they represent totally independent mantle derived magmas. (Further explanations are in the text).

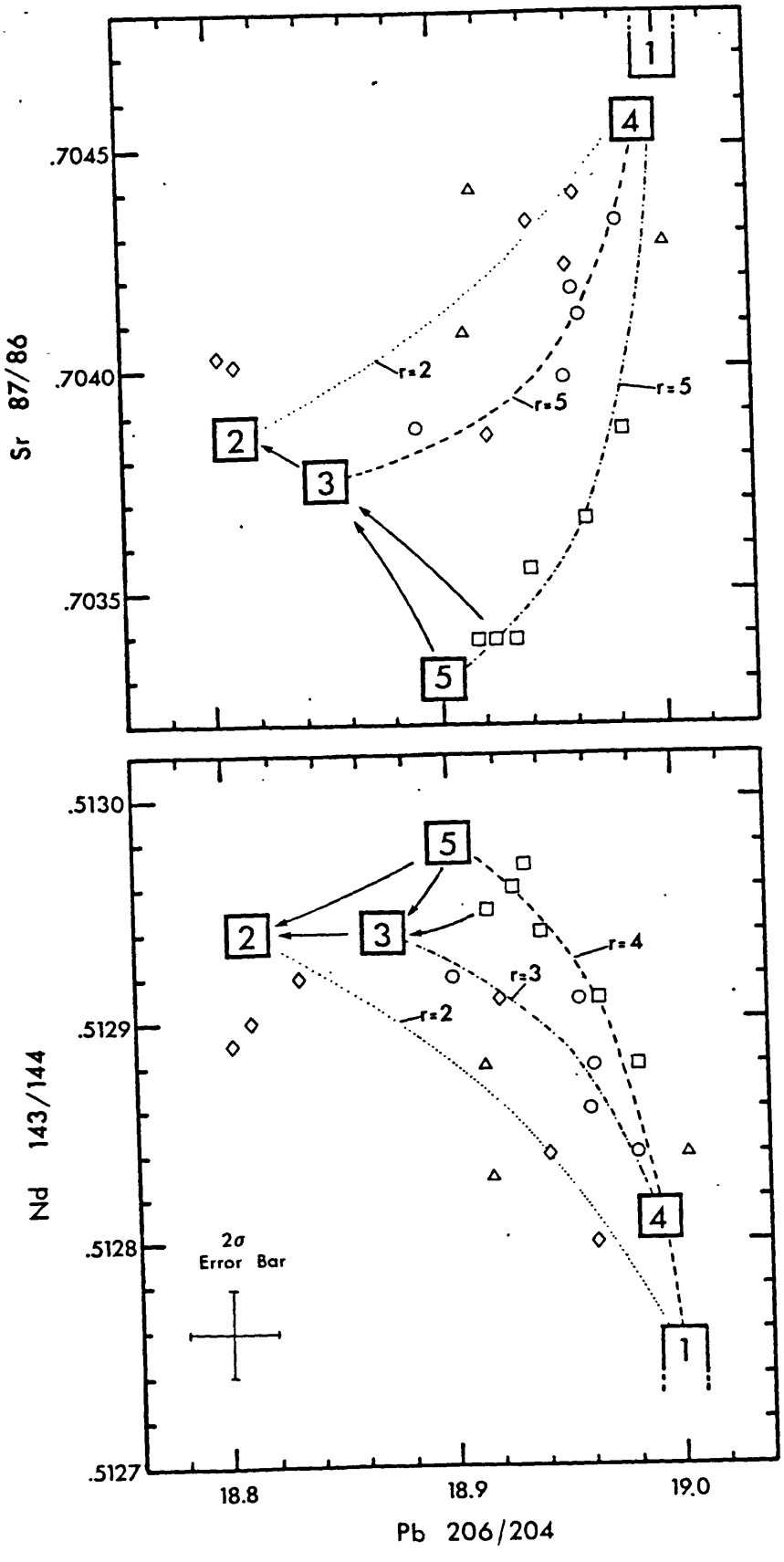
1
4
.7045
.7040
.7035
Sr 87/86
r=2
r=5
r=5
2
3
5
.5130
.5129
.5128
.5127
Nd 143/144
5
2
3
r=4
r=3
r=2
2σ
Error Bar
4
1
18.8
18.9
19.0
Pb 206/204

ilation of the existing cumulates within the magma chamber. End-members #2, #3, and #6 are derived from end-member #5, and end-member #4 is derived from end-member #1. The above interpretation is not in conflict with the statements made in the crustal contamination section, because the within-suite variations, that form the magma mixing trends are not directly related to crustal contamination. However, the actual process that creates the derivative end-members (#2, #3 and #6) involves crustal contamination, as well as differentiation.

Based on the end member compositions (Table-1.4), the HA basalts represent mixtures of end-members #5 and #1 (up to 30%). The Ararat Series can be generated by mixing #3 and #4 (up to 35%). The compositions of the Little Ararat Series can be obtained by mixing end-member #2 and #1 (up to 40%).

1.6.4 Mantle Source Characteristics

Although the demonstration of magma mixing between two isotopically distinct mantle derived magmas and, as a result, the observed correlated variations among Sr, Nd, and Pb isotope systems, clearly indicate that isotopic mantle heterogeneities exist beneath Ararat; the processes (magma versus mantle mixing), the timing (old versus recent), and the scale (large versus small) involved in the creation of these heterogeneities need to be further evaluated.

Conceptually, a number of permutations of the above parameters can be responsible for the creation of mantle heterogeneities (Zindler et al., 1979). In the following discussion, only the Ararat HA basalts will be considered, but the conclusions reached apply equally to the other Ararat suites, for the reasons given previously. Consideration of the large range observed in Pb 206/204 ratios along with the very steep slope on the Pb-Pb diagrams (Figure-1.22), automatically eliminates the possibility of young differentiation events, involving only the mantle, in the formation of the heterogeneities. Also, the existence of mixing trends between the two end members (#1 and #5), including all kinds of combinations of compatible and incompatible elements, eliminates the possibility of solid state mantle mixing (Langmuir et al., 1979). Finally, the eruption sequence of the lavas, which become increasingly enriched in isotopic characteristics, makes small scale heterogeneities (smaller than the melting scale) higly unlikely. For example, consider a mantle segment that is variably veined by an enriched end member. When partially melted, the first melts will be produced preferentially from the segments that have the highest vein/mantle ratios and carry the isotopic signatures of the enriched end member. Besides, once the case for magma mixing is established, models involving small scale heterogeneity (smaller than the melting scale) are eliminated automatically.

After the elimination of the above possibilities, the only permutation left is the large scale (~30km., chosen somewhat arbitrarily, but may be considered a good approximation for the melting scale), old (~200 m.y.), mixing of magmas, which corresponds to the LOM model of Zindler et al.,(1979). This model depicts a long-term mantle heterogeneity which exists between two separate mantle boxes. The depleted box is shallower than the enriched box. The oldest lavas originate from the shallow-depleted segment. The melts derived from this segment get contaminated at an increasing rate by the melts derived from the lower-enriched segment.

Being consistent with the parameters describing the heterogeneity (LOM) in the widest sense, a variant of the above model would be the contamination of the depleted mantle, not by an enriched mantle, but by sediment components, as suggested by the Ararat array which diverges significantly from the oceanic mantle trend on the 206-207-204 Pb diagram (Figure-1.22). Similar high-sloped divergent trends observed in other arc settings, are interpreted as being caused by contributions from subducted sediments, either in the form of partial melts or fluids carrying their isotope signatures (Tatsumoto, 1969; Kay et al.,1978; Sun, 1980; Morris et al., 1982; Barreiro, 1983; Davidson, 1983). However, the Ararat HA basalt data is not consistent with this model, because, the HA basalts plot right along the "oceanic regression line" on the Nd-Sr isotope correlation diagram (Figure-1.20). Mixing trends between sediments and depleted mantle end members that can create the observed range in the Nd 143/144 ratios would also cause a shift at least at the lower end of the Ararat HAB array towards more radiogenic Sr 87/86 values. Besides, positive correlations between compatible elements (such as Ni, Cr) and radiogenic Sr and Pb ratios are not consistent with a "typical" sediment contamination signature.

Once the sediment and crustal contamination possibilities are discounted, then the question is how can the observed isotopic characteristics of the Ararat lavas be generated within the mantle, and within the general framework of the LOM model.

End-member #5 (HA basalt end member) is apparently derived from a mantle that has had a time-integrated depletion in Rb/Sr and Nd/Sm ratios with respect to the bulk earth, as evidenced by its high Nd 143/144 and low Sr 87/86 relative to bulk earth. However, the LREE enriched patterns of the isotopically least enriched (least effected by magma mixing) Ararat HA basalts indicate a recent enrichment event (Figure-1.14). This end-member plots within the upper bound of the Pb oceanic array (Figure-1.22). It is within the radiogenic ends of the Tethian ophiolite fields. Considering the somewhat questionable degree of "purity" of this end-member (composition estimates are only an appproximation) and the somewhat anomalous isotope characteristics of the Tethian ophiolites (Hamelin et al., 1984), one may suggest that the mantle source of end-member #5 is analogous to the mantle sources of transitional MORB such as the Tethyan ophiolite source or continental arc basalts.

End-member #1 ("alkali basalt" end member) also appears to be derived from a mantle that has had a time-integrated depletion in Rb/Sr and Nd/Sm relative to bulk earth (but relatively enriched compared with end member #5). However the Pb isotopic composition of end-member #1 is quite radiogenic and similar to some of the OIB from the Indian Ocean (e.g. Crozet, Amsterdam; Figure-1.22).

Recent studies have suggested that magmas derived from ancient subducted oceanic crust or sediments can explain the rather anomalous isotopic characteristics of some of the OIB (Hofmann & White, 1980; Chase,1981; Zindler, et al., 1982; White & Hofmann, 1982; Kurz et al., 1982; Cohen & O'Nions, 1982; Dupre & Allegre, 1983). So, consistent

with the LOM heterogeneity model, magmas derived from an ancient subducted crust can potentially generate the Ararat end-member #1.

It is also interesting to note that paleomagnetic studies indicate that the "Turkish Plate" was part of the northern margin of Gondwanaland and in Permo-Triassic times (Lauer, 1982) was situated to the south of the present Arabian peninsula. If it is assumed that the thickening of the continental lithosphere by thermal accretion can create a stacked mantle memory (Brooks, et al., 1976; Allegre, 1982), then this mechanism may suggest the transportation of "Indian Ocean Signatures" to the site of Ararat. However, as suggested by Hart (1984), if the "Indian Ocean=DUPAL signatures" are confined only to the southern hemisphere, including continental volcanics, then another source with enriched U/Pb and depleted Rb/Sr and Nd/Sm characteristics may be required.

An alternative model, which depicts the presence of a depleted mantle, sediment-contaminated by a recent subduction process (not associated with the closure of the Bitlis-Zagros Ocean), is also capable of generating the isotopic composition of end member #1. Although it's polarity, location, and extent are still controversial, as a result of intense multi-orogenic deformation, geological evidence suggests that a Mid-Jurassic suture zone, formed by southward subduction, resulted in the elimination of the Paleo-Tethys (Khain, 1977; Sengor et al., 1980; Bergougnan & Fourquin, 1980). This suture zone can be traced as a discontinuous belt from southeastern Bulgaria, across northern Turkey, towards northeastern Iran. Melts derived from a mantle segment that was contaminated by sediments during the southward subduction of the Paleo-Tethys oceanic crust can potentially generate the isotopic characteristics of end member #1.

If the tectono-magmatic model proposed in Chapter 3 is correct, then the mantle source region for end member #5 should be shallower than that of end member #1. This

arrangement favors the second model, that is the mantle source of end member #1 is deeper and represents a mantle segment that was contaminated with sediments during a previous subduction event (during late Paleozoic-Early Mesozoic).

1.7 Conclusions

The Ararat volcano, which is one of the major calc-alkaline eruptive centers in the Tertiary to Quaternary volcanic province in eastern Turkey, is composed of mainly andesites, dacites and subordinate HA basalts, rhyolites.

Consistent with field observations, four eruptive suites have been distinguished on the basis of the major and trace element composition of the lavas. These are, from older to younger: Little Ararat, Old Ararat, High-Alumina Basalt, and Ararat series.

The wide ranges observed in the trace element compositions, as well as in Sr, Nd, and Pb isotopic compositions, are not consistent with the derivation of the different Ararat suites from a common parental magma through fractional crystallization. Also, within-suite compositional variations cannot be explained by fractional crystallization.

Various two-component magma mixing processes involving six end-members, that are derived from two distinct mantle-derived magmas by the interplay of fractional crystallization, limited crustal contamination and cumulate assimilation, can account for the major, trace, REE, and Sr, Nd, Pb isotopic composition of the Ararat lavas.

The HA basalt end-member (#5) has been derived from a mantle that has had a time-integrated depletion in Rb/Sr and Nd/Sm. This depleted mantle source is similar to that of continental arc basalts.

The "Alkali basalt" end member (#1) has been derived from a mantle source with relatively less depleted characteristics, but with quite radiogenic Pb 207/204 isotopic composition. Models involving both an ancient subducted oceanic crust source or a segment of depleted subcontinental mantle that has been contaminated by sediments (either in melt or fluid form) during a previous subduction event are considered plausible. However, considering all the geological and geochemical facts, the latter appears to be the most satisfactory petrogenetic model.

It is not possible to establish a convincing link between the subduction of the Bitlis-Zagros ocean crust and the Ararat volcanism. However, the assumption of a detached sinking slab following Miocene continental collision along the Bitlis-Zagros suture zone, can be viewed as a plausible trigger for the generation of the calc-alkaline magmas and their emplacement within the continental crust. The calc-alkaline volcanism may be maintained to present by the continued sinking and dehydration of this detached slab as well as by the continued tectonic deformations caused by continental collision (see the third chapter). This creates mantle upwelling which not only initiates the alkali volcanism, but also keeps the calc-alkaline volcanism alive.

Finally, I believe that this study demonstrates the power of detailed, comprehensive geochemical studies in revealing the complexities involved in geological processes, even among the products of one single volcano. This study suggests that geochemical characterization of a calc-alkaline volcano and it's mantle source is almost impossible with a few randomly collected samples.

CHAPTER 2

GEOCHEMISTRY OF THE ALKALINE VOLCANICS

2.1 Introduction

Alkaline volcanics are an integral part of the Tertiary to Quaternary volcanic province of eastern Turkey and northwest Iran. Alkaline products dominate the volcanics both as fissure lava flows and central volcanoes (Nemrut, Tendurek) in the Lake Van region (Figure-2.1). They consist of rocks ranging in composition from alkali basalts, through hawaiites, benmoreiites, mugearites and sodic trachytes to peralkaline commendites and pantellerites. The less differentiated compositions, hawaiites in particular, dominate the fissure lava flows and small spatter cones. The cone-forming lavas of Tendurek and Nemrut are more evolved and are mostly sodic trachytes. The most differentiated, silica oversaturated peralkaline compositions are dominant among the post-caldera products of Nemrut volcano.

The oldest age obtained by K/Ar dating of alkaline rocks is about 6my. b.p. in the Lake Van area (Innocenti et al. 1976, 1980). The most recent volcanic activity occurred in 1441, producing three small lava flows along a N-S trending radial fault that cuts the Nemrut caldera (Kanlitas flows, Oswald,1910). The presence of Eocene alkaline volcanics has been confirmed by K/Ar dating and paleontological studies of the associated sediments in the Azerbaijan region, northwest Iran (Comin-Chiramonti et al. 1978; Riou, 1979). Strongly undersaturated alkaline lavas (analcimites, phonolites, alkali basalts, trachytes) are interbedded with high-K calc-alkaline lavas in this region. Basanites post-date the Upper Miocene, high-K calc-alkaline volcanics, with 1.3-0.5 my. K/Ar ages in the Bijar region of Iran (Boccaletti et al. 1977). Although the presence of alkaline and calc-alkaline volcanics spanning an active period from Tertiary to present have been reported in the Caucasuses region (USSR), their volcanological and geochemical charecteristics have not been well-documented (Adamia et al. 1977; Koronovskii, 1979a,b).

Figure-2.1

Simplified geological map of the Lake Van area, showing the distribution of calc-alkaline and alkaline volcanics and major volcanoes. Key to the patterns: 1- Alkaline volcanic rocks, 2- Calc-alkaline volcanic rocks, 3- Neogene and Quaternary sedimentary deposits, 4- Pre-Neogene basement. Map after Innocenti et. al., 1976.

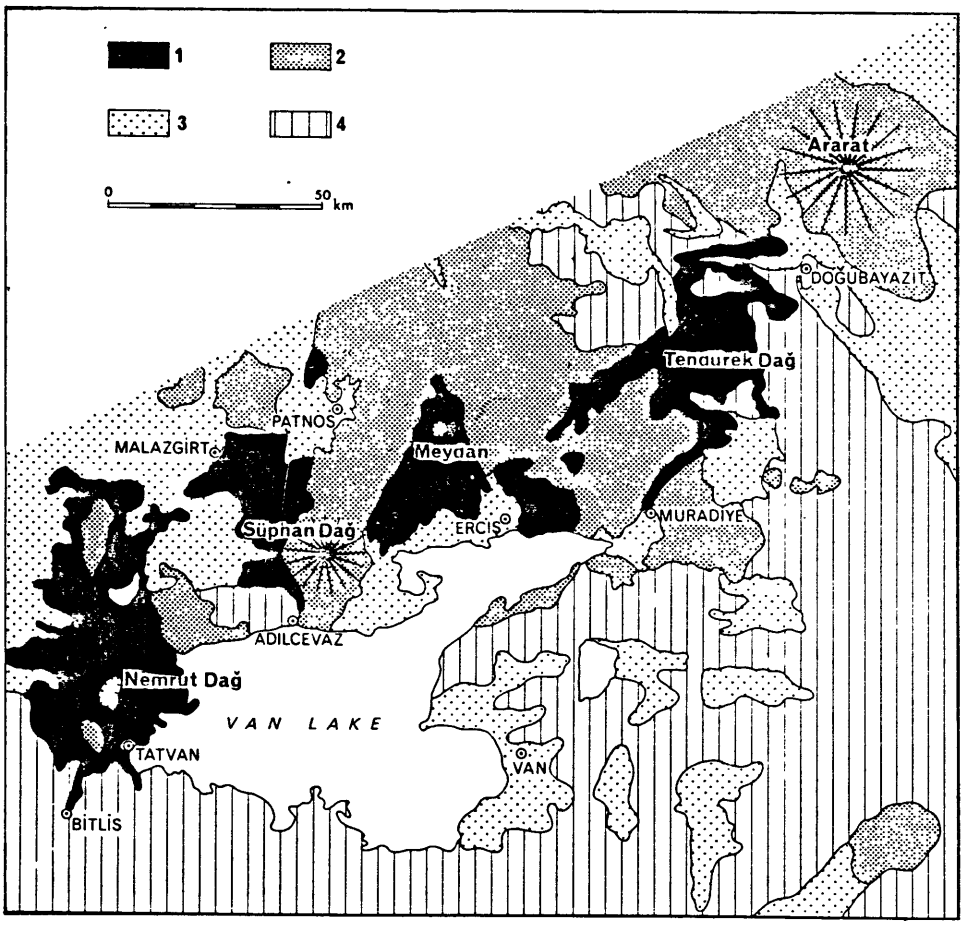
1
2
3
4
0
50 km
Ararat
DOGUBAYAZIT
Tendurek Dağ
PATNOS
MALAZGIRT
Meydan
Süphan Dağ
ERCIS
MURADIYE
ADILCEVAZ
Nemrut Dağ
VAN LAKE
TATVAN
VAN
BITLIS

2.2 Description of major volcanoes and fissure lavas

2.2.1 Tendurek Volcano

Tendurek volcano is situated about 50 km. to the southwest of Ararat volcano (Figure-2.1). A number of scattered spatter cones which produced mainly basaltic lava flows and basaltic scoria, represent the earliest phase of Tendurek volcano. Tendurek is a composite volcano which has two cones that are 4,5 km. apart. They both have small craters. Fumerolic activity is still present in the western crater. A small lake occupies the eastern crater. The cones were formed during the main phase of volcanic activity and produced mainly differentiated, sodic-trachytes. The main phase of activity also produced some silica oversaturated peralkaline lava flows and minor pyroclastics. Although a number of radial and circular concentric faults have been observed, that surround the two Tendurek cones, indicating the initial stages of a huge (ca. 10 km. diameter) caldera formation. The caldera has not fully developed and collapsed. However, these features indicate the presence of a large-shallow magma chamber beneath Tendurek.

2.2.2 Nemrut Volcano

Nemrut volcano is situated on the western shore of Lake Van. The main cone is composed largely of trachyte lava flows. A huge caldera ($\sim$8 km. diameter) dominates the upper portion of the volcano. The walls of the caldera were formed by ring faults and are cut by several radial faults. The eastern half of the caldera is filled with highly differentiated peralkaline lava flows, domes and pumice deposits representing post-caldera activity. The semicircular Nemrut Lake occupies the western half of the caldera. Nemrut volcano is surrounded by an extensive ignimbrite cover (400 sq. km.) which also contains pumice intercalations. Post-caldera peralkaline lava flows are also present on the flanks

of the volcano. The latest activity of Nemrut is represented by olivine-basalt lava flows which erupted through N-S trending radial faults on the northern flank of the volcano. Oswald (1910) reported that the latest eruptions occurred in 1441. A number of independent, relatively small, eruptive centers scattered in the immediate vicinity of Nemrut volcano also produced basaltic lava flows.

2.2.3 Fissure Lavas

Alkaline products are mainly represented by fissure lava flows and small cinder cones in the area to the north of Lake Van, between Nemrut and Tendurek volcanoes. Fissure volcanic activity started about 6 my. ago and continued up to Quaternary times. The calc-alkaline lava flows of Suphan volcano overlie surrounding alkaline fissure lavas. Fissure lavas contain the least differentiated compositions and were erupted through a network of NW-SE and NE-SW trending faults (see Chapter-3 for the details of tectonics and geology). These lavas form small volcanic plateaus which are localized along fault zones, and roughly conform the fault trends.

2.3 Petrography

Alkali basalts contain small amounts of phenocrysts (5%), consisting of calcic plagioclase and olivine (Fo 75-70). The quoted compositions are from the EMP work of Innocenti et al., (1980). The groundmass consists of zoned plagioclase, clinopyroxene ($Wo_{47}Fs_{42}En_{42}$-$Wo_{45}Fs_{16}En_{39}$), olivine (Fo70-60), Ti-magnetite and ilmenite. The phenocryst contents gradually increase going from hawaiites, mugearites to benmoreites. The most abundant phenochryst phases are invariably plagioclase and clinopyroxene and to a lesser extent olivine. Some hawaiite samples also contain nepheline in their groundmass. Apatite is also common.

The hawaiites that were erupted in the immediate vicinity of the calc-alkaline Suphan volcano exhibit disequilibrium features among their phenocrysts. These were referred to as the "Malazgirt Graben association" by Innocenti et al., (1980). Plagioclases show reverse zoning with andesine cores (An 50-40), a more basic intermediate zone (An 60-65) and more acid outer rims (An 35-50). The hawaiites also contain three types of pyroxenes: pigeonite, calcic augite and orthopyroxene. The coexistence of andesene plagioclase, Ca-rich augite and fayalitic olivine in the groundmass is also typical in these rocks.

2.4 Results

2.4.1 Major and trace element variation

Representative major element analyses for the alkaline rocks are presented in Table-2.1. The major element compositions have been normalized to 100% volatile-free, with all Fe expressed as FeO (designated FeOT). Subdivision of the samples (Tendurek, Nemrut, Malazgirt and Meydan) is based on geographic locality. The first row of the Tendurek group (A-1 to A-64) belongs to the earliest phase of activity of Tendurek volcano. They represent the basaltic eruptions associated with the small spatter cones. Representative analyses of the main phase of Tendurek activity are presented in the second and third rows (from T-11 to T-60).

Samples N-13-2 to N-34 are from Nemrut volcano. N-31-B belongs to the lava flows associated with the most recent (1441) eruptions. The rest of the Nemrut samples are from small individual eruption centers in the vicinity of Nemrut volcano.

TABLE 2.1

TENDUREK

	T-1	T-4	T-10	T-13	T-14	T-26	T-32	T-33	T-34	T-38	T-46	T-64	
SiO2	46.99	50.57	53.20	46.04	53.26	50.41	52.54	51.92	51.66	47.80	51.95	46.79	
Al2O3	17.52	17.66	17.08	18.83	17.32	17.51	17.97	18.16	18.16	17.01	17.79	17.62	
FeO(T)	11.79	10.43	9.95	11.10	9.07	10.52	9.55	9.49	9.35	11.14	8.70	11.44	
MgO	4.86	4.37	3.50	3.23	3.15	4.20	3.38	3.40	3.40	6.42	5.55	5.06	
CaO	9.26	7.54	6.96	9.80	6.37	6.62	6.84	6.68	6.91	10.50	8.45	9.43	
Na2O	5.06	5.34	5.28	7.40	6.44	5.76	5.48	5.77	5.65	3.96	4.76	5.47	
K2O	1.33	1.51	1.74	1.76	2.10	1.43	1.78	1.92	1.94	0.55	1.14	1.28	
TiO2	2.25	2.02	1.88	2.00	1.81	2.30	1.84	1.71	1.67	2.07	1.51	2.18	
MnO	0.20	0.18	0.20	0.19	0.19	0.22	0.19	0.19	0.19	0.19	0.16	0.20	
P2O5	0.58	0.71	0.50	0.67	0.58	1.13	0.89	0.91	0.88	0.34	0.36	0.58	
TOTAL	99.84	100.33	100.29	101.02	100.29	100.10	100.46	100.15	99.81	99.98	100.37	100.05	
Mg#	42.4	42.8	38.5	34.2	38.2	41.6	38.7	39.0	39.3	50.7	53.2	44.1	

	T-11	T-12	T-15	T-22	T-24	T-25	T-27	T-29	T-31-A	T-31-B	T-35	T-36-A	T-36-B
SiO2	58.00	58.42	58.16	59.04	58.33	58.40	58.09	62.39	59.34	58.14	58.14	58.10	58.32
Al2O3	17.76	18.72	20.04	18.67	18.45	18.70	18.54	18.46	18.51	18.32	18.51	18.31	18.64
FeO(T)	6.82	4.80	4.75	4.90	5.08	5.05	5.46	4.06	4.93	5.65	5.52	5.60	5.72
MgO	0.49	1.16	0.79	1.16	1.35	1.19	1.53	0.65	1.37	1.52	1.55	1.62	1.55
CaO	3.77	2.37	1.84	2.47	2.65	2.52	3.29	1.84	3.05	3.46	3.52	3.43	3.56
Na2O	7.86	8.12	8.78	7.75	8.41	8.36	7.54	7.23	7.59	7.50	7.38	7.39	6.71
K2O	4.41	4.44	5.07	4.42	4.00	4.36	3.88	4.27	3.91	3.96	3.88	3.68	3.75
TiO2	1.05	1.04	0.68	1.06	1.16	1.11	1.21	0.70	1.15	1.22	1.20	1.23	1.26
MnO	0.23	0.17	0.19	0.17	0.17	0.17	0.17	0.15	0.16	0.17	0.17	0.17	0.17
P2O5	0.19	0.40	0.27	0.38	0.49	0.48	0.55	0.23	0.51	0.55	0.52	0.56	0.54
TOTAL	100.58	99.64	100.57	100.02	100.09	100.34	100.26	99.98	100.52	100.49	100.39	100.09	100.22
Mg#	11.4	30.1	22.9	29.7	32.1	29.6	33.3	22.2	33.1	32.4	33.4	34.0	32.6

	T-39	T-40-A	T-40-B	T-48	T-49	T-50-B	T-51	T-52	T-53	T-55	T-58	T-59	T-60
SiO2	55.29	59.24	58.95	62.04	62.30	58.80	59.26	58.88	59.59	59.75	58.02	58.13	57.63
Al2O3	16.97	18.99	18.89	17.35	17.58	18.55	18.71	18.75	18.71	19.01	19.00	19.25	18.99
FeO(T)	8.50	4.88	4.82	5.31	4.65	5.14	5.11	4.96	5.01	4.79	5.74	5.48	5.70
MgO	1.62	1.11	1.08	0.49	0.54	1.35	1.29	1.18	1.27	1.06	1.24	0.95	1.05
CaO	5.28	2.29	2.30	1.21	1.08	2.77	2.55	2.37	2.46	2.12	2.73	2.09	2.32
Na2O	6.48	7.91	7.53	7.18	7.49	7.70	6.14	8.14	7.34	8.66	8.08	8.20	8.22
K2O	3.05	4.30	4.57	5.58	5.40	3.98	4.36	4.38	4.37	4.57	4.15	4.40	4.23
TiO2	1.84	1.05	1.03	0.63	0.63	1.16	2.55	1.10	1.11	1.03	1.04	0.96	1.04
MnO	0.22	0.17	0.17	0.20	0.19	0.18	0.18	0.17	0.17	0.16	0.21	0.19	0.20
P2O5	0.63	0.42	0.37	0.08	0.12	0.51	0.43	0.46	0.44	0.41	0.39	0.38	0.41
TOTAL	99.88	100.36	99.71	100.07	99.98	100.14	100.58	100.39	100.47	101.56	100.60	100.03	99.79
Mg#	25.4	28.8	28.5	14.1	17.2	31.9	31.0	29.8	31.1	28.3	27.8	23.6	24.7

TABLE 2.1 (Cont'd)

	NEMRUT														
	N-13-2	N-13-4	N-13-10	N-13-11	N-21	N-28A	N-31B	N-34A	N-36	N-40	N-41	N-42	N-47A	N-52	N-53
SiO2	63.22	63.46	48.92	64.83	58.46	73.83	46.96	58.49	52.32	53.51	50.34	50.73	61.54	56.76	60.76
Al2O3	18.25	18.18	17.26	16.67	16.95	12.15	16.71	18.44	16.23	16.95	17.84	17.71	18.18	16.56	16.24
FeO(T)	4.28	3.77	11.24	4.51	6.85	3.70	12.73	7.34	11.80	9.49	11.60	11.10	4.38	10.07	8.06
MgO	0.43	0.47	6.06	0.24	1.74	<0.2	6.46	1.72	3.40	4.22	4.27	3.89	0.48	1.60	0.93
CaO	2.79	1.91	8.61	1.72	4.15	0.19	9.60	4.04	6.82	7.53	7.08	6.93	1.34	4.98	4.15
Na2O	6.42	6.56	3.70	5.80	6.05	5.14	3.45	4.97	4.24	4.07	4.27	4.69	6.85	5.11	5.94
K2O	3.86	4.78	1.48	5.51	3.71	4.69	0.61	3.74	1.78	1.51	1.82	1.98	5.99	2.79	2.87
TiO2	0.55	0.54	2.10	0.46	1.22	0.24	2.78	1.20	2.27	2.12	2.59	2.55	0.55	1.50	0.93
MnO	0.16	0.11	0.18	0.13	0.18	0.09	0.19	0.19	0.24	0.16	0.18	0.17	0.13	0.32	0.20
P2O5	0.17	0.16	0.41	0.12	0.54	<0.05	0.34	0.48	1.39	0.42	0.49	0.50	0.13	0.74	0.42
TOTAL	100.13	99.94	99.96	99.99	99.85	100.28	99.83	100.61	100.49	99.98	100.48	100.25	99.57	100.43	100.50
Mg#	15.19	18.18	49.01	8.66	31.17	-	47.50	29.46	33.93	44.22	39.62	38.45	16.34	22.07	17.06

	MALAZGIRT													MEYDAN		
	S-41	S-43	S-60	S-63	S-64	S-65	S-66	S-68	S-69E	S-69F	S-70A	S-70B	S-75A	S-75B	S-72	S-73	S-77
SiO2	54.46	48.11	48.37	53.58	55.49	53.03	55.33	52.80	56.12	49.50	50.74	50.39	53.30	57.30	50.53	51.24	50.45
Al2O3	15.81	18.39	18.38	17.73	16.56	17.38	16.41	17.64	18.47	18.79	15.91	16.20	17.69	16.72	18.76	18.76	19.12
FeO(T)	10.60	10.47	10.29	10.13	10.37	9.94	10.19	9.84	6.98	9.67	11.98	11.73	9.78	8.73	9.17	8.13	8.94
MgO	3.01	6.82	7.52	3.35	2.97	3.40	2.97	3.57	3.21	6.39	5.83	5.20	3.48	2.67	6.18	5.32	5.51
CaO	6.16	10.14	9.88	7.51	6.17	7.53	6.15	7.54	6.39	9.49	8.05	8.20	7.62	5.68	8.91	9.62	8.85
Na2O	4.60	4.14	4.00	4.93	3.77	4.92	4.00	4.59	4.95	4.60	4.24	4.12	5.05	4.29	4.34	4.10	4.81
K2O	2.24	0.54	0.46	1.55	2.25	1.51	2.29	1.48	2.79	1.12	1.15	1.14	1.64	2.60	1.61	1.23	1.14
TiO2	2.24	1.68	1.64	2.12	2.08	2.06	2.09	2.10	1.25	1.67	2.28	2.26	2.07	1.52	1.51	1.26	1.40
MnO	0.15	0.17	0.18	0.15	0.13	0.14	0.13	0.15	0.13	0.18	0.18	0.18	0.17	0.15	0.18	0.18	0.17
P2O5	0.58	0.22	0.23	0.41	0.38	0.44	0.39	0.42	0.50	0.45	0.45	0.44	0.41	0.49	0.48	0.36	0.43
TOTAL	99.85	100.68	100.95	101.46	100.17	100.35	99.95	100.13	100.79	101.86	100.81	99.86	101.21	100.15	101.67	100.20	100.82
Mg#	33.6	53.7	56.6	37.1	33.8	37.9	34.2	39.3	45.0	54.1	46.5	44.1	38.8	35.3	54.6	53.8	52.4

The samples of the Malazgirt group represent the alkali fissure lava flows in the vicinity of Suphan volcano, and are older than the young calc-alkaline lava flows of Suphan volcano. The samples that are grouped under Meydan are from an area to the NNE of Suphan volcano, between Patnos and Meydan.

In Figure-2.2, total alkalies (Na2O+K2O) are plotted against SiO2. All of the samples plot in the alkaline field as defined by the alkaline-subalkaline division of Irvine and Baragar (1971). Tendurek lavas have the highest total alkali contents and Nemrut lavas occupy a relatively intermediate field on this plot. However, the Malazgirt and Meydan lavas plot very close to the alkaline-subalkaline dividing line. The major element variations are illustrated in Figures-2.3 and 2.4. All of the alkaline samples form broadly continous trends on these plots with their MgO, FeO, CaO and TiO2 contents correlating negatively with SiO2. The Nemrut samples have higher FeO(T) and TiO2 contents than the other alkaline groups. The basaltic compositions show a large range in TiO2 contents, from about 1.3 to 2.8%. All of the samples have high Al2O3 contents (see Table-2.1), independent of the plagioclase phenocryst contents. They also have high Na2O/K2O ratios, in general. The majority of the samples follow a typical Fe-enrichment trend on an AFM plot (Figure-2.5). However, a few samples, the Meydan group in particular, do not show any Fe-enrichment.

Molecular norms (Barth-Niggli Katanorm) have been calculated for all the samples after assigning %Fe2O3=%TiO2+1.5, following Irvine and Baragar (1971). All of the Tendurek and Meydan lava flows are nepheline and olivine normative. The Malazgirt and Nemrut lavas exhibit a transitional character and contain both hypersthene and nepheline normative compositions; however the majority of them are hypersthene normative.

Figure-2.2

Plot of total alkalies (K2O+Na2O) versus SiO2 for the alkaline volcanics. The dividing line for the "alkaline" and "subalkaline" fields is from Irvine & Baragar (1971). Tendurek lavas apparently have higher total alkali contents compared with the other alkaline suites. Nemrut lavas occupy an intermediate position. Malazgirt and Meydan lavas plot very close to the dividing line.

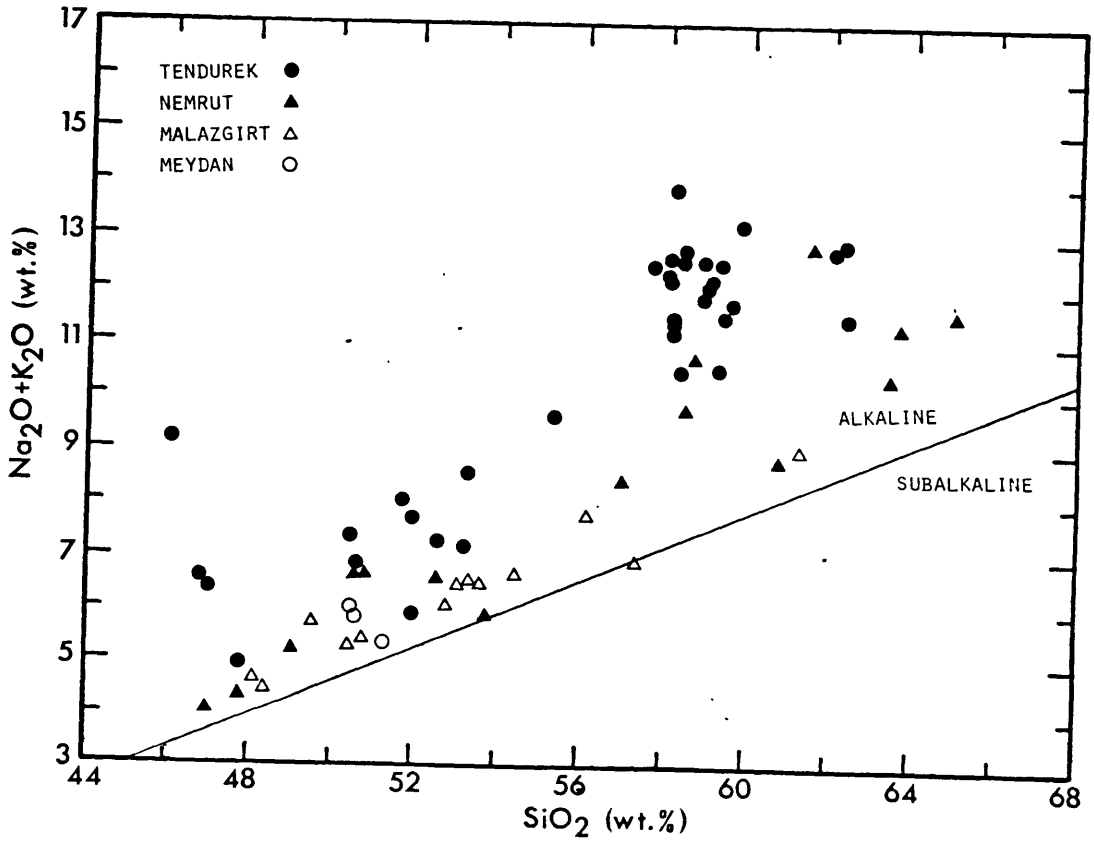
TENDUREK
NEMRUT
MALAZGIRT
MEYDAN
ALKALINE
SUBALKALINE
Na_2O+K_2O (wt.%)
SiO_2 (wt.%)
17
15
13
11
9
7
5
3
44
48
52
56
60
64
68

Figure-2.3 and 2.4

Diagrams showing the variation of MgO, FeO(T), CaO and TiO2 with SiO2 contents.

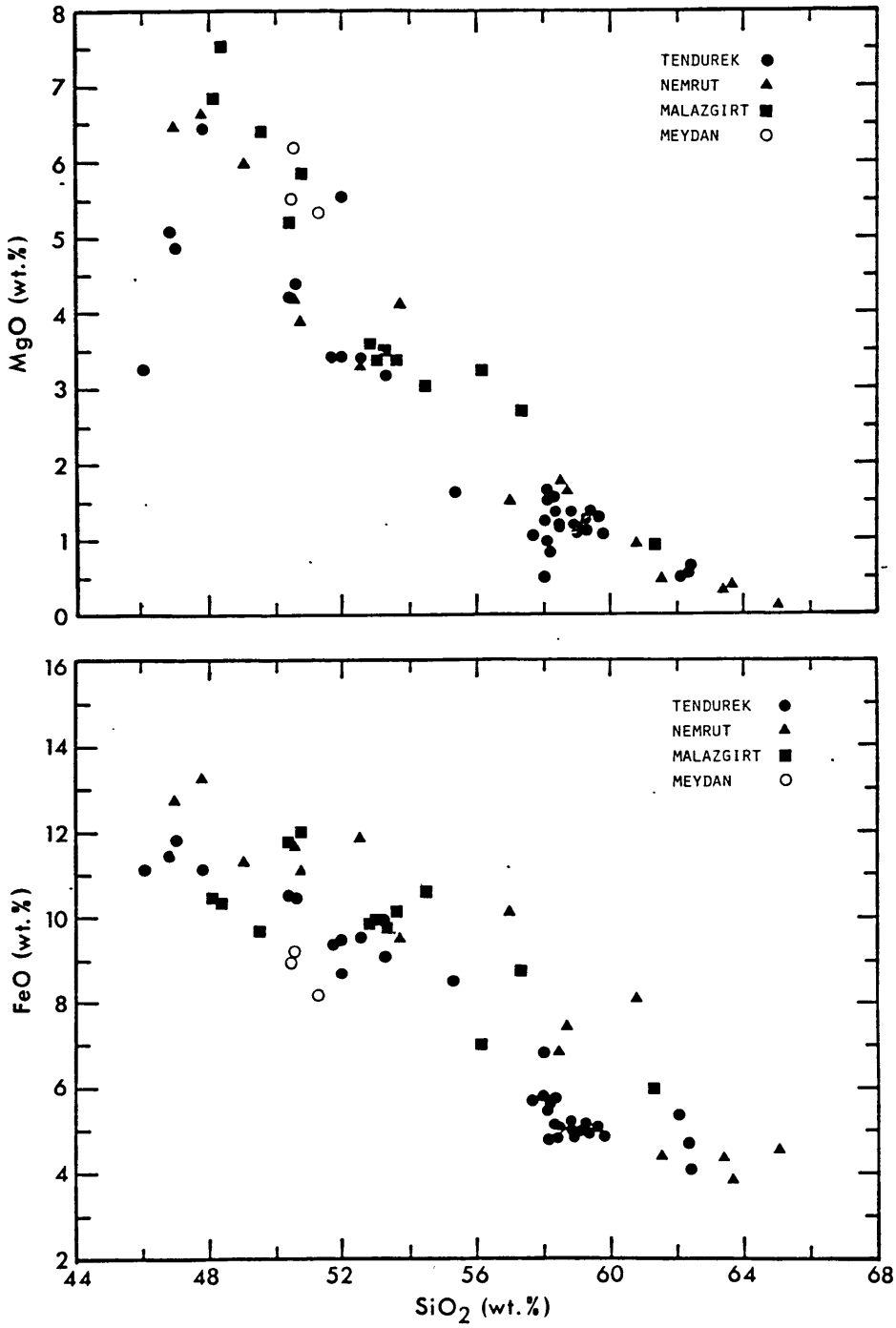
TENDUREK
NEMRUT
MALAZGIRT
MEYDAN
MgO (wt.%)
FeO (wt.%)
SiO2 (wt.%)
0
1
2
3
4
5
6
7
8
2
4
6
8
10
12
14
16
44
48
52
56
60
64
68

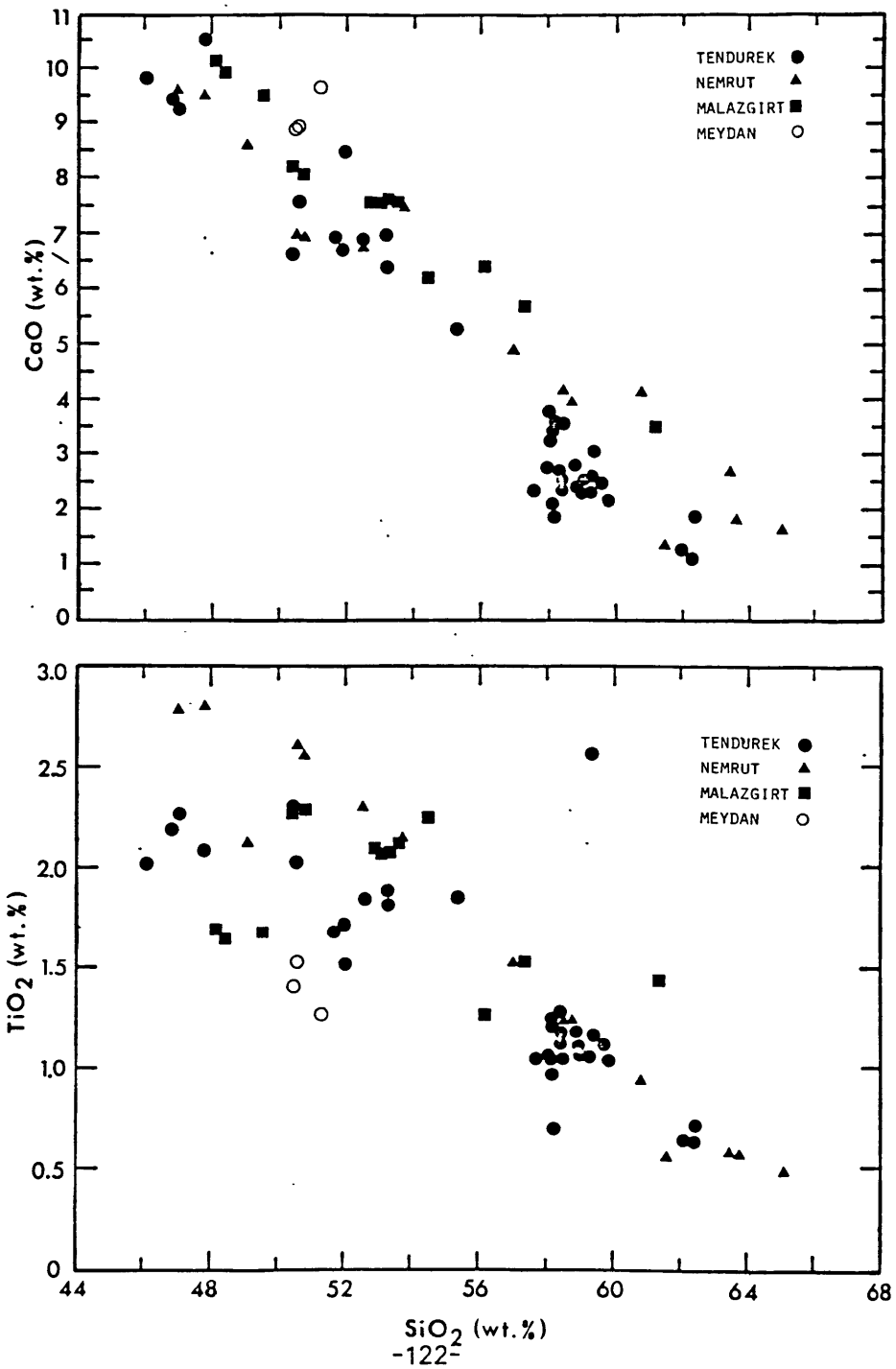
TENDUREK
NEMRUT
MALAZGIRT
MEYDAN
CaO (wt.%)
TiO2 (wt.%)
SiO2 (wt.%)
0
1
2
3
4
5
6
7
8
9
10
11
0.5
1.0
1.5
2.0
2.5
3.0
44
48
52
56
60
64
68

Figure-2.5

AFM diagram of the alkaline volcanics. Most of the samples form a broad curved trend indicative of Fe-enrichment. However the Meydan lavas and a few Malazgirt lavas show little or no Fe-enrichment.

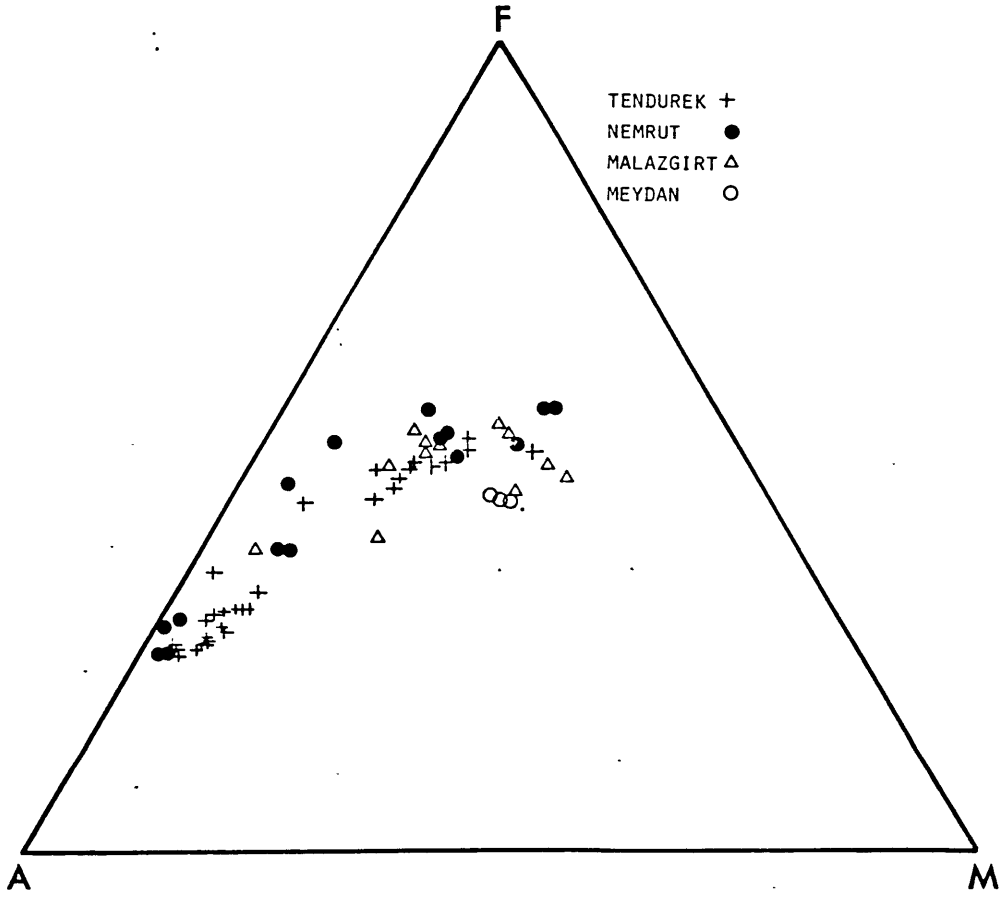
F
TENDUREK +
NEMRUT ●
MALAZGIRT △
MEYDAN ○
A
M

The trace element abundances of some representative samples are listed in Table-2.2. There is a broad positive correlation between the alkali element abundances and SiO2 contents. However, the incompatible element ratios such as K/Rb, K/Cs and K/Ba do not correlate well with SiO2 or K2O contents. For example, the K/Rb ratios exhibit a wide range from 400 to 720 for a limited K2O range (0.45-0.56%).

2.4.2 Rare Earth Elements

The REE abundances of representative samples are listed in Table-2.3 and their chondrite-normalized REE patterns are shown in Figure-2.6. The LREE abundances vary by a factor of 5 (31-155xchondrites), while the HREE abundances are relatively constant (17-22xchondrites). Although all of the analyzed samples are LREE enriched, they have a large range in the degree of LREE enrichment. (La/Yb) e.f. (enrichment factor relative to chondrites) range from 1.99 to 7.61. The (La/Yb) e.f. correlate positively with SiO2 contents and negatively with Mg#. Excluding S-60, there is also a positive correlation between the Sr87/86 ratios and the chondrite-normalized La/Yb ratios.

2.4.3 Isotope Geochemistry

Sr, Nd and Pb isotope compositions along with Rb, Sr, Sm, and Nd abundances for the alkaline rocks are listed in Table-2.4. Sr87/86 ratios range from 0.70341 to 0.70579 and Nd143/144 ratios range from 0.51269 to 0.51293. The observed Pb isotopic composition ranges are 18.827-19.185 for Pb206/204, 15.629-15.713 for Pb207/204 and 38.881-39.152 for Pb208/204.

Table 2.2 (+)

	K	Rb	Sr	Ba	Cs	K/Rb	K/Sr	K/Ba	K/Cs
					TENDUREK				
T-1	11036	24.4	585	326	0.58	452	19	34	19028
T-13	14434	30.8	834	428	0.89	469	17	34	16218
T-26	11837	18.5	662	452	0.30	640	18	26	39457
T-34	16091	35.0	653	603	0.80	460	25	27	20114
T-38	4595	6.4	420	147	0.12	718	11	31	38292
T-46	9468	21.5	426	242	0.54	440	22	39	17533
T-64	10627	22.9	589	314	0.56	464	18	34	18977
T-24	33247	102.2	245	617	2.88	325	136	54	11544
T-36-A	30536	93.0	290	595	2.65	328	105	51	11523
T-39	25296	78.0	590	754	2.63	324	43	34	9618
T-40-A	35670	113.4	205	594	3.05	315	174	60	11695
T-50-B	33012	100.0	247	616	2.76	330	134	54	11961
					NEMRUT				
N-13-10	12265	32.2	457	311*	1.12	381	27	39	10951
N-32	5275	7.3	421	104*	0.26	723	13	51	20288
N-36	14780	38.2	450	387*	1.50	387	33	38	9853
N-40	12551	35.0	389	213*	1.54	359	32	59	8150
N-41	15101	50.1	698	351*	3.04	301	22	43	4967
					MALAZGIRT				
S-41	18591	59.1	274	-	-	315	68		
S-43	4463	11.1	368	-	-	402	12		
S-60	3795	9.5	333	-	-	399	11		
S-63	14389	46.4	350	-	-	310	41		
S-68	12298	34.9	318	-	-	352	39		
S-70-A	9540	15.2	346	-	-	628	28		
S-75-A	13619	41.9	350	-	-	325	39		
					MEYDAN				
S-72	13387	33.9	831	-	-	395	16		
S-77	9483	22.0	743	-	-	431	13		

(+) Concentrations in ppm. by isotope dilution, with precision for K, Rb, Sr, Ba <=1% and for Cs <=5%.
(*) Determined by XRF.

TABLE 2-3

	T-34	T-38	T-64	S-60	S-70-A	CHONDRITIC ABUND.(1)
La	51.2	15.3	32.5	10.1	22.9	0.33
Ce	106.8	38.7	71.0	25.7	56.1	0.88
Nd	44.5 (44.03)(2)	21.8 (22.16)	34.0 (34.77)	15.0 (15.73)	28.2	0.60
Sm	8.36 (8.45)(2)	5.56 (5.55)	7.35 (7.36)	4.38 (4.24)	6.88	0.181
Eu	2.54	2.03	2.46	1.61	2.29	0.069
Tb	1.21	1.05	1.26	0.88	1.34	0.047
Yb	4.08	3.41	3.97	3.07	4.35	0.20
Lu	0.60	0.50	0.53	0.46	0.63	0.034
La/Ce	0.48	0.39	0.46	0.39	0.41	
La/Sm	6.06	2.76	4.42	1.37	3.33	
La/Yb	12.55	4.49	8.19	3.29	5.26	

(1) Chondrite abundances are from Frey et al., (1968).
(2) Concentrations in parentheses are determined by isotope dilution.

TABLE 2-4

SAMPLE #	Sr 87/86 (1) (5)	Nd 143/144 (2) (5)	Pb 206/204 (3)	Pb 207/204 (3)	Pb 208/204 (3)	Rb (4)	Sr (4)	Sm (4)	Nd (4)	Rb/Sr	Sm/Nd	Sr/Nd
				TENDUREK								
T-1	0.70533 ∓4	0.51277 ∓3	19.022	15.666	38.973	24	585	7.77	36.94	0.041	0.210	15.836
T-13	0.70533 ∓4	0.51278 ∓3	-	-	-	31	834	7.12	36.95	0.037	0.193	22.571
T-26	0.70579 ∓4	0.51279 ∓2	18.908	15.660	38.944	18	662	8.79	44.05	0.027	0.200	15.028
T-38	0.70433 ∓3	0.51289 ∓3	18.952	15.654	38.963	6.4	420	5.55	22.16	0.015	0.250	18.953
T-46	0.70492 ∓4	0.51283 ∓2	18.945	15.650	38.939	21	423	5.29	23.56	0.050	0.225	17.954
T-64	0.70511 ∓3	0.51283 ∓2	19.011	15.656	38.940	23	589	7.36	34.77	0.039	0.212	16.940
T-24	0.70538 ∓3	0.51282 ∓2	-	-	-	102	245	8.35	43.02	0.416	0.194	5.695
T-34	0.70575 ∓3	0.51275 ∓3	18.827	15.667	38.881	35	653	8.45	44.03	0.054	0.192	14.831
T-36-A	0.70562 ∓5	0.51281 ∓2	19.040	15.712	39.152	93	290	8.72	44.55	0.321	0.196	6.510
T-39	0.70564 ∓4	0.51275 ∓2	19.044	15.679	39.023	78	590	9.76	48.44	0.132	0.201	12.180
T-40-A	0.70531 ∓4	0.51278 ∓2	18.998	15.661	38.961	113	205	8.33	42.96	0.551	0.194	4.772
T-50-B	0.70542 ∓5	0.51276 ∓2	18.996	15.662	38.966	100	247	8.42	43.23	0.405	0.195	5.714
				NEMRUT								
N-13-10	0.70515 ∓3	0.51272 ∓3	19.185	15.713	39.288	32	457	6.40	28.30	0.070	0.226	16.150
N-32	0.70374 ∓4	0.51293 ∓3	19.069	15.629	38.917	7.3	421	5.87	23.15	0.017	0.254	18.190
N-36	0.70462 ∓4	0.51282 ∓2	19.067	15.674	39.097	38	450	12.30	54.14	0.084	0.227	8.310
N-40	0.70341 ∓3	0.51291 ∓2	19.139	15.677	39.127	35	389	6.86	29.93	0.090	0.229	13.000
N-41	0.70503 ∓3	0.51279 ∓2	-	-	-	50	698	6.55	30.56	0.072	0.214	22.840
				MALAZGIRT								
S-41	0.70558 ∓3	0.51278 ∓2	-	-	-	59	274	10.74	45.54	0.215	0.236	6.017
S-43	0.70467 ∓4	0.51277 ∓3	19.001	15.676	39.057	11	368	4.44	16.62	0.030	0.267	22.142
S-60	0.70462 ∓6	0.51273 ∓2	19.009	15.685	39.083	10	333	4.24	15.73	0.030	0.270	21.170
S-63	0.70479 ∓4	0.51277 ∓2	-	-	-	46	350	8.63	36.00	0.131	0.240	9.722
S-65	0.70489 ∓3	0.51276 ∓2	-	-	-							
S-68	0.70479 ∓3	0.51276 ∓2	-	-	-	35	318	-	-	0.110	-	-
S-70-A	0.70496 ∓3	0.51280 ∓2	19.032	15.662	39.023	15	346	6.88	28.20	0.043	0.244	12.270
S-75-A	0.70476 ∓4	0.51278 ∓3	-	-	-	42	350	8.36	35.05	0.120	0.239	9.986
				MEYDAN								
S-72	0.70538 ∓4	0.51269 ∓3	-	-	-	34	831	6.09	32.50	0.041	0.187	25.569
S-77	0.70535 ∓4	0.51270 ∓2	18.997	15.677	39.111	22	743	5.10	25.71	0.030	0.198	28.899

(1) Sr 87/86 ratios normalized to 0.70800 for E & A SrCO3 using Sr 86/88 = 0.1194
(2) Nd 143/144 ratios normalized to 0.51264 for BCR-1 using Nd 146/144 = 0.7219
(3) Pb isotope ratios are normalized for mass discrimination using that obtained for NBS SRM 981. Reproducibility is better than 0.05% AMU-1.
(4) Concentrations in ppm by isotope dilution, with precision for Sr, Nd, and Sm ~0.3% and for Rb ~1%.
(5) Quoted errors for Sr and Nd isotopic ratios are in-run statistics, and are representative of true precision as demonstrated by replicate analysis of various samples.

Figure-2.6

Chondrite-normalized REE patterns of representative lava flows of the alkaline suites. Chondrite normalization values are listed in Table-2.3. Note the large range and degree of enrichment observed for the LREE, compared with the relatively narrow range for the HREE.

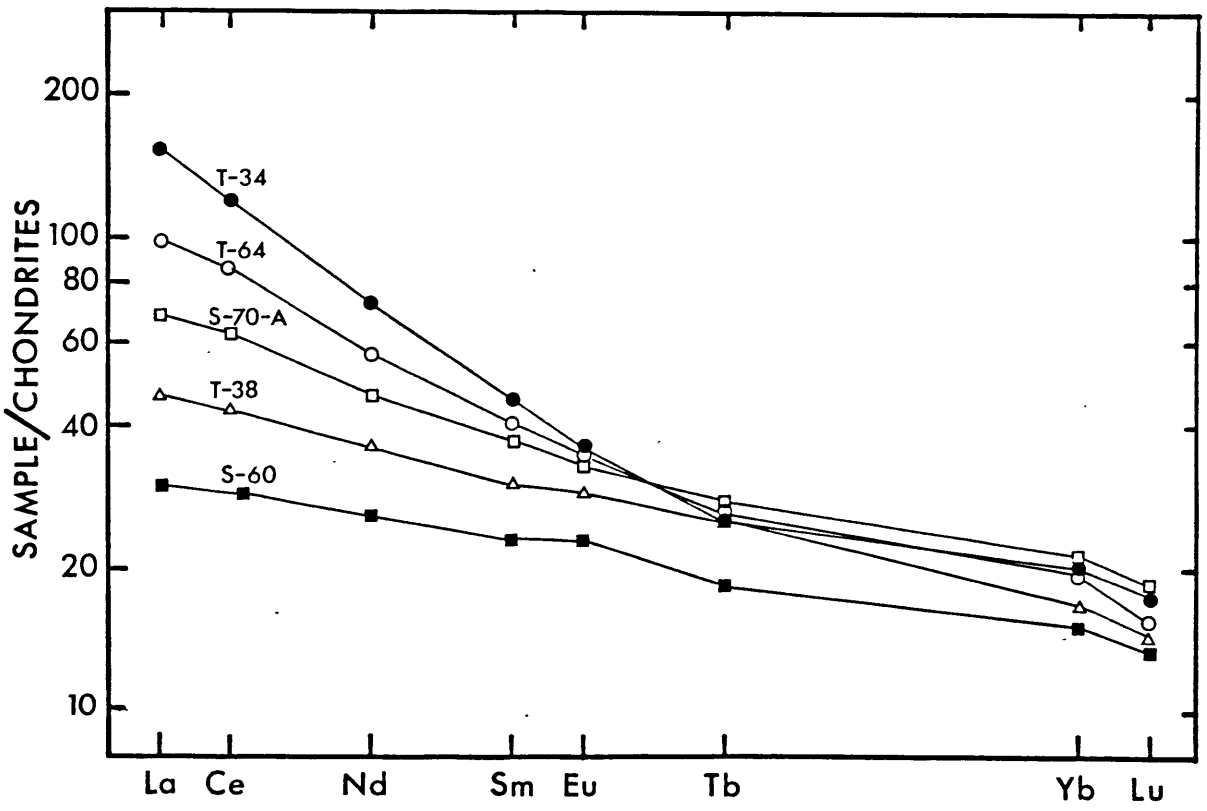
200
100
80
60
40
20
10
SAMPLE/CHONDRITES
T-34
T-64
S-70-A
T-38
S-60
La
Ce
Nd
Sm
Eu
Tb
Yb
Lu

2.4.3.1 Sr and Nd Isotope Variation

The Sr and Nd isotope composition of the alkaline suites are plotted on a Nd-Sr isotope correlation diagram in Figure-2.7. The fields of Ararat, Azores and Grenada are also shown for comparison. Only two samples from Nemrut, one of which is the 1441 lava flow, plot close to the Ararat field, while the rest are shifted significantly towards the more radiogenic Sr side of the diagram. Alkaline suites also have lower Nd143/144 ratios relative to the Ararat field. Tendurek lavas have higher Sr87/86 ratios compared with the other alkaline suites. The majority of Malazgirt lavas form a cluster and do not exhibit a negative correlation on the Sr-Nd isotope diagram. The Sr87/86 and Nd143/144 ratios do not show any recognizable correlations with the major element compositions. In Figure-2.8, the Sr87/86 ratios are plotted against Rb/Sr ratios. The basaltic compositions exhibit the largest variation in Sr87/86 ratio (from 0.7038 to 0.7058) for a range in Rb/Sr ratio of 0.02-0.05. However, the observed range in the Sr87/86 ratios of the more differentiated lavas is relatively small (from 0.7053 to 0.7058) with a Rb/Sr range of 0.02 to 0.55.

The Nd isotopic ratios are plotted against Sm/Nd ratios in Figure-2.9. Different alkaline suites form broad fields with different trends on this diagram. Tendurek lavas show a positive correlation between Nd isotope ratios and Sm/Nd ratios. Malazgirt samples exhibit a negative correlation between those ratios. Nemrut lavas have quite a large range in Nd143/144 ratios(from 0.51272 to 0.51293), despite a limited range in Sm/Nd ratios. The variation of isotopic ratios and reciprocal abundances for Sr and Nd display complex relations, both the among different alkaline suites as well as among within a given suite of lava flows (Figures-2.10 and 2.11). Most of the Tendurek lavas are more radiogenic in Sr87/86 compared with the Nemrut and Malazgirt series. Excluding one sample (S-41), the Malazgirt lavas form a cluster which has an average Sr87/86 ratio

Figure-2.7

Sr-Nd isotope correlation diagram for the alkaline rocks. Fields for Ararat, Azores, and Grenada are also shown for comparison. Bulk earth values and the "Oceanic Regression Line" are from Allegre et al., (1984). All Nd data are normalized to Nd146/144=0.51264 for BCR-1. Data sources: Hawkesworth et al., (1979), White and Hofmann (1982).

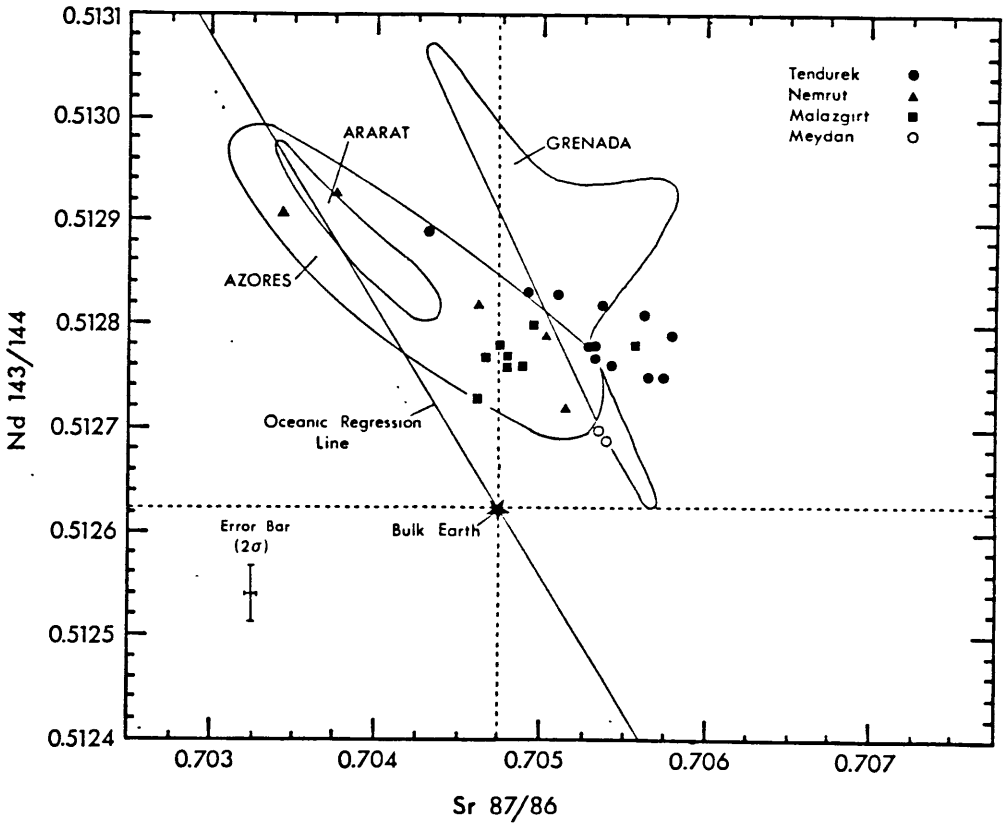
0.5131
0.5130
0.5129
0.5128
0.5127
0.5126
0.5125
0.5124
Nd 143/144
0.703
0.704
0.705
0.706
0.707
Sr 87/86
Tendurek
Nemrut
Malazgirt
Meydan
ARARAT
GRENADA
AZORES
Oceanic Regression Line
Bulk Earth
Error Bar (2σ)

Figure-2.8

Diagram illustrating the variation of Sr 87/86 ratios with Rb/Sr ratios for the alkaline rocks.

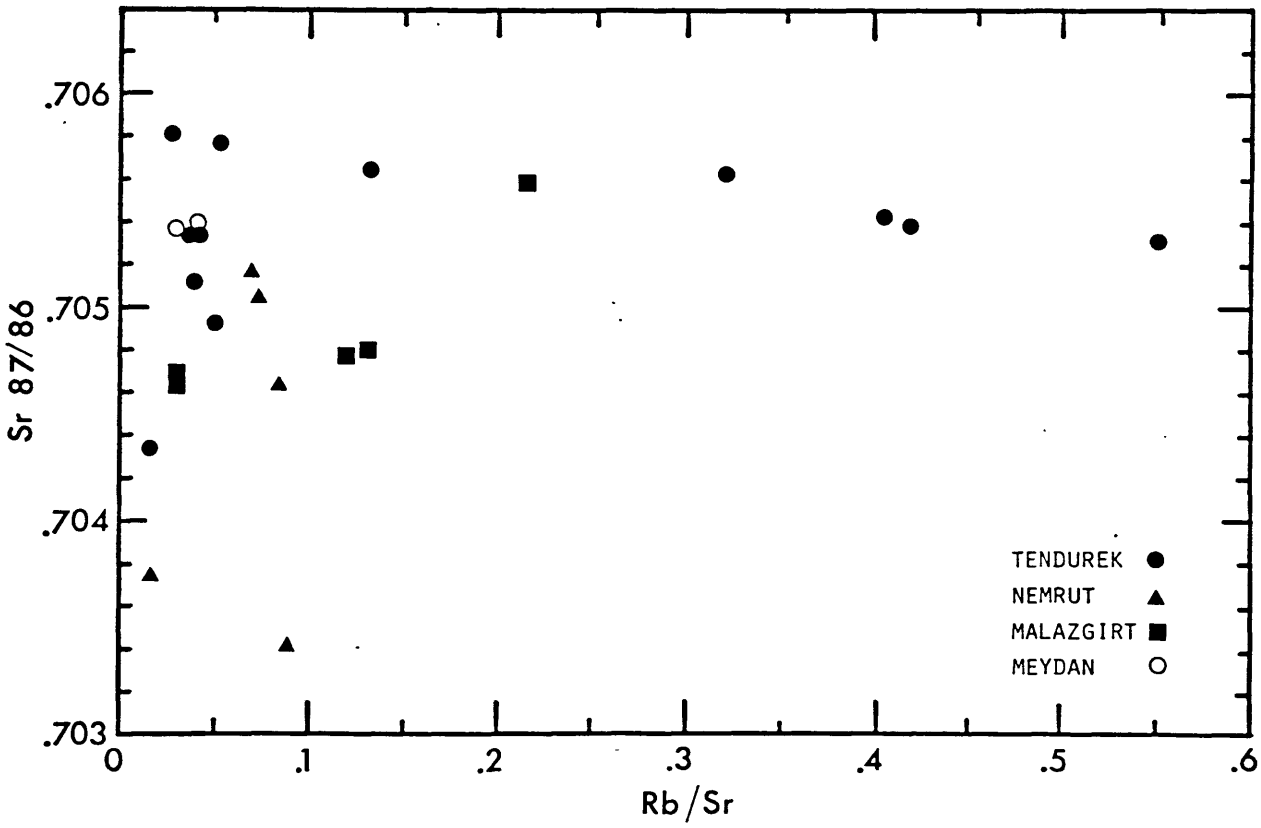
.706
.705
.704
.703
Sr 87/86
0
.1
.2
.3
.4
.5
.6
Rb/Sr
TENDUREK
NEMRUT
MALAZGIRT
MEYDAN

Figure-2.9

Plot of Nd143/144 versus Sm/Nd ratios for the alkaline volcanics. Different alkaline suites form broad fields with different trends.

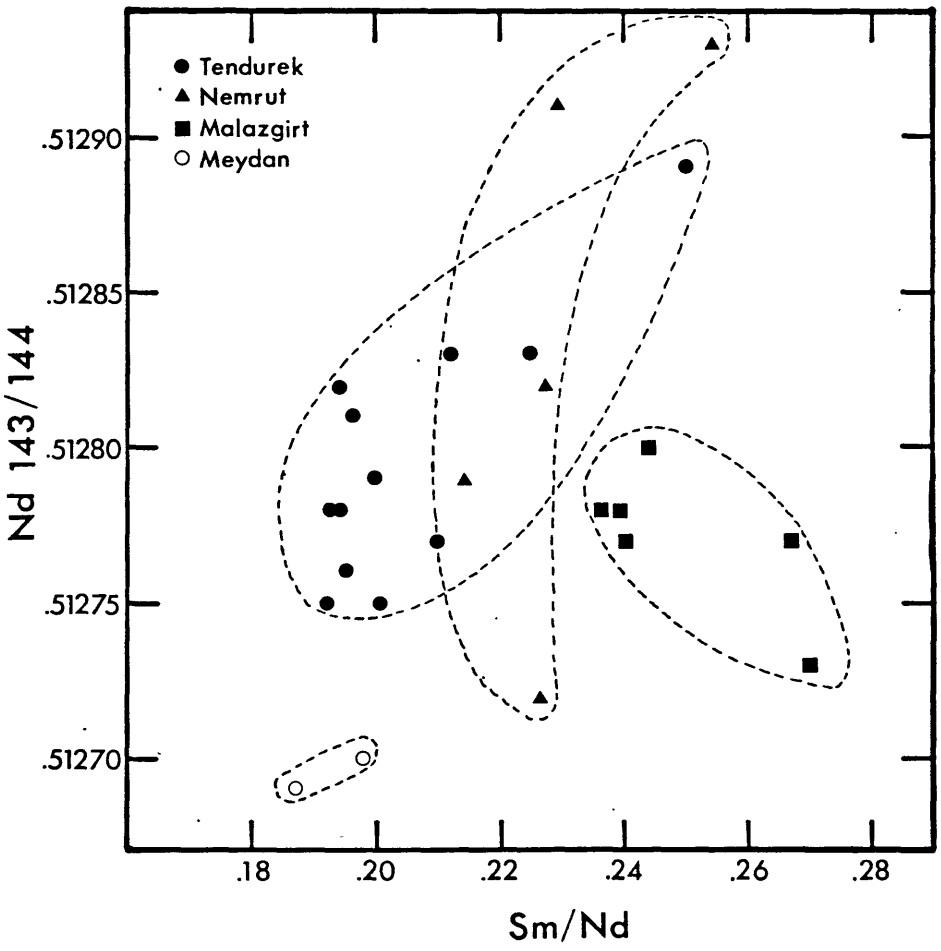
● Tendurek
▲ Nemrut
■ Malazgirt
○ Meydan
.51290
.51285
.51280
.51275
.51270
Nd 143/144
.18
.20
.22
.24
.26
.28
Sm/Nd

Figure-2.10

Variation between Sr87/86 ratios and reciprocal Sr abundances for the alkaline rocks.

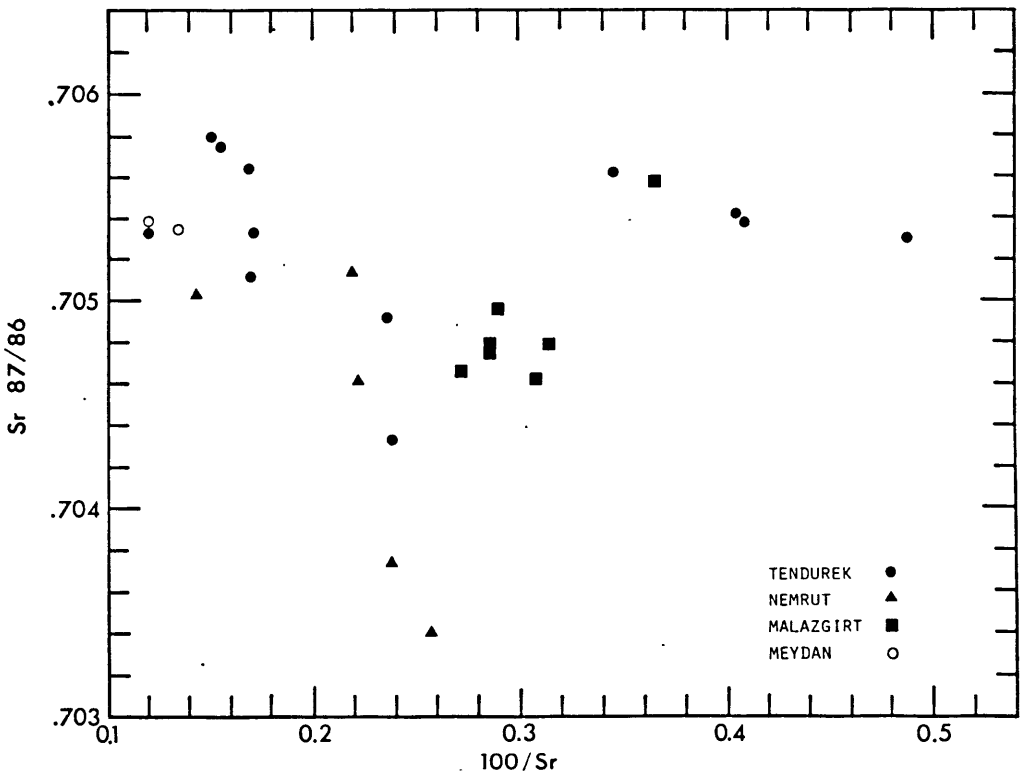
.706
.705
.704
.703
Sr 87/86
0.1
0.2
0.3
0.4
0.5
100/Sr
TENDUREK
NEMRUT
MALAZGIRT
MEYDAN

Figure-2.11

Variation between Nd143/144 ratios and reciprocal Nd abundances for the alkaline rocks. Note that the broad field defined by the Tendurek lavas appears to coincide with the positive linear trend formed by the Ararat HA basalts (Chapter-1). The Malazgirt lavas exhibit a wide range in Nd abundance, but a narrow range in Nd143/144 ratios.

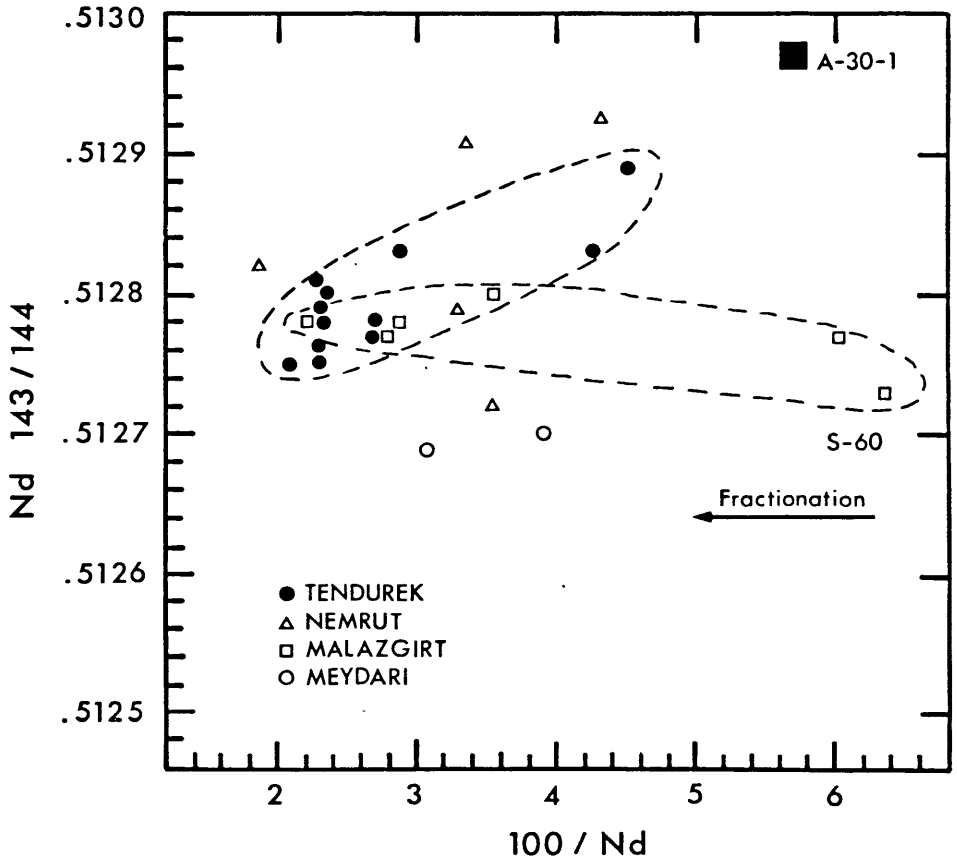
.5130
.5129
.5128
.5127
.5126
.5125
Nd 143 / 144
2
3
4
5
6
100 / Nd
A-30-1
S-60
Fractionation
TENDUREK
NEMRUT
MALAZGIRT
MEYDARI

and Sr abundance of 0.7048 and 340ppm., respectively (Figure-2.10). The Nemrut lavas, (with the exception of N-41) show a large range in Sr isotopic composition, (from 0.7034 to 0.7052) but a limited range in Sr abundance. The Meydan samples plot within the high-Sr side of the Tendurek field. In Figure-2.11, the Tendurek lavas form a broad field which appears to coincide with the positive linear trend defined by the Ararat HA basalts (Chapter 1). The Nemrut lavas broadly conform to this trend, though with a shift towards higher Nd143/144 values. The Malazgirt lavas form a distinct field which is characterized by a wide range in Nd abundance (from 16 to 46ppm.) but a limited range in Nd143/144 ratios.

2.4.3.2 Pb Isotope Variation

The Pb isotope ratios of the alkaline suites are plotted in Figure-2.12 on Pb isotope correlation diagrams, long with various island arc and ocean island basalt fields. The Alkaline suites form rather broad fields and extend the Ararat Pb-array towards more radiogenic compositions. The Nemrut lavas have more radiogenic Pb206/204 and Pb208/204 ratios than any of the other of the volcanics analyzed for Pb isotopes from eastern Turkey. These lavas form a steep trend on the 207-206-204 Pb diagram, with a large range in Pb 207/204 ratios (from 15.629 to 15.713). Most of the Tendurek lavas form a steep narrow trend overlapping with the upper part of the Ararat array, and extending it towards more radiogenic Pb 207/204 values. However, two samples from Tendurek have significantly lower Pb 206/204 ratios, indicative of lower crustal contamination. The Malazgirt lavas plot within the Tendurek field on the Pb-Pb isotope diagrams. Most of the samples from alkaline the suites (with the exception of the Nemrut lavas) plot within the Ararat field on the 208-206-204 Pb diagram.

Figure-2.12

Pb-Pb isotope correlation diagram for the alkaline rocks. Included for comparison are the fields for a variety of island arcs and ocean island basalts. Data sources are the same as in Figure-1.22.

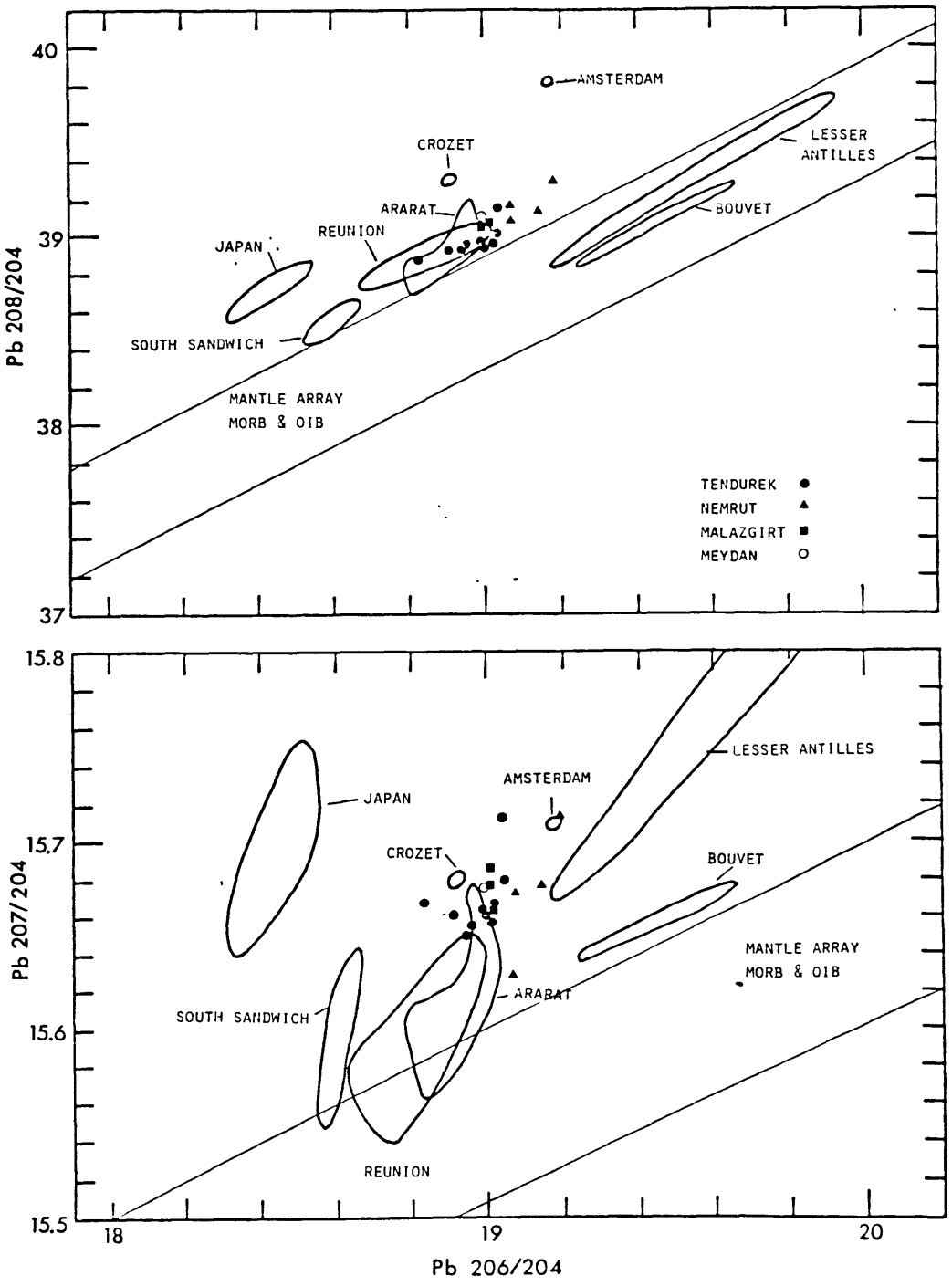
40
39
38
37
Pb 208/204
AMSTERDAM
CROZET
ARARAT
REUNION
JAPAN
SOUTH SANDWICH
LESSER ANTILLES
BOUVET
MANTLE ARRAY
MORB & OIB
TENDUREK
NEMRUT
MALAZGIRT
MEYDAN
15.8
15.7
15.6
15.5
Pb 207/204
18
19
20
Pb 206/204
LESSER ANTILLES
AMSTERDAM
JAPAN
CROZET
BOUVET
MANTLE ARRAY
MORB & OIB
ARARAT
SOUTH SANDWICH
REUNION

Figure-2.13

Sr-Pb and Nd-Pb isotope correlation diagrams for the alkaline rocks. Although the alkaline rocks as a whole form a "cloud", the Tendurek lavas by themselves appear to form positive and negative trends on the Sr87/86 versus Pb206/204 and Nd143/144 versus Pb206/204 diagrams, respectively.

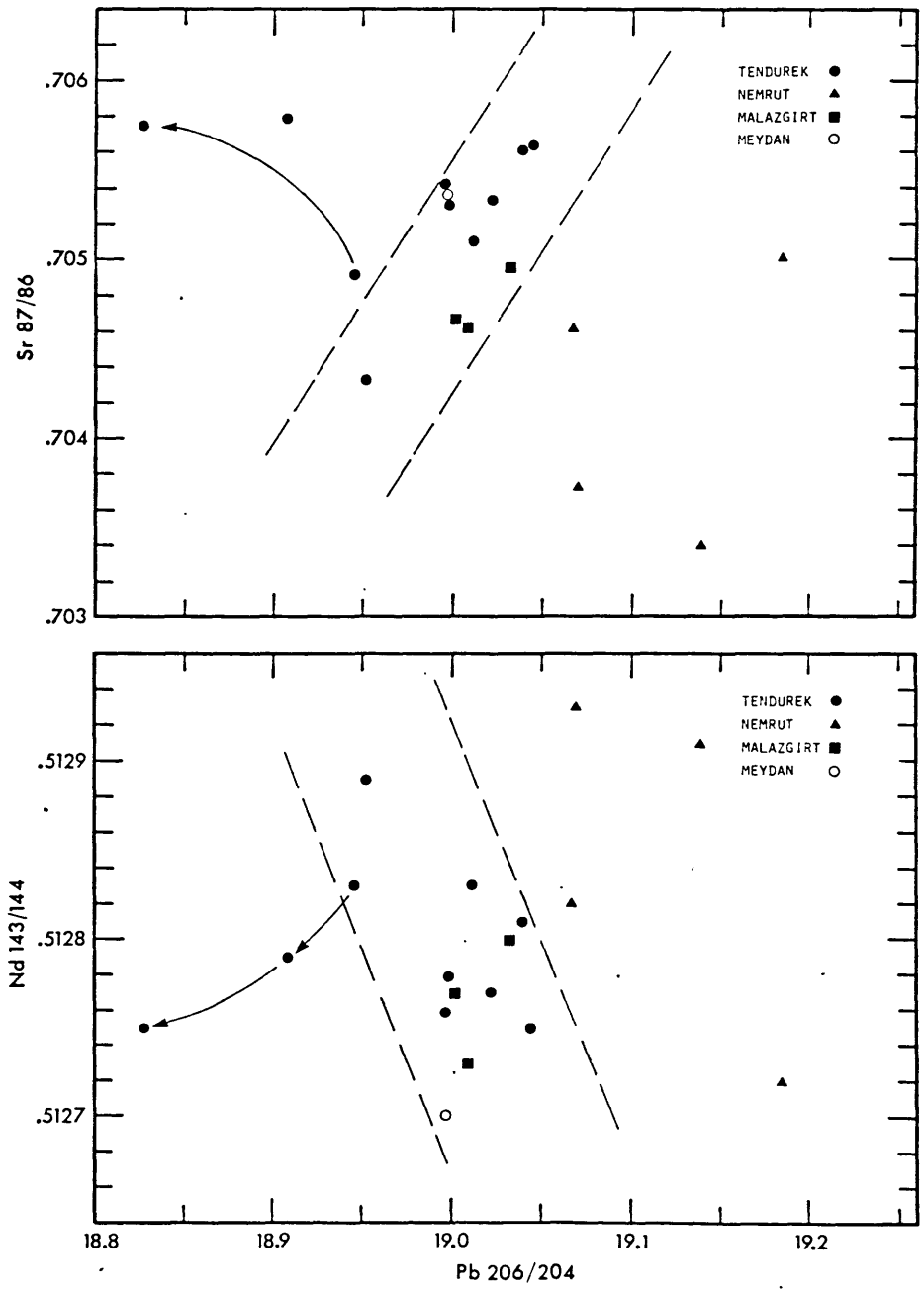
.706
.705
.704
.703
Sr 87/86
TENDUREK
NEMRUT
MALAZGIRT
MEYDAN
.5129
.5128
.5127
Nd 143/144
18.8
18.9
19.0
19.1
19.2
Pb 206/204

When considered together, the Isotopic compositions of the alkaline lavas form a "cloud" on the Sr-Pb and Nd-Pb isotope correlation diagrams (Figure-2.13). However, with the exclusion of potentially contaminated samples, the Tendurek lavas appear to exhibit positive and negative correlations on the Sr 87/86 versus Pb 206/204 and Nd 143/144 versus Pb 206/204 diagrams, respectively.

2.5 Discussion

2.5.1 Crustal Contamination

The fact that all of the alkaline lavas plot to the right of the oceanic Sr-Nd regression line (Figure-2.7), suggests involvement of a contamination process in their petrogenesis.

The Tendurek lavas exhibit a significant range in Sr 87/86 ratios (from 0.70433 to 0.70579). This range exceeds the range that is observed for the majority of the uncontaminated mantle derived magmas and indicates either crust or sediment contamination. However, the lack of a positive correlation between Rb/Sr ratios and Sr 87/86 ratios, the observed unradiogenic Pb 206/204 signatures, and the positive correlation between the degree of differentiation and the radiogenic Sr component (for basaltic compositions) implies crustal rather than sediment contamination as a principal cause for the observed variations. The nature of the crustal component and the contamination process can be inferred utilizing diagrams involving isotope ratios (Figures-2.8 to 2.13). The least evolved lavas representing the earliest phase of activity of Tendurek have consistently higher Sr abundances (>400ppm.) and lower Rb/Sr ratios (<0.1) in comparison with the more evolved lavas produced during the second phase of activity . There is a negative correlation between the Sr 87/86 ratios and reciprocal Sr abundances for the relatively

undifferentiated Tendurek lavas (Figure-2.10). Some of these lavas also have unradiogenic Pb 206/204 ratios, which correlate negatively and positively with Sr 87/86 and Nd 143/144 ratios, respectively (Figure-2.13). These characteristics are all consistent with contamination involving lower crust. As pointed out by DePaolo (1981), positive correlations between Sr abundances and Sr 87/86 ratios can be modelled by an assimilation-fractional crystallization process in which Sr behaves incompatibly in a lower crustal environment assuming existence of sufficiently high water pressures. Nd and Sr abundances and isotopic compositions of the "primitive" Tendurek lavas can be modelled by an assimilation-fractional crystallization (AFC) process assuming a bulk distribution coefficient of 0.15 for Nd, a range of 0.5 to 0.9 for the ratio of assimilation to fractional crystallization, a lower crustal composition of Nd=30ppm., Nd 143/144=0.51265, Sr=250ppm., Sr 87/86=0.70750, and an uncontaminated magma composition of Nd=19ppm., Nd 143/144=0.51288, Sr=400ppm., Sr 87/86=0.70460. The lower crustal composition given above is chosen because it satisfies the data. However, the question of the representativeness of this composition is a difficult one to answer due to lack of any data about the nature of lower crust in this region. However, the 5 to 7 fold increase in Rb, Ba and Cs abundances from T-38 to T-34 suggests contamination by a lower crustal melt rather than assimilation of pieces of lower crustal material. Thus the inferred abundances of Nd and Sr for the lower crust may not reflect the actual abundances in the solid.

It is also interesting to note the differences in the chondrite normalized patterns of T-38 and T-34 (Figure-2.6). While the chondrite-normalized Tb abundances of T-34 and T-38 are identical, T-34 is not only significantly enriched in LREE but is also slightly enriched in HREE. Considering the convex upward partition coefficient patterns of calcic amphiboles and clinopyroxenes (Mysen, 1977; Nicholls & Harris, 1980), either fractional crystallization of those phases or partial melting of rocks containing the above phases

can potentially cause enrichments in LREE and HREE. However, consideration of the following points makes it more likely that T-38 composition can be modified by addition of a small degree partial melt derived from an amphibole-bearing source:

1. 36% decrease in K/Rb ratio from T-34 to T-38
2. About a two-fold decrease in K/Cs ratio
3. 4 to 7 fold increase in K, Rb, Ba and Cs abundances
4. 40% increase in Sr abundance
5. Assumed high water pressures in order to explain the Sr abundance increase.

T-34 also has the most unradiogenic Pb 206/204 ratio among the Tendurek lavas. All the above facts are consistent with lower crustal contamination of magmas (with T-38 like composition) by small degree partial melts derived from lower crust that is metamorphosed to amphibolite facies. Among the first activity phase lavas of Tendurek, T-38, T-46, T-26 and T-34 appear to be consistent with the above scenario. However, T-1 and T-64 differ from them, in that they do not show any shift toward unradiogenic Pb 206/204 ratios as expected for lower crustal contamination. They are erupted through two major fault zones, Agri Fault and Caldiran Fault, respectively (see Chapter-3). This may not be of any significance as far as the chemistry of these lavas are concerned. However, it is worth noting that crustal contamination of a basaltic magma by a crustal melt is a liquid-state interdiffusion process, in which the relative diffusivities of elements and "exposure" times are very important in determining the contamination signatures for different elements (Watson, 1982). If the presence of a major fault zone reduces the residence time of a basaltic magma within a lower crustal environment, crustal contamination may be manifested selectively depending on the relative diffusivities of the elements concerned. If there is a large enough difference between the diffusivities of Pb relative to Nd, Sr, and the alkalies, then relatively rapid ascent utilizing existing major fault zones may provide an explanation for the lack of unradiogenic Pb 206/204 signa-

tures for T-1 and T-64. Alternatively, compositionally heterogeneous lower crust may be considered as a likely explanation.

Lavas produced during the second activity phase of Tendurek exhibit a large range in Rb/Sr ratios and Sr abundances (Figures-2.8 and 2.10), but a small range in Sr 87/86 ratios. They also form linear trends of negative slope on the Sr 87/86 versus Rb/Sr and Sr 87/86 versus 100/Sr diagrams. The large ranges in Rb/Sr ratios and Sr abundances can be accounted for by fractional crystallization involving plagioclase within a shallow crustal magma chamber. The observed negative correlations in Figures 2.8 and 2.10 can be explained in two ways. If fractionation of a single batch of magma is envisaged, crustal contamination during fractionation by wall-rocks which have less radiogenic Sr 87/86 ratios (0.7058 versus 0.7052), can produce those negative correlations. Alternatively, fractionation of a magma in a magma chamber that is repeatedly filled by magmas that become progressively less radiogenic can also produce the negative correlations. In this case, the erupted magmas will be progressively more fractionated, LIL element enriched but their Sr isotope ratios will be lower.

Malazgirt lavas form distinct fields on the diagrams involving isotope ratios. S-60 is the most primitive among them with 7.52% MgO content and 56.6 Mg# (Table-2.1). It also has the lowest K content (3795ppm.) among all of the alkaline rocks. K is an element which is most drastically affected by crustal contamination (De Paolo, 1981; Watson, 1982). Based on its low K content and primitive character, one would expect that S-60 is the least affected by crustal contamination. However, its Nd 143/144 ratio is among the lowest obtained from the alkaline suite. S-60 plots closest to the oceanic regression line on the Nd-Sr correlation diagram compared to the other alkaline samples (Figure-2.7). Malazgirt lavas do not show the unradiogenic character in Pb 206/204 ratios but they are quite radiogenic in Pb 207/204 ratios (Figure-2.12). In light of the

above geochemical characteristics, it is difficult to conclusively assess the viability of crustal contamination for S-60. However the following points argue against crustal contamination:

1. High MgO content and Mg# of S-60.
2. Lowest K content among alkaline suites (3795 ppm.)
3. Lower Sr 87/86 ratio (0.70462) than samples that are contaminated by crust.
4. Lack of unradiogenic Pb 206/204 signatures.

The overall trends formed by the Malazgirt lavas in Figure-2.7 to 2.11 appear to be consistent with two-component magma mixing between S-60 and a crustally contaminated basaltic magma (similar to T-46 and T-64).

The most striking characteristic of the basaltic Nemrut lavas is their more radiogenic Pb isotopic compositions with respect to the other alkaline suites (Figure-2.12 and 2.13). All of the basaltic lavas post-date the extensive ignimbrite eruptions of Nemrut. As emphasized in the third chapter, Nemrut volcano is situated in a rift-like environment (Mus-Van basin). The Mus basin is filled with recent (Tertiary to present) sediments reaching thicknesses of up to 8000m. Once the lower crust is partially melted, causing ignimbrite eruptions, and is replaced by upper mantle material, the basaltic magmas that are produced later would escape lower crustal contamination. However, upper crustal contamination by recent sediments would create radiogenic Pb signatures. This scenario seems to be consistent with the overall geochemical characteristics of the basaltic Nemrut lavas.

2.5.2 Mantle Source Characteristics

Study of mantle-derived xenolith-bearing alkali basalts is a generally accepted and widely used approach (in order to avoid complications arising from fractionation or crustal contamination of lavas) in the characterization of mantle sources. Because of the general lack of mantle xenoliths in tholeiitic lavas, an alternative is to choose lavas that closely approximate the equilibrium partial melts of assumed mantle compositions. These melts would have a Mg# in the range of 68-75 for up to 30% melting of peridotite, based on the Fe-Mg partitioning between olivine and liquid (0.3; Roeder & Emslie, 1970) and Mg values of 88-89 for upper mantle peridotites (Frey et al. 1978). Unfortunately, none of the analyzed samples meet the above criteria and most of them have been modified by crustal contamination and fractionation. Nevertheless, some broad generalization can be made based on the chemistries of the least modified lavas. In this respect S-60 is the best candidate among the alkaline lavas, but ironically its overall composition is tholeiitic rather than alkaline. Although S-60 is nepheline normative, the fact that it plots very close to the alkaline-subalkaline dividing line on the alkalies versus silica plot (Figure-2.2) and its chondrite normalized La/Yb ratio of 1.99 (relatively flat REE pattern), suggest a transitional character for S-60.

Frey et al.(1978) proposed a model in which associated melilitites, basanites, alkali basalts and tholeiites of Eastern Australia are produced from a common LREE-enriched pyrolite source (with lower Ti content) by 4-25% partial melting. However, this model is not applicable to the Eastern Turkey volcanics, because a pyrolite model implicitly or explicitly (Ringwood, 1975) assumes a "fertile" mantle source with chondritic Rb/Sr and Sm/Nd ratios. Including the alkali basalts, all the volcanics from Eastern Turkey indicate derivation from a mantle source(s) that has had time-integrated depletions in Rb/Sr and Nd/Sm ratios. This is in accord with the conclusions reached by Allegre et al., (1981,

1982) and Allegre (1982) regarding the depleted nature of subcontinental mantle. As proposed in Chapter-1, the highly radiogenic Pb 207/204 character of the alkali basalts and the steep trends obtained on 207-206-204 Pb diagrams necessitate a mantle source that is contaminated by LIL-element enriched fluids carrying sediment signatures. It has also been suggested that this contamination event is possibly related to the closure of Paleo-Tethys. It can be envisaged that such a contamination would cause enrichments in the depleted subcontinental mantle (in spinel-peridotite facies) and also create hydrous phases such as amphiboles. In fact, there is abundant evidence confirming the presence of heterogeneously metasomatized, hydrous phase-bearing subcontinental mantle as inferred by mantle xenolith studies (e.g. Frey & Green, 1974; Frey & Prinz, 1978; Menzies & Murthy, 1980). These studies propose the derivation of metasomatizing fluid or low degree melt (Component-B of Frey & Green, 1974) from a garnet peridotite source. This is not inconsistent with the proposed model here, as long as a sediment contamination is superimposed on it. Magmas derived from a heterogeneous, amphibole-bearing spinel-peridotite mantle source by varying degrees of partial melting can generate the alkaline to tholeiitic lavas. Along with the isotope data, the Na and Al-rich composition of the alkaline lavas (Table-2.1) is consistent with such a model. For example, Frey & Green (1974) reported major element composition of glasses that are formed by incongruent melting of hydrous phases in peridodite nodules during their rapid ascend to the surface. Examination of the major element compositions of these glasses (Table-6 of Frey & Green, 1974) reveals that the alkali abundances are correlated with associated hydrous phases (amphibole and/or phlogopite). Glasses derived mainly from amphibole have very low K2O contents (e.g. 0.05, 0.1%) and K2O/Na2O ratios, whereas the ones that have phlogopite melt components have very high K2O contents (up to 7%) and high K2O/Na2O ratios. Independent from the type of hydrous phase, all glasses are characterized by very high Al2O3 contents (up to 24.2%).

Table-2.5 Comparison of basalt compositions from different tectonic environments

	EASTERN TURKEY		ANOROGENIC BASALT						CONT. ARC HAB			AVE. MORB
Ref.	S-60	A-30-1	1 (a)	2 (a)	3 (a)	4 (a)	5 (b)	6 (c)	7 (d)	8 (d)	9 (d)	10 (e)
SiO2	48.37	51.84	51.42	50.43	50.56	50.75	52.41	52.46	52.2	51.89	50.1	49.56
Al2O3	18.38	18.30	13.87	15.44	13.83	13.51	13.65	14.13	19.1	20.36	17.7	16.09
FeO(T)	10.29	8.89	14.23	10.49	12.41	12.81	10.89	10.46	7.07	7.64	10.0	10.17
MgO	7.52	5.06	2.69	7.60	5.12	4.21	5.64	6.38	5.33	4.41	6.80	7.69
CaO	9.88	7.99	6.44	8.96	9.62	8.45	8.79	8.01	8.57	9.41	9.89	11.34
Na2O	4.00	4.60	4.02	3.21	2.65	2.80	2.28	2.78	4.32	3.50	3.34	2.80
K2O	0.46	0.37	2.52	0.98	0.93	1.58	1.72	0.42	0.80	0.64	0.48	0.24
TiO2	1.64	1.78	2.30	1.42	2.57	3.95	2.77	1.65	1.69	1.01	1.52	1.42
MnO	0.18	0.14	0.27	0.17	0.17	0.19	0.15	0.13	0.69	0.18	0.17	-
P2O5	0.23	0.28	1.55	0.28	0.22	0.66	0.49	0.24	0.20	0.21	0.14	0.12
Sr	333	424	296	430	219	732	316	279	280	436	380	121
Rb	9.5	9	58	18.2	15	44	19	10	10	22	18	2
Ba	-	93	1658	394	239	653	295	111	290	244	135	20
Zr	-	184	1195	143	203	398	134	142	-	-	-	90
Hf	3.57	4.09	23.4	3.25	4.49	7.22	-	-	-	2.55	-	2.44
Nb	-	6	112	14.1	15.9	37	5	12	-	-	-	4.6
Th	1.91	1.67	7.15	2.83	1.12	5.33	-	3	-	2.69	-	0.26
Zr/Nb	-	30.7	10.7	10.1	12.8	10.8	26.8	11.8	-	-	-	20

Sample Locations: 1- Craters of the Moon National Monument, U.S.A.; 2- New Grande Rift, New Mexico, U.S.A.;
3- Deccan, India; 4- Parana Basin, Brasil; 5- Average Sabie River form. (n = 27), Karoo, S. Africa;
6- Springsure Group, Southern Queensland, Australia; 7- Chiole Island, Chile;
8- Average (n=8) Andean HA basalt; 9- Mt. St. Helens.

(a) Thompson et al., (1983)
(b) Cox (1983)
(c) Ewart (1982)
(d) Escobar et al., (1977)
(e) Pearce (1976, 1982)

In Table-2.5, the compositions of the closest candidates for mantle-derived magmas from Eastern Turkey (S-60 and A-30-1) are listed with various, mostly tholeiitic, basalts from different tectonic environments for comparison (because of the transitional-tholeiitic composition of S-60). The most obvious differences between the major element compositions of S-60 and anorogenic basalts are the high contents of Al2O3 and Na2O in S-60. Once the accumulated plagioclase possibility is discounted (because of the practically aphyric nature of S-60), then this difference must be significant in terms of magmatic processes and/or mantle source compositions. Similar differences are also observed between high-alumina basalts and continental tholeiites. When these observations are combined together, probably the most likely explanation would be hydrous (including hydrous phase contributions) versus anhydrous melting of depleted upper mantle. Recently, Grove and Baker (1984) have emphasized the importance of early plagioclase fractionation (under dry conditions) in the generation of tholeiitic trends. When the already high-Al2O3 character of melts that are formed by partial melting of hydrous-peridotites are retained by the supression of plagioclase fractionation, then it would be possible to generate high-Al lavas like S-60 or typical high-alumina basalts.

The closest analogs to the eastern Turkish volcanics are the Cenozoic volcanics from the western U.S.A. (Hedge & Noble, 1971; Lipman et al., 1978 and its references; Menzies et al, 1983). Interestingly, the western U.S.A. is also the closest analog to eastern Turkey in terms of its geological evolution. In the western U.S.A., the cessation of a subduction-related regime was followed by initiation of extensional tectonics characterized by normal faulting. This is similar to eastern Turkey but without continental collision (see Chapter-3). Recent volcanism (including calc-alkaline and alkaline character) developed in response to this new tectonic regime. Alkali olivine basalts from the Southern Basin and Range province (SBRP) and Sierra Nevada province (SNP) span a large range in Sr and Nd isotopic compositions (0.70285-0.70689 and 0.51304-0.51215, respectively,

Menzies et al., 1983). SNP lavas are also characterized by unusually high Sr contents (700-2,500ppm.). Based on the lack of a negative correlation between Sr 87/86 and Nd 143/144 ratios, crustal contamination of the SNP lavas has been discounted (Hedge and Noble, 1971; Menzies et al., 1983). The latter authors have suggested an enriched-heterogeneous-hydrous garnet peridotite mantle source for the SNP lavas. However, the above argument against crustal contamination is not a strong one, as emphasized in the previous discussions. Moreover, "enriched mantle" and "crustal contamination" possibilities are not exclusive of each other. Probably better and more convincing conclusions can be reached without a prejudiced approach by considering more complex and geologically reasonable processes (e.g. contamination by partial melts derived from an already crustally-contaminated igneous body).

2.6 Conclusions

The alkaline volcanics of eastern Turkey span a wide composition range from alkali basalts, through hawaiites, benmoreiites, mugearites to silica oversaturated peralkaline lavas. Alkali volcanism in basically sodic in character and the most primitive lavas are transitional to tholeiites. All of the alkaline suites studied have been variously affected by lower and/or upper crustal contamination. The conclusions reached in Chapter 1 regarding the mantle source characteristics of end member #1, inferred from Sr, Nd and Pb isotopes, are basically valid for the alkaline volcanics. Derivation of the alkaline lavas by partial melting of a recently metasomatized, heterogeneous, hydrous phase-bearing, depleted peridotite mantle source followed by variable degrees of crustal contamination and fractional crystallization is consistent with their overall geochemical characteristics.

CHAPTER 3

DEFORMATIONAL DOMAIN CONTINENTAL TECTONICS IN THE LAKE VAN REGION, EASTERN TURKEY: IMPLICATIONS ON THE ORIGIN OF AN EXTENSIONAL REGIME ASSOCIATED WITH COMPRESSION

3.1 Introduction:

Our knowledge on continental tectonics has advanced significantly in the last decade, with the emphasis given to the study of deformational modes displayed by convergent boundaries and continental collision zones (e.g., McKenzie, 1972; Molnar & Tapponnier, 1975; Tapponnier & Molnar, 1976; Burchfiel, 1980, Royden et al., 1983). One of the major outcomes of these studies is the recognition of the differences in deformational styles between oceanic and continental crust. The seismic activity and deformation is confined to narrow zones within oceanic crust that allow the precise identification of plate boundaries and their interactions. Continents display much more complex internal deformational styles, that incorporate spatially and temporally coexisting compressional, extensional, and transform regimes evidenced by the heterogenous, diffuse seismic activity within broad zones. This makes the strict application of rigid-plate concepts almost impossible in intracontinental areas. These complications arise from a number of reasons that are inherently attributable to the nature of the continental crust. Among those the most important ones are: 1- Its buoyant character and resistance to subduction, 2- Its tendency to escape laterally away from continental collision zones along major transform boundaries. 3- Its ability to retain a tectonic memory by preservation of old zones of weaknesses that can be reactivated. Superposition of new and reactivated structures, particularly large fault zones, fragment the continental crust into a mosaic of blocks. By locking or unlocking of fault zones, blocks within the mosaic can escape laterally. Interaction between blocks can also transmit forces over great distances within the continental crust. 4- The mosaic structure exposed at the surface may not extend throughout the entire thickness of the continental crust, but may be present above major subhorizontal zones of decoupling. (Bak et.al, 1975; Grocott, 1977; Eaton, 1980; Burchfiel, 1980).

Eastern Turkey, particularly the Lake Van region, represents an area where we can identify the above characteristics of continental tectonics and, by studying the details of the crustal mosaic structure, potentially offers an in-depth understanding of the complex tectonic processes that occur in convergence and continental collision zones.

The present tectonic regime of eastern Anatolia is mainly dominated by the relative motions of the Arabian and Eurasian plates (Nowroozi, 1971; McKenzie, 1972; Dewey et al., 1973). As a result of the convergence between the Arabian and Eurasian plates, the existing southern branch of the Neo-Tethian ocean was consumed by a northward subduction, and continental collision took place in Miocene time along the Bitlis Suture Zone (Rigo de Righi & Cortesini, 1966; Dewey et al., 1973; Hall, 1976). Convergence is still active today, as shown by the folding and thrusting of Pliocene to recent sediments on the Arabian platform ("border folds" of Ketin (1966) in Turkey, Zagros ranges in Iran) and the diffuse seismic activity throughout the region (Nowroozi, 1971; McKenzie, 1972; Rotstein & Kafka, 1982).

McKenzie (1972) originally proposed that, as a manifestation of this continental collision, in order to avoid the thickening of the buoyant continental crust, the Anatolian plate moves away westward from a triple junction (known as the Karliova Junction, Figure-3.1) by consuming eastern Mediterranean sea floor along the Hellenic trench. McKenzie's model has received general acceptance, with some minor modifications, in the literature dealing with the tectonics of the eastern Mediterranean (e.g., Alptekin, 1973; Tapponnier, 1977; Dewey & Sengor, 1978; Mercier, 1981).

Detailed study of the tectonics in eastern Turkey (east of the Karliova Junction, here called the Lake Van region) has been neglected partly due to the extensive Tertiary to recent volcanics that obscure the structures in this region. Innocenti et al.(1976)

Figure-3.1

Major tectonic elements of Turkey. Only the deformational domains of eastern Turkey are shown. ADD: Anatolian, PDD: Pontide, EEDD: Erzincan-Erzurum, VDD: Van, AFDD: Arabian Foreland, AZDD: Azerbaijan, RDD: Rezayeh deformational domains. The major faults are: NAF: North Anatolian, EAF: East Anatolian, PFZ: Pasinler, AFZ: Ararat, HF: Hakkari, MRF: Main Recent, ECF: Ecemis, TGF: Tuz Golu fault. WAGS: West Anatolian Graben System, BSZ: Bitlis Suture Zone. LV: Lake Van, BM: Bitlis Massif, PM: Puturge Massif, GS: Gulf of Saroz, GI: Gulf of Iskenderun, M: Mudurnu region.

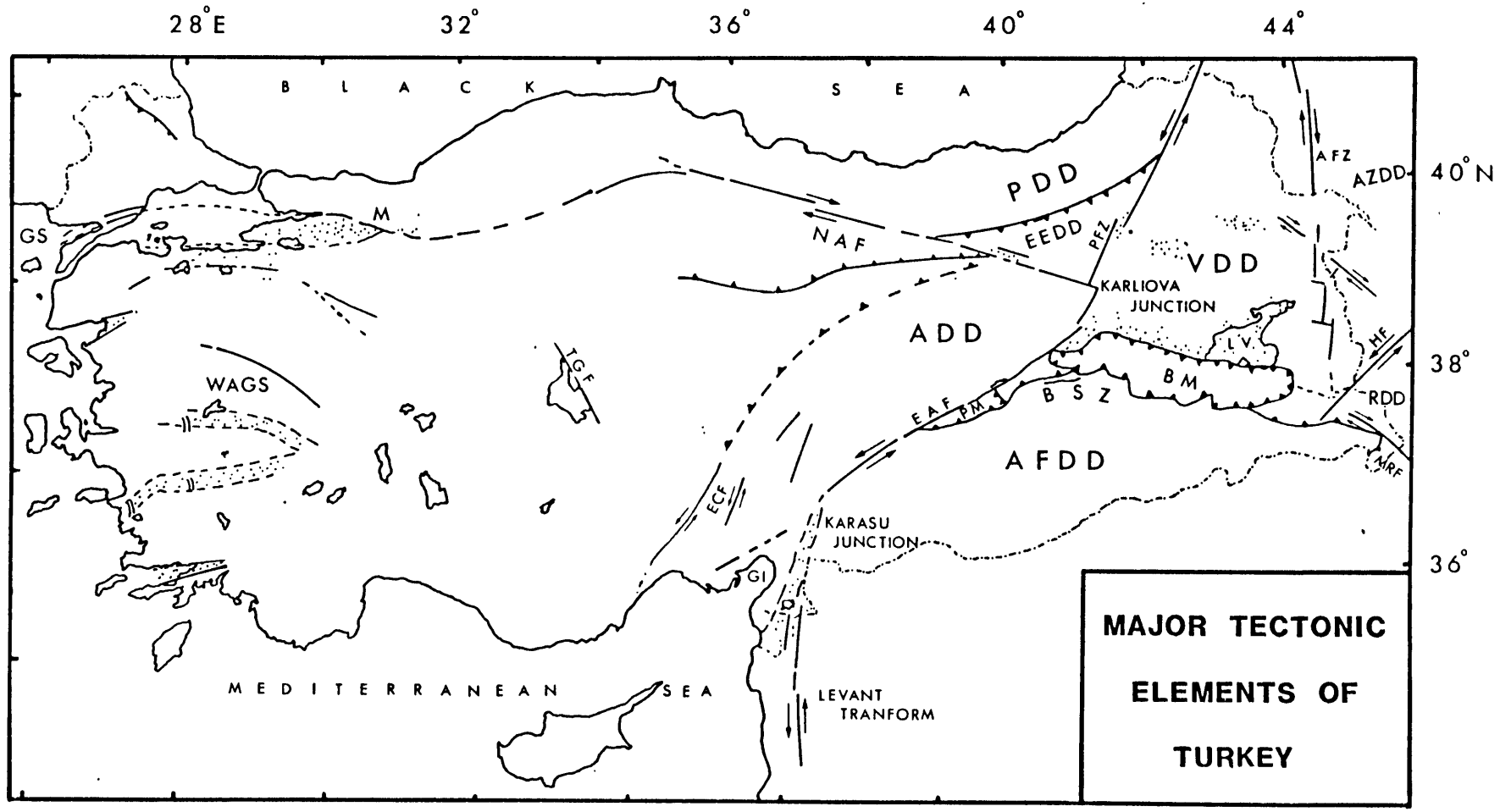
28°E
32°
36°
40°
44°
40°N
38°
36°
B L A C K S E A
MEDITERRANEAN SEA
GS
M
NAF
PDD
EEDD
PFZ
AFZ
AZDD
VDD
KARLIOVA JUNCTION
ADD
LV
HF
BM
BSZ
EAF
RDD
MRF
AFDD
WAGS
TGF
ECF
KARASU JUNCTION
GI
D
LEVANT TRANFORM
MAJOR TECTONIC ELEMENTS OF TURKEY

studied the volcanics in the Lake Van region and suggested that the calc-alkaline volcanism is a result of a relict subduction process following cessation of subduction in Upper Miocene time, and that the alkaline volcanism marked the onset of the continental fragmentation due to the divergent motion of the Anatolian and Iranian plates. Sengor & Kidd (1977) synthesized the accumulated geological data and tried to establish a similarity between the tectonics of the "Turkish - Iranian Plateau" and the "Tibet Plateau". They suggested that the post-collisional tectonics of the "Turkish Plateau" can be explained by shortening and thickening of the continental crust, whereby its lower levels are partially melted to give rise to the calc-alkaline volcanism. They also proposed that local longitudinal cracking of the crust, due to north-south shortening, produced the alkaline volcanism in eastern Turkey.

The purpose of this paper, based on the results of my field studies, aerial photograph, LANDSAT and SIR-A (Shuttle Imaging Radar) image analysis and also on the existing geological and geophysical data, is to present a tectonic model suggesting the development of an extensional tectonic regime within a broad compressional regime and to propose a generalized model for the initiation of extensional tectonics.

3.2 Geological Setting

The NE-SW trending Bitlis metamorphic massif is about 300 km. long and 40 km. wide. It is located to the south of Lake Van (Figure-3.1,2), and is part of a belt of metamorphic rocks that extends from the Nigde-Bolkar and Puturge massifs in the west to the Zagros mountains of Iran in the east (Sanandaj-Sirjan Zone of Stocklin, 1968). The Bitlis massif contains rocks of almandine-amphibolite facies in its core and a greenschist-facies in its cover (Boray, 1973; Yilmaz, 1975). Yilmaz (1972) has determined by Rb/Sr dating that the core metamorphism and associated granitic intrusions took place

Figure-3.2

Geological map of the Lake Van area. Simplified after Altinli, 1966-b. Key to the legend: 1-Quaternary, 2-Late Cenozoic volcanic rocks, 3-Neogene, 4-Oligo-Miocene, 5-Eocene, 6-Late Cretaceous-Paleocene ophiolitic melange, 7-Ophiolites, 8-Granitoids, 9-Metamorphic basement 10-Autocthonous Arabian platform sedimentary rocks (to the south of the Bitlis suture zone).

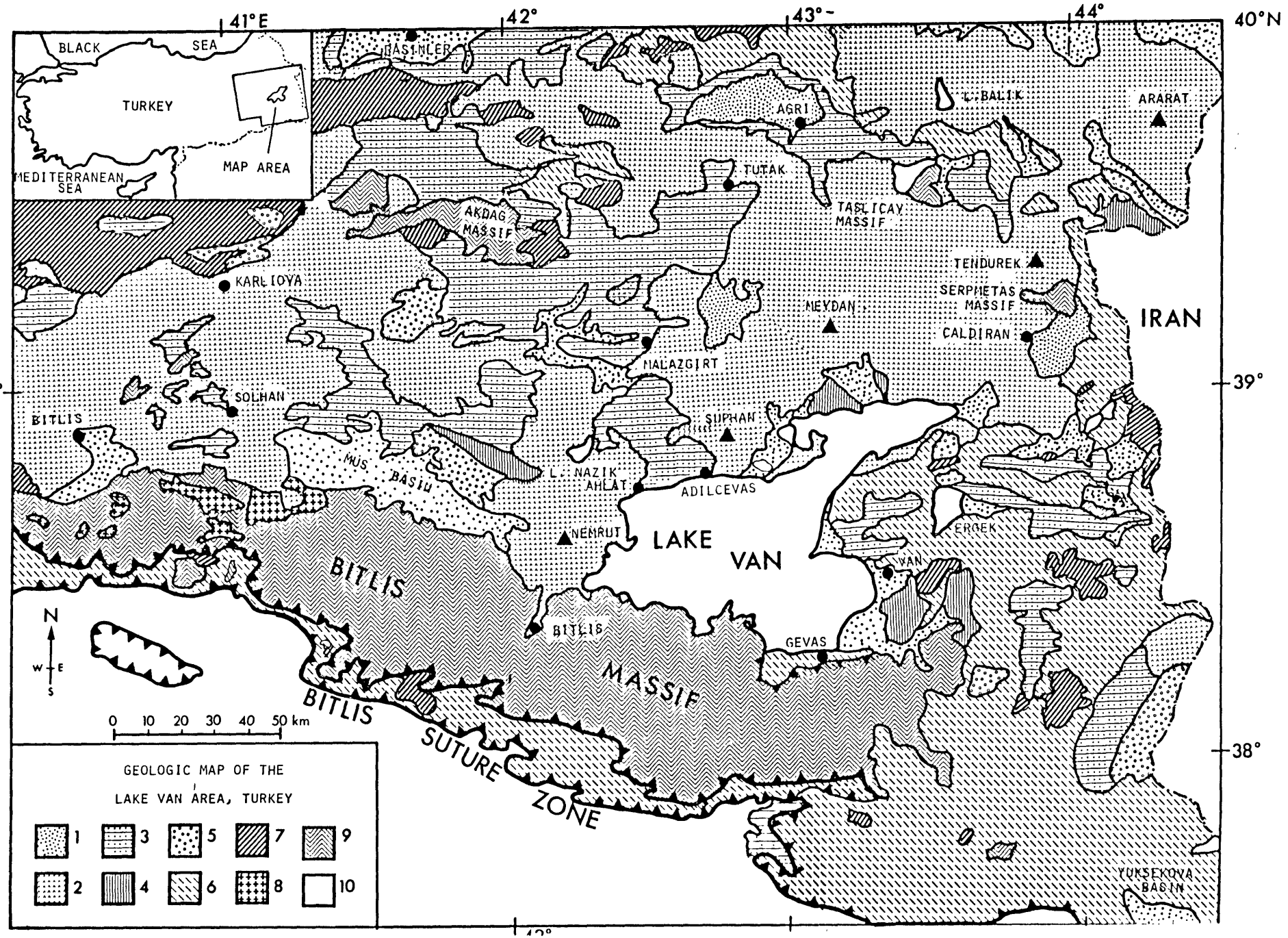
41°E
42°
43°
44°
40°N
39°
38°
BLACK SEA
TURKEY
MEDITERRANEAN SEA
MAP AREA
BASINLER
AGRI
L. BALIK
ARARAT
TUTAK
TASLICAY MASSIF
AKDAG MASSIF
KARLIOVA
TENDUREK
SERPHETAS MASSIF
NEYDAN
IRAN
CALDIRAN
NALAZGIRT
SOLHAN
BITLIS
SUPHAN
MUS BASIN
L. NAZIK
AHLAT
ADILCEVAS
NEMRUT
LAKE VAN
ERCEK
VAN
BITLIS MASSIF
GEVAS
BITLIS SUTURE ZONE
YUKSEKOVA BASIN
N
W
E
S
0 10 20 30 40 50 km
GEOLOGIC MAP OF THE LAKE VAN AREA, TURKEY
1
2
3
4
5
6
7
8
9
10

in the Paleozoic. The cover rocks are composed of Megalodont-bearing Upper Triassic marbles and schists intercalated with metavolcanics and Fusulinid-bearing marbles (Perincek, 1980). Perincek (1980) interpreted the presence of Upper Triassic(Norian) metavolcanics within the Bitlis massif as evidence of continental rifting and the opening of the south Neo-Tethyan ocean which separated the Anatolian and Arabian plates.

The Bitlis Suture Zone is situated to the south of the Bitlis massif and consists of arcuate, north dipping, internally-imbricated thrust sheets of ophiolitic melange and flysh units (Rigo de Righi & Cortesini, 1966; Hall, 1976; Ozkaya, 1982). The Bitlis massif is thrust southward over an ophiolitic melange complex which,in turn is thrust southward over sedimentary rocks of the Arabian platform (Altinli, 1966-b; Hall, 1976).

On the Arabian platform, autocthonous sedimentary rocks range from Paleozic to Upper Tertiary age in southeastern Turkey(Foothills structure belt of Rigo de Righi & Cortesini,1964 and Border Folds of Ketin,1966). The autochthonous rocks contain imbricated thrust faults and disharmonic folds, that affect rocks as young as Pliocene to Recent, that can be followed to the southeast into the Zagros ranges of Iran (Altinli, 1966-a; Stocklin, 1968; Haynes and McQuillan, 1974).

The area north of Lake Van, is largely covered by Late Cenozoic volcanic rocks but Paleozoic metamorphic rocks crop out as small inliers (e.g.,Akdag, Taslicay, Serpmetas massifs; Figure-3.2). The metamorphic rocks in these areas resemble those of the Bitlis massif. This crystalline basement and an Upper Cretaceous-Paleogene ophiolitic melange-flysh complex that crops out mainly to the west of the Lake Van, is overlain unconformably by wide-spread Miocene marine carbonate rocks and lacustrine and fluvial molassic sedimentary rocks.

In contrast to the Neogene formations, Eocene and Oligocene rocks are not wide-spread in the Lake Van region. They are present within depressions such as the "Mus Basin". The limited nature of Early Cenozoic rocks could be partly due to their removal by erosion following Late Tertiary uplift. However, analysis of their depositional environment and lithological character suggest that they were formed within pull-apart basins and fault troughs along major strike-slip faults. The Eocene rocks in the Lake Van region also contrast sharply with the wide-spread Eocene rocks to the west of the Karliova Junction, and on the Arabian platform, in terms of their depositional environment and lithology.

The Eocene rocks consist of several hundred meters of alternating very poorly sorted conglomerates and sandstones around Gevas, along the southern shore of the Lake Van. These conglomerates unconformably overlie either rocks of the Bitlis Massif or ophiolitic rocks near Gevas and contain angular clasts derived from the underlying lithologies (Yilmaz et al., 1981). The Gevas conglomerates contain Nummilites both within their clasts and within their matrix. These rocks have been interpreted by Yilmaz et al (1981) as debris flows deposited along a fault zone. Altinli (1966a) described the Eocene deposits in the Lake Van region as containing "confused bedding, lensing, intertonguing and cataclastic features".

Tertiary sediments are present within narrow, elongate basins unconformably overlying the metamorphic basement rocks or ophiolitic melange in the Lake Van area. Thickness of the Tertiary to Quaternary sedimentary formations reaches about 6500m. in the Erzurum-Pasinler, 4500m. in the Tekman, 7000m. in the Malazgirt, and 8000m. in the Mus basins (Kurtman and Akkus, 1971; Kurtman et al., 1978; Saroglu and Guner, 1981). These are composed of mainly alternating conglomerate, sandstone, marl, and reefal limestone that were deposited in a shallow marine environment from Lutetian to Middle Miocene.

However, rapid facies changes are typical in these basins. In fact, along the northwestern shore of the Lake Van, Ahlat-Adilcevaz area, the Tertiary is excusively represented by red-continental Ahlat conglomerates, reaching about 550m. thickness (Altinli, 1966-a; Kurtman et al., 1978). In general, Oligocene rocks unconformably overlie Eocene rocks. The post-Burdigalian sedimentation starts with an unconformity. It is generally lacustrine and becomes fluviatile upwards into Upper Pliocene and Quaternary time and includes volcanic intercalations.

The area north of Lake Van is extensively covered by Late Tertiary to recent volcanics. Calc-alkaline and alkaline rocks coexist spatially and temporally. The absence of any volcanogenic material in the Aquitanian-Burdigalian sediments underlying the volcanic cover implies that the volcanic activity in this region started after Late Burdigalian time (Innocenti et al., 1980). Calc-alkaline volcanism is represented by two main stages of activity. K/Ar dating by Innocenti et al.(1976) has revealed that the first phase of calc-alkaline, high-potassic activity came to an end with repeated ignimbrite eruptions about 6my. ago and was characterized by large lava domes and flows. The second stage calc-alkaline volcanic activity formed spectacular stratovolcanoes, such as Suphan and Ararat, whose heights reach 4058m. and 5165m. respectively. Andesitic and dacitic compositions dominate the calc-alkaline products, with subordinate basalts and pyroclastics.

The alkaline volcanism started as fissure basalt eruptions about 6my. ago and continued with the development of major cones such as the Nemrut and Tendurek volcanoes. Alkaline rocks include alkali basalts, hawaiites, mugearites, benmoreites and trachytes. Hawaiites are by far the most abundant lithology. Nemrut volcanoe is surrounded by an extensive ignimbritecover (about 400 sq.km.) which also contains pumice intercalations. Highly fractionated peralkaline lava flows (mostly commenditic) fill the eastern half of the

Nemrut caldera, which has a diatemeter of 8km. The youngest activity of Nemrut volcano is represented by minor olivine-basalt lava flows, which erupted in 1441 (Oswald, 1910). Tendurek volcano also produced some peralkaline lava flows and minor pyroclastics.

3.3 Tectonic Setting

A thorough understanding of the Late Cenozoic to Recent tectonic evolution of the Lake Van region requires at least some background knowledge of the major tectonic structures in eastern Turkey, such as the North and east Anatolian faults. I will present a brief review of these major features before discussing the tectonics of the Lake Van region.

In the LANDSAT and SIR-A image analysis, strike-slip faults have been identified by the determination of characteristic straight and narrow furrows (strike-slip rift) and adjacent hills, sharp traces in Quaternary alluvium, major bends and interruptions of streams and long linear paths of major streams (e.g. Tapponnier & Molnar, 1977). These determinations have been corroborated by field observations, seismicity, alignment of the earthquake epicenters, available geological maps and seismic reflection profiles across the Lake Van.

3.3.1 North Anatolian Fault

The North Anatolian Fault (hereafter referred to as the NAF) is an arcuate right-lateral strike-slip fault that extends about 1200km. westwards from Karliova Junction (the intersection of NAF and East Anatolian faults, Figure-3.1) all the way to the Gulf of Saroz (see Sengor's, 1979 detailed review). The fault zone is marked by high seismic activity and has been the locus of numerous destructive historic and recent

earthquakes (Allen, 1969, 1975; Toksoz et al. 1979). The fault-plane solutions of the major shocks along the fault zone give a well-defined pure right-lateral strike-slip motion between the Karliova Junction and about 31 E longitude, near Mudurnu. (Canitez & Ucer, 1967; McKenzie, 1972; Dewey, 1976). To the west of 31 E longitude, the NAF splays into several branches that display major en-echelon and anastomozing fault geometries and the fault plane solutions include a predominant normal faulting component in addition to the right-lateral strike-slip component (Canitez & Ucer, 1967a,b; McKenzie, 1972).

The NAF zone, between Karliova Junction and about 31 E longitude (Mudurnu region), consists of a number of strike-slip faults with different lenghts arranged in an en-echelon geometry and contains numerous pull-apart basins (i.e. from east to west they are Erzincan, Susehri, Niksar, Erbea, Ladik, Kargi, Tosya, Ilgaz-Cerkes, Gerede, Bolu etc.). The fault traces have been mapped in detail by Ketin & Roesli(1953) and Arpat & Saroglu(1979) in some parts of the NAF zone.

In spite of the large number of studies on the NAF, a general agreement has not been reached yet on its date of initiation and cumulative offset. However, an offset of about 85 km. since Burdigalian time has been documented by Seymen(1975) in the eastern part around Resadiye-Erzincan. The NAF seems to represent a tectonic feature older than Burdigalian (possibly Eocene time) so that the 85 km. displacement should be considered as a minimum displacement along the fault (discussed below).

It is also uncertain whether the eastern and western halves of the arc-shaped NAF represent two different faults, one left-lateral (in the west) and one right-lateral (in the east), that have been joined recently. This would require a reversal of movement from

left-lateral to right-lateral strike-slip along the western part of the fault (see Hancock & Barka, 1983 and its references).

3.3.2 East Anatolian Fault

The East Anatolian Fault (hereafter referred to as the EAF) takes up some of the motion between the Anatolian and Arabian plates and is a left-lateral strike-slip fault (Figure-3.1). It can be traced from the Karliova Junction, after making a slight bend around Bingol, extends to the SW about 410km. It intersects the left-lateral strike-slip Dead Sea Fault (Levant Transform) at the north end of the Karasu depression (Maras-Antakya graben of Arpat & Saroglu, 1975). Based on a LANDSAT interpretation McKenzie (1976) extended the EAF further to the southwest towards the Gulf of Iskenderun, giving a total length of about 550km. Fault traces have been mapped in detail by Arpat & Saroglu(1972, 1975) and Seymen & Aydin(1972). The EAF zone is similar to the NAF zone and contains several en echelon strike-slip fault segments and pull-apart basins, among which the Hazar pull-apart basin is the most prominent (Hempton et al. 1983). The fault plane solution for the May.22.1971 Bingol earthquake gives a left-lateral strike-slip motion that agrees well with the strike and sense of motion of the associated surface breaks (McKenzie, 1976). The date of origin and the cumulative off-set along the EAF are not well-constrained. Arpat & Saroglu(1972) documented a 22km. left lateral displacement of marine Miocene sediments along the EAF, close to the Karliova Junction. However, based on the geometry of the triangular Karasu pull-apart basin (EAF-Levant transform Junction), a cumulative offset of 40 km. can be estimated. Subsidence in the Karasu pull-apart basin has been about 400 m. since Upper Pliocene time, as indicated by the vertical displacement of lava flows (Arpat & Saroglu, 1975).

Figure-3.3

Location map showing the areas in which satellite (LANDSAT & ERTSA) and SIR-A (Shuttle Imaging Radar) images are discussed.

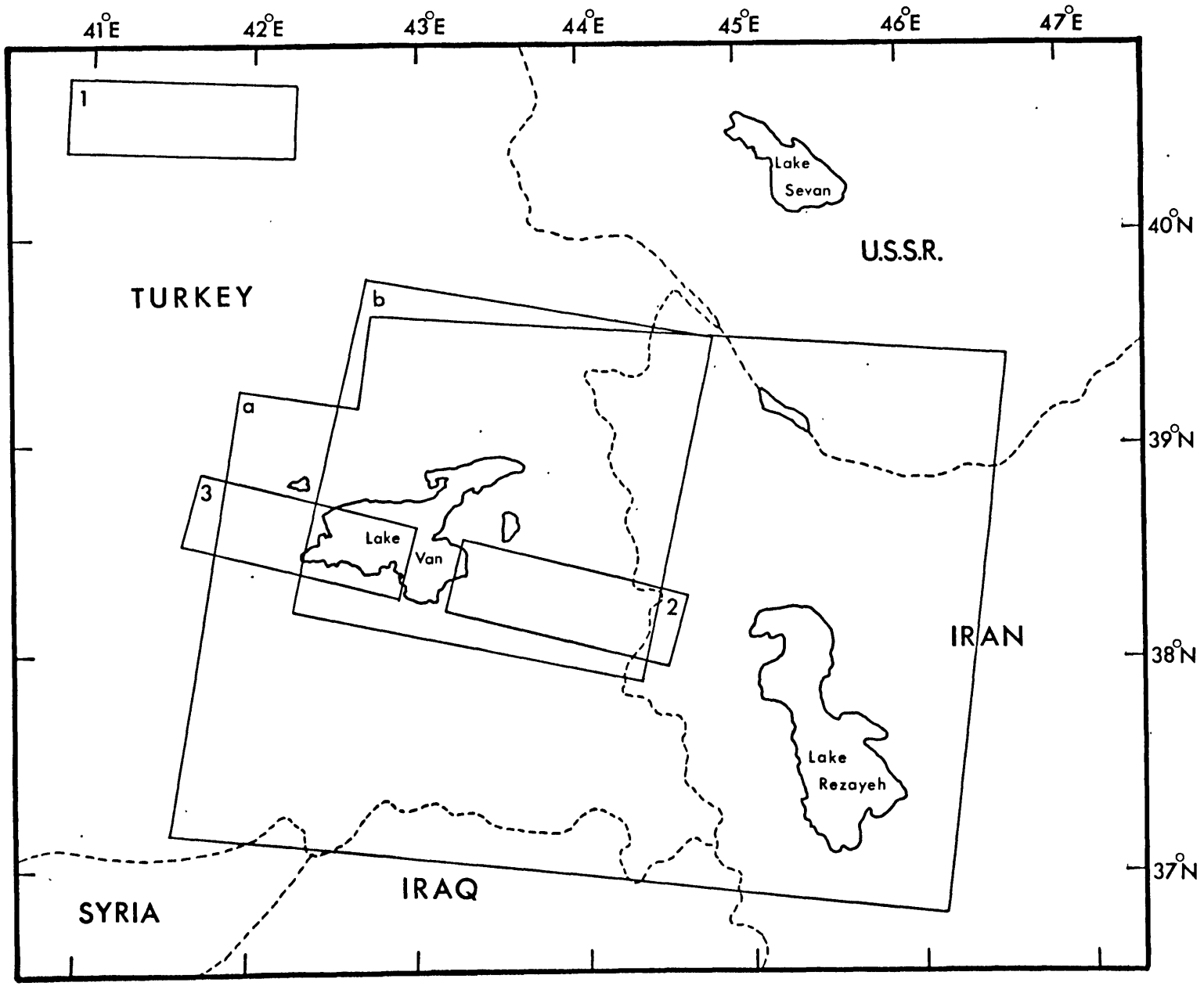
41°E
42°E
43°E
44°E
45°E
46°E
47°E
40°N
39°N
38°N
37°N
1
a
b
2
3
Lake
Sevan
U.S.S.R.
TURKEY
Lake
Van
IRAN
Lake
Rezayeh
IRAQ
SYRIA

3.3.3 Main Recent Fault

The Main Recent Fault was discovered by Braud and Ricou (1971) in the Neyriz region in Iran. Detailed studies of this fault confirmed its right-lateral, strike-slip character and its active seismicity (Tchalenko and Braud, 1974). The Main Recent Fault extends in a NW-SE direction from Neyriz Region in Iran towards the Yuksekova pull-apart basin in southeastern Turkey (Figures-3.4,8,11).

3.4 Van Deformational Domain

The term "Deformational domain" is introduced here as opposed to "plate" term, to describe continental areas that display coherent deformational styles. Deformational domains are bounded by major shear zones that, in general, have been repeatedly activated throughout the deformational history of the region. These major fault zones represent the first-order tectonic elements. The origin and evolution of the higher-order tectonic elements within the deformational domains are constrained by the domain defining first order faults and stresses that are distributed by them. Although regional seismicity helps somewhat in delineating deformational domains, it does not provide complete information, due to its diffuse nature in the continental crust. Detailed knowledge of the geology, tectonic structures and their trends, combined with seismicity, are required to define deformational domains for a given region. In eastern Turkey, seven such deformational domains can be distinguished (Figure-3.1). The Van Deformational domain is one of them.

The Van Deformational Domain (VDD) here is defined as the area, east of the Karliova Junction, which is bounded by the Pasinler fault zone in the west, Agri Fault in the north, Bitlis Massif in the south, and Ararat Fault Zone in the east (Figure-3.4). The

Figure-3.4

Landsat mosaic of eastern Turkey and northwestern Iran. The large lake on the left is Lake Van, and the one on the right is Lake Rezayeh. See Figure-3.3 for location (Box labeled with a).

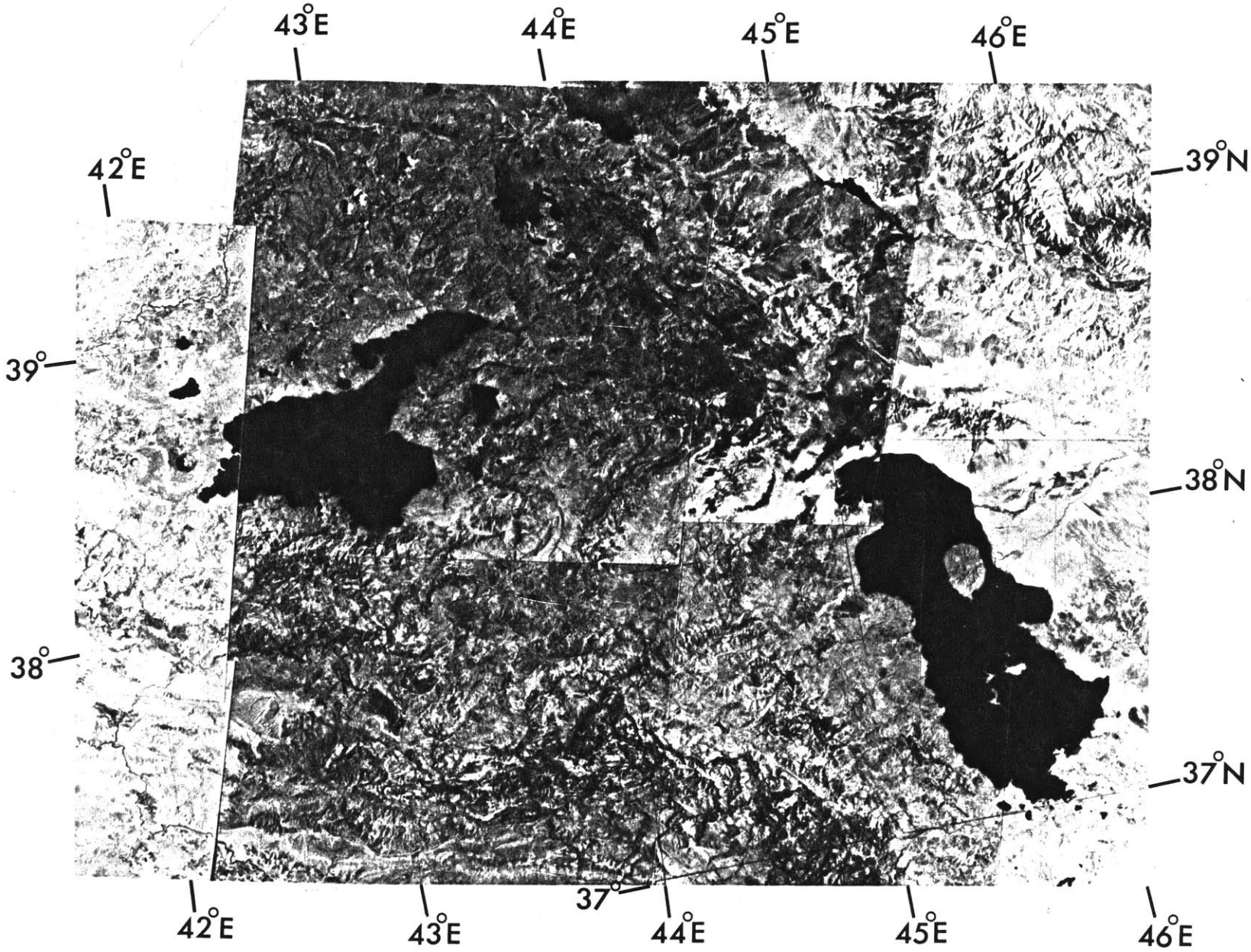
43°E
44°E
45°E
46°E
42°E
39°N
39°
38°N
38°
37°N
37°
42°E
43°E
44°E
45°E
46°E

Figure-3.5

ERTSA image of Lake Van area. Note the NW-SE trending faults that cut across Lake Van. In the upper right corner the southern lava flows of Ararat volcano can be seen. The recent lava flows of Tendurek volcano form a sharp contrast with its surroundings and is quite visible in the upper middle portion of the image. Suphan volcano is situated just to the north of Lake Van and indicated with a "S". In the lower right corner a segment of the NW-SE trending Hakkari fault is quite visible. See Figure-3.3 for location (box labeled with b).

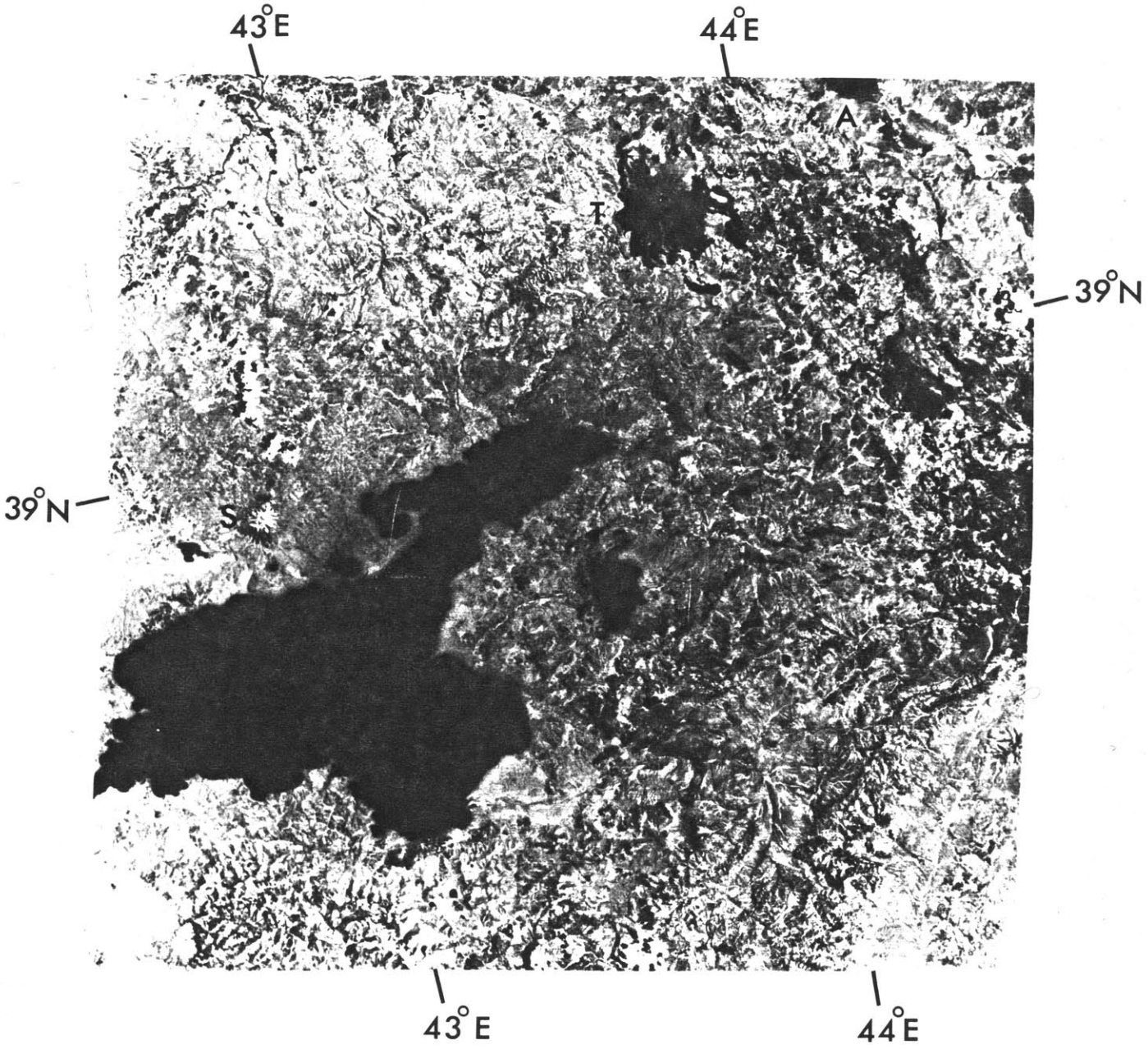
43°E
44°E
A
T
39°N
39°N
S
43°E
44°E

major style of deformation in the VDD is oblique faulting. The VDD contains a set of prominent NW-SE trending oblique faults and a set of less developed NE-SW trending oblique faults (Figures-3.4 and 3.5). These faults have major strike-slip and subordinate dip-slip components and they are arranged in an en-echelon geometry forming a set of conjugate shears. NW-SE trending faults are dextral and NE-SW trending faults are sinistral faults. This arrangement is consistent with the trends and sense of motions of the NAF and EAF. Some of these faults have been recently discovered following destructive earthquakes (Toksoz et al. 1977; Saroglu & Guner,1979; Saroglu person. comm., 1982). The following descriptions of these faults are preliminary, and extensive field work and geophysical study of the Lake Van area is required to document further the date of initiation and the vertical and horizontal displacements along these faults.

3.4.1 Pasinler Fault

The Pasinler fault zone forms the western boundary of the VDD (Figures-3.1,8,11). It also forms a NE-SW trending boundary for the Late Cenozoic volcanic province and the region of high seismic activity in eastern Turkey (see Figure-1.1 of Chapter 1 and Jackson & McKenzie, 1984; Figures 3 & 12). The NW-SE trending set of right-lateral oblique-slip faults of the VDD are terminated by the Pasinler fault (Figure-3.8). This fault zone extends from Erzurum-Pasinler basin towards Caucasuses. A smaller southern segment, which is about 75 km. long, extends after a left stepping, from Erzurum basin towards Haskoy, a small town in the vicinity of the North Anatolian fault. A segment of this fault zone can be seen on the SIR-A image in Figure-3.6. This fault zone is seismically active, as evidenced by more than eight earthquake epicenters lining up along the fault zone in the Erzurum-Pasinler area. Unfortunately this major fault zone has not been recognized previously, so that there are no existing geological studies regarding the amount of displacement and its date of origin. A recent destructive earthquake (Oct. 30.

Figure-3.6

SIR-A Image of northeastern Turkey. A small segment of the Pasinler fault is visible in the lower right corner of the image. A recent earthquake occurred recently (Oct.30.1983; M=7.1) along the southern continuation of this fault, giving left-lateral strike-slip fault plane solution (Toksoz et al., 1984). The earthquake also produced a 80cm. left-lateral displacement along the fault. See Figure-3.3 for location (box labeled with 1).

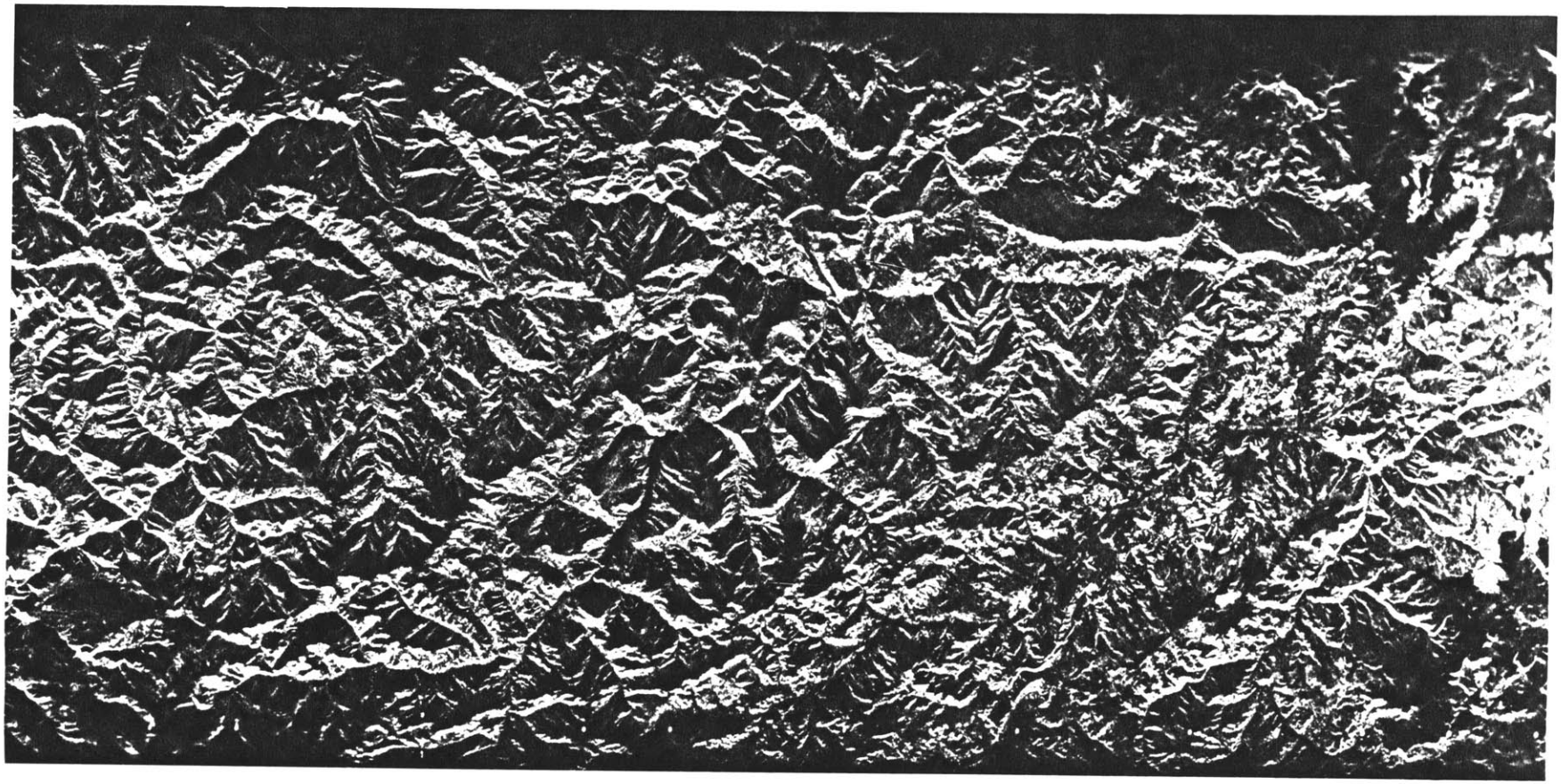

ILLUMINATION

N

0 10 20 km.

1983; M=7.1) occurred in this fault zone, producing 80cm. left-lateral displacement. The fault plane solution gives a left-lateral strike-slip motion consistent with the field observations (Toksoz et al.1984).

3.4.2 Ararat Fault

The Ararat fault forms the eastern boundary of the VDD. The NNE-SSW trend of this fault zone, like the Pasinler fault, is almost perpendicular to the Caucasian trend. The Ararat fault zone extends from east of Lake Van, towards Caucasuses, passing from west of the Ararat volcano and Lake Sevan. The fault zone is composed of a number of right-lateral strike-slip faults, some of which are displaced by younger faults. This fault zone is marked by a high anisotropy of seismic velocities (Yegorkina et al., 1977). The epicenters of six earthquakes that occurred in the period 1956-1976 (energy class K 10) are aligned along the northern segment of Ararat fault zone (Polshkov et al., 1979). The epicenters of the Igdir earthquake (Jan.3.1952, M=6) and the historic Satmanis earthquake (March.8.1715; Tchalenko, 1977) also coincide with the southern extension of this fault zone within Turkey.

3.4.3 Hakkari Fault

The Hakkari Fault zone is a major fault zone in the southeastern part of Turkey (Figure-3.8). It extends in a NE-SW direction from NW of the Yuksekova pull-apart basin in Turkey towards Iran and, after being right laterally displaced by the Tabriz fault, can be traced towards the Caspian Sea along the Araxes River. The Hakkari fault zone is a left-lateral shear zone. The fault traces and left-lateral displacements of streams can be clearly seen on LANDSAT and SIR-A images (Figures-3.4,5,7). A small event (Feb. 3. 1976; Mb=5.2) at the NE end of this fault zone, to the west of the Caspian Sea, gives

Figure-3.7

SIR-A image of southeastern Turkey. In the upper left corner the southeastern shore of Lake Van is seen. The NE-SW trending left-lateral strike-slip Hakkari fault zone is clearly visible in the right side of the image and indicated with a thick arrow. ee Figure-3.3 for location (box labeled with 2).

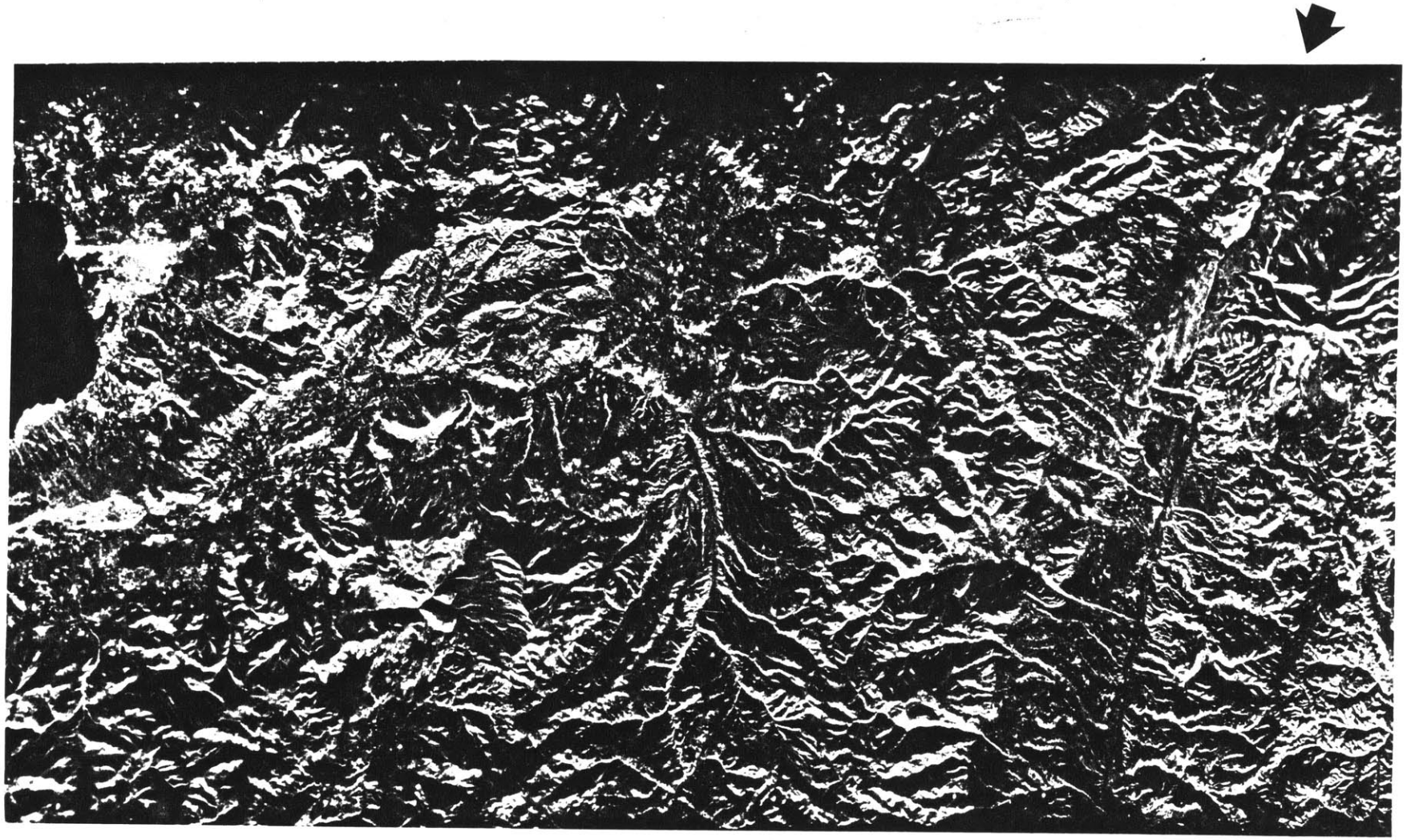

ILLUMINATION

N

0 10 20 km.

a left-lateral strike-slip fault-plane solution (see Figures-13 & 16 of Jackson & McKenzie, 1984). This fault zone seems to represent an old tear zone that disrupted the Anatolian-Iranian continental margin during the northward convergence of the Arabian plate, because the Bitlis Suture zone ophiolitic melange lithologies form a well defined, narrow zone to the south of the Bitlis metamorphic massif. However, in the southeastern corner of Turkey, not only does the Bitlis massif terminate, but the ophiolitic melange covers wide areas to the east of Lake Van. Based on his detailed field studies, Ketin (1977) describes them as an ophiolitic melange developed in an accretionary prism. The Sanandaj-Sirjan zone in Iran, which corresponds to the Bitlis metamorphic massif (Stocklin, 1968), extends after a left-lateral displacement as a continuous belt along the Zagros ranges, starting southwest of Lake Rezayeh. So the southeastern Anatolian ophiolitic melange may be interpreted as accretionary prism lithologies, obducted through the Hakkari left-lateral shear zone. However, this interpretation is quite different from the "East Anatolian Accretionary Complex" model of Sengor and Yilmaz (1981), in which they suggest that this accretionary complex represents a "continental hole" filled with oceanic island arc and melange complexes without any continental crust beneath them. The Hakkari Fault Zone has also been recognized as a major left-lateral fault by Khain (1969) and Gamkrelidze (1977). However, they extend this zone all the way from the Levant transform to the Caspian Sea, referring to it as the "Palmyra-Apsheron" fault. Apparently the Salmas earthquake of May.6.1930 reactivated a small segment of this fault zone near Derik; the displacement was left-lateral and the northern block subsided about 1m. (Tchalenko and Berberian, 1974).

The Hakkari-Yuksekova area in southeastern Turkey is an important junction where three major systems intersect: the right-lateral Ararat fault, the left-lateral Hakkari fault and the right-lateral Main Recent fault.

3.4.4 Agri Fault

The Agri fault is located just to the north of Tendurek volcano (Figures-3.4,5), and right-laterally displaces very young (Pliocene?) lava flows of Tendurek. It forms a junction with the Ararat fault and Lake Rezayeh fault swarm between The Tendurek and Ararat volcanoes and, extends northwestwards along the Murat River towards the Erzurum-Pasinler pull-apart basin (Figure-3.8). The fault traces are clearly visible on the LANDSAT images (Figures-3.4,5).

3.4.5 Caldiran-Tutak Fault

The Caldiran fault is situated to the south of the Tendurek volcano (Figures-3.4,5,8). The Tutak fault represents a northwestward continuation of the Caldiran fault. These two faults are combined and indicated with "TF" in Figure-3.8. The Caldiran fault was discovered after a destructive earthquake that occurred in Nov.24.1976 with a magnitude of M =7.3 (Arpat et al. 1977; Toksoz et al. 1977). This earthquake produced 250 cm. of right-lateral displacement. The fault plane is vertical at the surface. However, the fault plane solutions show a 60 degree dip to the SSW (Toksoz person. comm., 1983). A small sag pond (Lake Hidirmentes, about 2km. long and 1km. wide) is situated along the fault. After the Caldiran earthquake, the north shore of Lake Van was uplifted relative to the south shore by about 16cm. and this southward tilting of the lake has been interpreted as coseismic by Toksoz et al.(1977).

The Tutak fault has been documented by Saroglu & Guner(1979). This fault is also a right-lateral strike-slip fault and extends north-westward towards the Pasinler pull-apart. Even though the Caldiran and Tutak faults have been named separately, they seem to be

Figure-3.8

Schematized tectonic map of the Lake Van region. The abbreviations for the major fault names are the same used in Figure-1. The additional ones are: AF: Agri, TF: Tutak, CF: Caldiran, PF: Patnos, MF: Malazgirt, ADF: Adilcevaz, TABF: Tabriz fault. The pull-apart basins are shown as: EPPA: Erzurum-Pasinler, EP: Erzincan, YPA: Yuksekova. The fault plane solutions are from Shirokova,1962; McKenzie,1972; McKenzie,1975; Toksoz et al., 1978,1984; Eyidogan,1983. The locations of the earthquake epicenters are from Tchalenko,1977 and Toksoz et al.,1984.

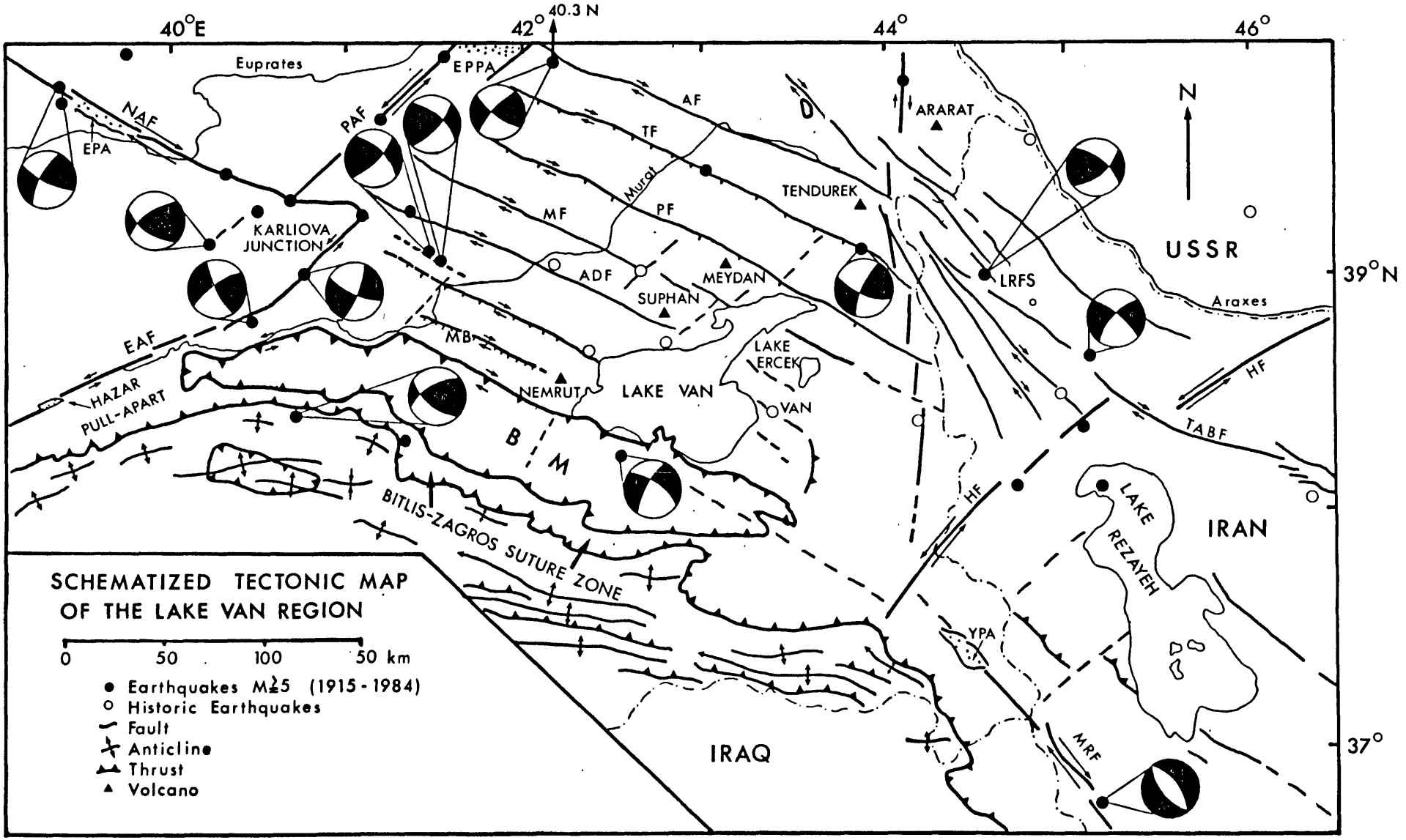
40°E
42°
40.3 N
44°
46°
Euprates
EPPA
NAF
EPA
PAF
AF
TF
D
ARARAT
N
Murat
MF
PF
TENDUREK
KARLIOVA
JUNCTION
ADF
MEYDAN
SUPHAN
USSR
LRFS
39°N
Araxes
EAF
MB
LAKE
ERCEK
HAZAR
PULL-APART
NEMRUT
LAKE VAN
VAN
HF
TABF
B
M
HF
LAKE
REZAYEH
IRAN
BITLIS-ZAGROS SUTURE ZONE
YPA
MRF
IRAQ
37°
SCHEMATIZED TECTONIC MAP
OF THE LAKE VAN REGION
0
50
100
50 km
Earthquakes M≥5 (1915 - 1984)
Historic Earthquakes
Fault
Anticline
Thrust
Volcano

two segments of a single fault, and assigning only one name (such as Tutak fault) may be more appropriate.

3.4.6 Patnos and Malazgirt Faults

These faults extend in a NW-SE direction and form the northern and southern boundaries of the Akdag metamorphic massif (Figure-3.2) along the northern shore of Lake Van (Figures3-4,5,8). The Malazgirt fault extends to the east of Lake Van, forming the northern shore of Lake Ercek. This fault is composed of a number of right-lateral strike-slip en-echelon faults that are displaced in places by NE-SW trending subordinate left-lateral strike-slip faults which bound Neogene and Quaternary basins. The Murat river makes almost a 90 degree turn on the Malazgirt fault, and narrow strips of fissure basalts line up with these fault zones. A destructive earthquake occurred in 28.April.1903 with a magnitude of M=6.3 near the town of Malazgirt causing about 3500 casualties (Tchalenko, 1977). Also, recent microseismic monitoring around the town of Ercis has revealed the presence of high seismic activity along these faults (Saroglu person. comm., 1982).

3.4.7 Adilcevaz Fault

Adilcevaz fault also extends in a NW-SE direction towards the Pasinler fault and crosses Lake Van (Figures-3.4,5,8). This fault is seismically very active and a number of destructive earthquakes have occurred in the vicinity of this fault (March.31.1648 Van, April.9.1857 Bulanik, February.6.1891 Adilcevaz, and July.11.1945 Van; see Tchalenko,1977; Ambraseys & Melville, 1982 for detailed descriptions of historic earthquakes in this region).

3.4.8 Lake Van Basin

Lake Van is the largest soda lake on earth and ranks fourth in volume (607 cubic km., with 3600 sq. km. surface area) among the closed lakes of the world (Degens et al., 1978). The elevation of the lake surface is 1648m., with the southern basin (south of a line connecting the towns of Adilcevaz and Van) being deeper than the northern one. The particular orientation of Lake Van and the NW-SE trending en-echelon faults that cross the lake provide an excellent opportunity to study the prevailing tectonic regime along the seismic reflection profiles. As clearly seen in Figure-3.9, and documented by Wong & Finckh (1978) along other profiles, the faults that cross Lake Van and the ones bounding the lake basin are oblique-faults with major dip-slip components, indicating the subsidence in the Lake Van basin. The continuation of these oblique faults in the basement rocks, coupled with the stratigraphic characteristics of the sediments, indicate the presence of half-grabens, in other words, unidirectional tilting of basement blocks towards the northeast. All these features suggest the development of an extensional tectonic regime accompanying continental collision and convergence in this region. However, note that the strike of the depressions and half-grabens are parallel to the collision front, which is represented by the uplifted Bitlis Massif. Thus, the original Mus-Lake Van basin appears to be formed by a complex mechanism which involves unidirectional tilting and subsidence of crustal basement blocks, bounded by en-echelon oblique faults, and possibly the coelescence of small pull-apart basins into larger ones.

Another indirect line of evidence for the presence of an extensional tectonic regime in this area comes from Nemrut Volcano. Nemrut volcano, with its alkaline character, extensive ignimbrite eruptions and peralkaline commenditic and pantelleritic lava flows is a typical rift volcano, similar to the ones in the East African Rift and Pantelleria. As originally suggested by Lahn(1948), the lavas that formed the Nemrut volcano apparently

Figure-3.9

Line drawing of seismic reflection profile across the Lake Van (from Wang & Finck, 1978). Note the increasing thickness and northward tilting of sedimentary horizons bounded by faults. These are oblique-slip faults, because they have both dip-slip and strike-slip displacements.

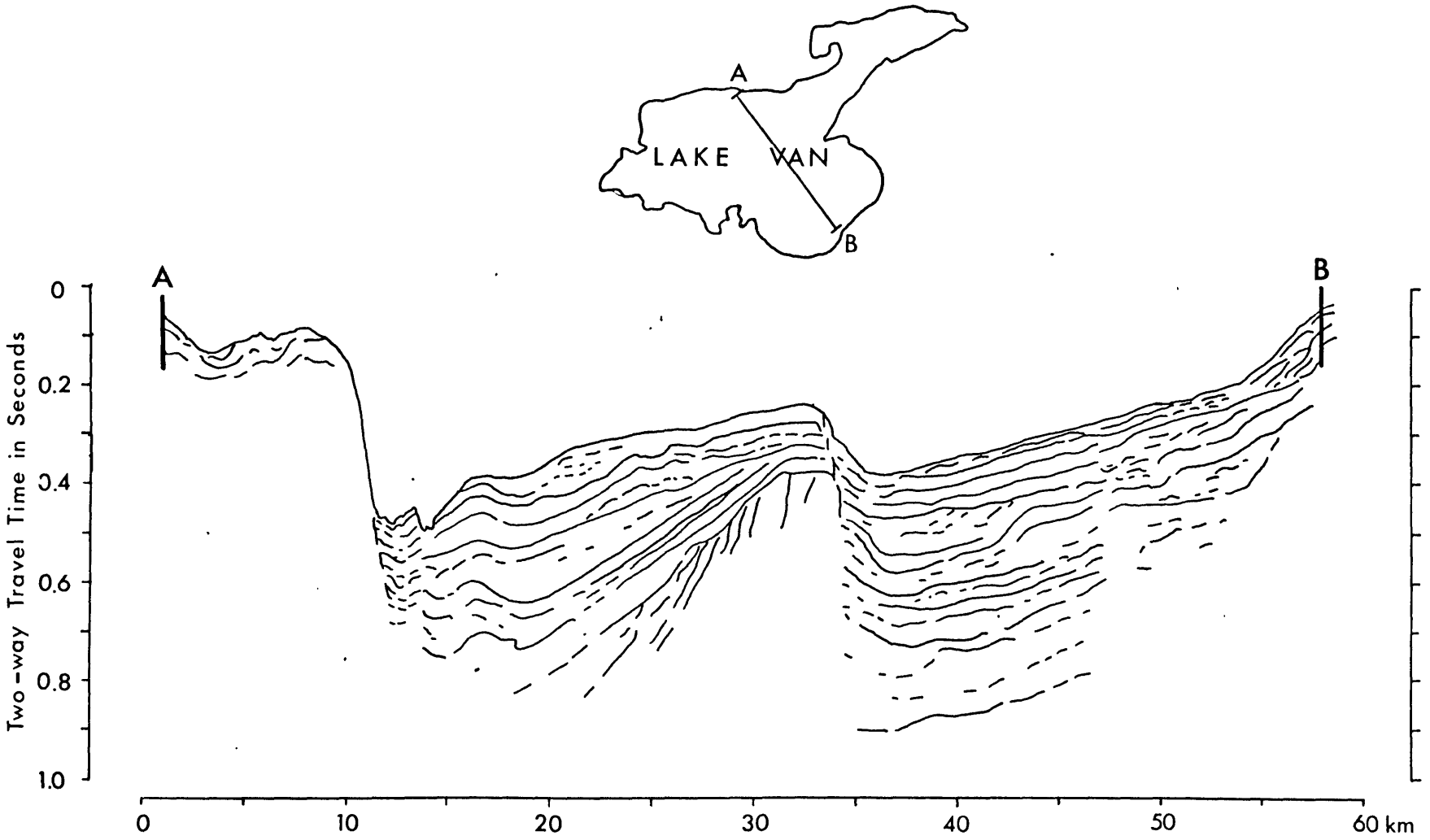
A
LAKE VAN
B
A
B
Two-way Travel Time in Seconds
0
0.2
0.4
0.6
0.8
1.0
0
10
20
30
40
50
60 km

Figure-3.10

SIR-A image of the southwestern portion of Lake Van and Mus basin. The large caldera of Nemrut volcano is located in the middle. The lavas of the Nemrut volcano apparently divided the original Mus-Lake Van basin into two separate basins, and caused the impoundment of the lake by damming the Lake Van basin. Mus basin is situated to the west of Nemrut and trends roughly in the E-W direction. The Bitlis massif metamorphics (located to the south of Mus basin and Lake Van) can be distinguished by their special drainage patterns. A number of oblique and normal fault traces are also visible to the west and northwest of Nemrut volcano. See Figure-3.3 for location (box labeled with 3).

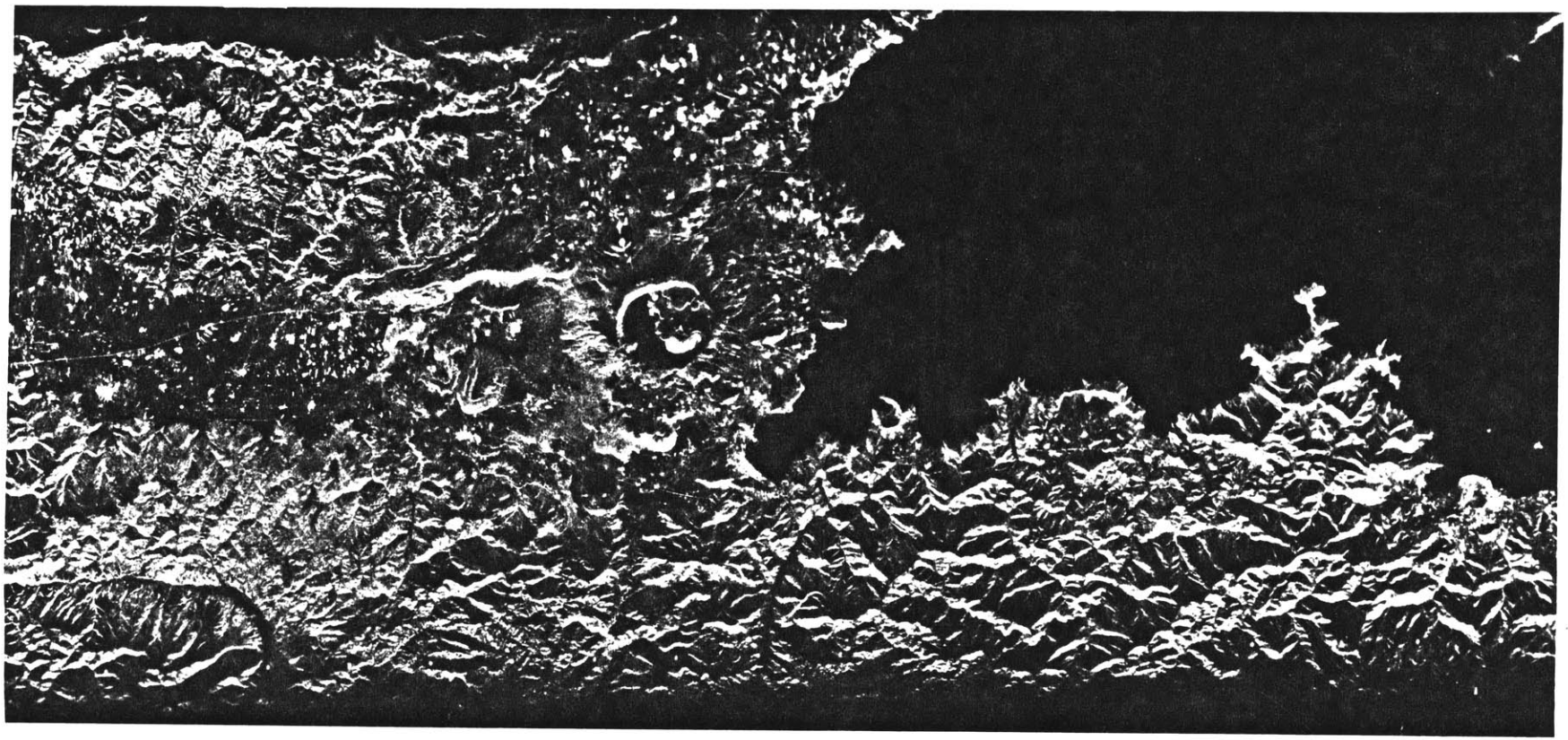

ILLUMINATION

N

0 10 20 km.

divided the original Mus-Lake Van basin into two separate basins, and caused the impoundment of the lake by damming the Lake Van basin (Figure-3.10). Mus basin is also bounded on the west by the Solhan volcanics; these are one of the earliest products of alkaline volcanic activity in this region (Saroglu et al.,1982).

The heat flow is apparently very high in the Lake Van region as there are 38 thermal springs in the vicinity of Lake Van (Kurtman & Baskan, 1978). Kempe et al. (1978) suggested that the heat flow in the Lake Van basin significantly exceeds the world average.

The southern edges of the Lake Van and Mus basins are bounded by the Bitlis metamorphic massif. Due to the continental collision and still continuing convergence, the Bitlis Massif is not only thrust southward over the ophiolitic melange-flysh complex of the Bitlis Suture zone, but is also thrust northward over Cretaceous and Paleogene lithologies. Imbricated thrusts and reverse faults are abundant within the Bitlis Massif. The ones on the northern flank dip southwards, whereas the ones on the southern flank dip northwards (Altinli,1966-b; Yilmaz et al., 1981). The geometrical configuration of the northern and southern thrusts and reverse faults indicates that the uplift of the massif has occurred under significant compression. This mechanism necessitates the presence of a major reverse fault along the northern edge of the Bitlis Massif, complementing the southern Bitlis Suture Zone thrust. In fact, there is well-documented field evidence suggesting the presence of reverse faulting along the northern margin of the Bitlis Massif, where Neogene lacustrine limestones of the Mus area are exposed at an altitude 700 m. lower than similar limestones found on the peaks of the Bitlis Massif (Hall, 1976).

3.5 Discussion and tectonic model

Although the origin of back-arc basins has attracted a great deal of interest in the past (e.g Karig, 1971; Toksoz & Bird, 1977; Uyeda & Kanamori, 1979), the significance of the extensional-compressional tectonics association in continental areas has become recognized only recently (Eaton, 1980; Dalmayrac and Molnar, 1981; Molnar et al., 1981; Royden et al., 1982; Suarez et al., 1983). The Basin and Range province of the western United States, the Altiplano of the Andes, the Aegean area (including northern Greece and western Turkey), the Carpathian Neogene basins, Tibet, Tyrrhenian Sea, and Jaz Murian Basin in Iran can be given as examples of areas where extensional tectonics are associated with compression.

The Basin and Range province of the western United States represents an area that has experienced about 30 m.y. of crustal extension, immediately following compressional deformation phases of the Sevier (Late Jurassic to Late Cretaceous) and Laramide (Late Cretaceous to Late Eocene) orogenies (Burchfiel and Davis 1972, 1975; Stewart, 1978; Davis, 1980; Eaton, 1980). Faulting follows older geologic patterns that developed especially during Mesozoic and Earlier Tertiary in the western United States. Eaton (1980), acknowledging the significant influence of the compressional regime on the mechanics and locus of the Cenozoic extension in the Basin and Range province, suggested that subhorizontal zones of sliding first developed as thrust soles during compression, and later evolved into extensional decollements However, Wernicke(1982), based on his detailed field studies in the Mormon Mountains (a thrust terrain formed during Sevier orogeny and located along the eastern margin of the Basin and Range province) produced evidence that the low-angle thrust faults have not evolved into extensional decollements. Contrasting with this, the dip-slip reactivation of the preexisting strike-slip faults are partly responsible for the early Tertiary extension in the Pacific Northwest (Davis, 1980). This

discrepancy may be reconciled by attributing the lack of reactivation of thrust faults during extension to the thin-skinned compressional nature of the Mormon thrust.

The tilted-block structure of the Basin and Range Province terminates rather abrubtly along the Garlock Fault (Davis & Burchfiel, 1973). The more stable Mojave Desert block is located to the south of the Garlock Fault. So models that involve stretching of the lower continental crust to produce extension and tilted-block structure can not satisfactorily explain this kind of a sudden change in deformational style.

The coexistence of active thrust faulting and normal faulting have been documented for the Andean Cordillera (Lavenu,1978; Mercier,1981; Dalmayrac and Molnar,1981; Suarez et. al.,1983). In particular, in the Cordillera Blanca region of Peru and around Lake Titicaca (Altiplano region of southern Peru and northern Bolivia), the strike of normal faulting is approximately parallel to the strike of folding and thrusting, indicating a component of extension perpendicular to the mountain ranges. Similarly, the coexistence of active compressional and extensional deformation has been observed in Tibet (Molnar et al. 1981). For both of these regions, the presence of extension has been explained by body forces produced by gravity and buoyancy forces exerted by the crustal roots of the elevated regions (Molnar et. al., 1981; Dalmayrac and Molnar, 1981; Suarez et. al., 1983).

The Neogene intra-Carpathian basins represent an area where extension developed contemporaneously with the Neogene thrusting in the foreland fold and thrust belt (Horvath and Royden, 1981; Burchfiel and Royden, 1982; Royden et. al., 1982,1983). The southward and westward dipping Cretaceous subduction along the Carpathian arc was terminated by the continental collision between Europe and smaller continental fragments in the Miocene. The northeast and northwest trending sets of conjugate shears, which

lead to the development of discrete basins (e.g. Pannonian, Vienna, Graz) , reflect N-S shortening and E-W extension within the Carpathian loop. A mechanism which involves downbending of the subducted slab causing a lithospheric flow to fill the space left by the retreating plate is suggested for the development of an extensional stress field in this region. The thrusting and apparent compression along the fold and thrust belt have been described as thin-skinned (because of the diffuculties involved in the subduction of ligth upper crustal material) resulting in the detachment of the crust from the underlying lithosphere (Burchfiel and Royden, 1982; Royden et. al., 1982,1983).

The Aegean area (including northern Greece and western Turkey) is one of the very seismically active regions on earth and is located to the north of the Aegean arc. As a result of the overall convergence between the Eurasian and African plates, and westward sideways escape of the so called "Anatolian Plate", the Mediterrenean sea floor subducts northwards with an angle of 30 and at a rate of 3-4 cm/year (Caputo et. al.,1970; Papazachos and Comminakis,1971; Le Pichon and Angelier, 1979). The prevailing tectonic regime in the Aegean is extensional as evidenced by the available fault plane solutions and the roughly E-W trending normal faults throughout the region which are subparallel to the Aegean arc (Alptekin,1973; McKenzie,1978). A close association of normal and thrust faults has been documented in northeastern Greece and Albania (Angelier,1976; McKenzie,1978). Based on the crustal thicknesses of 30 km. and 50 km., beneath the Aegean Sea and surrounding regions respectively, McKenzie(1978) has suggested that the Aegean has been stretched by a factor of two since Miocene. He also rejected the concept that the extension is not the direct result of the local release of gravitational energy in Aegea. Because there is no great difference in crustal thickness between the area south of the Aegean arc and the region undergoing extension. Dewey and Sengor(1978) have attempted to explain the extension in Aegea and surrounding regions by "locking" the two strands of the North Anatolian Fault where they change orientation

at the western end of the Marmara Sea. But, as pointed out by McKenzie(1978) "It is hard to believe that blocks in northwestern Greece and Albania have sufficient strength to act in the manner they proposed". He instead suggested a mechanism in which the cold lower parts of the lithosphere detach and sink as blobs through the mantle, due to the extension in the upper crust. Thus lithosphere, consisting of a thin continental crust, deforms easily, reflecting the convective motions in the mantle. Kaya (1979,1982) suggests that N-S extension in western Turkey is related to the NE-SW trending oblique-slip faults (in a manner similar to the development of extension in the Basin and Range Province and its relation to the Garlock fault (Davis & Burchfiel, 1973). He also points out the consistent southward tilted block structure of the region, and emphasises that simple stretching models cannot easily account for this structure.

The evolution of the present tectonic regime of the Lake Van region can be best described in the context of the convergence of the African-Arabian and Eurasian plates with the subduction of oceanic crust until Miocene time, followed by continental collision and continued convergence since Miocene time.

Although Sengor & Kidd (1978) suggested, active shorthening and crustal thickening, as did McKenzie (1972), and inferred the presence of numerous thrusts in the Lake Van region, the documented subsidence of the Lake Van and Mus basins, the dominance of oblique-slip faulting with major strike-slip compenents, and the lack of major thrusts and the very high heat flow do not support crustal thickening.

Numerous thrust faults are present within and south of the Bitlis Massif, but none are known to the north of the Bitlis Massif (Altinli, 1966-b, p.4 and plate II) and the deformation is dominated by the prominent NW-SE and NE-SW trending conjugate set of oblique-slip faults that have major strike-slip components in the VDD. A few minor

thrusts, that are related to strike-slip movements, are present particularly in the vicinity of the Karliova Junction.

The inefficient Sn and Rayleigh wave propagation in the uppermost mantle beneath the Lake Van region and the northern part of the Iranian Plateau suggest that zones of high-attenuation (low Q) are present (Molnar and Oliver, 1969; Toksoz and Bird, 1977; Kadinsky-Cade, 1981). Bouger anomaly values range from -125 to -150 mgal. in these regions (Wilcox et al., 1972; Ozelci, 1973). These negative Bouger anomalies, when combined with the seismic wave attenuation and high heat flow, can be best explained by a relatively thin crust in the Lake Van region.

Chen et al. (1980) estimated uppermost mantle P wave velocities of 7.73 +- 0.08 km/s beneath Turkey. They also pointed out that this value is comparable to that of the Basin and Range province (7.8 +- 0.1 km/s) and is significantly lower than that under Tibet (8.1 +- 0.1 km/s).

The plateau character of the Lake Van region, based on the above discussions, can be explained by the partial replacement of the lower continental lithosphere by the upwelling of hot upper mantle, without calling upon crustal thickening.

The depositional environment and stratigraphic characteristics of the Eocene and Neogene formations in the Lake Van region (particularly the ones in the vicinity of Mus, Gevas and Adilcevaz) possess almost all the characteristics of sediments deposited along major shear zones (such as very rapid sedimentation, great sedimentary thickness, and very limited, narrow basin size, extreme lateral facies variations, abundance of coarse clastics, etc. (Reading, 1980)). These characteristics suggest that the North Anatolian Fault, in particular only the eastern part including the eastward extension towards

Yuksekova (Proto NAF), represents an existing major shear zone (like the San Andreas dextral shear system in the Western United States, the Alpine dextral shear system in New Zealand, and the peri-Adriatic-Vardar dextral shear system of the Alps) that predates the Miocene continental collision. The evolution of the depositional and deformational history of the small sedimentary basins associated with all these major shear zones is strikingly similar (Crowell, 1974; Howell et al., 1980; Sporli, 1980; Prebble, 1980; Dickinson, 1983).

The proto-North Anatolian fault and NW-SE trending en-echelon strike-slip faults apparently have been disturbed and modified by the continental collision and still continuing continental convergence in the Lake Van region. Mainly three different, but nevertheless related deformational styles, take up the continental convergence that is the result of the relative N-NE motion of the Arabian plate. These are: 1-) Folding and thrusting within the leading edge of the Arabian plate (including the Bitlis Massif) and along the Caucasuses. 2-) Displacements along NE-SW and NW-SE trending sets of strike slip faults 3-) Rotation-tilting and lateral escape of crustal blocks and thrusting of these blocks over a decollement surface within the VDD.

Fault-bounded, vertical slab-like crustal blocks in the Lake Van region have responded to continental collision by vertical rotation, northeastwards tilting away from the collision front, and by southeastwards lateral escaping along the NW-SE trending set of en echelon strike-slip faults (Figures-3.8,11,12).

Because rotation and tilting effectively increase the surface area, by increasing the distance that is perpendicular to the long axis of the slabs, this process (and possible thrusting of these slabs over a decollement surface) necessitates a free space in the

Figure-3.11

Van Deformational Domain and its relations with the surrounding deformational domains. Strippled areas are depressions and Neogene basins. RD: Rioni, KD: Kura, EP: Erzurum-Pasinler, A: Agri, M: Mus, MA: Malazgirt, T: Tekman, LV: Lake Van, LR: Lake Rezayeh, LS: Lake Sevan. The chewron patterns denote fold zones; ATFZ: Adzhar-Trialety, TFZ: Talesh, Cross-hatched areas are the basaltic crusts of the Black and Caspian Seas. The thick dashed lines connecting them show the approximate boundaries of the original Black-Caspian Sea back-arc basin. ODU: Okriba-Dzurila uplift. The abbreviations for the names of the deformational domains and the major fault zones are the same used in Figure-3.1 and Figure-3.3. The additional one is the CDD: Caspian deformational domain. The faults in the area to the SW of the Caspian Sea are from Berberian, 1983. TAF: Talesh, SF: Sangevar, LF: Lahijan, KF: Khazar fault. The areas shown with vertical, thick wavy patterns denote the uplifted continental margin of the Anatolian-Iranian block. BM: Bitlis Massif, SS: Sanandaj-Sirjan Zone. The belt marked by oblique heavy lines is the Bitlis-Zagros Suture Zone. The area shown with vertical thin wavy pattern is the "Border Fold Zone"(BFZ) of the Arabian foreland deformational domain (AFDD).

KJ: Karliova Junction. The large arrow shows the N-NE motion of the Arabian plate. Small arrows along the Caucasuses represent the southwestward thrusting of the continental crust along the Main Caucasian Thrust.

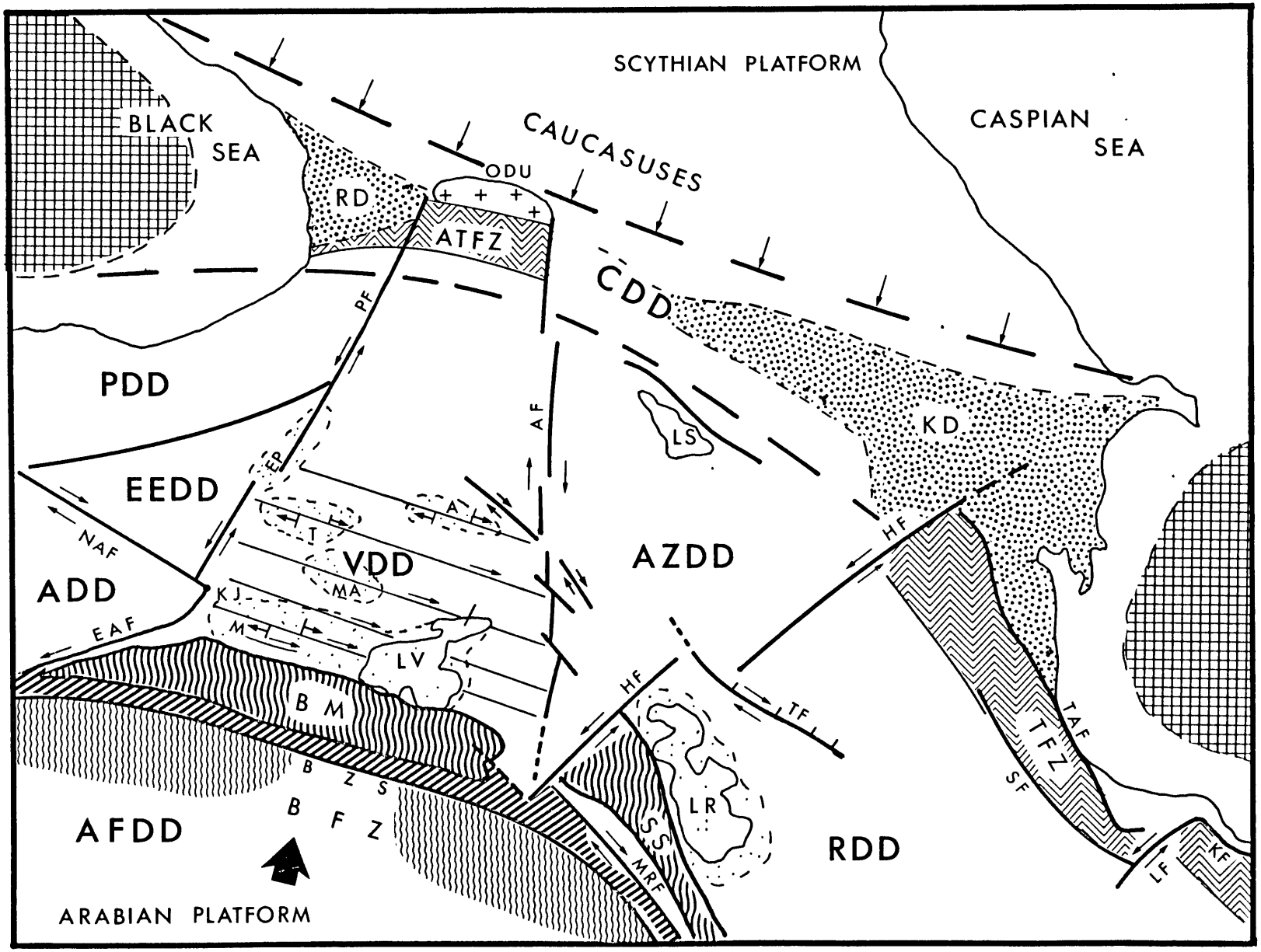
SCYTHIAN PLATFORM
BLACK SEA
CAUCASUSES
CASPIAN SEA
ODU
RD
ATFZ
CDD
PF
PDD
AF
LS
KD
EP
EEDD
A
T
NAF
VDD
AZDD
HF
ADD
KJ
MA
EAF
M
LV
B M
HF
TF
TAF
TFZ
SF
B Z S
LR
B F Z
AFDD
SS
MRF
RDD
LF
KF
ARABIAN PLATFORM

direction of tilting and thrusting, to accomodate the areal increase. In fact, this free boundary was available in the Caucasus region.

Geophysical studies have revealed that the Black Sea and the southern part of the Caspian Sea is floored by a basaltic basement (Neprochnov, 1968; Neprochnov et al., 1974; Balavadze et al., 1975). This 15-20 km. thick basaltic basement is covered with thick(15-25 km.), undeformed Late Mesozoic-Cenozoic sediments. Although there are a number of theories on the origin of the basaltic crusts of the Black and Caspian Seas (see Berberian, 1983), recent studies favor an origin in back-arc (marginal sea) basins as a result of northward subduction of the northern Neotethys (now represented by the Erzincan-Akera-Sevan-Quradagh suture (Adamia et al., 1977; Letouzey et al.,1977; Berberian, 1983)). The Black Sea and Caspian Sea back-arc basins were probably continuous and connected through the Caucasus. Deep seismic sounding studies along the Caucasuses have documented the presence of a basaltic layer, although tectonicly disturbed, beneath the folded, faulted Mesozoic-Cenozoic cover (Shempelev, 1978). The first mountain building period of the Alpine orogenesis in the Caucasuses was Miocene and preceded the intense tilting, uplifting and rapid subsidence of basins during the Pliocene and Quaternary (Tsagareli, 1974). Detailed field studies have revealed the presence of north-vergent thrusts in the Adzhar-Trialety zone of the Lesser Caucasus (Gamkarelidze, 1974). Berberian (1983) describes the southern Caspian Sea basin as "a compressional depression floored by a trapped, modified oceanic crust" that is being consumed along its periphery by overthrusting continental crust.

This data indicate that the present Caucasus region represents an area where the middle segment of the elongate Black Sea-Caspian Sea back-arc basin was completely eliminated by the overthrusting of continental crust, both from north and south, resulting

in intense deformation of the Late Mesozoic-Cenozoic sedimentary cover and separation of the Black Sea and Caspian Sea basins (Figure-3.11).

The Caucasus region that connects the Black Sea and the Caspian Sea can be divided into three segments, perpendicular to the Caucasian trend: the Rioni depression in the NW, the Okriba- Dzirula uplift and Adhzar-Trialety fold zone in the middle, and the Kura depression in the SE (Khain, 1975). The Okriba-Dzirula uplift is separated from the Rioni depression in the west, and the Kura depression in the east, by the northward extensions of the Pasinler and Ararat faults, respectively (Figure-3.11). As pointed out above, these fault zones form the eastern and western boundaries of the tilted-block structured Van deformational domain. This relation exemplifies the importance of the Pasinler and Ararat shear zones in transmitting the compressive stresses from the continental collision front (the Bitlis Massif) all the way to the Caucasuses. Apparently, the required extra space due to the unidirectional tilting of competent crustal blocks and northeastward thrusting of crustal slabs over a decollement surface within the VDD is accomodated by folding, overthrusting, and uplifting along the Okriba-Dzirula uplift and Adzhar-Trialety fold zone. However the Rioni and Kura depressions have largely escaped from this intense compression, due to the presence of the two major shear zones. More interestingly, the Talesh fold zone, which corresponds to the Adhzar-Trialety fold zone of Caucasuses (Khain, 1975), is located along the southwestern shore of the Caspian Sea. The Talesh fold zone is delimited by the Talesh (TAF) and the Sangavar (SF) active reverse faults (Berberian, 1983). The left-lateral Hakkari fault separates the Kura depression from the Talesh-Elbruz fold zone. The wedge-shaped Azerbaijan deformational domain (AZDD) that is defined by the right-lateral Ararat and the left-lateral Hakkari faults, protects the Kura depression from major shortening, whereas the effects of compression are manifested as folding and thrusting along the Talesh-Elbruz fold zone, immediately to the southeast of the Hakkari fault. After presenting evidence on the

availibility of an "escape space" in the Caucasuses, we can further elaborate on the implications of the tilting of crustal blocks.

Simultaneous tilting and lateral escape modifies the faults from strike-slip to oblique-slip in character, and has significant implications. Unidirectional tilting of crustal blocks can cause some limited thinning of the continental crust, above a detachment surface, while crustal thickening is avoided by the lateral escape. As indicated above, another important implication of the tilting of crustal blocks by continental collison and convergence is the possible formation of a detachment zone within the continental crust due to the transition from brittle to ductile deformation with increasing depth. Because of this gradual transition within the continental crust, listric faults (faults that have decreasing dip angles with increasing depth) can be formed by modification of oblique-slip faults under compression. This process may be described as bending of crustal blocks. Bending of crustal blocks superimposed on tilting can cause further thinning of part of the continental crust that is above a decollement surface. This process, in a very simplified cartoon representation, is shown in Figure-3.12.

In this figure, one vertical slab-like crustal block, which has an original thickness of d_o, is represented as a vertical bar. Simple tilting of this crustal slab reduces the vertical thickness to d_1. If the degree of tilting is expressed by θ, the angle with the horizontal surface, then the amount of thinning is:

$$\text{Thinning} = d_o - d_1 = d_o(1-\sin\theta)$$

If bending of this crustal slab is superimposed on tilting, the amount of thinning becomes even larger. If the curved slab is chosen as a circular arc, for the sake of simplicity, the following equations can be written:

$$\overset{\frown}{AB} = r\varphi = d_o \quad \text{..... (1)}$$

$$\overline{AB} = 2r\sin(\varphi/2) \quad \text{..... (2)}$$

Figure-3.12

Schematic cross-section showing the effects of tilting and bending of crustal blocks. d_o is the original thickness, d_1 is the thickness of the tilted crustal block, d_2 thickness of the crustal block after bending superimposed on tilting. Explanations are in the text.

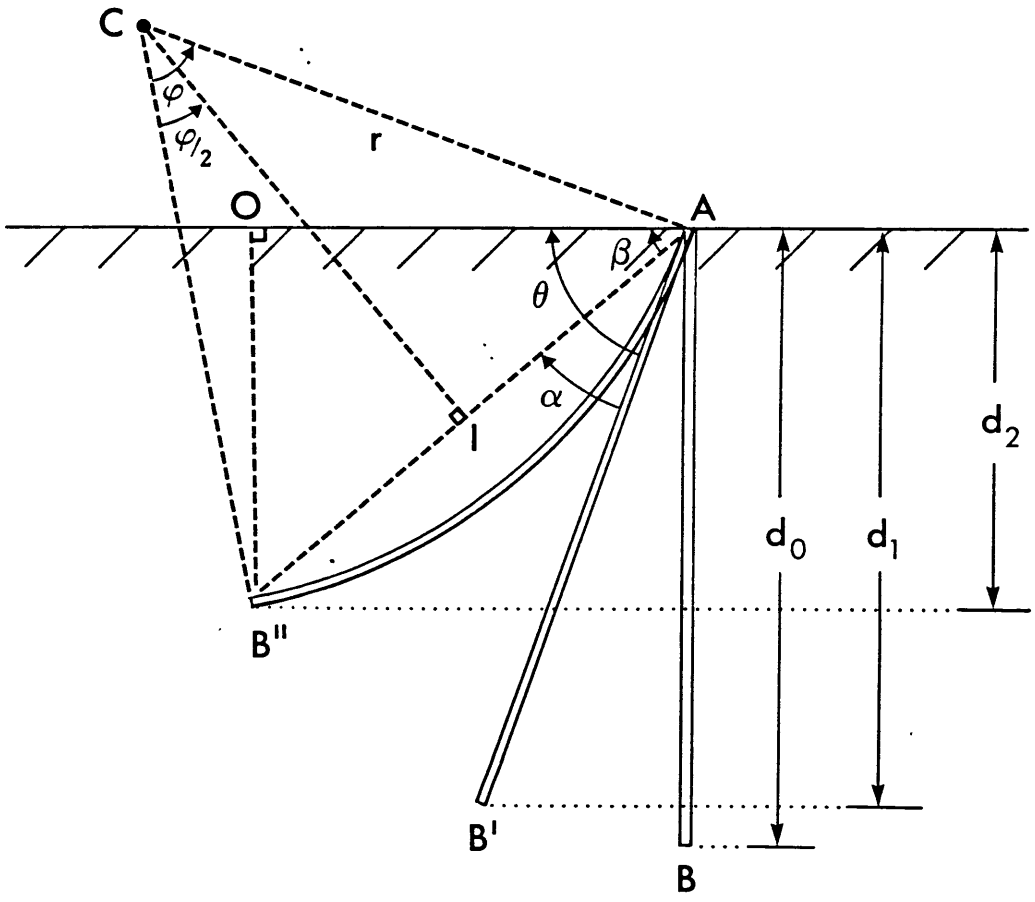
C
φ
φ/2
r
O
A
β
θ
α
l
d2
d0
d1
B''
B'
B

$$d_2 = OB'' = AB \sin(\theta - \varphi/2) \quad \text{..... (3)}$$

$$\overline{AB''}/\widehat{AB''} = 2r \sin(\varphi/2) / r\varphi \quad \text{..... (4)}$$

Combining equations (1) , (2) and (4)

$$\overline{AB''} = d_o 2\sin(\varphi/2) / \varphi \quad \text{..... (5)}$$

Then from equations (3) and (5)

$$d_2 = OB'' = d_o 2\sin(\varphi/2) / \varphi \sin(\theta - \varphi/2)$$

where d_2 is the final thickness.

The amount of thinning can be expressed with respect to the original thickness as:

$$\% \text{ Thinning} = (d_o - d_2) / d_o$$

by replacing the equations:

$$\% \text{ Thinning} = 1 - (2\sin(\varphi/2)/\varphi)\sin(\theta - \varphi/2) \times 100$$

The purpose of the above calculations is to demonstrate the viability of tilting and bending of crustal blocks in thinning the continental crust by compression. These calculations can be elaborated by using more realistic listric curvatures providing that we have a sufficient data base to model the variations in rheologic properties and the temperature profiles of the continental crust with depth.

Based on the above discussions, the following scenario can be proposed for the Alpine geological evolution of the VDD (Figure-3.13). During Paleogene time the Bitlis-Zagros oceanic crust was subducted northward, and the subduction related magmatism weakened the continental crust of the overriding Anatolian-Iranian plate. The brittle to ductile transition zone within the continental crust was raised to shallower levels in response to the steepened temperature gradient. Some of the preexisting zones of weakness on the Anatolian-Iranian continental block were reactivated by the compressional regime related to continued subduction (e.g. NAF, Hakkari Fault). During Miocene time, continental collision of the Anatolian-Iranian and Arabian blocks formed the

Figure-3.13

Schematic sequential cross sections showing the Alpine evolution of the Van Deformational Domain. Key to the abbreviations: BCSBAB: Black-Caspian Sea back-arc basin, ESASZ: Erzincan-Sevan-Akera suture zone, NAF: North Anatolian Fault, AP: Arabian Platform, BM: Bitlis Massif, BZS: Bitlis suture zone, LV: Lake Van. Deformational domains: CDD-Caucasus, VDD-Van, AFDD-Arabian Foreland.

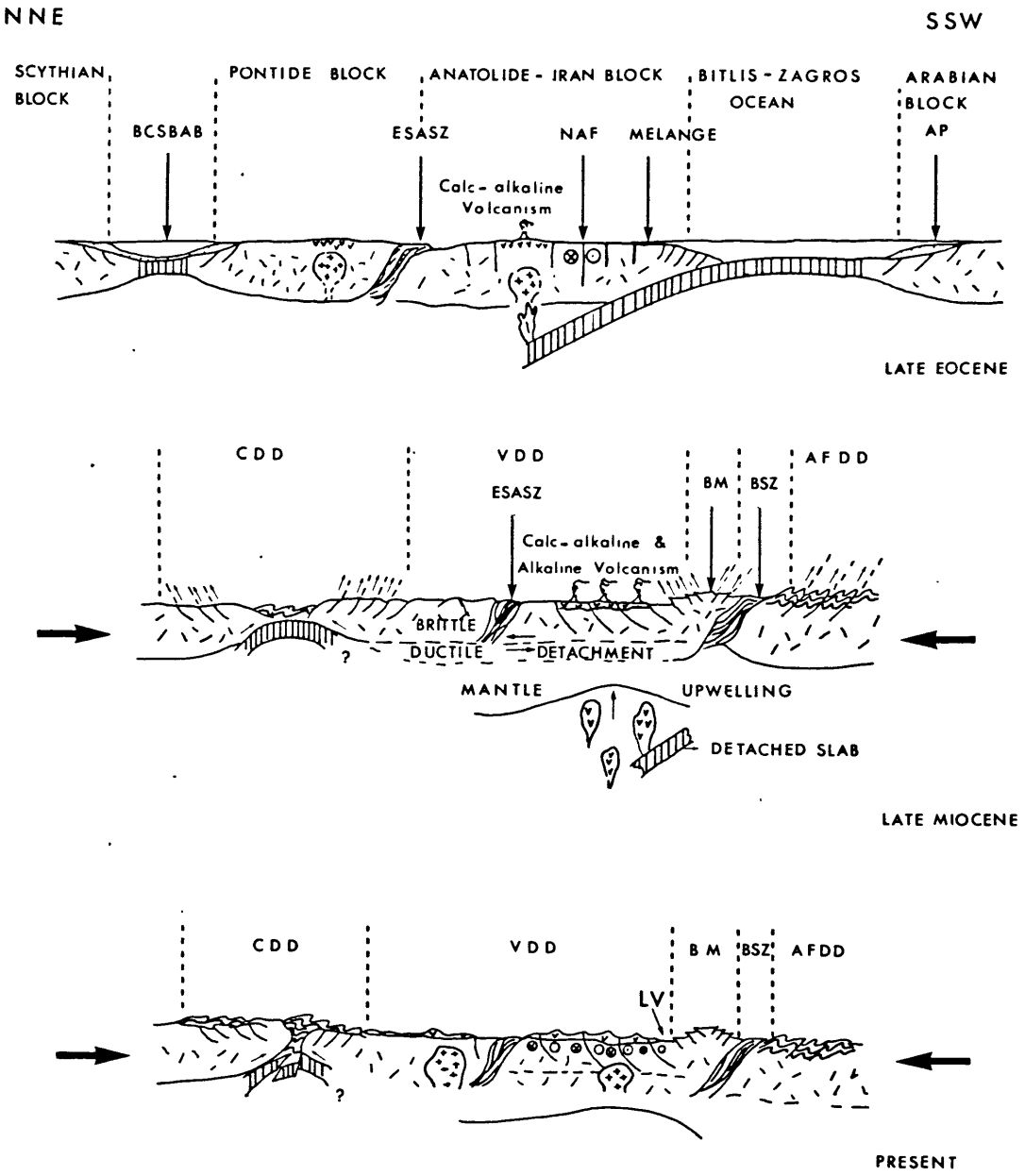
NNE
SSW
SCYTHIAN BLOCK
PONTIDE BLOCK
ANATOLIDE - IRAN BLOCK
BITLIS - ZAGROS OCEAN
ARABIAN BLOCK
BCSBAB
ESASZ
NAF
MELANGE
AP
Calc - alkaline Volcanism
LATE EOCENE
CDD
VDD
ESASZ
BM
BSZ
AFDD
Calc - alkaline & Alkaline Volcanism
BRITTLE
DUCTILE
DETACHMENT
MANTLE
UPWELLING
DETACHED SLAB
LATE MIOCENE
CDD
VDD
BM
BSZ
AFDD
LV
PRESENT

Bitlis-Zagros suture and uplifted the continental margin of the Anatolian-Iranian block (Bitlis Massif and Sanandaj-Sirjan Zone). The Bitlis Massif acted as a butress and forces were transmitted northward to the Caucasuses. Under the tectonic control of the left-lateral Pasinler fault zone and the right-lateral Ararat fault zone, not only a decollement surface formed, but also slab-like crustal blocks were bent and tilted northeastwards, causing some thinning of the continental crust. This period also witnessed the development of the Neogene basins that cover extensive areas. Thinning of the continental crust disturbed the mantle beneath the VDD and mantle upwelled by means of rising mantle diapirs. The forces exerted by the mantle upwelling and gravitational body forces of the crustal slabs caused more tilting and thinning of the crust. Because of the buoyant character of the Arabian continental crust, the subducted slab detached and started to sink, reviving the calc-alkaline volcanism. At the same time, the partial melting of the rising mantle diapirs produced alkaline magmas. These magmas either ascending alone or mixing with calc-alkaline magmas, produced alkali and transitional (hybrid) volcanics. The consumption of the available "escape space" along the Caucasuses prevented the further development of the extensional regime in the VDD. Continued convergence following the continental collision started to squeeze the crustal slab like-blocks that were trapped between the continental masses of the Arabian and Scythian platforms. Those competent crustal blocks, instead of thrusting over each other to thicken the crust, started to escape eastwards away from the maximum compression region along the NW-SE trending set of oblique-slip faults. This kind of deformational style is expected, because sideways motion utilizing existing fault zones requires less work than crustal thickening. The latter necessitates work that is done against gravity. Sideways escape also modifies the mosaic structure of the continental crust by locking some existing faults and distributing the stresses to create new faults. For example, the Ararat fault segment to the east of Lake Van probably represents such a locked shear

zone due to the eastward escape of the crustal blocks. The Hakkari fault is also locked by the intersecting Tabriz fault.

The availibility of an "escape space" adjacent to the extending terranes seems to be a very important factor in the development of extensional regimes. Although the extension along the mid-ocean ridges is compensated by the elimination of the oceanic crust subduction, we can categorize another type of subduction mechanism, that is, the Aegean Arc type subduction. In this category, subduction is not directly accompanied by a mid-ocean opening but originates as a result of thrusting of a continental crust over an existing oceanic crust. Because of their contrasting densities, the existing oceanic crust can be viewed as an "escape space" for the continental crust. For example, the Mediterranean seafloor is an escape space for the Aegean continental crust. Similarly the Caucasus back-arc basin was an "escape space" for the VDD. The California coast of the United States represents an area where a transition occurred, due to the subduction of the East Pacific Rise about 20 my. ago, from Andean type to Aegean type subduction. A steepening of the subduction angle of the Farallon-Juan de Fuca plate in this region has been suggested (Snyder et al., 1976). Interestingly the timing of this event based on the space-time patterns of the Cenozoic volcanism in the western United States, is also about 20 my. before present. Burchfiel and Royden (1982) also proposed a similar steeepening for the subducting slab in the Carpathian Arc, preceeding extension in the Pannonian basin. The steepening of the subduction angle may be caused by an increase in the convergence rate due to thrusting of continental crust over oceanic crust.

In conclusion, thinning of continental crust by tilting and bending of vertical slab like crustal blocks, pushing them over a decollement surface towards an "escape space" and pulling them apart to accomodate sideways escape, may provide a reasonable explanation

for the formation of Neogene basins, contemporaneous development of extensional-compressional tectonics and calc-alkaline - alkaline volcanics in the Lake Van area in particular. This model may offer plausible alternative explanations for the origin of extensional tectonics (Basin and Range type extensional terrains, back-arc spreading, ocean openings) either immediately following or developing contemporaneously with compressional tectonic regimes in an adjacent region.

REFERENCES:

Adamia, S. A., Lordkipanidze, M. B., and Zakariadze, G. S., 1977. Evolution of an active continental margin as exemplified by the Alpine history of the Caucasus., Tectonophysics, 40, 183-199.

Alberti, A. A., Comin-Chiaramonti, P., Sinigoi, S., Nicoletti, M., and Petrucciani, C., 1980. Neogene and Quaternary volcanism in Eastern Azerbaijan (Iran): some K-Ar age determinations and geodynamic implications. Geol. Rundschau., 69, 216-225.

Allegre, C. J., 1982. Chemical geodynamics. Tectonophysics, 81, 109-132.

Allegre, C. J., Dupre, B., Lambret, B. and Richard, P., 1981. The sub-continental versus sub-oceanic debate. I. Lead-neodymium-strontium isotopes in primary alkali basalts from a shield area: Ahaggar volcanic suite. Earth Planet. Sci. Lett., 52, 85-92.

Allegre, C. J., Dupre, B., Richard, P. and Rousseau, D., 1982. Sub-continental versus sub-oceanic mantle. II. Nd-Sr-Pb isotopic comparison of continental tholeiites with mid-ocean ridge tholeiites, and the structure of the continental lithosphere. Earth Planet. Sci. Lett., 57, 25-34.

Allegre, C. J., Hart, S. R. and Minster, J.-F., 1983. Chemical structure and evolution of the mantle and continents determined by inversion of Nd and Sr isotopic data, II. numerical experiments and discussion. Earth Planet Sci. Lett., 66, 191-213.

Allen, C. R., 1969. Active faulting in northern Turkey. Contrib. No. 1577, Div. Geol. Sci., Calif. Inst. Tech. 32.

Alptekin, O., 1973. Focal mechanism of earthquakes in western Turkey and their tectonic implications (Ph. D. thesis): Sorocco, New Mexico Inst. Mining & Tech., 189p.

Altinli, E., 1966-a. Geology of eastern and southeastern Anatolia. Bull. Miner Res. Explor. Inst., Ankara, 66, 35-75.

Altinli, E., 1966-b. Geology of eastern and southeastern Anatolia Part-II). Bull. Miner. Res. Explor. Inst., Ankara, 67, 1-22.

Ambraseys, N.N. & Melville, C.P., 1982. A history of Persian earthquakes., Cambridge Univ. Press, Cambridge, 219 p.

Anderson, A. T., 1976. Magma mixing: petrological process and volcanological tool. J. Volcan. Geotherm. Res., 1, 3-33.

Apted, M. J. and Boettcher, A. L., 1981. Partitioning of rare earth elements between garnet and andesite melt: an autoradiographic study of P-T-X effects. Geochim. Cosmochim. Acta, 45, 827-837.

Arculus, R. J. and Johnson, R. W., 1981. Island-arc magma sources: a geochemical assessment of the roles of slab-derived components and crustal contamination. Geochem. Jour., 15, 109-133.

Armstrong, R. L., Taubeneck, W. H. & Hales, P. O., 1977. Rb-Sr and K-Ar geochronometry of Mesozoic granite rocks and their Sr isotopic composition, Oregon, Washington, and Idaho. Bull. geol. Soc. Am., 88, 397-411.

Arpat, E. & Saroglu, F., 1972. The East Anatolian fault system: thoughts on its development. Bull. Miner. Res. Explor. Inst., Ankara, 78, 33-39.

Arpat, E. & Saroglu, F., 1975. Some recent tectonic events in Turkey. Bull. Geol. Soc. Turkey., 18, 91-101 (in Turkish).

Arpat, E., Saroglu, F., & Iz, H. B., 1977. Caldiran Depremi., Yeryuvari ve Insan., 2, 29-41.

Bak, J., Sorensen, K., Grocott, J., Korstgard, J., Nash, D., and Watterson, J., 1975. Tectonic implications of Precambrian shear belts in western Greenland. Nature, 254, 566-569.

Balavadze, B. K. and Mindeli, P. S., 1975. Methods of deep crustal studies in the Black Sea region. In: The Earth's Crust and the development of the Black Sea Basin., Ed. Nauka, Moskow, p. 274.

Ballance, P. F., and Reading, H. G., 1980, eds., Sedimentation in Oblique-slip Mobile Zones: Specs. Publ. 4, Int. Assoc. Sediment. Blackwell Scientific Publications, 265 p.

Barreiro, B., 1983. Lead isotopic compositions of South Sandwich Island volcanic rocks and their bearing on magmagenesis in intra-oceanic island arcs. Geochim. Cosmochim. Acta, 47, 817-822.

Basaltic Volcanism Study Project, 1981. Basaltic Volcanism on the Terrestrial Planets, Pergamon Press.

Berberian, M., 1983. The southern Caspian: A compressional depression floored by a trapped, modified Oceanic crust., Can J. Earth Sci. 20, 163-183.

Bergougnan, H. and Fourquin, C., 1982. Remnants of a pre-Late Jurassic ocean in northern Turkey: Fragments of Permian-Triassic Paleo-Tethys?: Discussion and reply. Geol. Soc Amer. Bull., 93, 929-936.

Boccaletti, M., Innocenti, F., Manetti, P., Mazzuoli, R., Motamed, A., Pasquare, G., Di Brozolo, F. R., and Sobhani, E. A., 1977. Neogene and Quaternary volcanism of the Bijar area (Western Iran). Bull. Volcan., 40, 1-12.

Boray, A., 1975. The structure and metamorphism of the Bitlis Area. Bull. Geol. Soc. Turkey., 18, 81-84 (in Turkish).

Bowen, N. L., 1928. The evolution of the igneous rocks. Princeton University Press (reprinted by Dover Press, 1956), 334p.

Braud, J. & Ricou, L.-E., 1971. L'accident due Zagros ou Main Thrust, un charriage et un coulissement. C. r. hebd. Seanc. Acad. Sci., Paris 272, 203-206.

Briqueu, L. and Lancelot, J. R., 1979. Rb-Sr systematics and crustal contamination models for calc-alkaline igneous rocks. Earth Planet. Sci. Lett., 43, 385-396.

Burchfiel, B. C., 1980. Eastern European Alpine System and the Carpathian Orocline as an example of collision tectonics. Tectonophysics, 63, 31-61.

Burchfiel, B. C., and Davis, G. A., 1972. Structural framework and evolution of the southern part of the Cordilleran orogen, Western United states. Amer. J. Sci., 272, 97-118.

Burchfiel, B. C. and Davis, G. A., 1975. Nature and controls of Cordilleran orogenesis, Western United States: Extensions of an earlier synthesis. Amer. J. Sci., 275-a, 363-396.

Burchfiel, B. C. and Royden, L., 1982. Carpathian foreland fold and thrust belt and its relation to Pannonian and other basins. Bull. Am. Assoc. Petrol. Geol. 66, 1179-1195.

Canitez, N. & Ucer, S. B., 1967. Computer determinations for the fault plane solutions in and near Anatolia. Tectonophysics, 4, 235-244.

Caputo, M., Panza, G. F. and Postpischl, D., 1970. Deep structure of the Mediterrenean Basins, J. Geophys. Res., 75, 4919-4923.

Carter, S. R., Evensen, N. M., Hamilton, P. J. and O'Nions, R. K., 1978. Neodymium and strontium isotope evidence for crustal contamination of continental volcanics. Science, 202, 743-747.

Chase, C. G., 1981. Oceanic island Pb: two-stage histories and mantle evolution. Earth Planet. Sci. Lett., 52, 277-284.

Chen, C. Y., Chen, W. P., and Molnar, P., 1980. The uppermost mantle P wave velocities beneath Turkey and Iran., Geophys. Res. Lett., 7, 77-80.

Cohen, R. S. and O'Nions, R. K., 1982. Identification of recycled continental material in the mantle from Sr, Nd and Pb isotope investigations. Earth Planet. Sci. Lett., 61, 73-84.

Cox, K. G., 1983. The Karoo province of southern Africa: Origin of trace element enrichment patterns. In: Hawkesworth, C. J. and Norry, M. J. (eds), Continental basalts and mantle xenoliths. Shiva, U. K.

Crowell, J. C., 1974. Origin of Late Cenozoic basins in southern California, Spec. Publ. Soc. Econ. Paleontol. and Mineral., 22, 190-204.

Dalmayrac, b. and Molnar, P., 1981. Parallel thrust and normal faulting in Peru and constraints on the state of stress. Earth Planet. Sci. Lett., 55, 473-481.

Davidson, J. P., 1983. Lesser Antilles isotopic evidence of the role of subducted sediment in island arc magma genesis. Nature, 306, 253-256.

Davis, G. A., 1980. Problems of the intraplate extensional tectonics, Western United States. In: Continental Tectonics, National Academy of Sciences, 84-95.

Davis, G. A. and Burhfiel, B. C., 1973. Garlock Fault: An intracontinental transform structure, southern California, Geol. Soc. Am. Bull., 84, 1407-1422.

Degens, E. T., Wong, H. K., Kurtman, F., & Finckh, P., 1978. Geological development of Lake Van: A summary. In: Degens, E. T. & Kurtman, F. (eds.) The Gelogy of Lake Van. Publ. No. 169., Miner. Res. Explor. Inst., Ankara, 134-146.

DePaolo, D. J. and Johnson, R. W., 1979. Magma genesis in the New Britain island arc: constraints from Nd and Sr isotopes and trace-element patterns. Contrib. Mineral. Petrol., 70, 367-380.

DePaolo, D. J. and Wasserburg, G. J., 1977. The sources of island arcs as indicated by Nd and Sr isotopic studies. Geophys. Res. Lett., 4, 465-468.

Dewey, J. W., 1976. Seismicity of northern Anatolia. Bull. Seism. Soc. Am., 66, 843-868.

Dewey, J. W., Pitman, W. C. III, Ryan, W. B. F., & Bonnin, J., 1973. Plate tectonics and the evolution of the Alpine system. Bull. Geol. Soc. Am., 84, 3137-3180.

Dewey, J. F. & Sengor, A.M.C., 1979. Aegean and surrounding regions: complex multi-plate and continuum tectonics in a convergent zone. Bull. Geol. Soc. Am. 90, 89-92.

Dickinson, W. R., 1983. Cretaceous sinistral strike slip along Nacimiento fault in Coastal California, Bull. Am. Ass. Petrol. Geol., 67, 624-645.

Dupre, B. and Allegre, C. J., 1983. Pb-Sr isotope variation in Indian Ocean basalts and mixing phenomena. Nature, 303, 142-146.

Eaton, G. P., 1980. Geophysical and geological characteristics of the crust of the Basin and Range province. In: Continental Tectonics, National Academy of Sciences, 96-113.

Eichelberger, J. C., 1975. Origin of andesite and dacite; evidence of mixing at Glass Mountain in California and at other circuum-Pacific volcanoes. Geol. Soc. Am. Bull., 86, 1381-1391.

Ewart, A., 1982. Petrogenesis of the Tertiary anorogenic volcanic series of southern Queensland, Australia, in the light of trace element geochemistry and O, Sr and Pb isotopes. J. Petrol., 23, 344-382.

Eyidogan, H., 1983. Bitlis-Zagros bindirme ve kivrimli kusaginin sismotektonik ozellikleri. Ph.D. thesis (unpublished), Istanbul Tech. Univ., 111p.

Frey, F. A. and Green, D. H., 1974. The mineralogy, geochemistry and origin of lherzolite inclusions in Victorian basanites. Geochim. Cosmochim. Acta, 38, 1023-1059.

Frey, F. A., Green, D. H., 1978. Integrated models of basalt petrogenesis: a study of quartz tholeiites to olivine melilitites from South Eastern Australia utilizing geochemical and experimental petrological data. J. Petrol., 19, 463-513.

Frey, F. A. and Prinz, M., 1978. Ultramafic inclusions from San Carlos, Arizona: petrologic and geochemical data bearing on their petrogenesis. Earth Planet. Sci. Lett., 38, 129-176. Frey, F. A., Haskin, M. A., Poetz J. A. and Haskin, L. A., 1968. Rare earth abundances in some basic rocks. J. Geophys. Res., 73, 6085-6098.

Gamkrelidze, I. P., 1974. Mekhanism formirovania tectonicheskikh struktur (na primere Adzharo-Trialetskoy zony) i nekotoryye obshchiye problemy tectoniki. Avtoref. dokt. dissert, Tbilisi.

Gamkrelidze, I. P., 1977. Tectonic development of the Anatolia-Caucasus-Iran segment of the Mediterranean belt., Geotectonics, 11, 173-181.

Garcia, M. O., Jacobson, S. S., 1979. Crystal clots, amphibole fractionation, and the evolution of calc-alkaline magmas. Contrib. Mineral. Petrol 69, 319-332.

Gast, P. W., 1968. Trace element fractionation and the origin of tholeiitic and alkaline magma types. Geochim. Cosmochim. Acta, 32, 1057-1086.

Gill, J. B., 1978. Role of trace element partition coefficients in models of andesite genesis. Geochim. Cosmochim. Acta, 42, 709-724.

Gill, J. B., 1981. Orogenic andesites and plate tectonics, Springer Verlag, New York, 390p.

Green, T. H., 1980. Island arc and continent-building magmatism-a review of petrogenetic models based on experimental petrology and geochemistry. Tectonophysics, 63, 367-385.

Green, T. H., 1981. Experimental evidence for the role of accessory phases in magma genesis. Jour. Volcan. Geotherm. Res., 10, 405-422.

Gulen, L., 1982. Sr, Nd and Pb isotope systematics of Ararat and Suphan volcanoes, Eastern Turkey. EOS, Trans. Am. Geophys. Un., 63, 1145.

Grocott, J., 1977. The relationship between Precambrian shear belts and modern fault systems. J. Geol. Soc. Lond. 133, 257-262.

Grove, T. L. and Baker, M. B., 1984. Phase equilibrium controls on the tholeiitic versus calc-alkaline differentiation trends. J. Geophys. Res., 89, 3253-3274.

Grove, T. L., Gerlach D. C. and Sando, T. W., 1982. Origin of calc-alkaline series lavas at Medicine Lake volcano by fractionation, assimilation and mixing. Contrib Mineral Petrol, 80, 160-182.

Hall, R., 1976. Ophiolite emplacement and the evolution of the Taurus suture Zone, south-eastern Turkey. Bull. Geol. Soc. Am., 87, 1078-1088.

Hamelin, B., Dupre, B. and Allegre, C. J., 1984. The lead isotope systematics of ophiolite complexes. Earth Planet. Sci. Lett., 67, 351-366.

Hancock, P. L. & Barka, A. A., 1983. Tectonic interpretations of enigmatic structures in the North Anatolian fault zone. J. Struc. Geol., 5, 217-220.

Hart, S. R. , 1971. K, Rb, Cs and Ba contents and Sr isotope ratios of ocean floor basalts. Philos. Trans. R. Soc. London Ser. A., 268, 578-587.

Hart, S. R., 1984. The DUPAL anomaly: a large scale isotopic mantle anomaly in the southern hemisphere. Submitted, Nature.

Hart, S. R. and Brooks, C., 1977. The geochemistry and evolution of early Precambrian mantle. Contrib. Mineral. Petrol., 61, 109-128.

Hart, S. R. and Nalwalk, A. J., 1969. K, Rb, Cs and Sr relationships in submarine basalts from the Puerto Rico trench. Geochim. Cosmochim. Acta, 34, 145-155.

Hawkesworth, C. J., Norry, M. J., Roddick, J. C. and Vollmer, R., 1979. 143Nd/144Nd and 87Sr/86Sr ratios from the Azores and their significance in LIL-element enriched mantle. Nature, 280, 28-31.

Hawkesworth, C. J., O'Nions, R. K., and Arculus, R. J., 1979. Nd and Sr isotope geochemistry of island arc volcanics, Grenada, Lesser Antilles. Earth Planet. Sci. Lett., 45, 237-248.

Hawkesworth, C. J. and Powell, M., 1980. Magma genesis in the Lesser Antilles island arc. Earth Planet. Sci. Lett., 51, 297-308.

Haynes, S. J. and McQuillan, H., 1974. Evolution of the Zagros Suture Zone, southern Iran., Geol. Soc. Am. Bull., 85, 739-744.

Hedge, C. E. and Noble, D. C., 1971. Upper Cenozoic basalts with high Sr 87/86 and Sr/Rb ratios, southern Great Basin, western United States. Geol. Soc. Am. Bull., 82, 3503-3510.

Hellman, P. L. and Green, T.H., 1979. The role of sphene as an accessory phase in the high-pressure partial melting of hydrous mafic compositions. Earth Planet. Sci. Lett., 42, 191-201.

Hempton, M. R., Dunne, L. A., and Dewey, J. F., 1983. Sedimentation in an active strike-slip basin, southeastern Turkey. J. Geol., 91, 401-412.

Hofmann, A. W. and White, W. M., 1980. The role of subducted oceanic crust in mantle evolution. Carnegie Inst. Wash. Yrbk., 79, 477-483.

Horvath, F. and Royden, L., 1981. Mechanism for the formation of the Intra-Carpathian Basins: A Review. Earth Evolution Sci., 3, 307-316.

Howell, D. G., Crouch, J. K., Greene, H. G., McCulloch, D. S., and Vedder, J. G., 1980. Basin development along the late Mesozoic and Cainozic California Margin: a plate tectonic margin of subduction, oblique subduction and transform tectonics. In: Ballance, P. F. and Reading, H. G. (eds) Sedimentation in Oblique-slip mobile zones. Spec. Publ. Int. Ass. Sediment. 4, 43-62.

Innocenti, F., Manetti, P., Mazzuoli, R., Pasquare, G. and Villari, L., 1982. Anatolia and north-western Iran. In: Thorpe, R. S., (ed) Andesites: Orogenic Andesites and Related Rocks, 327-349.

Innocenti, F., Mazzuoli, R., Pasquare', G., Radicati di Brozolo, F., and Villari, L., 1976. Evolution of the volcanism in the area of interaction between the Arabian, Anatolian, and Iranian plates (Lake Van, eastern Turkey). J. Volcan. Geotherm. Res., 1, 103-112.

Innocenti,F., Mazzuoli, R., Pasquare, G., Serri, G., and Villari, L., 1980. Geology of the volcanic area north of Lake Van (Turkey). Geol. Rundschau, 69, 292-322.

Irvine, T. N., 1977. Origin of chromitite layers in the Muskox intrusion and other stratiform intrusions: a new interpretation. Geology, 5, 273-277.

Irvine, T. N. and Baragar, W. R. A., 1971. A guide to the chemical classification of the common volcanic rocks. Can. J. Earth Sci., 8, 523-548.

Irving, A. J., 1978. A review of experimental studies of crystal/liquid trace element partitioning. Geochim. Cosmochim. Acta, 42, 743-770.

Irving, A. J. and Frey, F. A., 1978. Distribution of trace elements between garnet megacrysts and host volcanic liquids of kimberlitic to rhyolitic composition. Geochim. Cosmochim. Acta, 42, 771-787.

Jakes, P. and White, A.J.R., 1970. K/Rb ratios of rocks from island arcs. Geochim. Cosmochim. Acta, 34, 849-856.

Jakes, P. and White, A.J.R., 1972. Major and trace element abundances in volcanic rocks of orogenic areas. Geol. Soc. America Bull., 83, 29-40.

Jackson, J. and McKenzie, D., 1984. Active tectonics of the Alpine-Himalayan Belt between western Turkey and Pakistan. Geophys. J. R. astr. Soc., 77, 185-264.

James, D. E., 1982. A combined O, Sr, Nd, and Pb isotopic and trace element study of crustal contamination in central Andean Lavas, I. Local geochemical variations. Earth Planet. Sci. Lett., 57, 47-62.

Kadinsky-Cade, K., Barazangi, M., Oliver, J., and ISACKS, B., 1980. Lateral variations of high-frequency seismic wave propagation at regional distances across the Turkish and Iranian Plateaus, J. Geophys. Res, 86, 9377-9396.

Karig, D. E., 1971. Origin and development of marginal basins in the Western Pacific., J. Geophys. Res., 76, 2542-2561.

Kay, R. W., 1980. Volcanic arc magmas: implications of a melting-mixing model for element rcycling in the crust-upper mantle system, J. Geol., 88, 497-522.

Kay, R. W., Sun, S.-S. and Lee-Hu, C.-N., 1978. Pb and Sr isotopes in volcanic rocks from the Aleutian Islands and Pribilof Islands, Alaska. Geochim. Cosmoshim. Acta, 42, 263-273.

Kaya, O., 1979. Orta Dogu Ege cokuntusunun (Neojen) stratigrafisi ve tektonigi. TJK Bult., 35-58.

Kaya, O., 1982. Tersiyer sirt yitmesi: Dogu Ege bolgelerinin yapisi ve magmatikligi icin olasili bir mekanizma. In: Bati Anadolu'nun genc tektonigi ve magmatizmasi paneli, 39-58.

Kempe, S., Khoo, F., & Gurleyik, Y., 1978. Hydrography of Lake Van and its drainage area. In: Degens, E. T. & Kurtman, F. (eds.) The Geology of Lake Van. Publ. No. 169., Bull. Res. Explor. Inst., Ankara, 30-44.

Ketin, I., 1966. Tectonic units of Anatolia. Bull. Miner. Res. Explor. Inst., Ankara, 66, 23-34.

Ketin, I., 1977. Van Golu ile Iran siniri arasindaki bolgede yapilan jeoloji gozlemlerinin sonuclari hakkinda kisa bir aciklama., Bull. Geol. Soc. Turkey., 20, 79-85.

Ketin, I. & Roesli, F., 1953. Macroseismische Untersuchungen uber das nordwest-anatolische Beben vom 18. Marz 1953, Eclogae Geologicae Helvetiae, 46, 187-208.

Khain, V. E., 1969. Main structural features of the Alpine belt of Eurasia, the near and Middle East. Vestn. Mosk. Univ., No.1.

Khain, V. E., 1975. Structure and main stages in the tectono-magmatic development of the Caucasus: an attempt at geodynamic interpretation. Am. J. Sci., 275-a, 131-156.

Khain, V. E., 1977. Critical comparison of mobilistic models of tectonic development of the Caucasus. In: B. Biju-Duval and L. Montadert(eds.) Structural history of the Mediterranean Basins, Edition Technip, Paris, 353-362.

Kistler, R. W. & Peterman, Z. E., 1973. Variations in Sr, Rb, K, Na and initial 87Sr/86Sr in Mesozoic granitic rocks and intruded wall rocks in central California. Bull. geol. Soc. Am., 84, 3489-512.

Koronovskii, N. V., 1979a. The Paleogene vulcanism in the geologic history of the near and middle east, I. Geologiya, 34, 3-16.

Koronovskii, N. V., 1979b. Paleogene volcanism in the geological history of the near and middle east, II. Geologiya, 34, 30-42.

Kuno, H., 1950. Petrology of Hakone Volcano and the adjacent areas, Japan. Geol. Soc. Am. Bull., 61, 957-1020.

Kurtman, F. and Akkus, M. F., 1971. Inter-mountain basins in eastern Anatolia and their oil possibilities, Bull. Miner. Res. Explor. Inst., Ankara, ? , 1-9.

Kurtman, F., Akkus, M. F., and Gedik, A., 1978. The geology and oil potential of the Mus-Van Region. In: Degens, E. T. & Kurtman, F. (eds.) The Geology of Lake Van. Publ. No. 169., Miner. Res. Explor. Inst., Ankara, 124-133.

Kurtman, F. & Baskan, E., 1978. Mineral and thermal waters in the vicinity of Lake Van. In: Degens, E. T. & Kurtman, F. (eds.) The Geology of Lake Van. Publ. No. 169., Miner. Res. Explor. Inst., Ankara, 50-55.

Lahn, E., 1948. Contribution a l'etude geologique et geomorphologique de lacs de la Turquie. Publ. No. B-12., Miner. Res. Explor. Inst., Ankara.

Lauer, J.P., 1982. The geodynamic evolution of Turkey and Cyprus according to new paleomagnetic data. Abstract, Geol. Evolu. Eastern Mediterranean, Edinburgh, 21.

Langmuir, C. H., Vocke, R. D. Jr, Hanson, G. N., and Hart, S. R., 1978. A general mixing equation with applications to Icelandic basalts, Earth Planet. Sci. Lett., 37, 380-392.

Lavenu, A., 1978. Neotectonique des sediments Plio-Quaternaires du Nord de L'Altiplano Bolivien (region de La Paz-Ayo-Ayo-Umela), Cah. ORSTROM. Ser. Geol. X/1, 115-126.

LePichon, X. and Angelier, J., 1979. The Hellenic arc and trench system: A key to the Neotectonic evolution of the eastern Mediterranean arc. Tectonophysics, 60, 1-42.

Letouzey, J., Biju-Duval, B., Dorkel, A., Gonnard, R., Kristchev, K., Montadert, L., and Sungurlu, O., 1977. The Black Sea: A marginal basin, geophysical and geological data. In: B. Biju-Duval and L. Montadert(eds.) Structural history of the Mediterranean Basins, Edition Technip, Paris, 363-376.

Lipman, P. W., Doe, B. R., Hedge, C. E. and Steven, T. A., 1978. Petrologic evolution of the San Juan volcanic field, southwestern Colorado: Pb and Sr isotope evidence. Geol. Soc. Am. Bull., 89, 59-82.

Lopez-Escobar, L., Frey, F. A., and Vergara, M., 1977. Andesites and high alumina basalts from the Central-South Chile high Andes: geochemical evidence bearing on their petrogenesis. Contrib. Mineral Petrol., 63, 199-228.

Luhr, J. F. and Carmichael, I. S. E., 1980. The Colima volcanic complex, Mexico I. Post-Caldera andesites from volcan Colima. Contrib. Mineral. Petrol., 71, 343-372.

Manhes, G., Minster, J-F., and Allegre, C. J., 1978. Comparative uranium-thorium-lead and rubidium-strontium study of the Saint-Severin amphoterite: consequences for early solar system chronology, Earth Planet. Sci. Lett., 39, 14-24.

McCallum, I. S. and Charette, M. P., 1978. Zr and Nb partition coefficients: implications for the genesis of mare basalts, kreep, and sea floor basalts. Geochim. Cosmochim. Acta, 42, 859-869.

McKenzie, D., 1972. Active tectonics of the Mediterranean Region., Geophys. J. R. astr. Soc., 30, 109-185.

McKenzie, D., 1976. The East Anatolian Fault: A major structure in eastern Turkey., Earth Planet. Sci. Lett., 29, 189-193.

McKenzie, D., 1978. Active tectonics of the Alpine-Himalayan belt: the Aegean Sea and surounding regions. Geophys. J. R. ast. Soc., 55, 217-254.

Meijer, A., 1976. Pb and Sr isotopic data bearing on the origin of lavas from the Mariana arc system. Geol. Soc. Amer. Bull., 87, 1358-1369.

Menzies, M. A. and Murthy, V. R., 1980. Nd and Sr isotope geochemistry of hydrous mantle nodules and their host alkali basalt: implications for local heterogeneities in metasomatically veined mantle. Earth Planet. Sci. Lett., 46, 323-334.

Menzies, M. A., Leeman, W. P., and Hawkesworth, C. J., 1983. Isotope geochemistry of Cenozoic volcanic rocks reveals mantle heterogeneity below western USA., Nature, 303, 205-209.

Mercier, J. L., 1981. Extensional-compressional tectonics associated with the Aegean Arc: comparison with the Andean Cordillera of south Peru-north Bolivia. Phil. Trans. R. Soc. Lond. A 300, 337-355.

Mercier, J., Carey, E., Phillip, H., and Sorel, D., 1976. La neotectonique plio-quaternaite de l'arc egeen externe et de la mer Egee et ses relations avec seismicite. Bull. Soc. Geol. Fr.(7), 18, 355-372.

Molnar, P. and Oliver, J., 1969. Lateral variations of attenuation in the upper mantle and discontinuities in the lithosphere., J. Geophys. Res., 74, 2648-2682.

Molnar, P. & Tapponnier, P. 1975. Cenozoic Tectonics of Asia: Effects of a continental collision. Science, 189, 419-426.

Molnar, P., Tapponnier, P., and Chen, W. P., 1981. Extensional tectonics in central and eastern Asia: a brief summary. Phil. Trans. R. Soc. Lond. A-300, 403-406.

Moorbath, S. and Thompson, R. N., 1980. Strontium isotope geochemistry and petrogenesis of the early Tertiary lava pile of the Isle of Skye, Scotland, and other basic rocks of the British Tertiary province: an example of magma-crust interaction. J. Petrology, 21, 295-321.

Morris, J. D. and Hart, S. R., 1983. Isotopic and incompatible element constraints on the genesis of island arc volcanics from Cold Bay and Amak Island, Aleutians, and implications for mantle structure. Geochim. Cosmochim. Acta 47, 2015-2030.

Myers, J. D., Sinha, A. K. and Marsh, B. D., 1984. Assimilation of crustal material by basaltic magma: strontium isotopic and trace element data from the Edgecumbe volcanic field, SE Alaska. J. Petrology, 25, 1-26.

Neprochnov, Y. P., 1968. Structure of the Earth's crust of epicontinental seas. Caspian, Black, and Mediterranean. Can. J. Earth Sci., 5, 1037-1043.

Neprochnov, Y. P., Neprochnova, A. F., and Mirlin, Y. G., 1974. Deep structure of the Black Sea basin. In: E. T. Degens and D. A. Ross(eds.) The Black Sea geology, chemistry and biology. Amer. Assoc. Petrol. Geologists, Memoir 20, 35-49.

Nicholls, I. A. and Harris, K. L., 1979. Experimental rare earth element partition coefficients for garnet, clinopyroxene and amphibole coexisting with andesitic and basaltic liquids. Geochim. Cosmochim. Acta, 44, 287-308.

Nowroozi, A. A., 1971. Seismo-tectonics of the Persian Plateau, Eastern Turkey, Caucasus, and Hindu-Kush regions. Bull. seism. Soc. Am., 61, 317-341.

O'Hara, M. J., 1977. Geological evolution during fractional crystallization of a periodically refilled magma chamber. Nature, 266, 503-507.

Oswald, F. 1910. Zur tectonishen entwickhungsgeschichte des Armenischen hochlandes., Peterm. Mitt. Heft 13.

Oversby, V. M., 1971. Lead in oceanic islands: Faial, Azores and Trindade. Earth Planet. Sci. Lett., 11, 401-406.

Oversby, V. M., 1972. Genetic relations among the volcanic rocks of Reunion: chemical and lead isotopic evidence. Geochim. Cosmochim. Acta, 36, 1167-1179.

Oversby, V. M. and Ewart, A., 1972. Lead isotopic compositions of Tonga-Kermadec volcanics and their petrogenetic significance. Contrib. Mineral. Petrol., 37, 181-210.

Ozelci, F., 1973. Zagros tektonik zonu ve bu zonun Anadolu'da uzanimi ile ilgili Jeofizik gozlenimler. Turkiye Birinci Jeofizik Bilimsel ve Teknik Kongre Tebligleri, 241-249.

Ozkaya, I., 1981. Origin and tectonic setting of some melange units in Turkey., J. Geol., 90, 269-278.

Papazachos, B. C. and Comminakis, P. E., 1971. Geophysical and tectonic features of the Aegean arc, J. Geophys. Res., 76, 8517-8533.

Pearce, J. A., 1976. Statistical analysis of major element patterns in basalt. J. Petrol., 17, 15-43.

Pearce, J. A., 1982. Trace element characteristics of lavas from destructive plate boundaries. In: Thorpe, R. S., (ed) Andesites: Orogenic Andesites and Related Rocks, 525-548.

Pearce, J. A., 1983. Role of the subcontinental lithosphere in magma genesis at active continental margins. In: Hawkesworth, C. J. and Norry, M. J. (eds), Continental basalts and mantle xenoliths. Shiva, U. K.

Pearce, J. A. and Cann, J. R., 1973. Tectonic setting of basic volcanic rocks determined using trace element analysis. Earth Planet. Sci. Lett., 19, 290-300.

Pearce, J. A. and Norry, M. J., 1979. Petrogenetic implications of Ti, Zr, Y, and Nb variations in volcanic rocks. Contrib. Mineral. Petrol., 69, 33-47.

Peccerillo, A. and Taylor, S. R., 1976. Geochemistry of Eocene calc-alkaline volcanic rocks form the Kastamonu area, northern Turkey. Contrib. Mineral. Petrol., 58, 63-81.

Pegram, W. J., 1984. The isotope, trace element and major element geochemistry of the Mesozoic Appalachian tholeiite province, Ph.D. thesis, Massachusetts Institute of Technology.

Perfit, M. R., Gust, D. A., Bence, A. E., Arculus, R. J. and Taylor, S. R., 1980. Chemical characteristics of island-arc basalts: implications for mantle sources. Chem. Geol., 30, 227-256.

Perincek, D., 1980. Volcanics Triassic age in Bitlis metamorphic rocks., Bull. Geol. Soc. Turkey., 23, 201-211 (in Turkish).

Polshkov, M. K., Urupov, A. K., and Yegorkina, G. V., 1979. Anisotropy of the earth's crust in the Lesser Caucasus., Izvestiya, Earth Physics, 15, 98-101.

Prebble, W. M., 1980. Late Cainozoic sedimantation and tectonics of the East Coast Deformed Belt, in Marlborough, New Zealand. In: Ballance, P. F. and Reading, H. G.

(eds) Sedimentation in Oblique-slip mobile Zones. Spec. Publ. Int. Ass. Sediment. 4, 217-228.

Reading, H. G., 1980. Characteristics and recognition of strike-slip fault systems. In: Ballance, P. F. and Reading, H. G. (eds) Sedimentation in Oblique-slip mobile Zones. Spec. Pub. Int. Ass. Sediment. 4, 217-228.

Rhodes, J. M., Dungan, M. A., Blanchard, D. P. and Long, P. E., 1979. Magma mixing at mid-ocean ridges: evidence from basalts drilled near 22 degree N on the Mid-Atlantic ridge. Tectonophysics, 55, 35-61.

Rigo de Righi, M. & Cortesini, A., 1964. Gravity tectonics in Foothills structure belt of southeast Turkey., Bull. Am. Assoc. Petrol. Geol. 48, 1911-1937.

Ringwood, A. E., 1975. Composition and petrology of the earth's mantle. McGraw-Hill, New York, 618p.

Riou, R., 1979. Petrography and geochemistry of the Eocene alkaline lavas of the northern Azerbaijan (Iran). N. Jb. Geol. Palaont. Mh., 9, 532-559.

Rotstein, Y. & Kafka, A. L., 1982. Seismotectonics of the southern boundary of Anatolia, Eastern Mediterranean Region: Subduction, collision and arc jumping. J. Geophys. Res., 87, 7694-7706.

Royden, L. H., Horvath, F., and Burchfiel, B. C., 1982. Transform faulting, extension, and subduction in the Carpathian Pannonian region. Geol. Soc. Am. Bull., 93, 717-725.

Royden, L. H., Horvath, F., and Rumpler, J., 1983. Evolution of the Pannonian Basin system, 1- Tectonics. Tectonics, 2, 63-90.

Sakuyama, M., 1979. Evidence of magma mixing: petrological study of Shirouma-Oike calc-alkaline andesite volcano, Japan. J. Volcan. Geothern. Res., 5, 179-208.

Sanver, M., 1968. A palaeomagnetic study of quaternary volcanic rocks from Turkey. Phys. Earth Planet. Interiors, 1, 403-421.

Saroglu, F. & Guner, Y., 1979. Tutak diri fayi, ozellikleri ve Caldiran Fayi ile iliskisi, Yeryuvari ve Insan, 4, 11-14.

Saroglu, F. & Guner, Y., 1981. Factors effecting the geomorphological evolution of the eastern Turkey: relationships between geomorphology, tectonics, and volcanism. Bull. Geol. Soc. Turkey, 24, 39-50(in Turkish).

Saroglu, F., Guner, Y., & Yilmaz, Y., 1982. Initiation of the Neomagmatism eastern Anatolia: The geology of Solhan volcanics. Proc. 36th Geol. Congress Turkey, Ankara, 90.

Saunders, A. D., Tarney, J. and Weaver, S. D., 1980. Transverse geochemical variations across the Antarctic peninsula: implications for the genesis of calc-alkaline magmas. Earth Planet. Sci. Lett., 46, 344-360.

Schroeder, B, Thompson, G., Sulanowska, M., Ludden, J. N., 1980. Analysis of geologic materials using an automated x-ray fluorescence system, X-Ray Spectrom., 9, 198-205.

Sengor, A.M.C., 1979. The North Anatolian transform fault: its age, offset and tectonic significance. J. Geol. Soc. Lond., 136, 269-282.

Sengor, A.M.C. & Kidd, W.S.F., 1979. Post-collisional tectonics of the Turkish-Iranian Plateau and a comparison with Tibet. Tectonophysics, 55, 361-376.

Sengor, A.M.C., and Yilmaz, Y., 1981. Tethyan evolution of Turkey: A plate tectonic approach: Tectonophysics, 75, 181-241

Sengor, A.M.C., Yilmaz, Y., and Ketin, I., 1980. Remnants of a pre-Late Jurassic ocean in northern Turkey: Fragments of Permian-Triassic Paleo-Tethys? Geol. Soc. Amer. Bull., I, 91, 599-609.

Seymen, I., 1975. Kelkit vadisi kesiminde Kuzey Anadolu Fay Zonunun tektonik ozellligi. ITU Maden Fak. Yay., Istanbul, 192 pp.

Seymen, I. & Aydin, A., 1972. The Bingol Earthquake fault and its relation to the North Anatolian Fault zone. Bull. Miner. Res. Explor. Inst., Ankara, 79, 1-8.

Shempelev, A. G., 1978. Deep expression of the Main Caucasian Overthrust., Geotectonics, 12, 437-443.

Shimizu, N. and Kushiro, I., 1975. The partitioning of rare earth elements between garnet and liquid at high pressures: preliminary experiments. Geophys. Res. Lett., 2, 413-416.

Shirokova, E. I., 1962. Stresses effective in earhquake foci in the Caucasus and adjacent districts. Izv. Akad. Nauk SSSR., Ser. Geofiz., 10, 809-816.

Snyder, W.S., Dickinson, W.R., and Silberman, M.L., 1976. Tectonic implications of space-time patterns of Cenozoic volcanism in the western United States. Earth Planet. Sci. Lett., 32, 91-106.

Sparks, S. R. J., Sigurdson, H. and Wilson, L., 1977. Magma mixing: a mechanism for triggering acid explosive eruptions. Nature, 267, 315-318.

Spooner, E. T. C. and Gale, N. H., 1982. Pb isotopic composition of ophiolitic volcanogenic sulphide deposits, Troodos Complex, Cyprus. Nature, 296, 239-242.

Sporli, K. B., 1980. New Zealand and oblique-slip margins: tectonic development up to and during the Cainozoic. In: Ballance, P. F. and Reading, H. G. (eds). Sedimentation in Oblique-slip mobile Zones. Spec. Publ. Int. Ass. Sediment. 4, 147-170.

Stewart, J. H., 1980. Basin-range structure in western North America: A review. In: R. B. Smith and G. P. Eaton(eds). Cenozoic Tectonics and Regional Geophysics of the Western Cordillera., Geol. Soc. Am. Mem.# 152, 1-31

Stocklin, J., 1968. Structural history and tectonics of Iran: a review Bull. Am. Assoc. Petrol. Geol., 52, 1229-1258.

Suarez, G., Molnar, P., and Burchfiel, B. C., 1983. Seismicity, fault plane solutions, depth of faulting, and active tectonics of the Andes of Peru, Ecuador, and southern Colombia., J. Geophys. Res. 88, 10,403-10,428.

Sun, S. S., 1980. Lead isotopic study of young volcanic rocks from mid-ocean ridges, oceanic islands, and island arcs. Philos. Trans. R. Soc. London, A 297, 409-445.

Tapponnier, P., 1977. Evolution tectonique du systeme alpin en Mediterranean: painconnement et ecrasement rigide-plastique. Bull. Soc. Geol. France, 7, 437-460.

Tapponnier, P. & Molnar, P., 1976. Slip-line field theory and large-scale continental tectonics. Nature, 264, 319-324.

Tapponnier, P. & Molnar, P., 1977. Active faulting and tectonics in China. J. Geophys. Res. 82, 2905-2930.

Tatsumoto, M., 1969. Lead isotopes in volcanic rocks and possible ocean-floor thrusting beneath island arcs. Earth Planet. Sci. Lett., 6, 369-376.

Tatsumoto, M., 1978. Isotopic composition of lead in oceanic basalts and its implications to mantle evolution. Earth Planet Sci. Lett., 38, 63-87.

Taylor, H. P. Jr., 1980. The effects of assimilation of country rocks by magmas on 18O/16O and 87Sr/86Sr systematics in igneous rocks. Earth Planet. Sci. Lett., 47, 243-254.

Tchalenko, J. S., 1977. A reconnaissance of the seismicity and tectonics of the northern border of the Arabian plate (Lake Van region). Revue Geog. Phys. Geol. Dyn. (1), 19, 189-208.

Tchalenko, J. S. & Berberian, M., 1974. The Salmas (Iran) earthquake of May 6th, 1930., Ann. di Geofis., 27, 151-186.

Tchalenko, J. S. & Braud, J., 1974. Seismicity and structure of the Zagros (Iran): The Main Recent Fault between 33 and 35 degree N. Phil. Trans. R. Soc. Soc. Lond. A, 277, 1-25.

Thompson, R. N., Morrison, M. A., Dickin, A. P. and Hendry, G. L., 1983. Continental flood basalts... Arachnids rule ok? In: Hawkesworth, C. J. and Norry, M. J. (eds), Continental basalts and mantle xenoliths. Shiva, U. K.

Tilton, G. R. and Barreiro, B. A., 1980. Origin of lead in Andean calc-alkaline lavas, southern Peru. Science, 210, 1245-1247.

Toksoz, M. N., Arpat, E., and Saroglu, F., 1977. East Anatolian earthquake of 24 November 1976. Nature, 270, 423-425.

Toksoz, M. N. and Bird, P., 1977. Formation and evolution of marginal basins and continental plateaus. In: Talwani, M. and Pitman, W. (eds.), Island Arcs, Deep Sea Trenches and Back-Arc Basins, Maurice Eusing Ser., Vol. 1, 379-393.

Toksoz, M. N., Guenetle, M., Gulen, L., Keough, G., and Pulli, J. J., (1984) Source mechanism of Oct.30.1983 earthquake in northeastern Turkey (in prep).

Toksoz, M. N., Nabelek, J., and Arpat, E., 1978. Source properties of the 1976 earthquake in east Turkey. A comparison of field data and teleseismic results. Tectonophysics, 49, 199-205.

Tsagareli, A. L., 1974. Geology of Western Caucasus. In: E. T. Degens & D. A. Ross (eds.), The Black Sea-Geology, chemistry, and biology., Amer. Assoc. Petrol. Geologists, Memoir 20, 77-89.

Uyeda, S. and Kanamori, H., 1979. Back-arc opening and the mode of subduction., J. Geophys. Res., 84, 1049-1061.

Wang, H. K. & Degens, E. T., 1978. The bathymetry of Lake Van, eastern Turkey. In: Degens, E. T. & Kurtman, F. (eds). The Geology of Lake Van. Publ. No. 169., Miner. Res. Explor. Inst., Ankara, 6-10.

Wang, H.K. & Finckh, P., 1978. Shallow structures in Lake Van. In: E.T. Degens & F. Kurtman (eds.) The Geology of Lake Van. Publ. No. 169., Miner. Res. Explor. Inst., Ankara, 6-10.

Watson, E. B., 1982. Basalt contamination by continental crust: some experiments and models. Contrib Mineral Petrol, 80, 73-87.

Watson, E. B. and Jurewicz, S. R., 1984. Behavior of alkalies during diffusive interaction of granitic xenoliths with basaltic magma.

Wernicke, B. P., 1982. Processes of extensional tectonics, Unpublished Ph. D. thesis, M.I.T., 169p.

White, W. M. and Hofmann, A. W., 1982. Sr and Nd isotope geochemistry of oceanic basalts and mantle evolution. Nature, 296, 821-825.

White, W. M. and Patchett, J., 1984. Hf-Nd-Sr isotopes and incompatible element abundances in island arcs: implications for magma origins and crust-mantle evolution. In press, Earth Planet. Sci. Lett.

Wilcox, L. E., Rothermel, W. J., and Voss, J. T., 1972. A geophysical geoid of Eurasia., EOS Trans, Am. Geophys. Un., 53, 343. Res. Explor. Inst., Ankara, 20-28.

Wood, D. A., Joron J.-L., and Treuil, M., 1979. A re-appraisal of the use of trace elements to classify and discriminate between magma series erupted in different tectonic settings. Earth Planet. Sci. Lett., 45, 326-336.

Wright, T. L. and Fiske, R. S., 1971. Origin of the differentiated and hybrid lavas of Kilauea Volcano, Hawaii. J. Petro., 12, 1-65.

Yegorkina, G. V., Rakitov, V. A., Garetovskaya, I. V., and Yegorova, L. M., 1977. Stress state of the crust in Armenia, from seismic data., Geotectonics, 11, 125-130.

Yilmaz, O., 1971. Etude petrographique et geochronologique de la region de Cacas (Partie meridionale du massif de Bitlis, Turquie). These de Doct. 3e cycle, Universite de Gronoble-France, 230 pp.

Yilmaz, O., 1975. Etude petrographique et stratigraphique de la region de Cacas (Massif de Bitlis, Turquie). Bull. Geol. Soc. Turkey, 18, 33-40 (in Turkish).

Yilmaz, Y., Dilek, Y., & Isik, H., 1981. The geology of Gevas ophiolite and a synkinematic shear zone. Bull. Geol. Soc. Turkey., 24, 37-44 (in Turkish).

Zartman, R. E., 1974. Lead isotopic provinces in the Cordillera of the western United States and their geologic significance. Econ. Geol., 69, 792-805.

Zindler, A., Hart, S. R. and Brooks, C., 1981. The Shabogamo intrusive suite, Labrador: Sr and Nd isotope evidence for contamination of mafic magmas in the Proterozoic. Earth Planet Sci. Lett., 54, 217-135.

Zindler, A., Hart, S. R., Frey, F. A., and Jakobsson, S. P., 1979. Nd and Sr isotopic ratios and rare earth element abundances in Reykjanes Peninsula basalts: Evidence for mantle heterogeneity beneath Iceland. Earth Planet. Sci. Lett., 45, 249-262.

Zindler, A., Jagoutz, E. and Goldstein, S., 1982. Nd, Sr and Pb isotopic systematics in a three-component mantle: A new perspective. Nature, 298, 519-523.

APPENDIX

Sample Locations:

ARARAT:

Sample Number	Latitude(N) Deg.	Min.	Longitude(E) Deg.	Min.
A-1	39	54.8	44	16.1
A-4	39	56.7	44	14.7
A-5	39	57.3	44	12.2
A-6	39	55.9	44	09.7
A-8-B	39	51.8	44	05.3
A-9	39	47.6	44	07.4
A-10	39	35.1	44	09.3
A-12	39	36.3	44	12.4
A-13	39	36.1	44	13.2
A-14	39	36.2	44	14.4
A-17	39	35.0	44	14.2
A-19	39	34.1	44	14.6
A-23	39	32.0	44	19.2
A-25	39	32.1	44	20.3
A-26	39	32.2	44	20.4
A-30	39	30.4	44	19.3
A-32	39	33.4	44	20.7
A-33	39	33.7	44	20.3
A-34	39	34.1	44	20.3
A-36	39	33.4	44	19.0
A-42	39	44.3	44	19.6
A-43	39	43.2	44	28.3
A-45	39	42.1	44	23.3
A-46	39	39.6	44	23.9
A-47	39	40.4	44	21.9
A-48	39	38.6	44	21.7
A-51	39	40.1	44	21.0

Sample Locations:

TENDUREK:

Sample Number	Latitude(N) Deg.	Min.	Longitude(E) Deg.	Min.
T-1	39	32.4	43	59.2
T-4	39	31.6	43	46.8
T-10	39	28.3	43	49.2
T-11	39	27.7	43	49.4
T-12	39	27.3	43	48.6
T-13	39	29.5	43	46.3
T-14	39	29.6	43	49.2
T-15	39	28.0	43	53.9
T-22	39	27.4	43	57.9
T-24	39	27.6	44	00.0
T-25	39	26.4	43	59.3
T-26	39	25.7	44	01.6
T-27	39	23.7	44	00.0
T-29	39	22.7	43	59.0
T-31	39	22.4	43	58.5
T-32	39	22.3	44	01.3
T-33	39	20.5	44	01.1
T-34	39	20.1	44	01.4
T-35	39	20.1	44	00.1
T-36	39	17.0	44	00.0
T-38	39	12.7	44	00.3
T-39	39	13.9	43	54.6
T-40	39	23.7	43	48.1
T-46	39	14.1	43	44.4
T-48	39	24.6	43	59.3
T-49	39	25.0	43	58.9
T-50	39	23.5	43	56.2
T-51	39	21.4	43	53.4
T-52	39	21.2	43	53.1
T-53	39	21.1	43	54.0
T-55	39	21.5	43	52.6
T-58	39	22.0	43	56.0
T-59	39	22.3	43	56.4
T-60	39	22.0	43	56.7
T-64	39	10.2	43	58.5

Sample Locations:

Sample Number	Latitude(N) Deg.	Min.	Longitude(E) Deg.	Min.
NEMRUT:				
N-13	38	36.2	42	11.5
N-21	38	31.5	42	18.2
N-28	38	37.0	42	13.6
N-31	38	39.2	42	11.8
N-34	38	37.1	42	07.6
N-36	38	39.4	42	00.7
N-40	38	50.0	42	18.2
N-41	38	25.6	42	06.9
N-42	38	26.1	42	06.5
N-47	38	32.9	42	09.2
N-52	38	35.3	42	01.0
N-53	38	37.4	42	00.1
T-27	39	23.7	44	00.0
MALAZGIRT:				
S-41	38	57.3	42	55.1
S-43	39	00.0	42	55.0
S-60	39	04.1	43	09.2
S-63	39	07.8	42	51.5
S-64	39	06.8	42	51.1
S-65	39	05.7	42	52.8
S-66	39	05.2	42	49.3
S-68	39	06.4	42	43.8
S-69	39	07.3	43	24.9
S-70	39	07.8	43	18.3
S-75	39	05.5	42	34.6
MEYDAN:				
S-72	39	05.3	43	11.0
S-73	39	09.7	43	05.6
S-77	39	11.6	43	06.9